Downstream Processing of *Synechocystis* for Biofuel Production

by

Jie Sheng

A Dissertation Presented in Partial Fulfillment
of the Requirements for the Degree
Doctor of Philosophy

Approved October 2011 by the
Graduate Supervisory Committee:

Bruce E. Rittmann, Chair
Paul Westerhoff
Willem F. J. Vermaas

ARIZONA STATE UNIVERSITY

December 2011

ABSTRACT

Lipids and free fatty acids (FFA) from cyanobacterium *Synechocystis* can be used for biofuel (e.g. biodiesel or renewable diesel) production. In order to utilize and scale up this technique, downstream processes including culturing and harvest, cell disruption, and extraction were studied.

Several solvents/solvent systems were screened for lipid extraction from *Synechocystis*. Chloroform + methanol-based Folch and Bligh & Dyer methods were proved to be "gold standard" for small-scale analysis due to their highest lipid recoveries that were confirmed by their penetration of the cell membranes, higher polarity, and stronger interaction with hydrogen bonds. Less toxic solvents, such as methanol and MTBE, or direct transesterification of biomass (without pre-extraction step) gave only slightly lower lipid-extraction yields and can be considered for large-scale application.

Sustained exposure to high and low temperature extremes severely lowered the biomass and lipid productivity. Temperature stress also triggered changes of lipid quality such as the degree of unsaturation; thus, it affected the productivities and quality of *Synechocystis*-derived biofuel.

Pulsed electric field (PEF) was evaluated for cell disruption prior to lipid extraction. A treatment intensity > 35 kWh/m^3 caused significant damage to the plasma membrane, cell wall, and thylakoid membrane, and it even led to complete disruption of some cells into fragments. Treatment by PEF enhanced the potential for the low-toxicity solvent isopropanol to access lipid molecules during

subsequent solvent extraction, leading to lower usage of isopropanol for the same extraction efficiency.

Other cell-disruption methods also were tested. Distinct disruption effects to the cell envelope, plasma membrane, and thylakoid membranes were observed that were related to extraction efficiency. Microwave and ultrasound had significant enhancement of lipid extraction. Autoclaving, ultrasound, and French press caused significant release of lipid into the medium, which may increase solvent usage and make medium recycling difficult.

Production of excreted FFA by mutant *Synechocystis* has the potential of reducing the complexity of downstream processing. Major problems, such as FFA precipitation and biodegradation by scavengers, account for FFA loss in operation. Even a low concentration of FFA scavengers could consume FFA at a high rate that outpaced FFA production rate. Potential strategies to overcome FFA loss include high pH, adsorptive resin, and sterilization techniques.

ACKOWLEDGMENTS

Well, I guess this is the only part in my Ph.D. that I can write freely without worrying about criticisms about the logic and the validity of data. Being the first Bachelor and the only Ph.D. in my extended family, I would like to write some thinking here to myself, my family, a lot of people that I owe thanks, and possible readers who feel interested and inspired (if any).

I always envy those who have a luxurious childhood, which I was not lucky enough to have. No, I don't have engineer relatives to enlighten my education and career; no, I don't have a middle-class family to support my life or study. When I came to U.S., the only asset I have was $1,000 borrowed from a friend. For a young man like me, a reasonable life may be an ordinary blue-collar worker in a remote hinterland of China. So, when I retrospect, I am quite proud of what I have achieved, or at least I have reasons to be proud.

14 years ago, when my father passed away after a 6-year chronic illness, leaving only my mother and me in a small city of northeast China and a medical debt four times larger than our annual income, my family was in an extremely desperate situation. As a young boy, I observed my mother fighting to save the family. At that time, I made a wish: "I want a better life. I want a change." It was this small wish that sparked my journey to 2,700 km away and to become the #1 student of a top university with the most prestigious scholarships. It also was this small wish that carried me even 14,000 km further to U.S., a country that states: "*We hold these truths to be self-evident, that all men are created equal, that they are endowed by their Creator with certain unalienable Rights, that among these*

are Life, Liberty and the pursuit of Happiness." It turns out to be not bad, and…it is not easy.

I would like to confirm to myself and also to those who are still struggling in the mud of the fate that life, or at least part of it, can be changed by one's wish and effort, and you have to believe it. Change is always hard, but it can be achieved little by little, as long as you hold on that belief and keep moving forward. But even holding on is hard, especially when you are in the dark and cannot foresee any chance of success. There is a trick in this situation: just follow your heart and try one more step. It will not guarantee success, but at least you will not regret.

I have nothing to complain. Instead, I am grateful to a lot of people who really helped me in my life. I especially thank my advisor Dr. Bruce E. Rittmann, who generously provided me a life-changing chance of studying in his research group and thereafter, enormous help to my research. I also thank my committee members Dr. Willem F. J. Vermaas and Dr. Paul Westerhoff for their advice. I thank Science Foundation Arizona (SFAz) for funding my study at Arizona State University.

I also owe thanks to a lot of my colleagues, including Dr. Raveender Vannela, Dr. Rosa Krajmalnik-Brown, Dr. Robert W. Roberson, Dr. David Nielsen, Dr. Hyun Woo Kim, Dr. Xinyao Liu, Dr. Wei Yuan, Dr. Sawsan Hamad, Dr. Shuqin Li, Dr. James Banaszak, Dr. Mark Holl, Dr. Rhett Martineau, Dr. Daniel Brune, David Lowry, Jonathan P. Badalamenti, Chao Zhou, Joshua McIlwain, Jared Alder, Rod Caldwell, Rebecca Allen, Vicky Moore, Jesse Lynch,

Swathi Sridharakrishnan, Cody Anderson, Andrew Olsen, Alexander Zevin, and etc. I would like to express my sincere thanks to the motherlike lab and office administrators Diane Hagner and Saunia Calloway, all members of Swette Center for Environmental Biotechnology, the Biodesign Institute at Arizona State University, and those you know who you are. It is my honor to work with them for four years, an invaluable experience in my life. I am also grateful to British Petroleum (BP) and U.S. Department of Energy (US DoE) through ARPA-E funding for their support of the projects that I participated in.

When the Lord closes a door, somewhere He opens a window. Life may not have all we expect, it may even be tough, but it is still good. Just like the Soothsayer said to Po in *Kung Fu Panda 2*: "*Your story may not have such a happy beginning, but that doesn't make you who you are. It is the rest of your story, who you choose to be.*" Getting a Ph.D. is not the end but just another milestone in my journey: follow my passion, live my life. To continue this journey, I do need a little bit of bravery, patience, and belief. Good luck and don’t forget to smile!

DEDICATION

To my mother ZHAO Shumei who always supports me with love and teaches me the right things

To my father SHENG Zhenhua who always lives in my heart

And,

To my step-father YU Zhixiang and step-brother YU Yonglong who share the same pain, hope, effort, and happiness

TABLE OF CONTENTS

Page

LIST OF TABLES

Table Page

Table Page

Table Page

LIST OF FIGURES

Figure Page

Figure Page

Figure Page

ABBREVIATION

AC	Autoclaving
AOCS	American Oil Chemists' Society
ASE	Accelerated solvent extraction
BB	Bead beating
BPR	Biomass production rate
BT-PBR	Bench-top photobioreactor
C	Carboxysome
CAPS	3-(Cyclohexylamino)-1-propanesulfonic acid
CED	Cohesive energy density
DAG	Diacylglycerols
DGDG	Digalactosyl diacylglycerol
DI	Deionized
DO	Dissolved oxygen
DW	Dry weight
ESI-MS	Electrospray Ionization Mass Spectrometry
FAME	Fatty acid methyl ester
FCM	Flow cytometry measurement
FD	Freeze drying
FFA	Free fatty acid
FID	Flame ionization detector
FIU	Fluorescence intensity units
FP	Focused Pulsed (in Chapter 5)

FP	French press (in Chapter 6)
FPR	Free-fatty-acid production rate
Gal	Galactose
Gal_2	Digalactose
GC	Gas chromatography
HC	Hydrocarbons
HRT	Hydraulic retention time
IUPAC	International Union of Pure and Applied Chemistry
LC	Liquid chromatography
LI	Light irradiance
LPR	Lipid production rates
MEC	Microbial electrolysis cell
MFC	Microbial fuel cell
MGDG	Monogalactosyl diacylglycerol
MS	Mass spectrometry
MTBE	Methyl *tert*-butyl ether
MW	Microwave
nFPR	Net free-fatty-acid production rate
NO_x	Nitrogen oxides
OD	Optical density
OM	Outer membrane
PAR	Photosynthetically active radiation
PBR	Photobioreactor

PCC6803	*Synechocystis* PCC6803
PD	Peptidoglycan layer
PEF	Pulsed electric field
Pg	Phosphoglycerol
PHB	Poly-3-hydroxybutyrate
PG	Phosphatidyl diacylglycerol
PM	Plasma membrane
PS II	Photosystem II
R_i	Alkyl group
SCOD	Soluble chemical oxygen demand
Sq	Sulfoquinovose
SQDG	Sulfoquinovosyl diacylglycerol
SS	Suspended solid
ST-PBR	Single-tube roof-top photobioreactor
T	Thylakoid membranes
TAG	Triacylglycerols
TC	Total carbon
TE	Thioesterase
TEM	Transmission electron microscopy
TES	N-tris(hydroxymethyl)methyl-2- aminoethanesulfonic acid
TI	Treatment intensity
TLC	Thin layer chromatography
TOC	Total organic carbon

T-RFLP	Terminal restriction fragment length polymorphism
US	Ultrasound
VIPP-1	Vesicle-inducing protein in plastids 1
VSS	Volatile suspended solids

1 Introduction

1.1 World energy and biofuel

Energy is fundamental to human civilization. Modern human society is now consuming more than 16 terawatts (1 TW = 10^{12} W = 3.2 EJ/year = 3.03 quadrillion Btu/year) of energy worldwide (Brown et al., 2011; International Energy Agency, 2010). As reported by the U.S. Energy Information Administration in Figure 1.1 and Figure 1.2, fossil fuels, including petroleum oil, coal, and natural gas, play a pivot role, comprising more than 80% of the world total and U.S. energy supplies. However, as shown in Figure 1.3, the International Energy Agency (2010) projects that world crude-oil production will stay flat, because the decline of currently producing fields will barely be offset by the increase of output from newly developed fields.

The overwhelming addiction of human society to fossil fuels, coupled with the shrinkage of natural reserves, will spark global competition and conflict over scarce resources. Furthermore, ever since the initiation of the Industrial Revolution in the early 1800s, combustion of fossil fuels has released massive amount of CO_2 into the atmosphere, which already has lifted atmosphere CO_2 concentration from 280 ppm prior to the Industrial Revolution to a then-record high of 380 ppm in 2005 (IPCC, 2007). The accelerating influx of new CO_2 into the atmosphere is the key reason of the well-documented global warming. Unless this trend is stopped, severe climate change is expected and may threaten the existence of human society as we know it today.

In order to overcome the depletion of fossil fuels, meet the ever-growing energy demand, and relieve global warming, human society must make it a priority to develop renewable and carbon-neutral energy sources. Renewable and carbon-neutral energy can be defined, respectively, as energy that is produced from naturally replenished resources and does not generate net influx of CO_2 to atmosphere. In order to overcome the above-noted challenges, renewable and carbon-neutral substitutes for fossil fuels must be implemented on a comparable scale as fossil fuels (> 10 TW, 1 TW = 3.03 quadrillion Btu/year). Among all candidates, biofuel derived from biomass and biological activities is promising for its renewability, carbon neutrality, and scalability (Rittmann, 2008).

The production and utilization of biofuel can be traced back to the ancient ages, as people produced methane and alcohols by fermentation of biomass. Before the rise of cheap gasoline, bioethanol and vegetable oil were widely used as engine fuels, including Nikolaus August Otto's spark ignition engine in 1860s, Rudolf Diesel's diesel engine in 1890s, and Henry Ford's Model T in 1930s (Antoni et al., 2007; Kovarik, 1998). Recently, biofuels have gained renewed attention. Nowadays, biofuels of various types constitute about 10% of the world's primary energy supply (Antoni et al., 2007; International Energy Agency, 2010).

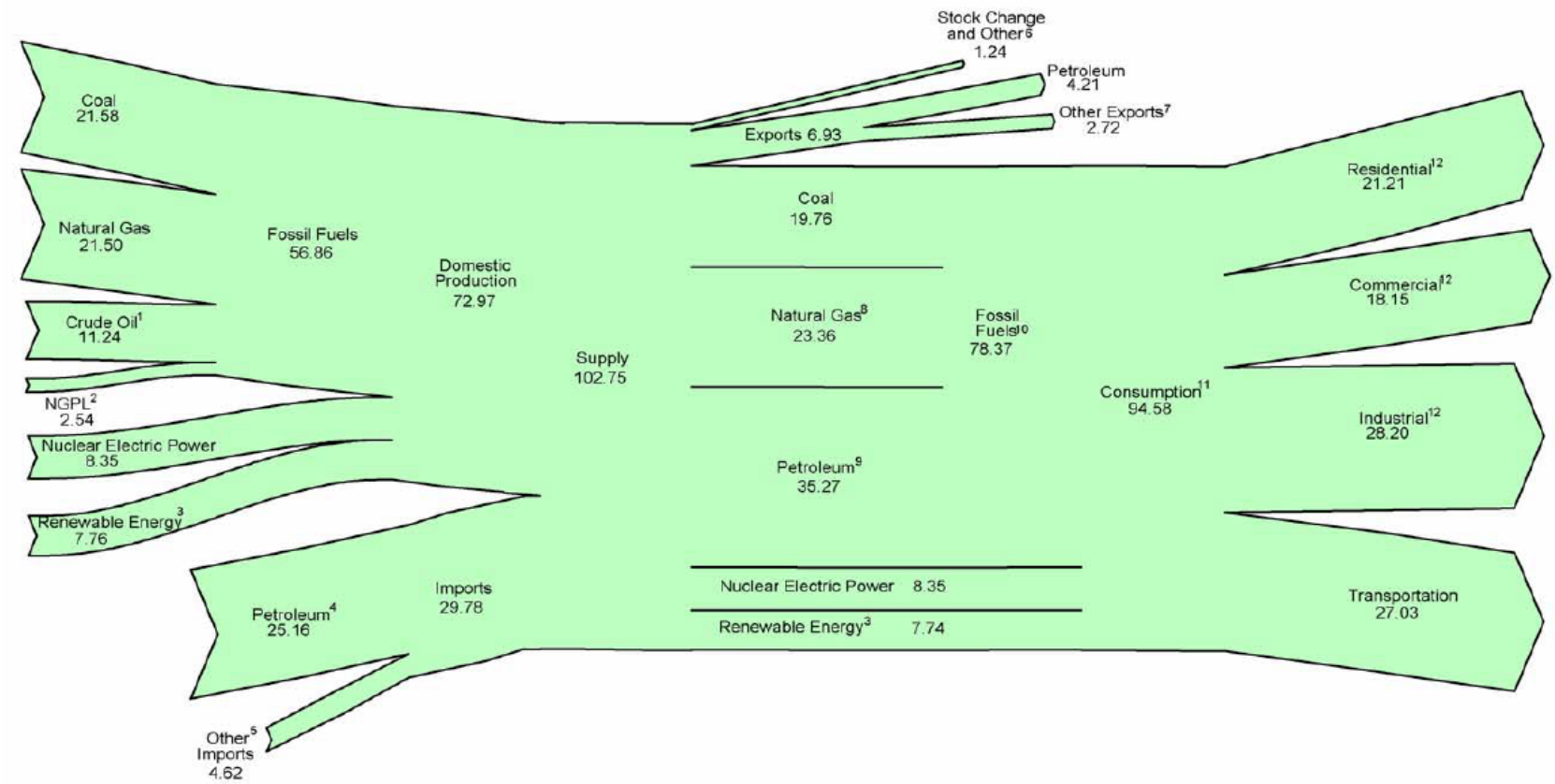

Figure 1.1. Energy flow in the United States, 2009.

The unit is quadrillion Btu (1 quadrillion Btu = 10^{15} Btu = 1.055 EJ = 0.33 TW·year) (U.S. Energy Information Administration, 2010a).

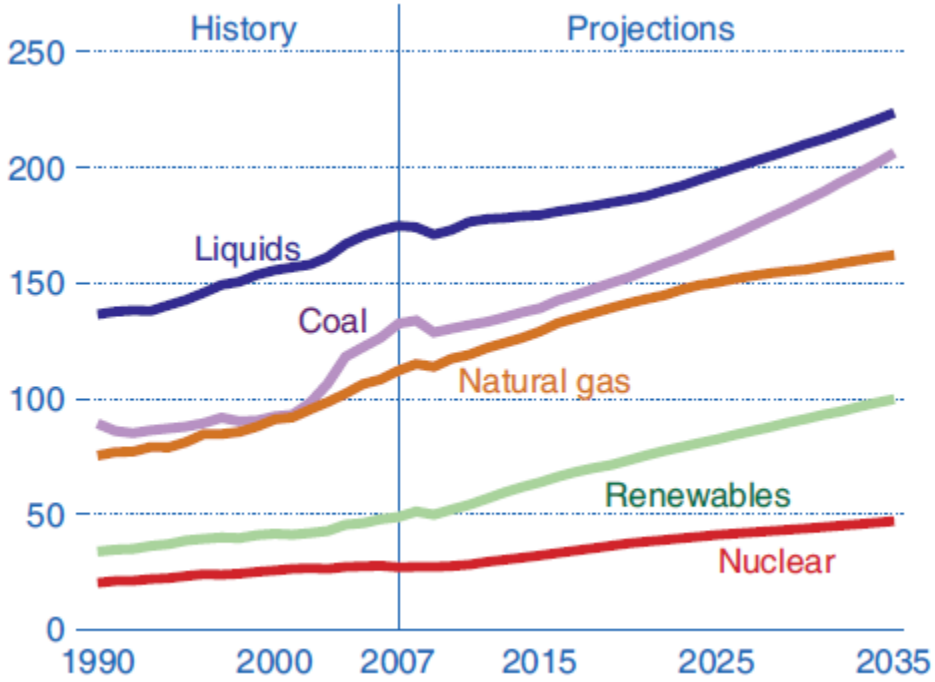

Figure 1.2. World-market energy use by fuel type (1990-2035).

The unit is quadrillion Btu = 0.33 TW·year (U.S. Energy Information Administration, 2010b).

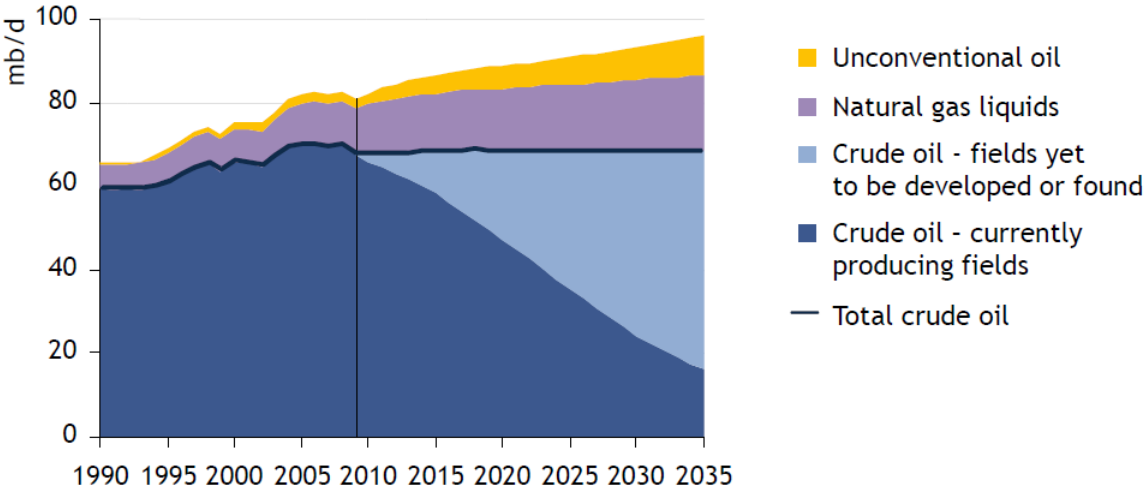

Figure 1.3. World oil production by type.

Crude oil production is projected to plateau between now to 2035 (International Energy Agency, 2010).

Major biofuel products include biomethanol, bioethanol, biobutanol, biomethane, biohydrogen, and biodiesel. Among them, only bioethanol and biodiesel are presently produced at industrial scale, and they comprise about 90% of the biofuel market (Mata et al., 2010). A biofuel can be blended with other fuels, or it can be used in a pure form.

Biodiesel is a promising substitute for petroleum diesel and has already been produced in industrial scale in the U.S., European Union, and other countries. It is defined as a fuel comprised of monoalkyl esters of long-chain fatty acids (such as fatty acid methyl ester, FAME) that can be produced by a transesterification reaction from triacylglycerol (TAG) or diacylglycerol (DAG) lipids (Knothe et al., 2005). Compared with petroleum diesel, which is a long-chain hydrocarbon mixture ($C_{10}H_{20}$ to $C_{15}H_{28}$ with average chemical formula $C_{12}H_{23}$), biodiesel has similar chemical properties and energy density so that it can be used in existing diesel engine with only minor engine changes (Van Gerpen et al., 2004). Biodiesel has been used successfully in a blend of up to 20% with petroleum diesel (B20), and application of pure biodiesel (B100) is being tested (Pinto et al., 2005).

Feedstock for biodiesel production is derived from lipids that come from highly concentrated sources, such as vegetable oils or animal fats. The lipids from these sources are extracted and then converted to biodiesel via an acid- or base-catalyzed transesterification reaction, as shown in Figure 1.4 (Li et al., 2008). The typical reaction condition at industrial scale is: 6:1 (v:v) of methanol: triglyceride, 1% NaOH or 0.5% $NaOCH_3$, and 60^{o}C under 1 atm pressure. Nearly 80% yield

can be achieved within 1 h, with more than 90% possible after 3 – 4 h (Knothe et al., 2005).

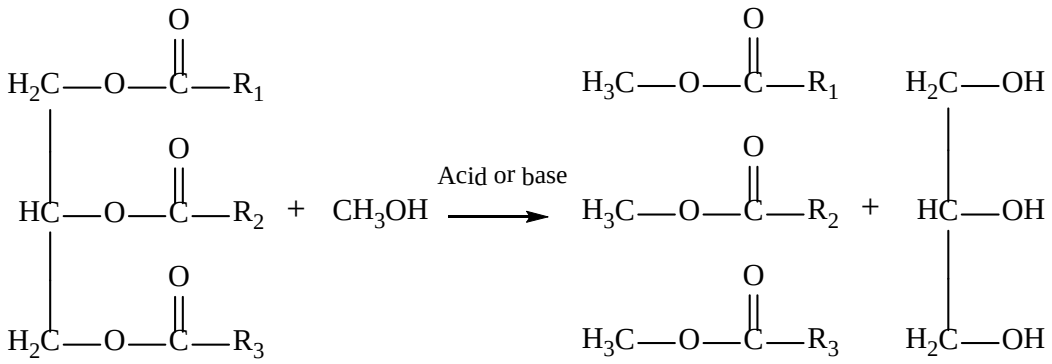

Figure 1.4. The transesterification reaction. R, alkyl group.

1.2 Biofuel from microalgae and cyanobacteria

Traditional feedstock for biofuel includes vegetable and animal tissue. In the case of biodiesel, although vegetable and animal wastes can be used as feedstock (Zhang et al., 2003), the supply of wastes cannot meet the demand for feedstock. In addition, the low quality of concentrated waste oils can be troublesome for the production process: e.g., a high content of free fatty acids that forms soap and brings about emulsification (Wang et al., 2010). As a result, massive growth of oil-rich vegetables would be required to make enough high-quality feedstock for biodiesel to meet demands, and this would bring about even more severe problems similar as those of bioethanol: diverting food crops, competing arable land and irrigation water, and increasing water pollution (Pimentel et al., 2008; U.S. National Research Council, 2008). For example, corn-

to-ethanol already is implicated as a threat to the food supply of human society and as a reason for surges in food prices (van der Horst and Vermeylen, 2011).

In contrast, phototrophic microorganisms, i.e., microalgae and cyanobacteria, have several advantages that make them more suitable for large-scale production of feedstock for biofuel: (1) They have a much higher photosynthetic efficiency and faster growth rate; thus, they have a much higher areal biomass and lipid production rates than plants (Dismukes et al., 2008; Zhu et al., 2008). (2) They can grow and be harvested all year around, providing a continuous and stable supply of feedstock (Schenk et al., 2008). (3) They can grow in non-arable land, such as desert, and with recycling of water and nutrients, which minimizes the competition with the food supply for human society or contamination of water resources (Chisti, 2007; Hu et al., 2008; Karaosmanoglu, 1999; Kim et al., 2010). (4) The microbial biomass is relatively simple (e.g., no lignocellulose), which avoids the technical complexities and economic burdens associated with the processing of lignocellulose plant tissue.

The concept of producing renewable and carbon-neutral biofuel by photosynthetic microorganisms is illustrated in Figure 1.5. Through photosynthesis, eukaryotic microalgae and prokaryotic cyanobacteria capture energy from sunlight and fix CO_2 from atmosphere or a combustion source. Direct products such as lipids and fatty acids can be converted to nonpetroleum-based diesel such as biodiesel and renewable diesel. The rest of the biomass can be further converted by anaerobic microorganisms to other valuable energy outputs, such as methane, hydrogen, and electricity by fermentation, the microbial

electrolysis cell (MEC), and the microbial fuel cell (MFC), respectively (Quintana et al., 2011; Rittmann et al., 2008a). The decomposition of photosynthetic biomass also releases useful nutrients, particularly N and P, which can be recovered and recycled. After the consumption of biofuel, the same amount CO_2 that was fixed by photosynthetic microorganisms is released back to the environment, completing the closed-loop, carbon-neutral CO_2 cycle.

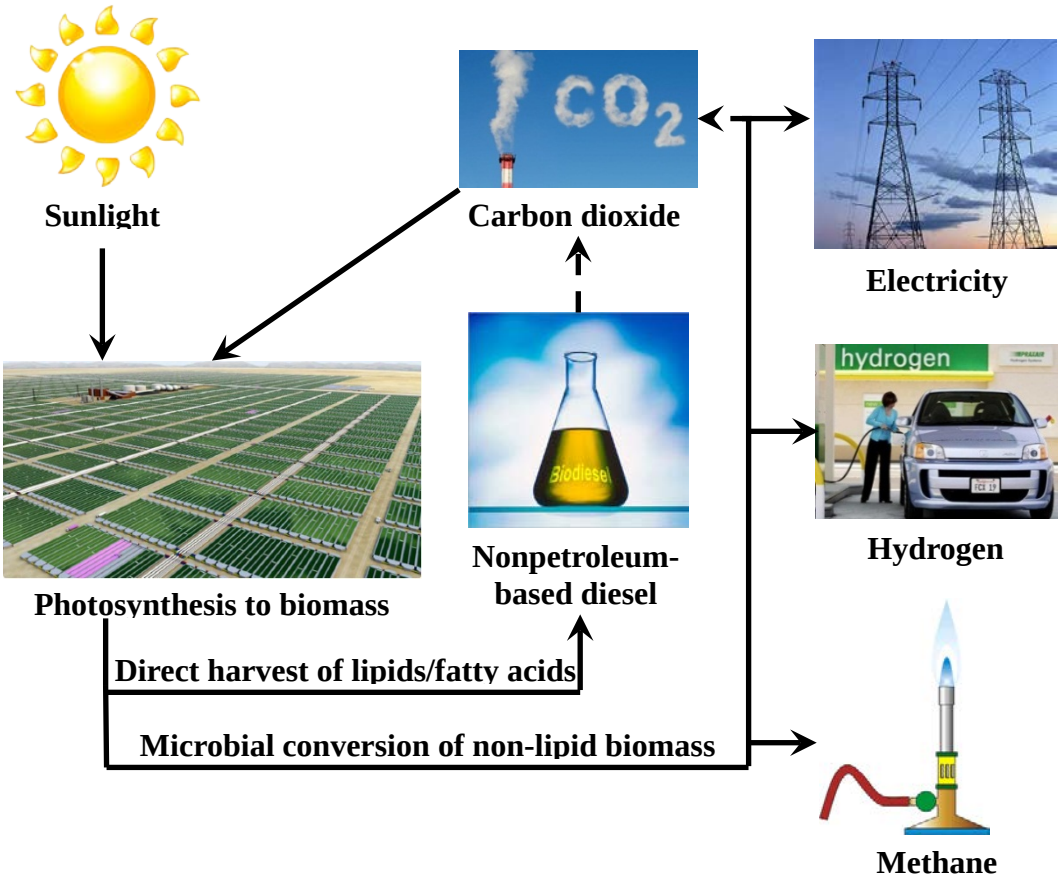

Figure 1.5. Renewable and carbon-neutral cycle of bioenergy based on photosynthetic microorganisms.

Photosynthetic microorganisms capture sunlight energy and fix CO_2 to produce biomass that can be harvested and converted to several useful energy forms. The released CO_2 equals to the captured CO_2 in photosynthesis, making the process carbon neutral.

Although algae and cyanobacteria can be used to generate raw materials for biofuel production, cyanobacteria have certain advantages over algae. First, lipid accumulation in oleaginous algae is mostly achieved by either imposing stress (i.e., adverse environmental conditions such as nutrient deficiency) or adding sugar (Huang et al., 2010; Li et al., 2007; Miao and Wu, 2006). In contrast, enrichment of lipids in cyanobacteria can be accomplished by over-expressing thylakoid membranes, which are positively correlated with photosynthetic rate and biomass production rate (Liberton et al., 2006; Mullineaux, 1999); thus, the highest density of lipids in cyanobacteria biomass occurs together with the highest biomass-production rate. Second, cyanobacteria are much more amenable to metabolic engineering to improve lipid content beyond that of the wild type (Kaneko et al., 1996; Liu et al., 2011a). For example, the entire genome sequence of cyanobacterium *Synechocystis* PCC 6803 is published, yielding precise information for gene modifications for a variety of metabolic pathways to optimize quality and quantity of lipids for nonpetroleum-based diesel production (Aseeva et al., 2004; Nakamura et al., 1998; Vermaas, 1996; Westphal et al., 2001). Other genetic modifications, such as production and excretion of free fatty acids (FFA) (Kaczmarzyk and Fulda, 2010; Liu et al., 2011b), FAME (Steen et al., 2010), and alkane (Schirmer et al., 2010) as valuable energy forms, also have been reported.

1.3 Phototroph stoichiometry of *Synechocystis*

In order to estimate the theoretical biomass and biofuel productivity from *Synechocystis*, I built a model of phototroph stoichiometry of *Synechocystis*. This work is founded on the energetics and stoichiometry approach in Chapter 2 of Rittmann and McCarty (2001), but has special modifications needed for phototrophy, which was not addressed in the past by the method. Important adaptations include making the chemical formula for *Synechocystis* biomass variable depending in its lipid content, identifying an internal electron donor that is produced when photosynthesis oxidizes H_2O to generate O_2 and high energy electrons, and developing the proper analogy between the synthesis of photoautotrophs to the synthesis of heterotrophs and chemoautotrophs.

1.3.1 Molecular composition of *Synechocystis* PCC 6803

First, I assumed a chemical formula for wild-type *Synechocystis* PCC 6803 of $C_{4.6}H_{7.5}O_{1.9}NP_{0.053}$ to calculate the electron distribution between fatty acids and non-fatty acids (Kim et al., 2011; Shastri and Morgan, 2005). Table 1.1 presents a typical fatty-acid profile of lipids from *Synechocystis* PCC 6803 (Sheng et al., 2011d). I express lipids as FAME so that I can focus on the desired final product from fatty-acid chains and eliminate non-convertible group such as sulfoquinovose and phosphoglycerol in *Synechocystis* DAG. The profile in Table 1.1 gives the formula for a typical composite FAME molecule derived from *Synechocystis* PCC 6803, shown at the bottom of Table 1.1: $C_{15.7}H_{30.9}COOCH_3$.

I then calculated the general formula of non-FAME compounds by subtracting FAME from total biomass based on mass balance. For wild-type *Synechocystis* PCC 6803, FAME typically constitutes 5% of the total biomass (w/w) (Sheng et al., 2011d). As shown in Table 1.2, the general formula of non-FAME compounds is $C_{4.25}H_{6.84}O_{1.86}NP_{0.053}$.

Table 1.1. Typical fatty acid profile of wild-type *Synechocystis* PCC 6803 (as FAME) and the composite formula

FAME	**Formula**	**Percentage (wt. %)**
C16:0*	$C_{15}H_{31}COOCH_3$	60%
C16:1	$C_{15}H_{29}COOCH_3$	5%
C18:0	$C_{17}H_{35}COOCH_3$	5%
C18:1	$C_{17}H_{33}COOCH_3$	5%
C18:2	$C_{17}H_{31}COOCH_3$	10%
C18:3	$C_{17}H_{29}COOCH_3$	15%
Composite FAME	$C_{15.7}H_{30.9}COOCH_3$	100%

* CX:Y denotes the compound that has a fatty acid chain of X carbons and Y double bonds (e.g. C16:0 — palmitic acid methyl ester or $C_{15}H_{31}COOCH_3$).

Table 1.2. Calculation of general chemical composition of non-FAME compounds in *Synechocystis* PCC 6803

Element	Atomic Weight	Biomass*	FAME**	Non-FAME***	Non-FAME (Normalized to N)
C	12	4.6	17.7	= 1 / 108.74 × 4.6 - 0.05 / 278.3 × 17.7 = 0.039	4.25
H	1	7.5	33.9	= 1 / 108.74 × 7.5 - 0.05 / 278.3 × 33.9 = 0.063	6.84
O	16	1.9	2	= 1 / 108.74 × 1.9 - 0.05 / 278.3 × 2 = 0.017	1.86
N	14	1	0	= 1 / 108.74 × 1 - 0.05 / 278.3 × 0 = 0.0092	1
P	31	0.053	0	= 1 / 108.74 × 0.053 - 0.05 / 278.3 × 0 = 0.00049	0.053
MW (g/mol)		108.74	278.3		103.3
e^- eq		19.36	100.7		17.4
e^- eq/g		0.18	0.36		0.17

* Assuming that wild-type *Synechocystis* PCC 6803 has a formula as $C_{4.6}H_{7.5}O_{1.9}NP_{0.053}$ and contains 5% (wt.) lipids (as FAME)

** The lipid profile of *Synechocystis* PCC 6803 can be represented by a composite FAME formula $C_{15.7}H_{30.9}COOCH_3$, from Table 1.1

*** The formula of non-FAME compounds is calculated by subtracting FAME from total biomass based on mass balance.

Table 1.2 also shows the electron density of FAME (e^- eq/g) and non-FAME biomass. The average oxidation state of C in FAME is -1.69, while it is -0.091 for non-FAME. Thus, the electron density in FAME is:

$$[4-(-1.69)]\times 17.7 = 100.7 \text{ e}^- \text{ eq/mol FAME} \quad (1.1)$$

or

$$\frac{100.7 \text{ e}^- \text{ eq/mol FAME}}{278.3 \text{ g FAME/mol FAME}} = 0.36 \text{ e}^- \text{ eq/g FAME} \quad (1.2)$$

In contrast, the electron density of non-FAME is 17.4 e^- eq/mol non-FAME, or 0.17 e^- eq/g, which is significantly lower than FAME.

Table 1.3 shows the molar coefficients of *Synechocystis* biomass calculated from the combination of FAME (Table 1.1) and non-FAME (Table 1.2) formulae as lipids become a larger percentage of the total biomass of *Synechocystis*. This calculation assumes that the composition of non-FAME compounds will not change after genetic modification to give a higher FAME content. Increasing the fatty acid content causes the relative amounts of H and C to increase much more than O, and the oxidation state of C becomes more negative. Table 1.3 also shows the electron density of the total biomass (e^- eq/g) and the electron distribution of FAME (e^- eq/total e^-) and of non-FAME biomass (e^- eq/total e^-) calculated from equations similar as (1.1) and (1.2). Because FAME has a higher electron density than non-FAME (Table 1.2), the increase of FAME content from 5% to 32% (corresponding to an increase in lipid content from 7% to 46% according to Sheng et al. (2011d) makes the electron density of the biomass increase steadily from 0.18 e^- eq/g to 0.23 e^- eq/g. Consequently, the

electron fraction in FAME also increases as the fatty acid content goes up. When FAME makes up 5% of the total biomass (corresponding to 7% lipid content), only 10.2% of total electrons is located in FAME, but this number increases to 50.3% when the FAME content goes up to 32% of total biomass (corresponding to 46% lipid content). Thus, increasing the FAME content by enriching the biomass in lipids directs more energy to the feedstock for nonpetroleum-based diesel such as biodiesel.

Table 1.3. Chemical composition of biomass (normalized to N) with different lipid contents (as FAME, wt. %)

FAME %	**5%**	**8%**	**11%**	**14%**	**17%**	**20%**	**23%**	**26%**	**29%**	**32%**
					*Molar coefficients**					
C	4.60	4.83	5.07	5.32	5.60	5.90	6.22	6.56	6.94	7.35
H	7.50	7.93	8.39	8.89	9.41	9.98	10.60	11.26	11.98	12.76
O	1.90	1.93	1.95	1.98	2.01	2.05	2.08	2.12	2.16	2.21
N	1.00	1.00	1.00	1.00	1.00	1.00	1.00	1.00	1.00	1.00
P	0.05	0.05	0.05	0.05	0.05	0.05	0.05	0.05	0.05	0.05
Total e^- eq/g**	0.18	0.18	0.19	0.20	0.20	0.21	0.21	0.22	0.22	0.23
FAME (% e^-/total e^-)	10.2	15.7	21.0	25.9	30.6	34.9	39.1	43.0	46.7	50.3
Non-FAME (% e^-/total e^-)	89.8	84.3	79.0	74.1	69.4	65.1	60.9	57.0	53.3	49.7

* Calculated from the combination of FAME (Table 1.1) and non-FAME (Table 1.2) formulae

** Calculated from equations similar as (1.1) and (1.2).

1.3.2 Stoichiometry calculation of energy flow and synthesis reaction

Figure 1.6 summarizes a simplified set of electron-transfer and energetics reactions in *Synechocystis* carrying out oxygenic photosynthesis. Light-photon energy is captured by photosystems I and II (PS I and PS II). Water is split, O_2 is generated, and electrons enter into the system via PS II. The typical non-cyclic photophosphorylation (the Z scheme) uses PS II and PS I sequentially, produces ATP in PS II, and produces NADPH in PS I. Cyclic electron flow from PS I to PS II also happens significantly in *Synechocystis*, and it only produces ATP (Vermaas, 2001).

For applying the energetics and stoichiometry model of Rittmann and McCarty (2001), I make three reasonable assumptions to make the model consistent with photosynthesis: (1) no respiration during light and dark times; (2) the energy and electrons used to fix CO_2 in the Calvin cycle are from ATP and NADPH produced by non-cyclic photophosphorylation; and (3) the energy and electrons required after the Calvin cycle come from ATP and NADPH produced by cyclic and non-cyclic photophosphorylation.

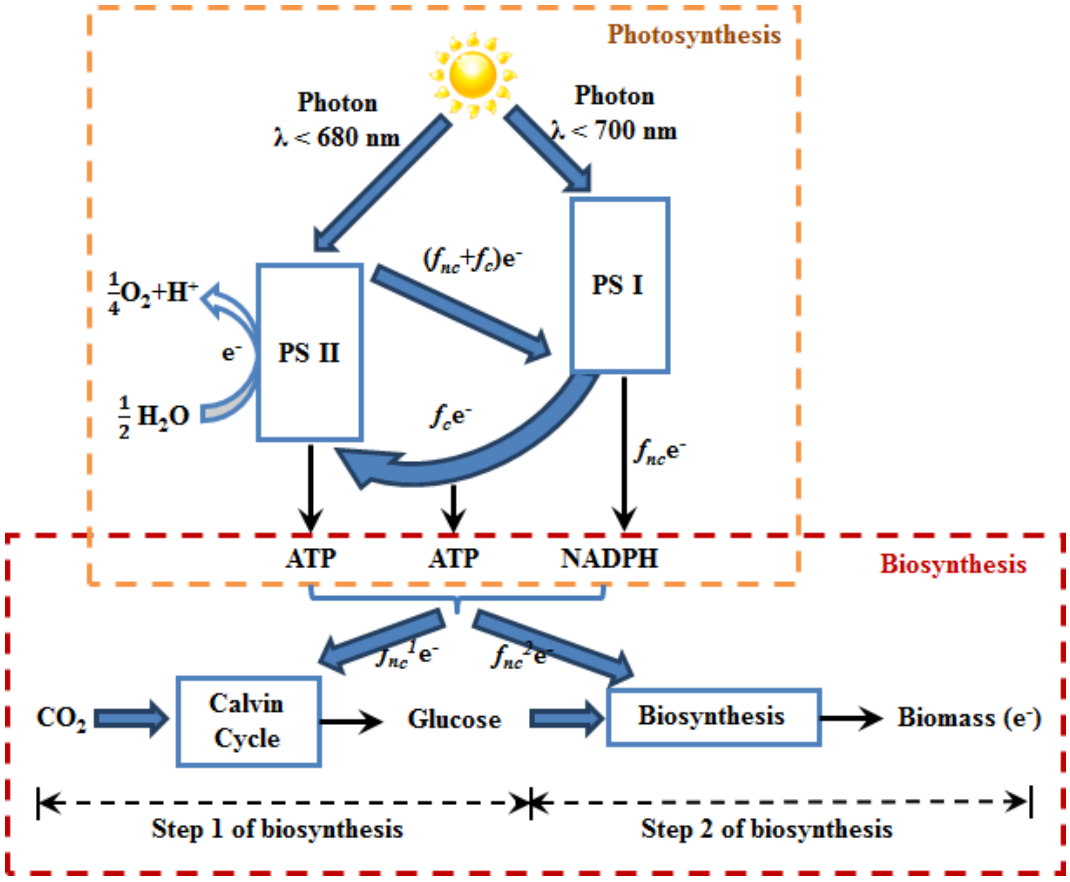

Figure 1.6. The energy flows and electron transfers in photosynthesis and biosynthesis of *Synechocystis*.

f_c: the electron fraction to cyclical photophosphorylation; f_{nc}: the electron fraction to non-cyclical photophosphorylation that passes to NADPH; f_{nc}^1: the electron fraction to step 1 of biosynthesis; f_{nc}^2: the electron fraction to step 2 of biosynthesis.

The immediate product of the Calvin cycle is glyceraldehyde-3-phosphate, but it is readily converted to glucose. Therefore, I use glucose to separate the biomass-synthesis reaction (R_c) into two steps, as shown in equations (1.3) and (1.4) (Rippka et al., 1979; Rittmann and McCarty, 2001):

Step 1 (R_c^1): $CO_2 \rightarrow$glucose through the Calvin cycle:

$$\frac{1}{4}CO_2 + \frac{3}{4}ATP + \frac{1}{2}NADPH + \frac{1}{2}H^+ + e^- \rightarrow \frac{1}{24}C_6H_{12}O_6 + \frac{3}{4}ADP + \frac{1}{2}NADP^+ + \frac{3}{4}P_i + \frac{1}{4}H_2O \quad (1.3)$$

Step 2 (R_c^2): glucose$\rightarrow$biomass, NO_3^- is the N source:

$$\left(\frac{n}{6h}\right)C_6H_{12}O_6 + \left(\frac{c}{h}\right)NO_3^- + \left(\frac{d}{h}\right)HPO_4^{2-} + \left(\frac{a-2b+6c+7d}{h}\right)H^+ + e^- \rightarrow \left(\frac{1}{h}\right)C_nH_aO_bN_cP_d + \left(\frac{n-b+3c+4d}{h}\right)H_2O \quad (1.4)$$

where $h = a - 2b + 5c + 5d$; a, b, c, d, and n are from Table 1.3. NO_3^- is the N source here, and the coefficients change when NO_2^- or NH_4^+ were the N source. The electrons are provided by NADPH.

Step 2 is conversion of glucose to biomass, and it is the same as occurs for heterotrophs and chemoautotrophs. To integrate photosynthesis with the method of Rittmann and McCarty (2001), I separate step 2 into two parts. The first part involves conversion into the representative carbon-containing intermediate used by Rittmann and McCarty (2001), i.e., pyruvate ($\Delta G^{o'}$ = 35.09 kJ/ e^- eq). The free energy of glucose is $\Delta G_c^{o'}$ = 41.35 kJ/ e^- eq (McCarty, 2007). Thus, conversion of glucose to pyruvate (ΔG_p) yields a small amount of energy:

$$\Delta G_p = 35.09 - \Delta G_c^{o'} = 35.09 - 41.35 = -6.26 \text{ kJ/e}^- \text{ eq} \quad (1.5)$$

The second part involves the conversion of pyruvate to cellular carbon. The energy requirement for this step (ΔG_{pc}) is 3.33kJ/g cells × X g cells/e^- eq, and the values of X g cells/e^- eq are shown in Table 1.3 (e.g., in "Total e^- eq/g").

The energy for step 2 of biosynthesis (ΔG_s^2) is then:

$$\Delta G_s^2 = \frac{\Delta G_p}{\varepsilon_s^n} + \frac{\Delta G_{pc}}{\varepsilon_s} = \frac{\Delta G_p}{\varepsilon_s^{-1}} + \frac{\Delta G_{pc}}{\varepsilon_s} \quad (1.6)$$

where ε_s is the energy-transfer efficiency for biosynthesis, which I set to 0.6, similar to the efficiency typically used for heterotrophs in Rittmann and McCarty (2001); for $\Delta G_p < 0$, $n = -1$.

The energetic reactions must supply the energy and electron requirements of biosynthesis. In *Synechocystis*, all energy for synthesis can be assumed to be in the form of ATP from cyclical and non-cyclical photophosphorylation, and the required electrons are from NADPH produced by non-cyclical photophosphorylation. Figure 1.6 shows how the electron flow is fractionated. For every e^- eq transferred from H_2O to biomass, the fractions of electron flows to different pathways have following relationship:

$$f_{nc} = f_{nc}^1 + f_{nc}^2 = 24 \times \frac{n}{6h} f_{nc}^2 + f_{nc}^2 = 1 \quad (1.7)$$

$$f_{nc}^2 = \frac{1}{(1 + 24 \times \frac{n}{6h})} \quad (1.8)$$

where f_{nc} is the electron fraction to non-cyclical photophosphorylation that passes to NADPH, f_{nc}^1 is the electron fraction to step 1 of biosynthesis, and f_{nc}^2 is the

electron fraction to step 2 of biosynthesis. The relationship between f_{nc}^{1} and f_{nc}^{2} (i.e., $f_{nc}^{1} = 24 \times \frac{n}{6h} \times f_{nc}^{2}$) is based on the stoichiometry from equations (1.3) and (1.4) with n and h from equation (1.4).

The relationships of electron flows with ATP and NADPH generation are:

Cyclical photophosphorylation: 1 e^- eq is transferred to produce 1 mol ATP, no net NADPH is produced

Non-cyclical photophosphorylation: 1 e^- eq is transferred to produce ¾ mol ATP and ½ mol NADPH

I assume that all energy and electrons for step 1 of biosynthesis (f_{nc}^{1}) are from non-cyclical photophosphorylation, as ¾ mol ATP and ½ mol NADPH are produced and used to transfer 1 e^- eq to 1/24 mol glucose (equation (1.3)). Thus, the energy and electron balance are fixed in step 1.

The energy and electron requirements of step 2 of biosynthesis are provided, respectively, by ATP from cyclical and non-cyclical photophosphorylation and by NADPH from non-cyclical photophosphorylation. ATP provides –32 kJ/mol of energy:

$$\text{ATP} \rightarrow \text{ADP}+\text{P}_\text{i} \ (\Delta G_r = -32 \text{ kJ/mol ATP}) \qquad (1.9)$$

Equation (1.10) balances the energy and electron requirements of step 2 of biosynthesis:

$$\varepsilon_r f_c \Delta G_r + \varepsilon_r f_{nc}^2 (\frac{3}{4} \times \Delta G_r) = -f_{nc}^2 \Delta G_s^2 = -f_{nc}^2 (\frac{\Delta G_p}{\varepsilon_s^{-1}} + \frac{\Delta G_{pc}}{\varepsilon_s}) \qquad (1.10)$$

where f_c is the electron fraction to cyclical photophosphorylation; ε_r is the energy-transfer efficiency for energy reaction from NADPH and ATP, which I set to 0.9.

The left part of the equation represents ATP from cyclical and non-cyclical photophosphorylation.

The yields of biomass ($Y_{Biomass}$) and FAME (Y_{FAME}) are:

$$Y_{Biomass}(\text{g VSS/e}^{-}\ \text{eq}) = f_{nc}^{2}\frac{1}{h}(\text{mol VSS/ e}^{-}\ \text{eq}) \times MW(\text{g VSS/mol VSS}) \quad (1.11)$$

and

$$Y_{FAME}(\text{g FAME/e}^{-}\ \text{eq}) = Y_{Biomass}(\text{g VSS/e}^{-}\ \text{eq}) \times \text{FAME \%} \quad (1.12)$$

where h is from equation (1.4)

Table 1.4 shows the stoichiometric calculations for *Synechocystis* with different lipid content: stoichiometric constants are calculated from equations (1.3) and (1.4), f_{nc}^{1} and f_{nc}^{2} from equations (1.7) and (1.8), f_c from equation (1.10), and Y values from equations (1.11) and (1.12).

Table 1.4. Stoichiometric calculations for the biomass-synthesis reaction (R_c), electron fractions between non-cyclical photophosphorylation and cyclical photophosphorylation, and yields of biomass and FAME using NO_3^- as the N source

FAME %	**5%**	**8%**	**11%**	**14%**	**17%**	**20%**	**23%**	**26%**	**29%**	**32%**
					*Stoichiometric constants**					
CO_2	0.513	0.516	0.519	0.523	0.526	0.529	0.532	0.534	0.537	0.540
NO_3^-	0.112	0.107	0.103	0.098	0.094	0.090	0.086	0.081	0.077	0.074
HPO_4^-	0.006	0.006	0.005	0.005	0.005	0.005	0.005	0.004	0.004	0.004
Biomass	0.112	0.107	0.103	0.098	0.094	0.090	0.086	0.081	0.077	0.074
f_{nc}^{2}**	0.33	0.33	0.32	0.32	0.32	0.32	0.32	0.32	0.32	0.32
f_{nc}^{1}	0.67	0.67	0.68	0.68	0.68	0.68	0.68	0.68	0.68	0.68
f_c***	0.84	0.82	0.81	0.80	0.78	0.77	0.76	0.75	0.73	0.72
$Y_{Biomass}$**** (g VSS/e^- eq)	3.97	3.92	3.87	3.82	3.77	3.72	3.67	3.62	3.58	3.53
Y_{FAME} (g FAME/e^- eq)	0.20	0.31	0.43	0.53	0.64	0.74	0.84	0.94	1.04	1.13

* Stoichiometric constants are calculated from equations (1.3) and (1.4)

** f_{nc}^{1} and f_{nc}^{2} are calculated from equations (1.7) and (1.8)

**** f_c is calculated from equation (1.10)

**** Y values are calculated from equations (1.11) and (1.12).

Based on energetics, most electrons are used for non-cyclical photophosphorylation ($f_{nc} > f_c$) in all cases. The fraction of electrons to non-cyclical photophosphorylation increases (f_c decreases) as the FAME% increases, because more reducing power is need in step 2 of biosynthesis. The biomass yield ($Y_{Biomass}$ in g VSS/mol photon) decreases as the FAME content increases, and this is caused by the increase of electron density of the biomass. However, this slight decrease does not prevent the important trend that the FAME yield (Y_{FAME} in g FAME/mol photon) increases as the fatty acid content increases. Since the yield of FAME is almost proportional to the fatty acid content, a genetic mutation with the purpose of increasing intracellular lipid significantly enhances the output of feedstock for nonpetroleum-based diesel such as biodiesel.

1.3.3 Conversion of light energy into biomass and biodiesel

In collaboration with Chao Zhou, I input sunlight energy into the model to calculate biomass and biodiesel (assuming main component is FAME) productivity. Sunlight data from a typical year of Phoenix, AZ are derived from National Renewable Energy Laboratory (NREL, http://rredc.nrel.gov/solar/old_data/nsrdb/1961-1990/tmy2/). Typical daily solar energy for spring, summer, fall, and winter are 12,500 kJ/m^2/d, 42,400 kJ/m^2/d, 32,800 kJ/m^2/d and 7,460 kJ/m^2/d, respectively. *Synechocystis* can absorb light ranging from 400-700 nm, which accounts for about 46% of total energy of solar irradiance.

There are two major units to present light irradiance: radiance (e.g., W/m^2) and photosynthetically active radiation (PAR; e.g., $\mu mol/m^2/s$). Radiance is widely used in solar engineering, usually converted directly from the total energy from sun light (or a range of light by multiplying energy fraction). PAR, on the other hand, focuses only on light with wavelength 400-700 nm, which can be used by the photosystems. It also considers the quantum flux of light, which is directly relevant to the photochemical basis of the photosystems. Although radiance is more recognized by the general public, PAR is more useful in theoretically calculation of light modeling.

It has been reported that 1 W/m^2 radiation in 400-700 nm equals to about 4.6 $\mu mol/m^2/s$ PAR (McCree, 1981); therefore, the average energy of photosynthetically active photon is 1/4.6 × 1,000 = 211 kJ/mol photon. The loss of photons by reflection is about 10% (Zhu et al., 2008). Thus, the calculation of total usable photons from solar irradiance is:

$$N_{photon}(\text{mol photon}) = \frac{\text{Solar Irradiance } (\text{kJ/m}^2/\text{d}) \times 46\%}{211 \text{ kJ/mol photon}} \times 0.9 \qquad (1.13)$$

For non-cyclical photophosphorylation, 1 mol photon is absorbed in PS II and another 1 mol in PS I to transfer 1 e^- eq. For cyclical photophosphorylation, 1 mol photon is absorbed in PS I to transfer 1 e^- eq during the cycling. We can then estimate the areal biomass and FAME production rates from the relationship of photons and electrons and $Y_{Biomass}$ and Y_{FAME} from Table 1.4.

$$\text{Areal Biomass Yield}(\text{gVSS/m}^2\text{/d}) = \frac{Y_{Biomass}(\text{gVSS/e}^-\ \text{eq}) \times N_{photon}(\text{mol photon/m}^2\text{/d})}{(1+ f_{nc} + f_c)(\text{mol photon/e}^-\ \text{eq})} \quad (1.14)$$

$$\text{Areal Biodiesel Yield}(\text{g/m}^2\text{/d}) = \text{Areal Biomass Yield}(\text{gVSS/m}^2\text{/d}) \times \text{FAME \%}(\text{gFAME/gVSS}) \quad (1.15)$$

The calculation results for areal biomass and biodiesel yields are shown in Figure 1.7. The model estimates that, by growing *Synechocystis* with FAME content from 5% to 32%, using NO_3^- as N source, and under Phoenix, AZ sunlight condition, the annual areal biomass yield can reach 2.1×10^5 to 2.4×10^5 kg/ha/yr, which is close to the estimations from other reports (Dismukes et al., 2008; Kebede and Ahlgren, 1996; Zittelli et al., 1996). The corresponding areal biodiesel yield (assuming a density 0.9 kg/L) can reach 1.3×10^4 to 7.9×10^4 L/ha/yr. Thus, a genetic mutation with the purpose of increasing intracellular lipid can significantly increase the production rate of the lipid precursor of nonpetroleum-based diesel. Table 1.5 shows that the biodiesel productivity rate of *Synechocystis* is approximately 20 – 70 times higher than from plant sources that can be grown in North America. This superior productivity mainly results from a much higher biomass growth rate of *Synechocystis* than that of plants, but it is accentuated by a high lipid content of modified *Synechocystis*. The much higher productivity rate supports that *Synechocystis* is a more suitable feedstock for massive production of biofuel than are plants. The productively values also give

insight into the potential for using *Synechocystis* to produce renewable feedstock for nonpetroleum-based diesel such as biodiesel.

Certain errors occur with this model. The biggest error may come from the neglect of the photoinhibition under the high light irradiance, which may overestimate the productivity results of this model. In order to address photoinhibition, a more sophisticated light model is required, which is beyond the scope of this study. In addition, neglecting respiration in the light and dark time also may overestimate the results. The selection of ε also influences the final output. Other N sources — NO_2^-, N_2, and NH_4^+ — can also be used, and predictions from the model are discussed in section 1.7 Appendix for Chapter 1.

Table 1.5. Comparison of biodiesel production rates for *Synechocystis* and oil-rich plants

Organism	**Biodiesel production (L/ha/yr)**	**Reference**
Synechocystis	13,000 – 79,000	Predicted by model in this chapter
Sunflower	570 – 1030	Huber et al. (2006)
Soybean	380 – 650	Huber et al. (2006)

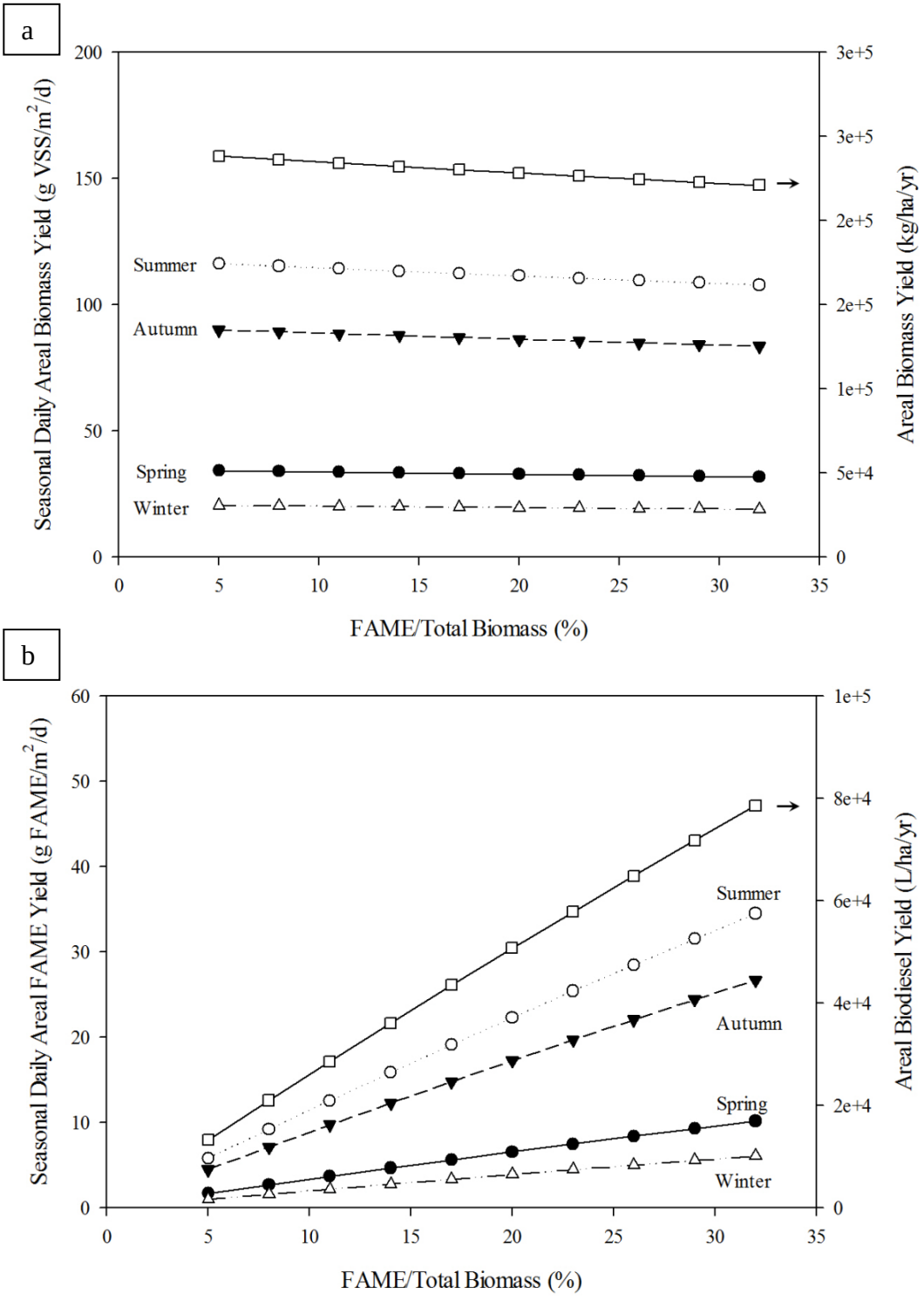

Figure 1.7. Seasonal daily and annual areal production rates for ***a.*** biomass and ***b.*** biodiesel (main component is FAME) as a function of the FAME content of *Synechocystis* under the sunlight condition of Phoenix, AZ.
The areal biodiesel yield was calculated by assuming a density 0.9 kg/L.

1.4 Photobioreactors

Growth of phototrophic *Synechocystis* requires suitable environmental conditions, such as light irradiation, temperature, pH, inorganic carbon, and nutrients such as N and P. Open ponds and closed photobioreactors (PBRs) have been applied for mass culture of microalgae and cyanobacteria. Examples are illustrated in Figure 1.8. Both approaches have been used at industrial scale (Figure 1.8b and d).

As shown in Figure 1.8a, an open pond is raceway, which is a looped recirculation channel with a paddlewheel for mixing and circulation and baffles placed in the flow channel for guiding flows around bends (Terry and Raymond, 1985). Although an open pond is low-cost due to its simple configuration, the major drawbacks of open pond include temperature fluctuations, water loss via evaporation, and less efficient usage of carbon dioxide. Some open ponds are poorly mixed, which leads to less efficient usage of sunlight and a low biomass concentration due to the consistent existence of dark zone. Contamination with unwanted microorganisms, such as predators that feed on *Synechocystis* and heterotrophic bacteria that compete for nutrients, also reduces productivity (Afi et al., 1996; Ding and Sun, 2005). As a result, open ponds have lower biomass productivity compared with closed PBRs (Chisti, 2007).

Unlike open ponds, closed PBRs provide a more controllable environment for the growth of photosynthetic biomass. Systematically designed PBR have been successfully applied in industrial scale for massive production of photosynthesis biomass (Carvalho et al., 2006; Molina Grima et al., 1999; Pulz,

2001; Tredici and Zittelli, 1998). The most popular form of PBR is a tubular PBR that consists of an array of straight transparent plastic or glass tubes for the growth of photosynthesis biomass and the capture of sunlight energy. Figure 1.8c shows a typical tubular PBR system. The diameter of tubes is usually limited to minimize the negative impact of light attenuation with depth. The culture that grows inside the tube also is intensively agitated by mechanical or airlift pumps to supply inorganic carbon and prevent biomass precipitation or a constant dark zone inside the tube. The temperature is usually controlled by putting the reactor in temperature-controlled water pond or greenhouse or by installing a thermal jacket around the tube for heat exchange. As a closed system insulated from the open air, evaporation loss and contamination with unwanted microorganisms can be significantly reduced. In comparison with open-raceway pond, tubular PBR systems are reported to have nearly 30 times of the biomass concentration and 13-fold greater volumetric biomass productivity rate, which significantly reduced the cost of medium and biomass recovery (Chisti, 2007; Molina Grima et al., 2003).

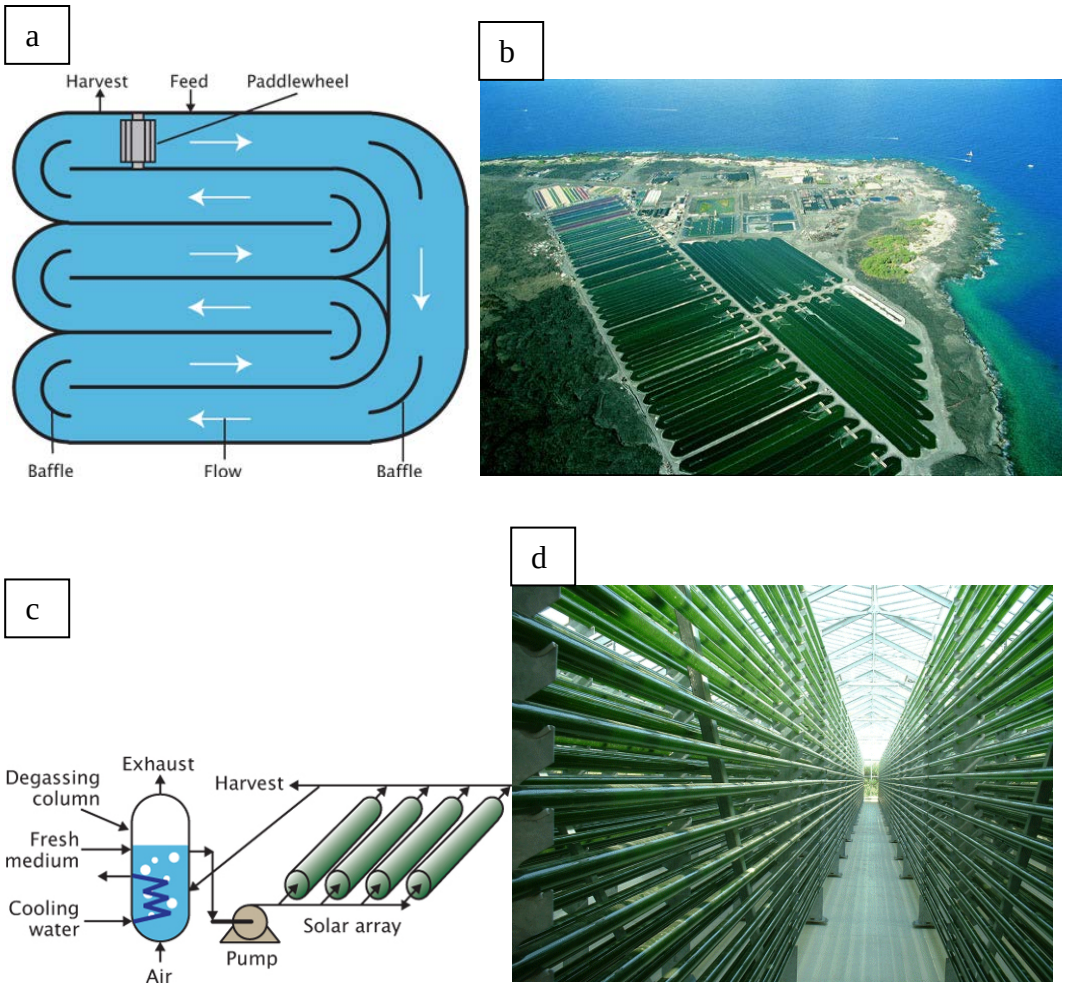

Figure 1.8. Schematics and real-world applications of open ponds and closed photobioreactors.

a. Schematic of a raceway pond. ***b.*** A raceway pond fed with ocean water for mass cultivation of algae on a 90-acre facility (Chisti, 2007). ***c.*** Schematic of a closed photobioreactor. ***d.*** Vertically stacked arrays of closed PBRs with annual production to be 130 – 150 tons (Pulz, 2001).

1.5 Downstream processing of *Synechocystis*

After cell growth and harvesting, downstream processing of *Synechocystis* biomass is necessary for recovering valuable materials, such as usable energy feedstock. A typical series of steps needed to produce nonpetroleum-diesel fuel and other forms of biofuels from *Synechocystis* biomass is illustrated in Figure 1.9a, which is based on Cooney et al. (2009). Biomass is harvested and then dewatered by filtration, centrifugation, or other means to remove and recycle medium. Cell disruption is usually performed to facilitate extraction of intracellular lipids by either an organic-solvent system or other extraction reagents, such as supercritical carbon dioxide (Couto et al., 2010). Extracted lipids are further converted to useful forms of nonpetroleum-based diesel such as biodiesel that can be mixed with petroleum diesel or used alone. Non-lipid biomass can be further utilized as feedstock for the production of other useful bioenergy outputs, such as methane, hydrogen, and electricity (Rittmann, 2008).

Recently, a breakthrough via genetic modification of *Synechocystis* makes it produce and excrete more valuable materials — FFA — for biofuel production (Kaczmarzyk and Fulda, 2010; Liu et al., 2011b). FFA can be further decarboxylated to long-chain alkanes, generally known as renewable diesel, which has nearly identical composition to petroleum diesel (Knothe, 2010). When mutant *Synechocystis* is grown in a PBR with FFA as the main product, the downstream treatment has to be modified to accommodate this shift of focus. Figure 1.9b shows a series of steps for biofuel production from mutant *Synechocystis*. Excreted FFA is extracted directly from medium by bio-

compatible organic solvent or hydrophobic or ion-exchange resin. Extracted FFA is further decarboxylated to long-chain alkane under the existence of hydrogen and catalyst (Na et al., 2010) When mutant-*Synechocystis* becomes incapable of producing FFA or when biomass is removed to maintain the desired solids retention time (SRT), the *Synechocystis* biomass is harvested and processed in a procedure similar with Figure 1.9a to retrieve intracellular lipids and for conversion of non-lipid biomass to valuable forms of biofuel, as noted above.

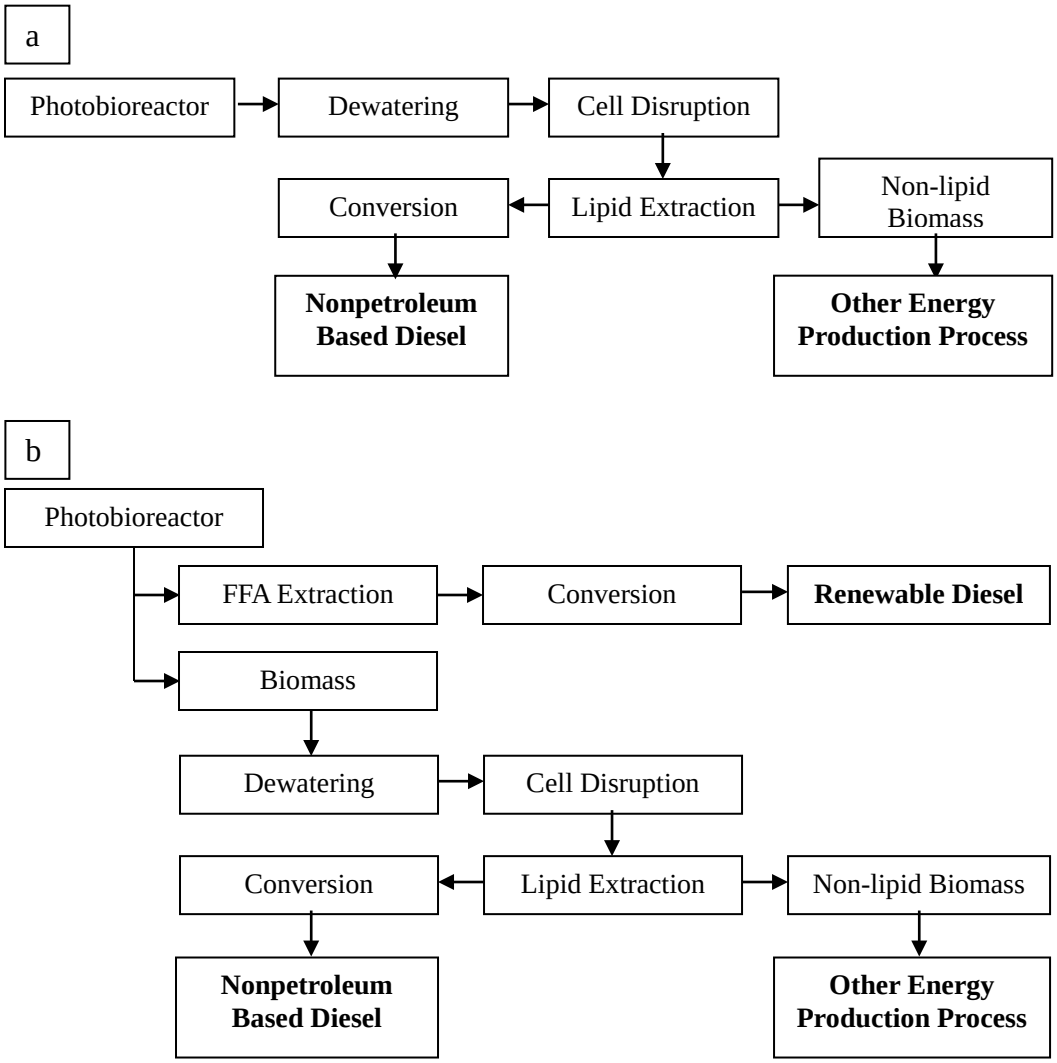

Figure 1.9. Schemes of downstream treatment of *Synechocystis* for biofuel production.

a. Focus on *Synechocystis* biomass and lipids: Harvested biomass from the photobioreactor is dewatered, disrupted, and extracted. Extracted lipids are transformed to engine-compatible diesel fuel, while non-lipid biomass can be further utilized for production of other biofuel (Rittmann, 2008). ***b.*** Focus on FFA: Excreted FFA is recovered and transformed to renewable feedstock (long chain alkane), while the *Synechocystis* biomass, after harvest, is processed according to Figure 1.9a.

1.6 Objectives and dissertation outline

The main objective of my work is to provide an integrated understanding of the downstream processing of *Synechocystis* for biofuel production. This understanding is critical to success, because downstream processing often is the most cost-intensive part of the entire production process. My work follows each step of downstream process from cell growth to the retrieval of valuable products: lipids or FFA. I investigate the influence of cultivation conditions to the quality and quantity of lipids, which has direct impact on the productivity and quality of biofuel. I also investigate different techniques (including a newly developed pulsed-electric-field technique) for cell disruption for the purpose of retrieving intracellular lipids. I then screen for suitable organic solvent systems for small-scale lipid extraction which focuses on maximum yield and for large-scale lipid extraction which requires cost-efficient and environmental-friendly solution without big sacrifice of productivity loss. In order to accommodate to the recent breakthrough of genetic modification of *Synechocystis,* which enables *Synechocystis* to synthesize and excrete free fatty acids (FFA), I also investigate the potential loss of FFA product and provide solutions for the recovery of FFA product.

My specific objectives are:

1. Establish reliable and accurate quantitative methods for lipid and FFA measurement produced by *Synechocystis*.
2. Study the effect of growth conditions on the quality and quantity of lipid production in *Synechocystis* biomass.

3. Study and compare the cell-disruption techniques to facilitate the extraction of intracellular lipids from *Synechocystis* biomass.
4. Study and develop the most suitable organic solvent system for lipid extraction for small and large scales.
5. Identify the potential challenges for scaling up newly developed mutant *Synechocystis* that can produce and excrete FFA, including product loss from chemical precipitation and biodegradation. Provide solutions to overcome these potential losses.

My dissertation is organized into the following chapters:

Chapter 2 provides an extensive investigation and qualitative and quantitative evaluation of methods for measuring lipids and free fatty acid (FFA) to meet my specific research needs (Objective 1). The results were published as Supplementary Data in a manuscript in *Bioresource Technology* (Sheng et al., 2011d).

Chapter 3 screens a number of extraction methods using organic solvents to develop the most suitable systems for lipid extraction from *Synechocystis* biomass for small-scale analytical purposes and large-scale mass production (Objective 4). It also provides experimental and theoretical demonstrations to support the applicability of certain solvent system. The results were published in the main manuscript in *Bioresource Technology* (Sheng et al., 2011d).

Chapter 4 investigates the effect of environmental conditions, particularly temperature, on the growth and lipids (quality and quantity) in *Synechocystis* (Objective 2). It provides information about the optimum growth condition for

Synechocystis in terms of optimum biomass and lipid productivity. It also evaluates the negative effect of extreme temperature on biomass growth and lipid quality and quantity. The results were published in *Bioresource Technology* (Sheng et al., 2011a).

Chapter 5 describes an innovative cell-disruption method — pulsed electric field (PEF) — and its effect on *Synechocystis* (Objective 3). It identifies the different mechanisms that lead to observable cell damages during the PEF treatment. It also discusses the benefit of implementing this technique into the downstream processing of *Synechocystis* for biofuel production. The results were published in an article in *Environmental Science & Technology* (Sheng et al., 2011c).

Chapter 6 describes how a range of cell-disruption methods — such as autoclaving, bead beating, freeze drying, French press, microwave, PEF, and ultrasound — affect lipid extraction from *Synechocystis* biomass (Objective 3). It identifies the types of damage to the cells after different treatment methods. It also indicates which methods enhance lipid extraction and which might be inappropriate in large application. This work was presented at the *8th IWA Leading-Edge Conference on Water and Wastewater Technologies* (Amsterdam, The Netherlands, 2011) and is in press for publication in *Water Science & Technology* (Sheng et al., 2011b).

Chapter 7 focuses on the production of excreted FFA by mutant *Synechocystis* strains (Objective 5). It monitors and identifies one major operation problem — FFA loss. It discusses mechanisms for FFA loss, such as FFA

precipitation via chemical reaction and biodegradation by FFA scavengers. It provides possible solutions to overcome these potential product losses for the purpose of maximizing net FFA productivity.

Chapter 8 summarizes and synthesizes all topics in my dissertation. It also discusses the significance of my work and the future studies.

1.7 Appendix for Chapter 1 — Phototroph stoichiometry of *Synechocystis* using different N sources

The results applying the new method for phototroph stoichiometry when using NO_3^- as N source are presented in section 1.3. Other N sources — NO_2^-, N_2, and NH_4^+ — can also be used. The change when using different N sources is in step 2 of biosynthesis (equation (1.4) in section 1.3).

When using NO_2^- as N source, equation (1.4) in section 1.3 is changed to:

$$\left(\frac{n}{6h}\right)C_6H_{12}O_6+\left(\frac{c}{h}\right)NO_2^-+\left(\frac{d}{h}\right)HPO_4^{2-}+\left(\frac{a-2b+4c+7d}{h}\right)H^++e^-\rightarrow \left(\frac{1}{h}\right)C_nH_aO_bN_cP_d+\left(\frac{n-b+2c+4d}{h}\right)H_2O \quad (1.16)$$

where $h = a - 2b + 3c + 5d$

When using N_2 as N source, equation (1.4) in section 1.3 is changed to:

$$\left(\frac{n}{6h}\right)C_6H_{12}O_6+\left(\frac{c}{2h}\right)N_2+\left(\frac{d}{h}\right)HPO_4^{2-}+\left(\frac{a-2b+7d}{h}\right)H^++e^-\rightarrow \left(\frac{1}{h}\right)C_nH_aO_bN_cP_d+\left(\frac{n-b+4d}{h}\right)H_2O \quad (1.17)$$

where $h = a - 2b + 5d$

When using NH_4^+ as N source, equation (1.4) in section 1.3 is changed to:

$$\left(\frac{n}{6h}\right)C_6H_{12}O_6+\left(\frac{c}{h}\right)NH_4^++\left(\frac{d}{h}\right)HPO_4^{2-}+\left(\frac{a-2b-4c+7d}{h}\right)H^++e^-\rightarrow \left(\frac{1}{h}\right)C_nH_aO_bN_cP_d+\left(\frac{n-b+4d}{h}\right)H_2O \quad (1.18)$$

where $h = a - 2b - 3c + 5d$

I performed similar calculation as in section 1.3, and the results are showed in Table 1.6 – Table 1.8; these can be compared directly to Table 1.4 and Table 1.5 when using NO_3^- as the N source. Because the oxidization state becomes more negative from NO_3^- to NH_4^+, less reducing power is required in the step 2 of biosynthesis, and this means that more biomass can be produced per electron transferred in step 2 of biosynthesis (Row "Biomass" in Table 1.6 – Table 1.8). This trend also is confirmed by several changes in Table 1.4 – Table 1.8. For example, when switching from NO_3^- to NH_4^+, smaller fractions of electrons are invested in non-cyclic photophosphorylation to produce NADPH ($f_{nc}/(1 + f_c)$ decreases); in addition, fewer fraction of electrons was used in step 2 of biosynthesis (f_{nc}^2 decreases). As a result, when switching N sources from NO_3^- to NH_4^+, the areal biomass yield and areal biodiesel yield under the sunlight condition in Phoenix, AZ increase from $2.1 \times 10^5 – 2.4 \times 10^5$ kg/ha/yr to $2.7 \times 10^5 – 3.2 \times 10^5$ kg/ha/yr and from $1.3 \times 10^4 – 7.9 \times 10^4$ L/ha/yr to $1.8 \times 10^4 – 9.8 \times 10^4$ L/ha/yr, respectively. This means an increase in areal yield of around 30%. However, whether NH_4^+ should be used instead of NO_3^- in massive cultivation of *Synechocystis* also depends on the price and toxicity of NH_4^+ versus NO_3^-, a topic beyond the scope of this study.

Table 1.6. Stoichiometric calculations for the biomass-synthesis reaction (R_c), electron fractions between non-cyclical photophosphorylation and cyclical photophosphorylation, and yields of biomass, FAME, and biodiesel using NO_2^- as the N source

FAME %	**5%**	**8%**	**11%**	**14%**	**17%**	**20%**	**23%**	**26%**	**29%**	**32%**
Stoichiometric constants										
CO_2	0.660	0.657	0.653	0.650	0.647	0.644	0.641	0.638	0.636	0.633
NO_2^-	0.144	0.136	0.129	0.122	0.116	0.109	0.103	0.097	0.092	0.086
HPO_4^-	0.008	0.007	0.007	0.006	0.006	0.006	0.005	0.005	0.005	0.005
Biomass	0.144	0.136	0.129	0.122	0.116	0.109	0.103	0.097	0.092	0.086
$f_{nc}^{\ 2}$	0.27	0.28	0.28	0.28	0.28	0.28	0.28	0.28	0.28	0.28
$f_{nc}^{\ 1}$	0.73	0.72	0.72	0.72	0.72	0.72	0.72	0.72	0.72	0.72
f_c	0.58	0.57	0.55	0.54	0.53	0.51	0.50	0.49	0.48	0.47
$Y_{Biomass}$ (g VSS/e^- eq)	4.29	4.21	4.14	4.07	4.01	3.94	3.88	3.82	3.76	3.71
Y_{FAME} (g FAME/e^- eq)	0.21	0.34	0.46	0.57	0.68	0.79	0.89	0.99	1.09	1.19
Areal Biomass Yield ($\times 10^5$ kg/ha/yr)	2.82	2.79	2.76	2.73	2.70	2.67	2.64	2.61	2.59	2.56
Areal Biodiesel Yield ($\times 10^4$ L/ha/yr)	1.57	2.48	3.37	4.25	5.10	5.94	6.75	7.55	8.33	9.10

Table 1.7. Stoichiometric calculations for the biomass-synthesis reaction (R_c), electron fractions between non-cyclical photophosphorylation and cyclical photophosphorylation, and yields of biomass, FAME, and biodiesel using N_2 as the N source

FAME %	**5%**	**8%**	**11%**	**14%**	**17%**	**20%**	**23%**	**26%**	**29%**	**32%**
					Stoichiometric constants					
CO_2	1.160	1.110	1.066	1.026	0.990	0.958	0.928	0.901	0.877	0.854
N_2	0.126	0.115	0.105	0.096	0.088	0.081	0.075	0.069	0.063	0.058
HPO_4^-	0.013	0.012	0.011	0.010	0.009	0.009	0.008	0.007	0.007	0.006
Biomass	0.252	0.230	0.210	0.193	0.177	0.162	0.149	0.137	0.126	0.116
$f_{nc}^{\ 2}$	0.18	0.18	0.19	0.20	0.20	0.21	0.21	0.22	0.22	0.23
$f_{nc}^{\ 1}$	0.82	0.82	0.81	0.80	0.80	0.79	0.79	0.78	0.78	0.77
f_c	0.78	0.75	0.73	0.70	0.68	0.65	0.63	0.61	0.59	0.57
$Y_{Biomass}$ (g VSS/e^- eq)	4.86	4.75	4.64	4.54	4.44	4.34	4.25	4.16	4.08	4.00
Y_{FAME} (g FAME/e^- eq)	0.24	0.38	0.51	0.64	0.75	0.87	0.98	1.08	1.18	1.28
Areal Biomass Yield ($\times 10^5$ kg/ha/yr)	2.98	2.94	2.90	2.86	2.82	2.78	2.75	2.71	2.68	2.65
Areal Biodiesel Yield ($\times 10^4$ L/ha/yr)	1.65	2.61	3.54	4.45	5.33	6.19	7.03	7.84	8.64	9.41

Table 1.8. Stoichiometric calculations for the biomass-synthesis reaction (R_c), electron fractions between non-cyclical photophosphorylation and cyclical photophosphorylation, and yields of biomass, FAME, and biodiesel using NH_4^+ as the N source

FAME %	**5%**	**8%**	**11%**	**14%**	**17%**	**20%**	**23%**	**26%**	**29%**	**32%**
					Stoichiometric constants					
CO_2	4.767	3.585	2.891	2.434	2.110	1.869	1.682	1.533	1.412	1.311
NH_4^+	1.036	0.743	0.571	0.457	0.377	0.317	0.271	0.234	0.204	0.178
HPO_4^-	0.055	0.039	0.030	0.024	0.020	0.017	0.014	0.012	0.011	0.009
Biomass	1.036	0.743	0.571	0.457	0.377	0.317	0.271	0.234	0.204	0.178
$f_{nc}^{\ 2}$	0.05	0.07	0.08	0.09	0.11	0.12	0.13	0.14	0.15	0.16
$f_{nc}^{\ 1}$	0.95	0.93	0.92	0.91	0.89	0.88	0.87	0.86	0.85	0.84
f_c	1.04	0.99	0.95	0.90	0.86	0.83	0.79	0.76	0.73	0.70
$Y_{Biomass}$ (g VSS/e^- eq)	5.62	5.44	5.27	5.12	4.97	4.83	4.70	4.57	4.45	4.34
Y_{FAME} (g FAME/e^- eq)	0.28	0.44	0.58	0.72	0.84	0.97	1.08	1.19	1.29	1.39
Areal Biomass Yield ($\times 10^5$ kg/ha/yr)	3.15	3.10	3.05	3.00	2.95	2.91	2.86	2.82	2.78	2.74
Areal Biodiesel Yield ($\times 10^4$ L/ha/yr)	1.75	2.75	3.72	4.67	5.58	6.46	7.32	8.15	8.96	9.75

2 Quantification of Lipids and Free Fatty Acids[*]

2.1 Introduction

Obtaining a reliable and precise quantification method for lipids and free fatty acids (FFA) is crucial for all research on the production and processing of these products. Several lipid-quantification methods have been reported in literature, including gas chromatography (GC), liquid chromatography (LC), dry weight, fluorescence staining, and saponification + titration (Foglia et al., 2004; Lee et al., 2010b; Lee et al., 1998; Sato and Murata, 1988). Each method has its advantages and limitations.

The dry weight measurement of lipids is easy and straightforward, but it counts all crude extract as lipids, which may seriously overestimate the real lipid content when non-lipid impurities exist (even after purification steps). In addition, dry weight measurement can only provide total amount of extract, but not a detailed profile of the lipids. Saponification followed by acid titration easily and rapidly quantifies saponifiable lipids (American Society for Testing and Materials, 2009) but cannot provide detailed lipid profile and may even generate losses of non-saponifiable lipids.

The other methods such as fluorescence and LC are deficient when the target is lipids in cyanobacteria. Cyanobacterial lipids are mainly membrane lipids located in the cell membrane and the thylakoid membranes. Unlike

[*] Several sections of this chapter were published as Supplementary Data of Sheng, J., Vannela, R., Rittmann, B.E. 2011. Evaluation of methods to extract and quantify lipids from *Synechocystis* PCC 6803. *Bioresource Technology*, **102**(2), 1697-1703.

triacylglycerols (TAG) lipids in algae, cyanobacterial lipids are diacylglycerols (DAG), having only two fatty acid chains and one non-fatty acid group connected with glycerol backbone. As shown in Figure 2.1, the non-fatty acid group can be a phosphoglycerol (Pg), sulfoquinovose (Sq), galactose (Gal), or digalactose (Gal_2), which correspond to four major DAG groups — phosphatidyl diacylglycerol (PG), sulfoquinovosyl diacylglycerol (SQDG), monogalactosyl diacylglycerol (MGDG), and digalactosyl diacylglycerol (DGDG). Quantification methods that are capable of measuring TAG may not be well suited for DAG. Fluorescence could be a swift and semi-quantitative method if a suitable dye is available, but common dyes do not target thylakoid membranes well. The fluorescent dye Nile Red has been reported to specifically target lipid deposits (mainly TAG), and it usually presents a linear relationship between fluorescent emission intensity and TAG amount in algae (Greenspan et al., 1985; Lee et al., 1998). However, Nile Red has a poor fluorescent response with membrane DAG. Another lipophilic dye, DiI, was reported to trace lipid diffusion in membranes, but this dye penetrates poorly into cells and tends to precipitate around cells (Casadevall et al., 2009). In addition to poor penetration, dyes also suffer the limitation of not being able to generate a lipid profile.

a.

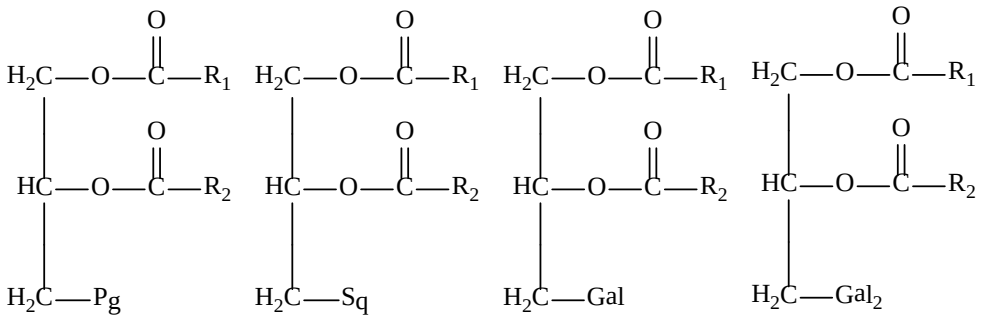

b.

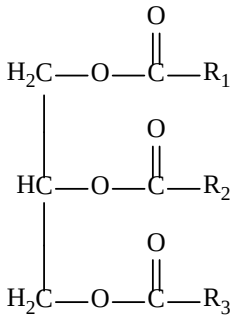

Figure 2.1. ***a.*** Major diacylglycerol groups of *Synechocystis* PCC 6803. ***b.*** Triacylglycerol in algae, plant, or animal tissue.

PG, phosphatidyl diacylglycerol; SQDG, sulfoquinovosyl diacylglycerol; MGDG monogalactosyl diacylglycerol; DGDG digalactosyl diacylglycerol; Pg, phosphoglycerol; Sq, sulfoquinovose; Gal, galactose; R, alkyl group.

LC in combination with mass spectrometry (MS) can provide a full view of lipid composition by yielding detailed charge-mass ratio of each compound (Foglia et al., 2004). However, in contrast to it excellence for TAG quantification, utilizing LC-MS for DAG measurement turns to a challenge due to the lack of commercial standards for diverse DAG compounds. Alternatively, some reports used single standard to represent a sort of compounds by assuming same peak response among all compounds (Balogi et al., 2005). This data-treatment method will generate errors if different compounds have different signal responses.

GC typically cannot yield reliable quantification results for direct quantification of DAG or TAG due to their high polarity, low volatility, and high tendency to form hydrogen bonds (Brondz, 2002). However, transesterification by acid or base catalysis with methanol gives lower-boiling-point derivatives — fatty acid methyl esters (FAME) — that have been widely measured by GC (Carvalho and Malcata, 2005; Liu et al., 2005; Sato and Murata, 1988). A big advantage of transesterification + GC measurement is its capability of providing accurate and detailed quantification of fatty acid profile in lipids, which is well tuned to the most valuable parts of the DAG molecule for biofuel production (Knothe, 2006). However, as the bonds between fatty acid group and glycerol are cleaved during transesterification, no information is provided about the original position of fatty acids in lipids. In order to assign the fatty acids to specific lipids, thin layer chromatography (TLC) or LC can be used ahead of transesterification + GC to separate different DAG groups (PG, SQDG, MGDG, DGDG) (Christie, 1986; Sato and Murata, 1988).

Compared with DAG, long-chain FFA have a much simpler molecular structure and can be measured by GC and LC (Brondz, 2002). However, quantification of long-chain FFA via GC or LC still needs careful attention. For example, most of FFAs do not have a good chromatophore or luminiphore that can be observed by the commonly used UV detector of LC (Cason and Sumrell, 1951). Thus, combining LC with other detectors, often MS, is required to obtain better signal strength.

The major concern of measuring long-chain FFA directly by GC is their high molecular weights, high boiling points, and high polarity, all of which result in broad peaks and low resolution and potential damage to non-polar or weak polar columns. As a result, derivatization of FFAs often has been applied to improve separation and sensitivity (Brondz, 2002). The most widely used derivatization is to esterify FFA to FAME via acid catalysis. This method has been adopted as a standard method by many authorities, such as International Union of Pure and Applied Chemistry (IUPAC) (1992) and American Oil Chemists' Society (1992).

Recently, direct measurement of long-chain FFA by GC has been reported by using Supelco Nukol column, a polar column that is specifically coated to endure long-chain FFA and improve peak shapes and responses (Lalman and Bagley, 2004). This method may avoid derivatization and significantly reduce processing time and workload without sacrificing accuracy and reliability of quantification results.

In this chapter, I evaluated several methods for quantification of lipids and FFA. I develop and optimize quantification methods and then confirmed their accuracy and reliability by applying them to lipid and FFA standards and *Synechocystis* samples.

2.2 Materials and methods

2.2.1 Cell cultures and standards

I obtained lipid producing strains wild-type *Synechocystis* PCC 6803 and mutant-type High VIPP and FFA producing strain TE/Δ*slr1609* from Dr. W. F. J. Vermaas. I also obtained FFA producing strain mutant-type SD243 from Dr. Roy Curtiss III of Arizona State University. *Synechocystis* High VIPP was constructed by overexpress vesicle-inducing protein in plastids 1 (VIPP-1) (Aseeva et al., 2004; Westphal et al., 2001). *Synechocystis* TE/Δ*slr1609* was constructed by expressing California bay acyl-ACP thioesterase (TE) in a background strain with overexpressed AccABCD and PAP yielding the TE strain. Then *slr1609* was knockout by insertion of a chloramphenicol resistance cassette (Kaczmarzyk and Fulda, 2010). *Synechocystis* SD243 was made by 8 successive genetic modifications starting with introducing genes for acyl-acyl carrier protein thioesterases, including overexpressing plant thioesterase genes, Acetyl-CoA carboxylase genes, deleting poly-3-hydroxybutyrate (PHB) synthesis genes, acyl-ACP synthetase gene, hemolysin-like surface layer protein gene, and cyanophycin synthetase genes (Liu et al., 2011b).

I maintained the pure strains on sterile BG-11 plates with 10-mM TES-NaOH (pH 8.0) (TES is N-tris(hydroxymethyl)methyl-2- aminoethanesulfonic acid), 1.5% agar, and 0.3% sodium thiosulfate (Rippka et al., 1979; van de Meene et al., 2006). I collected and transferred colonies to a 250-mL autoclaved flask containing 100 mL sterile BG-11 medium and allowed cells to grow for 4 to 5 d at a light intensity of 100 µmol photons/m^2-s and a constant temperature of 30^{o}C.

In addition to obtain lipids and FFA from *Synechocystis*, I also performed analysis by lipids, FAME, and FFA standards. If not specified, all chemical standards were purchased from Sigma-Aldrich (St. Louis, MO) with GC-standard purity.

2.2.2 Cell harvest and lipid extraction

I harvested the cells by centrifugation (Beckman Coulter, Avanti J-26 XPI) at 15,000*g* for 15 min. I suspended the cell pellet in deionized water and re-centrifuged two times to remove residual medium. For lipid extraction, I used the Folch (chloroform:methanol = 2:1, v/v; solvent:sample = 20:1, v/v) method (Folch et al., 1957). After the extraction step, I filtered the solvent-biomass mixture through a 0.45-µm PTFE membrane and evaporated the filtrate completely under N_2 (Labconco RapVap N_2 evaporation system) to eliminate residual solvent, maintaining the evaporation temperature below 60^{o}C to prevent lipid loss (Cantrell and Walker, 2009).

2.2.3 Separation of major DAG groups

I performed thin-layer chromatography (TLC) according to Sato and Murata (1988) and Christie (1993) to separate major DAG groups in *Synechocystis*. Two-dimensional TLC employed chloroform:methanol:water (75:25:2.5 by volume) in the first development and chloroform:methanol:acetic acid:water (80:9:12:2 by volume) in the second (perpendicular) development. Typical separation results are shown in Figure 2.4. I identified lipid groups by Electrospray Ionization Mass Spectrometry (ESI-MS) (Han and Gross, 2005).

2.2.4 Transesterification and quantification of FAME

I performed transesterification of the dried crude lipid using a method modified from Sato and Murata (1988) and Liu et al. (2005). Briefly, I added 1 mL of 3-N methanolic HCl (Supelco, St. Louis, MO) to the dried lipid in a test tube and heated it in a water bath at 85^{o}C for 2.5 h. After cooling the mixture to room temperature, I added 0.5 mL DI water and 1 mL of hexane and mixed the contents well by hand, collected the hexane layer containing the transesterification FAME, and extracted the remaining methanol/water two times again with 1 mL hexane. I pooled the three 1-mL volumes of hexane prior to GC analysis.

I identified and quantified FAME using gas chromatography (Shimadzu GC 2010) equipped with a Supelco SP2380 capillary column (30 m × 0.25 mm × 0.20 μm) and flame ionization detector (FID). Operating conditions were as follows: split ratio 1:10; inject volume 1 μL; helium carrier gas with constant

linear velocity 20 cm/s; H_2 40 mL/min, air 400 mL/min, make up gas (helium) 30 mL/min; injector and detector temperature 240^{o}C; and oven temperature started at 140^{o}C for 1 min and increased at a rate of 4^{o}C/min to 220^{o}C.

2.2.5 Extraction of excreted FFA from medium

For extraction of excreted FFA by mutant-type *Synechocystis* TE/Δ*slr1609* or SD243, I shook the whole culture by hand to achieve homogeneous distribution of FFA. I took a 1-mL sample and added 20 µL of 0.5 M EDTA to retrieve FFA precipitate (mainly calcium fatty acids) back to the dissolved phase. I then centrifuged the sample at 13,000*g* for 2 min to remove biomass. I transferred supernatant into an 8-mL glass tube and adjusted the pH and ionic strength by adding 80 µL of 50% H_2SO_4 and 0.05 g NaCl. I then added 2 mL hexane and vortexed (VWR Vortex Mixer) the mixture for full extraction. I centrifuged the samples at 1,900*g* for 5 min to separate the aqueous and hexane layers. In order to let FFA concentration fall into the linear range of calibration curve, resizing the volume of hexane was performed if necessary. I also performed similar extraction by using 14.17 mg lauric acid dissolved in 300 mL BG-11 and adjusting the pH to ~9 to mimic the real excretion by mutant-type *Synechocystis* TE/Δ*slr1609* and evaluate step-by-step extraction efficiency.

2.2.6 Quantification of FFA

I identified and quantified FFA using GC equipped with a Supelco Nukol capillary column (30 m × 0.53 mm × 0.50 µm) and FID. Operating conditions

were as follows: split ratio 1:10; inject volume 1µL; helium carrier gas with constant flow rate 30 mL/min; H_2 40 mL/min, Air 400 mL/min, make up gas (helium) 5 mL/min; injector and detector temperature 250^{o}C; and oven temperature started at 100^{o}C and increased at rate of 10^{o}C/min to 220^{o}C and hold for 5 min.

2.3 Results and discussion

2.3.1 Lipid quantification

Standards and calibration curve. Figure 2.2a showed GC chromatogram of Supelco 37 FAME mixed standards. Each peak was identified by the manual provided by the manufacturer and by GC-MS. Figure 2.2b shows calibration curves of major FAME compounds derived from *Synechocystis* DAG. CX:Y denotes the compound that has a fatty acid chain of X carbons and Y double bonds (i.e. C16:0 — palmitic acid methyl ester). A linear relationship with $R^2 >$ 0.9996 was reached between 0 to ~100mg/L for all major FAME.

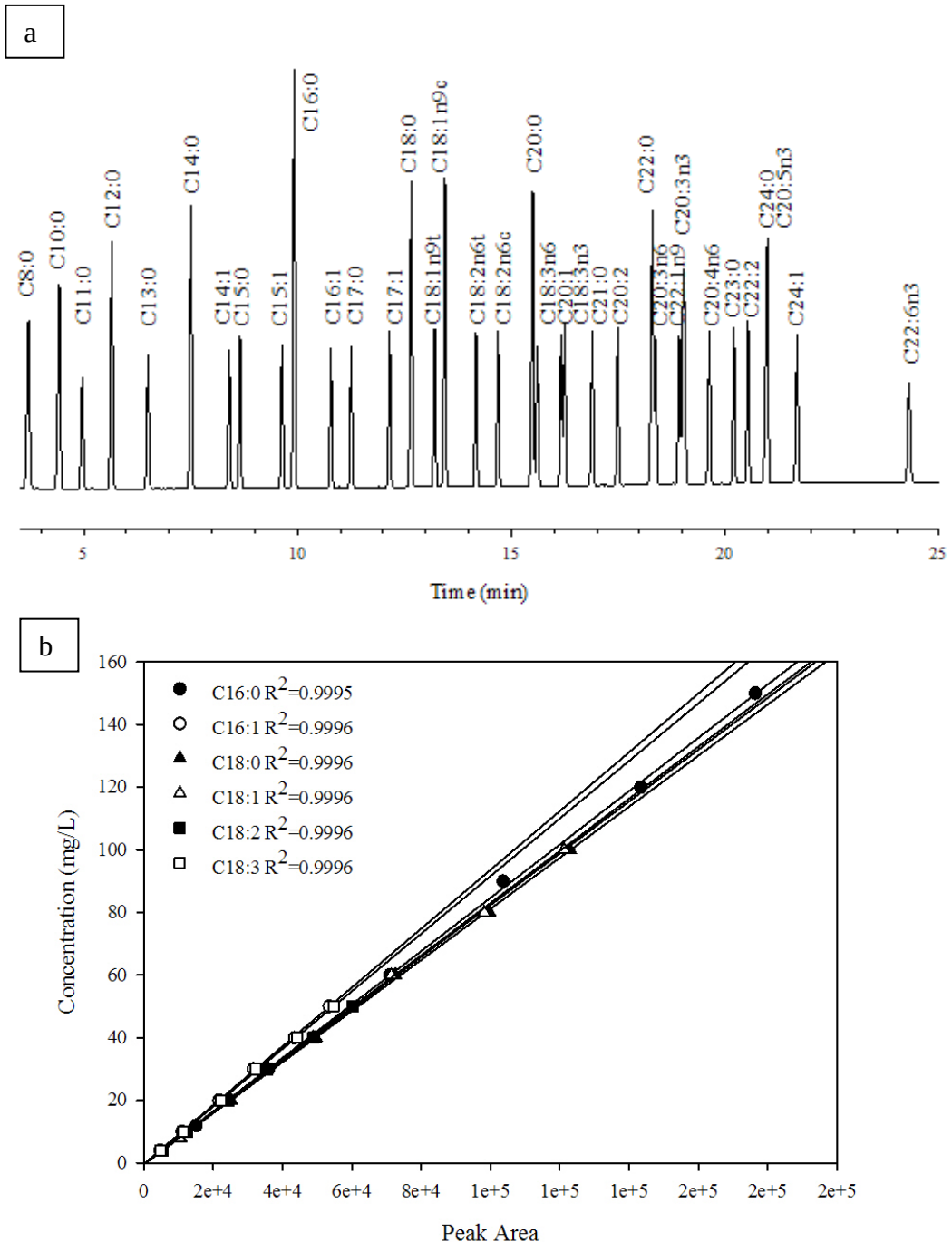

Figure 2.2. ***a.*** GC chromatogram of Supelco FAME 37 standards (some peaks are not shown). ***b.*** Calibration curve of FAME corresponding to typical fatty acids in *Synechocystis* DAG.

C16:0 denotes palmitic acid methyl ester.

Extraction efficiency of lipids from biomass. In order to use FAME to represent fatty acids in lipids accurately, the efficiencies of extraction and transesterification must be high enough to minimize losses. To test lipid-extraction efficiency, I performed three sequential lipid extractions from *Synechocystis* PCC 6803 biomass, as shown in Figure 2.3. The first extraction was sufficient to reach more than 97% of the maximum recovery; so, second and third extractions of biomass were not necessary. I also investigated extraction kinetics and found that a 2-h extraction time was as effective as a 24-h extraction (data not shown).

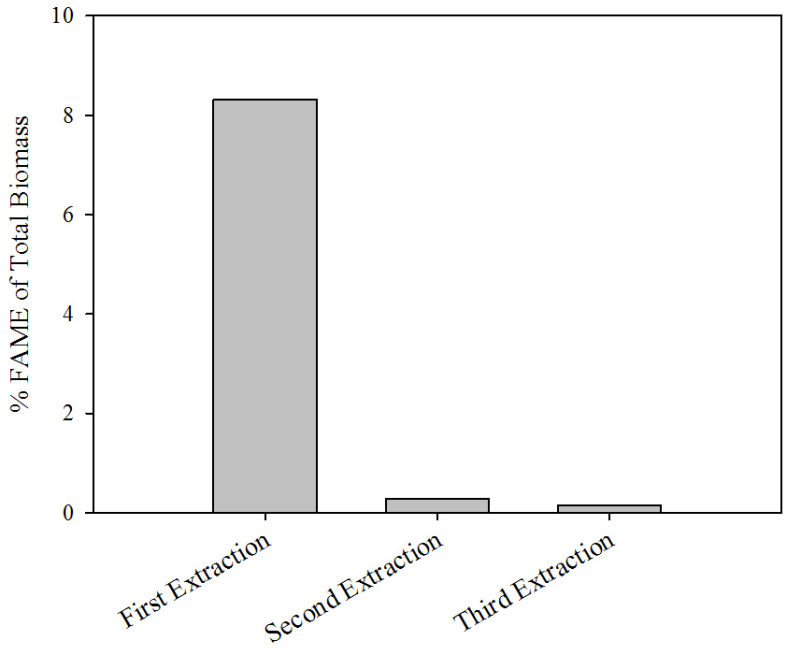

Figure 2.3. Comparison of first, second, and third extractions of lipid from *Synechocystis* PCC 6803 biomass by the Folch method.

Transesterification efficiency of TAG and DAG. In order to test transesterification efficiency, I first used standards for TAG vegetable oils — rapaseed oil, sunflowerseed oil, soybean oil, and peanut oil to perform transesterification reaction. For an ideal conversion from TAG to FAME, the FAME mass should equal the TAG mass. As shown in Table 2.1, all four samples yielded nearly 100% recovery of fatty acids with FAME/lipid, which means almost all TAG were converted to FAME via transesterification.

I also used DAG standards including two phospholipid standards, one MGDG and one DGDG, to test the transesterification efficiency to convert DAG to FAME. Only the phospholipid standards were pure compounds, while MGDG and DGDG, provided by Sigma, were mixed standards. Information about the standards is listed in Table 2.2.

Due to the existence of non-fatty acid group in DAG (Pg, Sq, Gal, or Gal_2), the mass of FAME does not correspond to the DAG mass. The theoretical FAME/DAG mass ratio was calculated based on the molecule structure of each standard compound and compared against the transesterification results, as shown in Table 2.3. Two phospholipid standards yielded satisfactory conversion efficiencies (96% and 93%), with experimental ratios of FAME/DAG close to theoretical ratios (69.6% vs. 72.5% and 69.2% vs. 74.3%). Because MGDG and DGDG standards are mixed standards, I used the most abundant compounds in these samples to calculate the theoretical ratio of FAME/DAG. As a result, MGDG standard yielded 90% recovery (65.5% vs. 72.5%), while DGDG standard

yielded 101% recovery (61.1% vs. 60.0%). In short, transesterification gave higher than 90% conversion efficiency for phospholipids, MGDG, and DGDG.

Table 2.1. TAG standard quantification by transesterification and GC analysis

Sample	Fatty acid profile (% Individual FAME/total FAME)						FAME (mg)	TAG (mg)	FAME /TAG (%)
	C16:0	C16:1	C18:0	C18:1	C18:2	C18.3			
Rapeseed	1.6	1.1	0.0	69.1	22.0	6.2	10.8	10.6	102
Sunflowerseed	3.2	0.0	0.0	26.5	70.4	0.0	10.6	9.8	109
Soybean	7.4	0.0	0.7	21.9	62.9	7.2	10.1	10.1	100
Peanut	7.3	0.0	0.0	59.8	32.9	0.0	10.2	9.9	103

Table 2.2. Commercial DAG standards

Standard	Composition	Amount	Provider
Phospholipid #1*	C16:0, C16:0**	5mg (5mg/L in 1mL)	Avanti, #154582
Phospholipid #2***	C18:0, C18:1	5mg (5mg/L in 1mL)	Avanti, #154582
MGDG	Mix	0.1mg	Sigma, G9523-1MG
DGDG	Mix	0.1mg	Sigma, D4651-1MG

* Dipalmitoyl phosphatidyl glycerol

** Denotes that both fatty acid chains in DAG are palmitic acid group

*** 9-Octadecenoic acid (9Z)-, 3-[[(2,3-dihydroxypropoxy)hydroxyphosphinyl]oxy]-2- [(1-oxooctadecyl)oxy] propyl ester.

Table 2.3. DAG standard quantification by transesterification and GC analysis

Sample	**C16:0 (mg)**	**C16:1 (mg)**	**C18:0 (mg)**	**C18:1 (mg)**	**C18:2 (mg)**	**C18:3 (mg)**	**FAME (mg)**	**FAME /DAG ***	**Theore -tical FAME /DAG**
Phospholipid #1**	3.43	0.022	0	0.027	0	0	3.48	69.6%	72.5%
Phospholipid #2***	0.094	0.013	1.81	1.54	0	0	3.46	69.2%	74.3%
MGDG	0.015	0.002	0	0.003	0.046	0	0.066	65.5%	72.5%
DGDG	0.018	0.003	0	0.003	0.037	0	0.061	61.1%	60.0%

* Calculated by dividing experimental FAME amount over theoretical DAG amount in Table 2.2

** Dipalmitoyl phosphatidyl glycerol

*** 9-Octadecenoic acid (9Z)-, 3-[[(2,3-dihydroxypropoxy)hydroxyphosphinyl]oxy]-2- [(1-oxooctadecyl)oxy] propyl ester.

***Hexane extraction efficiency of FAME after transesterification*. A**fter transesterification, FAME was extracted by hexane from the water/methanol mixture for further GC injection. Results of hexane extraction of FAME from transesterification solution are shown in Table 2.4. Almost all FAME were successfully extracted during the first and second extraction; so, the third extraction was not necessary.

Table 2.4. Evaluation of hexane extraction efficiency of FAME after transesterification

	C16:0	**C16:1**	**C18:0**	**C18:1**	**C18:2**	**C18:3**
First Extraction	97.4%	93.4%	100.0%	96.3%	99.1%	99.6%
Second Extraction	2.7%	4.3%	0.0%	3.2%	0.9%	0.4%
Third Extraction	0.0%	2.3%	0.0%	0.6%	0.0%	0.0%

TLC separation of major DAG groups. Figure 2.4 shows separation of different DAG groups (SQDG, PG, DGDG, and MGDG) on a TLC gel after two perpendicular developments. Each spot on the TLC gel represents one group of DAG and was identified by LC-MS, as shown in Figure 2.5. On the TLC gel, SQDG has the largest spot, which corresponds to the fact that SQDG makes up ~50% of total DAG. The spot of PG is very small, which results from the fact that PG only constitutes for ~10% of total lipids. The MS graph shows that most of the unsaturation fatty acids (C18:1, C18:2, and C18:3) came from DGDG and MGDG.

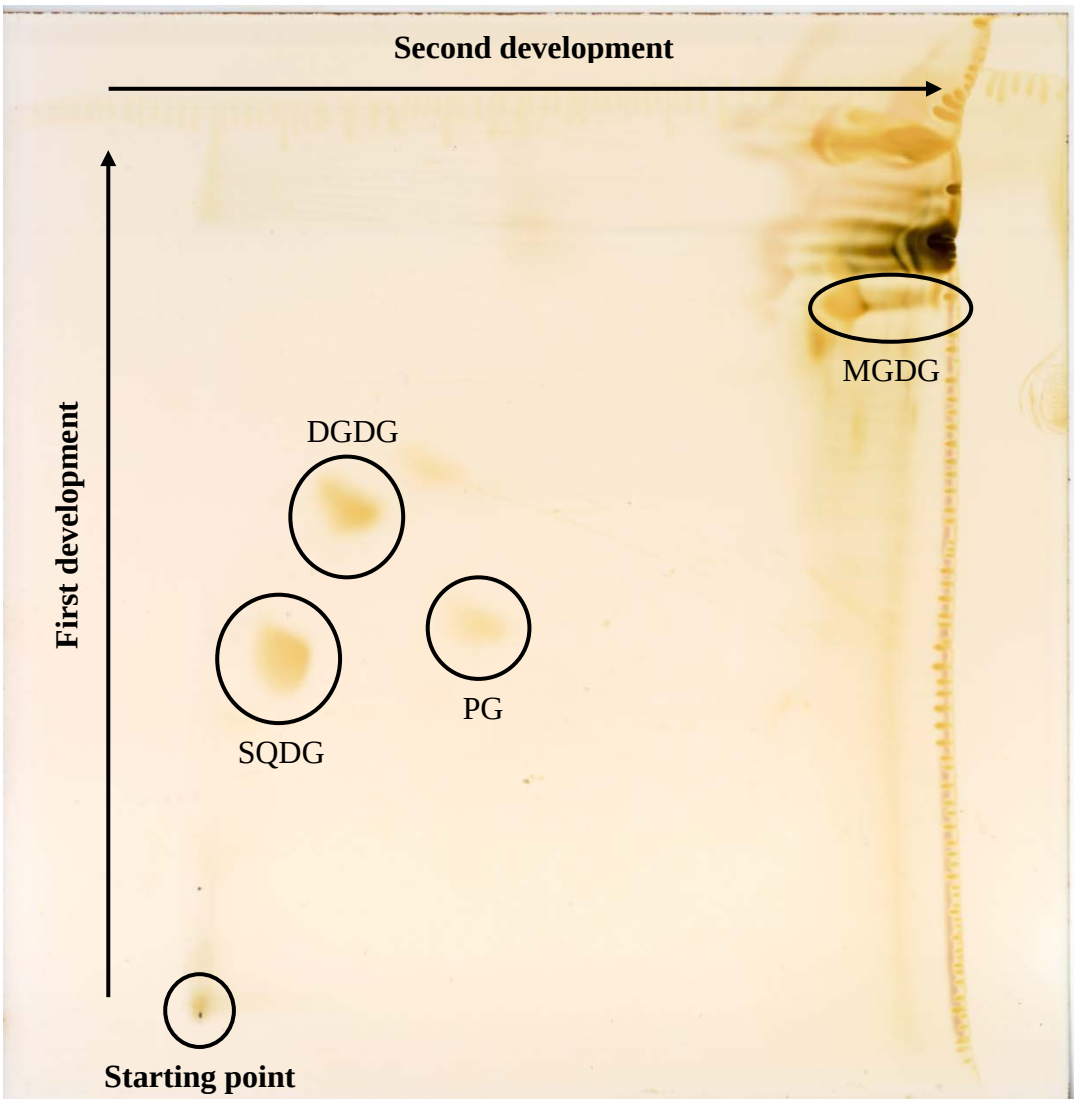

Figure 2.4. Thin-layer chromatogram of *Synechocystis* crude lipid (extracted by the Folch method) separated by two perpendicular developments on a silica gel. Each spot was identified by LC-MS, as illustrated in Figure 2.5.

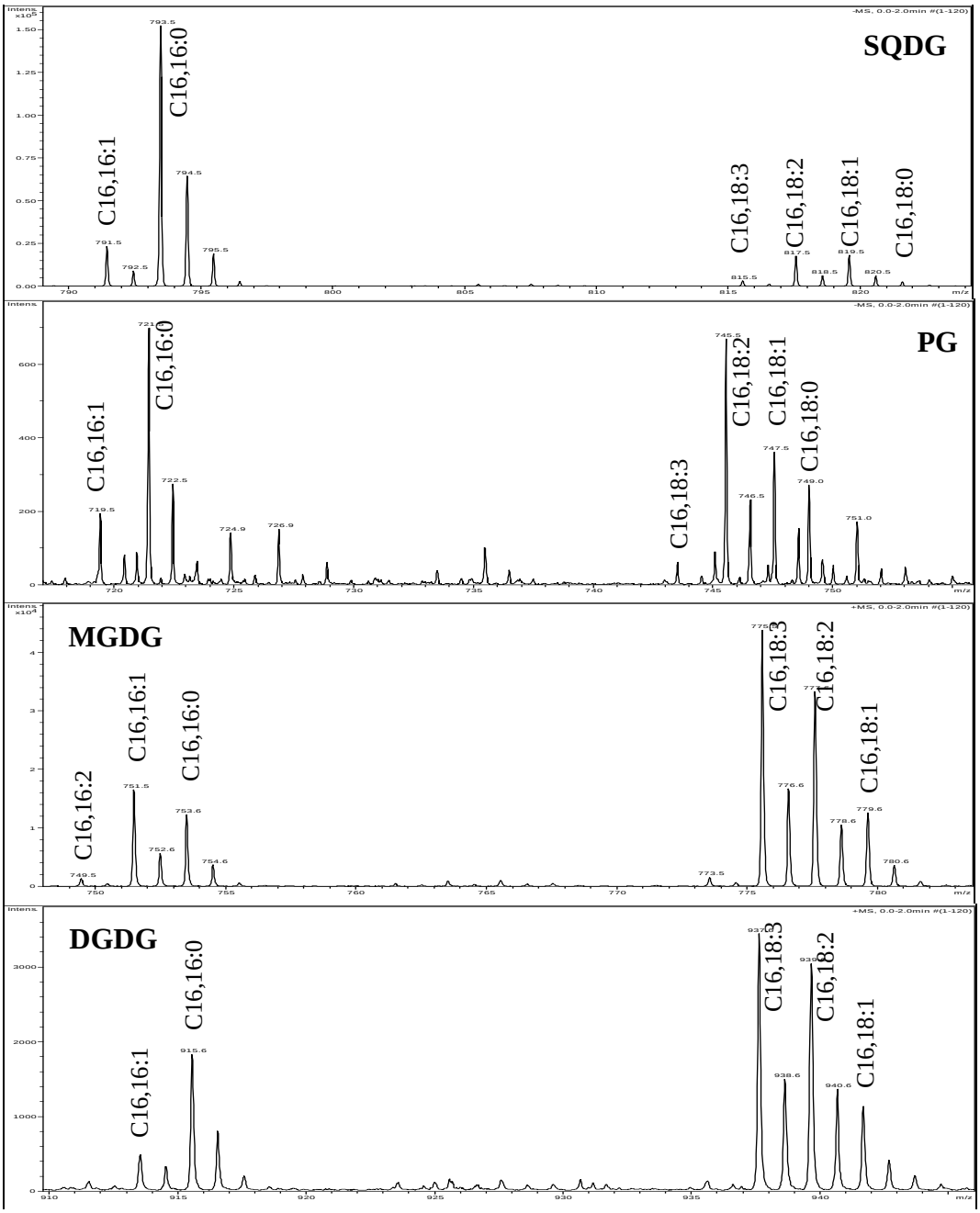

Figure 2.5. Identification of each DAG group (as separated by TLC) by LC-MS. C16, 18:3 denotes one C16 chain and one C18 chain with a total of three double bonds.

***Typical fatty acid profile of* Synechocystis.** A typical FAME chromatogram of wild-type *Synechocystis* PCC6803 is shown in Figure 2.6. C16:0 (the unsaturated member of the palmitoyl fatty acid group) was the predominant fatty acid in *Synechocystis* PCC 6803, constituting about 60% of the total fatty acids (by wt.). Other abundant fatty acids were C16:1 (~9.5%), C18:0 (~1.2%), C18:1 (~2%), C18:2 (~9.8%), and C18:3 (~16.5%). Some other natural fatty acid groups – such as C16:2, C17:0, and C18:4 – were detected in trace amounts.

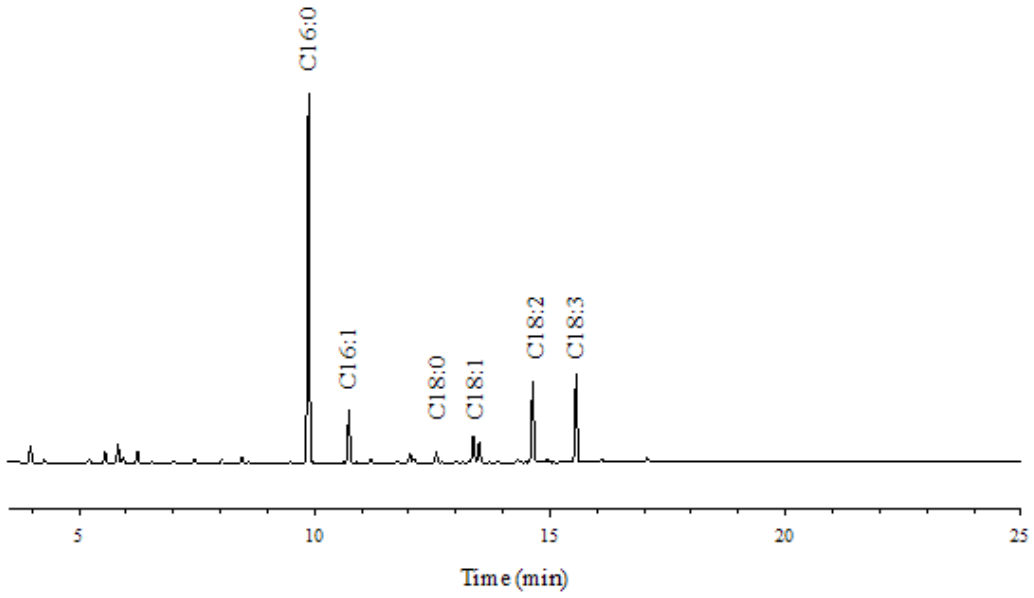

Figure 2.6. Typical FAME peaks of *Synechocystis* PCC 6803. C16:0 (palmitic acid) is the dominant component.

Comparison of wild-type Synechocystis PCC 6803 with mutant-type Synechocystis High VIPP. When the protein for producing thylakoid membrane — VIPP-1 — was over expressed, the lipid content in mutant *Synechocystis* High VIPP was significantly enriched (Aseeva et al., 2004; Westphal et al., 2001). Under similar cultivation and extraction (Folch method) conditions, the lipid content in *Synechocystis* High VIPP was more than doubled that of wild type *Synechocystis* sp. PCC 6803 (i.e., 8.80 ± 0.24% as FAMEs of total biomass, wt. % versus 4.20 ± 0.01%). A detailed comparison of the fatty acid profile indicated that all fatty acid species except C18:0 were enriched to some extent, while C16:0 became even more dominant (> 70% in High VIPP vs. ~60% in PCC 6803). Since diesel fuel requires shorter and saturated fatty acid chain, the higher percent of C16:0 should be more favorable for diesel production (Meher et al., 2006).

2.3.2 FFA quantification

Standards and calibration curve. Figure 2.7a shows a GC chromatogram of FFA mixed standards (C8 – C18), while Figure 2.7b shows the corresponding calibration curves. Obvious linear relationships with $R^2 > 0.9999$ were obtained for 0 to ~100 mg/L for all FFA. However, compared with shorter-chain FFA (C8 – C14), the peaks of longer-chain FFA (C16 – C18) were broader and lower, which reduced the sensitivity of peak response at low concentrations.

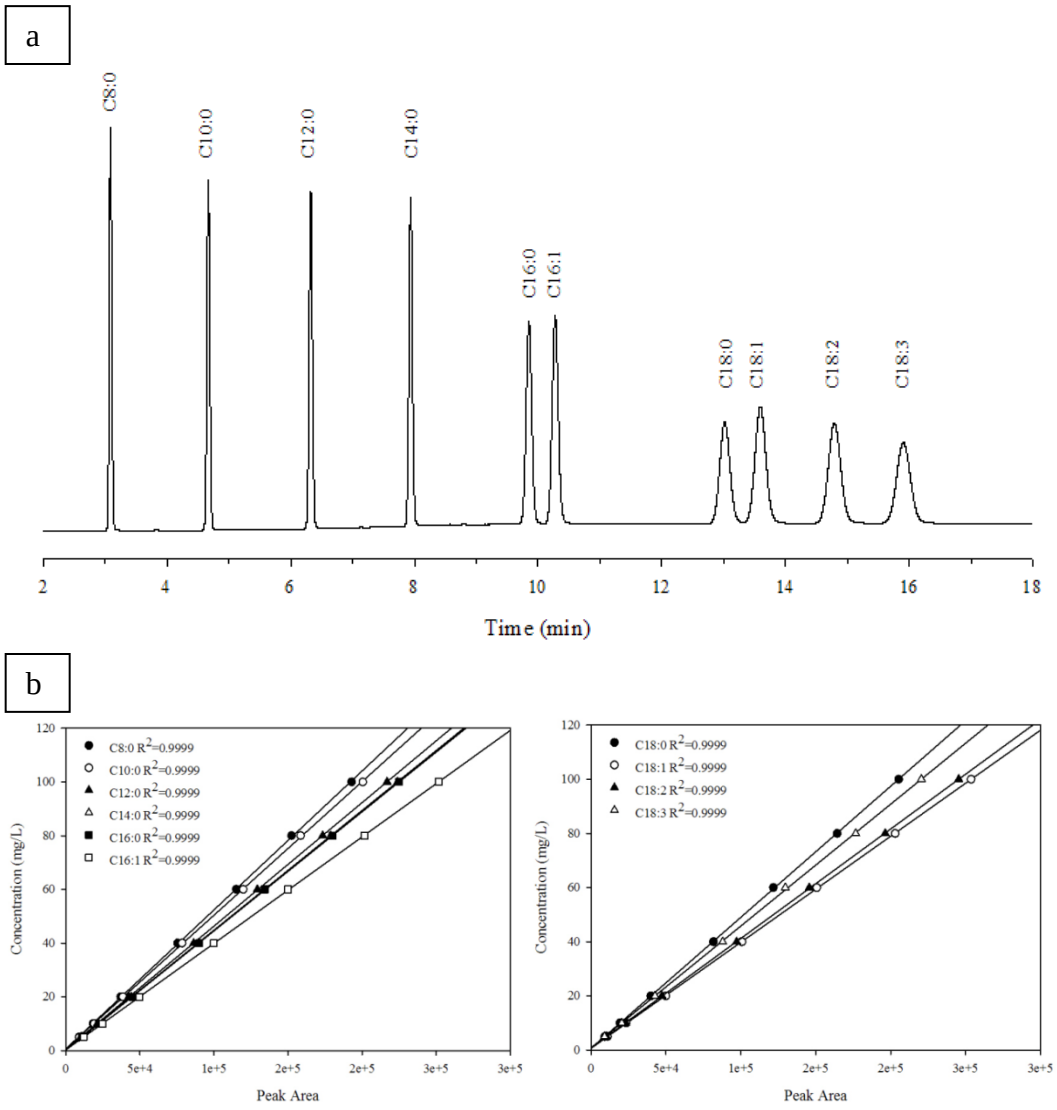

Figure 2.7. ***a.*** GC chromatogram of FFA standards. ***b.*** calibration curve of typical FFA excreted by mutant-type *Synechocystis*.

Extraction efficiency of FFA from medium. Step-by-step evaluation of extraction efficiency by using lauric acid standard indicated that the extraction efficiency was strongly affected by pH of the medium. Under the condition of culture growth and FFA secreation (pH = 8 – 9), without acidification, almost no lauric acid was extracted from the medium extracted by hexane. However, after acidification (pH < 1) and adjustment of the ionic strength (> 1 mol/kg), the solubility of lauric acid in aqueous phase was sufficiently reduced and the extraction efficiency jumped to 87%.

Excreted FFA profile of mutant-type Synechocystis. Typical FFA chromatograms of mutant-type *Synechocystis* TE/Δ*slr1609* and SD243 are shown in Figure 2.8a and Figure 2.8b, respectively. CX:Y denotes fatty acid with X carbons and Y double bonds. In contrast to a domination of C16:0 in intracellular lipids, C12:0 (lauric acid) appears to be the sole dominant FFA (> 90% wt.) excreted by *Synechocystis* TE/Δ*slr1609*. C14:0 also was detected in a small amount (< 10% wt.). Other FFA, such as C16:0, C18:0, C18:2 and C18:3, were in trace amounts.

In contrast to *Synechocystis* TE/Δ*slr1609*, *Synechocystis* SD243 showed a different profile of excreted FFA. C12:0 (~40% wt.), C14:0 (~11%), and C16:0 (~22%) appeared to be the major compounds among all FFA. Other FFA, such as C10:0 (~6%), C16:1 (~5%), C18:0 (~2%), C18:2 (~5%), C18:3 (~7%), also were detectable.

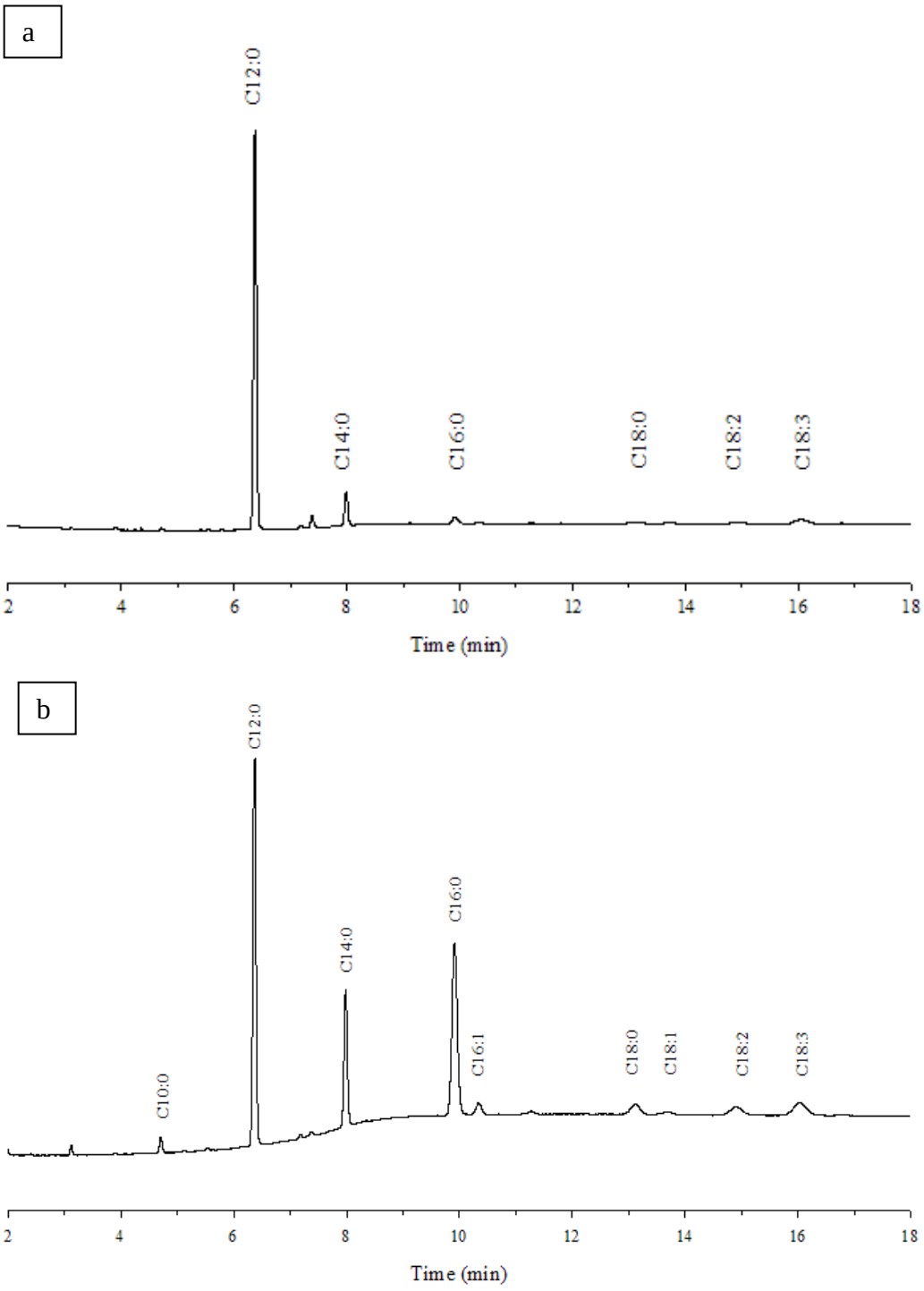

Figure 2.8. Typical FFA peaks of mutant-type ***a.*** *Synechocystis* TE/Δ*slr1609* and ***b***. SD243.

C12:0 denotes lauric acid.

2.4 Conclusions

This Chapter demonstrated that the fatty acids in intracellular lipids of *Synechocystis* PCC 6803 and mutant strain High VIPP can be precisely quantified via transesterification + GC-FID measurement as a form of FAME. When precise lipid profile is demanded, a pre-separation of different DAG groups can be performed by using TLC technique. Long-chain FFA produced by mutant strain *Synechocystis* TE/Δ*slr1609* and SD243 can be directly measured by GC-FID if suitable column and performance conditions are chosen. Direct measurement of long-chain FFA can significantly save the time and labor otherwise needed for derivatization. By genetically mutation, the quality and quantity of lipids and fatty acids of *Synechocystis* can be modified in favor of biofuel production.

3 Evaluation of Methods to Extract and Quantify Lipids from *Synechocystis* PCC 6803[*]

3.1 Introduction

Nonpetroleum-based diesel fuel can be a carbon-neutral substitute for petroleum diesel (Campbell et al., 2009; Pinto et al., 2005; Ragauskas et al., 2006; Rittmann, 2008). Traditional feedstock for nonpetroleum diesel includes vegetable oil and animal fat. Unless these materials come from food residuals, they divert materials from the food supply of human society and already have led to surges in food prices (Karaosmanoglu, 1999). In contrast, feedstock lipids generated from phototrophic microorganisms, i.e., algae and cyanobacteria, have higher areal yields than plants and do not compete with the food supply or contaminate water resources (Antoni et al., 2007; Chisti, 2007; Hu et al., 2008; Kim et al., 2010).

Although eukaryotic algae and prokaryotic cyanobacteria can be used to generate raw materials for nonpetroleum-based diesel production, cyanobacteria have certain advantages over algae. First, lipid accumulation in oleaginous algae is mostly achieved by either imposing stress (i.e., adverse environmental conditions) or adding sugar (Li et al., 2007; Miao and Wu, 2006). In contrast, enrichment of lipids in cyanobacteria can be accomplished by over-expressing thylakoid membranes, which are positively correlated with photosynthetic rate

[*] This chapter was published as Sheng, J., Vannela, R., Rittmann, B.E. 2011. Evaluation of methods to extract and quantify lipids from *Synechocystis* PCC 6803. *Bioresource Technology*, **102**(2), 1697-1703.

and biomass-production rate (Liberton et al., 2006; Mullineaux, 1999); thus, the highest density of lipids in cyanobacteria biomass occurs together with the highest biomass-production rate. Second, cyanobacteria are much more amenable to metabolic engineering to improve lipid content beyond that of the wild type (Kaneko et al., 1996). For example, the entire genome sequence of *Synechocystis* PCC 6803 is published, yielding precise information for gene modifications for a variety of metabolic pathways to optimize quality and quantity of lipids for nonpetroleum-based diesel production (Aseeva et al., 2004; Nakamura et al., 1998; Vermaas, 1996; Westphal et al., 2001).

Lipids in algae, vegetable, and animal tissue are mainly triacylglycerols (TAG). Lipid extraction from these materials is well studied (Fajardo et al., 2007; Lee et al., 2010b; Lee et al., 1998; Molina Grima et al., 1994). Methods based on using chloroform + methanol, such as the Folch and Bligh & Dyer methods, have been widely used for lipid extraction from animal tissue, plants, and algae (Bligh and Dyer, 1959; Folch et al., 1957; Iverson et al., 2001; Liu et al., 2005; Smedes and Thomasen, 1996). While these methods usually are effective, they have a serious drawback, because chloroform has been classified as Group B2 — possibly carcinogenic — by the U.S. EPA (Andersen et al., 2000); thus, large-scale lipid extraction using these methods is precluded by environmental and health risks. For this reason, ethanol, isopropanol, butanol, methyl *tert*-butyl ether (MTBE), acetic-acid esters, hexane, and various combinations have been investigated as less-toxic substitutes for lipid extraction (Fajardo et al., 2007; Lee et al., 1998; Lin et al., 2004; Miao and Wu, 2006; Molina Grima et al., 1994; Xu

et al., 2006). Additionally, direct transesterification (i.e., with no pre-extraction treatment) for biodiesel production has been investigated at small scale (Lepage and Roy, 1984; Liu and Zhao, 2007; Tran et al., 2009). Accelerated solvent extraction (ASE), using heat or pressure, also has been used to maximize lipid recovery, shorten extraction time, and recover solvent (Cooney et al., 2009).

Compared to lipid extraction from algae, little work has been performed on extraction of lipids from cyanobacteria, which are mostly diacylglycerols (DAG). The experience from the previous work on TAG may be misleading, because algae lipids and cyanobacteria lipids differ in important ways that were illustrated in Figure 2.1 of Chapter 2. First, the DAG (Figure 2.1a) are much more polar than the TAG (Figure 2.1b) (Weier et al., 2005). Second, DAG in cyanobacteria are mainly located throughout the cytoplasm in thylakoid membranes, while TAG are usually deposited in densely packed lipid bodies in the algae (Hu et al., 2008). Third, membrane DAG may be associated with protein and photosynthesis components by hydrogen bonding, which may interfere with extraction of DAG (Gabashvili et al., 1998; Mullineaux, 1999). Fourth, despite the Gram-negative structure of cyanobacteria, their peptidoglycan layer and the outer membrane are considerably thicker than for most Gram-negative bacteria. The degree of cross-linking between peptidoglycan chains within the murein also is far higher than those in most other Gram-negative bacteria, which results in more resistance to organic-solvent penetration to release intracellular lipids (Hoiczyk and Hansel, 2000). For these reasons, efficient extraction of DAG in cyanobacteria may require a different solvent or solvent system than that for TAG.

Interactions between solute and solvent can be assessed by several indicators: e.g., the dipole moment, solubility parameter, and polarity index (Lalman and Bagley, 2004). The dipole moment measures the polarity of a molecule as a net sum of the dipole moments of its polar bonds. The solubility parameter reveals the relationship of internal energy (by adding energies from dispersion bonds, polar bonds, and hydrogen bonds) of solvents and solutes through the concept that molecules having the same cohesive energy density (CED) are most effective in attracting and interacting each other (Hansen and Erickson, 1969). In some cases, the hydrogen-bond energy is important in its own right. The polarity index is defined as the measure of the ability of the solvent to interact with various polar test solutes, and it increases with solvent polarity (Snyder, 1974).

In this work, we used wild-type *Synechocystis* PCC 6803 as a feedstock for lipid extraction. We investigated a wide range of solvents and solvent mixtures that have been reported for lipid extraction from other feedstock sources. The over-arching purpose of this study was to identify the most suitable solvent or solvent mixture for high-throughput analysis for bench-top research and large-scale application. For all measurements, we converted extracted lipids to fatty acid methyl esters (FAME) via acid-catalyzed transesterification for assaying the lipid quality and quantity. We used transmission electron microscopy (TEM) to support and illustrate the mechanistic information associated with crude lipid extraction. Finally, we computed the indicators of solute/solvent interactions to

help explain why certain solvents are more or less efficient for extraction of DAG versus TAG.

3.2 Materials and methods

3.2.1 Cell cultures

We obtained wild-type *Synechocystis* PCC 6803 from Dr. W. F. J. Vermaas of Arizona State University. We maintained the pure strain on sterile BG-11 plates with 10-mM TES-NaOH (pH 8.0) (TES is N-tris(hydroxymethyl)methyl-2- aminoethanesulfonic acid), 1.5% agar, and 0.3% sodium thiosulfate (Rippka et al., 1979; van de Meene et al., 2006). We collected and transferred colonies to a 250-mL autoclaved flask containing 100 mL sterile BG-11 medium and allowed PCC 6803 to grow for 4 to 5 d at a light intensity of 100 µmol photons/m^2-s and a constant temperature of 30^{o}C. We then transferred biomass from the liquid culture into a 25-L carboy holding 20 L of sterile BG-11 medium to which sterile air (filtered by a glass-fiber filter) was sparged into the bottom through a pipette at a rate of 10 L/h to mix the culture and provide CO_2 for cell synthesis. We harvested biomass after 1 to 2 weeks, when sufficient biomass was available.

3.2.2 Cell harvest and lyophilization

We harvested the cells by filtration using a Millipore Pellicon Cassette (0.45µm) and then concentrated the biomass further by centrifugation (Beckman Coulter, Avanti J-26 XPI) at 15000 *g* for 15 min. We suspended the cell pellet in

deionized water and re-centrifuged two times to remove residual medium. We then lyophilized (Labconco FreeZone) the cell pellet at -50^{o}C under a vacuum for 2 d until the weight of biomass became constant. We ground the dried biomass into a powder with an agate mortar pestle and stored the powder at -80^{o}C until use. We used one source biomass powder (from the same batch of culture) for all the experiments reported in this study.

3.2.3 Lipid extraction

For lipid extraction using solvents, we used 15 ± 0.2 mg of lyophilized biomass powder, which corresponded to approximately 100 mL of culture at OD_{730} = 0.8. Table 3.1 shows the 14 different solvents and solvent combinations that we tested. The combinations included the Bligh & Dyer (chloroform:methanol:water = 1:2:0.8, v/v) (Bligh and Dyer, 1959) and Folch (chloroform:methanol = 2:1, v/v; solvent:sample = 20:1, v/v) (Folch et al., 1957) methods, along with less-toxic substitutes that have been reported as efficient for extraction of TAG from plant and animal tissues and algae. All solvents were purchased from Sigma-Aldrich (St. Louis, MO) and were HPLC grade. Only glass containers were used for organic solvent handling to prevent contamination. We performed all experiments in duplicate.

Table 3.1. Solvents and solvent mixtures used in this study for lipid extraction from dried *Synechocystis* PCC 6803 biomass

Solvent	Reference
Chloroform/Methanol 2:1, solvent:sample > 20:1 (v/v*) (Folch Method)	Folch et al. (1957)
Chloroform/Methanol/Water 1:2:0.8 (Bligh & Dyer Method)	Bligh and Dyer (1959)
Methanol/MTBE 1.5:5	Matyash et al. (2008)
Hexane/Ethanol 1:2.5	Molina Grima et al. (1994)
Hexane/Ethanol 1:0.9	Molina Grima et al. (1994)
Hexane/Isopropanol 2:3	Molina Grima et al. (1994)
Hexane/Isopropanol 3:2	Lee et al. (1998)
Acetic ester/Ethanol 1:1	Lin et al. (2004)
Acetic ester/Ethanol 2:1	Lin et al. (2004)
Methanol	Smedes and Thomasen (1996)
Ethanol	Fajardo et al. (2007)
Isopropanol	NA**
Butanol	Molina Grima et al. (1994)
Hexane	Miao and Wu (2006); Xu et al. (2006)
Direct transesterification (No solvent extraction)	Lepage and Roy (1984); Liu and Zhao (2007); Tran et al. (2009)

* All ratios are v/v

** None found in the literature.

To maximize the possibility to achieve high extraction yields, we mixed the powder sample with 3 mL of solvent (or solvent combination); this maintained a solvent:sample ratio of at least 20 (v/v). First, we mixed the biomass-powder sample with solvent(s) and vortexed (VWR Vortex Mixer) the mixture for 24 h at room temperature. Secondary extraction of biomass was not necessary, as one-time extraction was sufficient enough to reach more than 97% of maximal recovery for each extraction method (Figure 2.3 of the Chapter 2). After the extraction step, we filtered the solvent-biomass mixture through a 0.45-µm PTFE membrane. We did not add water during phase separation (purification), because we used FAME to analyze specifically for lipids. We evaporated the filtrate completely under N_2 (Labconco RapVap N_2 evaporation system) to eliminate residual solvent, maintaining the evaporation temperature below 60^{o}C to prevent lipid loss (Cantrell and Walker, 2009).

We also performed Soxhlet extraction by using a Soxtherm system (Gerhardt, Germany). During the extraction, we heated solvent/solvent systems to 200^{o}C. The full extraction cycle took 2 h. After extraction, we evaporated residual solvent as described above for further transesterification.

3.2.4 Transmission electron microscopy

We initially fixed cells in 2% glutaraldehyde in 50 mM $NaPO_4$, pH 7.2, and post-fixed them with 1% osmium tetroxide in the same buffer. Following acetone dehydration, the cells were infiltrated and embedded in Spurr's epoxy resin and polymerized at 60°C for 36 h. We cut 60-nm sections and post-stained

in uranyl acetate and lead citrate. We generated images on a Philips CM12 TEM operated at 80 kV with a Gatan model 791 camera.

3.2.5 Separation of major lipid groups

We performed thin-layer chromatography (TLC) according to Sato and Murata (1988) and Christie (1993) to separate major DAG groups in *Synechocystis*. Two-dimensional TLC employed chloroform:methanol:water (75:25:2.5 by volume) in the first development and chloroform:methanol:acetic acid:water (80:9:12:2 by volume) in the second (perpendicular) development. Typical separation results were shown in Figure 2.4 of Chapter 2. We identified lipid groups by Electrospray Ionization Mass Spectrometry (ESI-MS) (Han and Gross, 2005).

3.2.6 Transesterification and quantification of fatty acid methyl esters

We performed transesterification of the dried crude lipid using a method modified from Sato and Murata (1988) and Liu et al. (2005). Briefly, we added 1 mL of 3-N methanolic HCl (Supelco, St. Louis, MO) to the dried lipid in a test tube and heated it in a water bath at 85^{o}C for 2.5 h. After cooling the mixture to room temperature, we added 0.5 mL DI water and 1 mL of hexane and mixed the contents well by hand, collected the hexane layer containing the transesterification FAME, and extracted the remaining methanol/water two times again with 1 mL hexane. We pooled the three 1-mL volumes of hexane prior to GC analysis. By measuring the FAME content in each extract of serial extractions,

we found that over 99% of FAME was recovered after three hexane extractions (as shown previously in Table 2.4 of Chapter 2).

We also performed direct transesterification without prior extraction. For this, we used a 15 ± 0.2 mg lyophilized biomass powder and transesterified it directly (Lepage and Roy, 1984; Tran et al., 2009) by following the procedure given above.

We identified and quantified FAME using gas chromatography (Shimadzu GC 2010) equipped with a Supelco SP-2380 capillary column (30 m × 0.25 mm × 0.20 μm) and flame ionization detector (FID). Operating conditions were as follows: split ratio 1:10; inject volume 1 μL; helium carrier gas with constant linear velocity 20 cm/s; H_2 40 mL/min, air 400 mL/min, make up gas (helium) 30 mL/min; injector and detector temperature 240^{o}C; and oven temperature started at 140^{o}C for 1 min and increased at a rate of 4^{o}C/min to 220^{o}C. The Supelco 37-Component FAME Mix standard (Supelco, St. Louis, MO) provided the calibration curve for each FAME compound. We identified the peaks from a sample by comparing retention times with those of standard compounds, and we also confirmed the identities by GC-MS. Compound concentrations in samples were quantified based on the area under the chromatogram peak in comparison with the standards.

3.2.7 Molecular modeling of solute/solvent interactions

In order to investigate the likely impacts of molecular properties, we calculated the dipole moments and Hansen's 3-D solubility parameters (including

the hydrogen-bond energy) of each solvent and solvent mixture in comparison with the major DAG groups of *Synechocystis.* We employed Chem3D V11.0 with the MOPAC interface (CambridgeSoft, Cambridge, MA) and Molecular Modeling Pro (ChemSW, Fairfield, CA). A purchase link can be found at http://www.cambridgesoft.com/software/details/?fid=17&pid=228 (Chem3D) and http://www.chemsw.com/13052.htm (Molecular Modeling Pro). We retrieved the solubility parameters and polarity indices of all solvents from literature (Byers, 2003; Gupta et al., 1997; Snyder, 1974; Speight, 2005) and computed the solubility parameter and polarity index of solvent combinations from the volume fractions of each component using equations (3.1) and (3.2), respectively:

$$\delta(\text{mixture}) = \phi_1\delta_1 + \phi_2\delta_2 + \ldots \quad (3.1)$$

$$\text{PI}(\text{mixture}) = \phi_1\text{PI}_1 + \phi_2\text{PI}_2 + \ldots \quad (3.2)$$

where ϕ is volume fraction of a mixture component 1 or 2, δ is the solubility parameter, and PI is the polarity index.

3.3 Results and discussion

FAME quantification results after lipid extraction using the different solvent systems are shown in Figure 3.1. The Folch (4.20 ± 0.01%, wt. %) and Bligh & Dyer methods (4.22 ± 0.00%), both using chloroform + methanol, had the highest lipid yields in terms of total amount of fatty acids in the dry biomass. The water content in the Bligh & Dyer method played a quite important role in extraction. Decreasing the water content to the same level as that of the Folch method lowered the lipid-extraction efficiency to 4.00 ± 0.03%. Although these

chloroform + methanol-based methods were developed for extracting neutral lipids like TAG, we show that they also are suitable for extracting the polar lipids that exist in *Synechocystis*. Because they had the highest extraction efficiencies, the Folch or Bligh & Dyer methods can be considered the "gold standards" for bench-scale lipid extraction from *Synechocystis*. However, the toxicity of chloroform and methanol make them unsuitable for large-scale extraction, which also makes it essential to compare the efficiencies of other solvent systems.

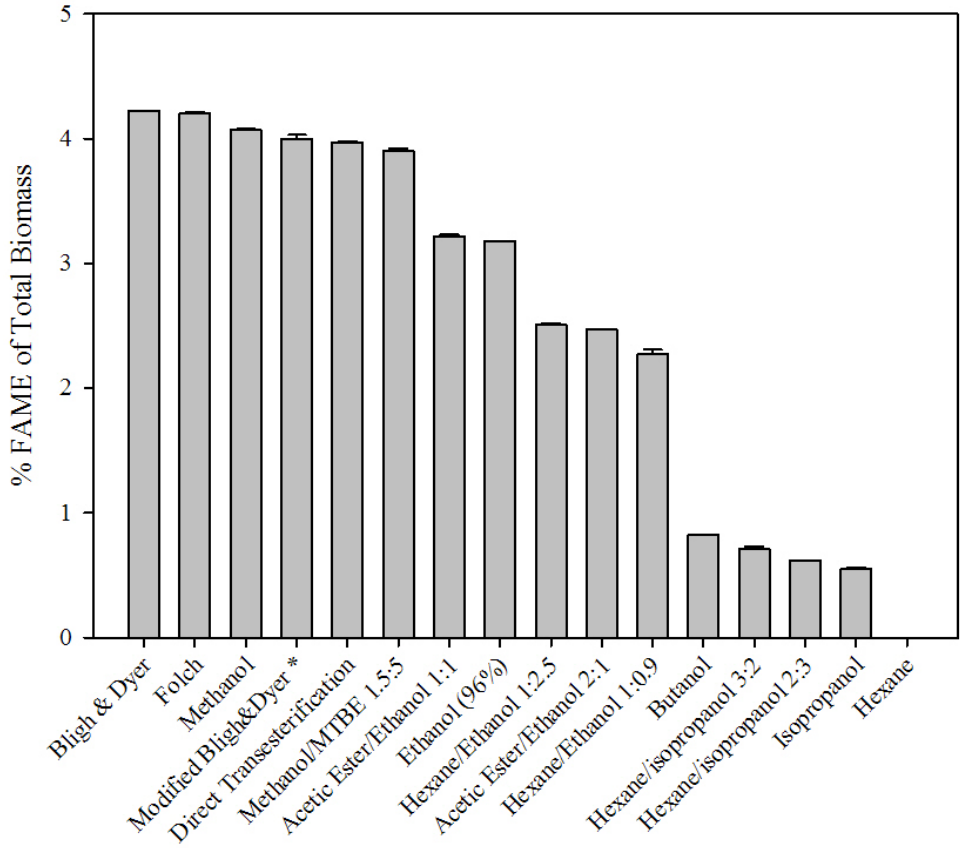

Figure 3.1. Percent FAME of total biomass after total lipid was extracted using different solvents/solvent combinations from *Synechocystis* PCC 6803.
All ratios are v/v. * Modified Bligh & Dyer refers to decreasing water content to the level of Folch method.

Several other methods achieved lipid-extraction efficiencies of at least 93% of that achieved by the Folch and Bligh & Dyer methods. Even though it was reported to be ineffective for extracting TAG (Smedes and Thomasen, 1996), methanol alone had a extraction yield of 4.07 ± 0.01%, or 96% of the *Synechocystis* lipids extractable by Folch and Bligh & Dyer methods. The methanol/MTBE solvent system also gave a similar yield (3.90 ± 0.02%). While methanol may be too toxic to use alone (U.S. EPA, 2009), the methanol/MTBE system may be a better candidate for large-scale extraction, since MTBE reduces methanol usage and lowers the toxicity and environmental impact of the extraction process.

Direct transesterification of biomass (without a solvent-extraction step) also yielded 3.97 ± 0.01% fatty acid mass/dry biomass, corresponding to 94% of the best yield found with solvent extraction before transesterification. While direct transesterification combines lipid extraction and biodiesel production into one step, it requires a more extensive water removal from biomass, as water interferes with the transesterification reaction and phase separation (Lepage and Roy, 1984). Meanwhile, residual water remained in biomass sample due to incomplete drying may require acid catalysis for transesterification, which is more difficult at large scale than base catalysis (Belarbi et al., 2000). For these reasons, direct transesterification has not been applied at large scale.

Other solvents/solvent systems — including acetic ester, ethanol in combination (1:1), and ethanol (96%) alone — gave lower lipid yields, around 3.2% of the dry biomass. Isopropanol, butanol, hexane, and combinations thereof

showed very poor lipid extraction capabilities (< 2.5%) from *Synechocystis* biomass. Although suitable for extraction of non-polar lipids like TAG (Fajardo et al., 2007; Lee et al., 1998; Lin et al., 2004; Miao and Wu, 2006; Molina Grima et al., 1994; Xu et al., 2006), these solvents proved to be inefficient for extraction of DAG from *Synechocystis*.

When heated to 200^{o}C during Soxhlet extraction, hot isopropanol yielded 84% lipid recovery of that achieved by the Folch method, a major improvement (over 13%) in comparison with no heat (Figure 3.2). However, heating gave no significant increase of lipid yield with the Folch solvent, methanol, or MTBE; similar findings have been reported in other cases (Schafer, 1998). Heat is not helpful for these solvent(s), as nearly all the lipids can be extracted out at room temperature. Although heating may promote solvent recovery and shorten extraction time, it should be carefully considered for large-scale application, as it is a large energy burden for the whole process.

We obtained TEM images before and after several types of extraction. The images are provided in Figure 3.3 for cells without extraction (Figure 3.3a) against cell residuals after Folch extraction (Figure 3.3b), isopropanol extraction (Figure 3.3c), and hexane extraction (Figure 3.3d). After isopropanol and hexane extractions, the cell's membrane system was only mildly damaged. The intracellular thylakoid membrane was still in a well aligned form, which indicates the inefficiency of these two solvents to penetrate into the cell and extract membrane lipids. However, after Folch extraction, the outer S-layer was completely dissolved, although the peptidoglycan layer and outer membrane were

still identifiable. The thylakoid membranes were severely disrupted, which indicates successful penetration of chloroform + methanol. Other cell organelles, such as the carboxysomes, also were disrupted during Folch extraction. The more successful penetration and destruction of intracellular membranes could be one of the reasons of the maximum lipid recovery by the chloroform + methanol-based method.

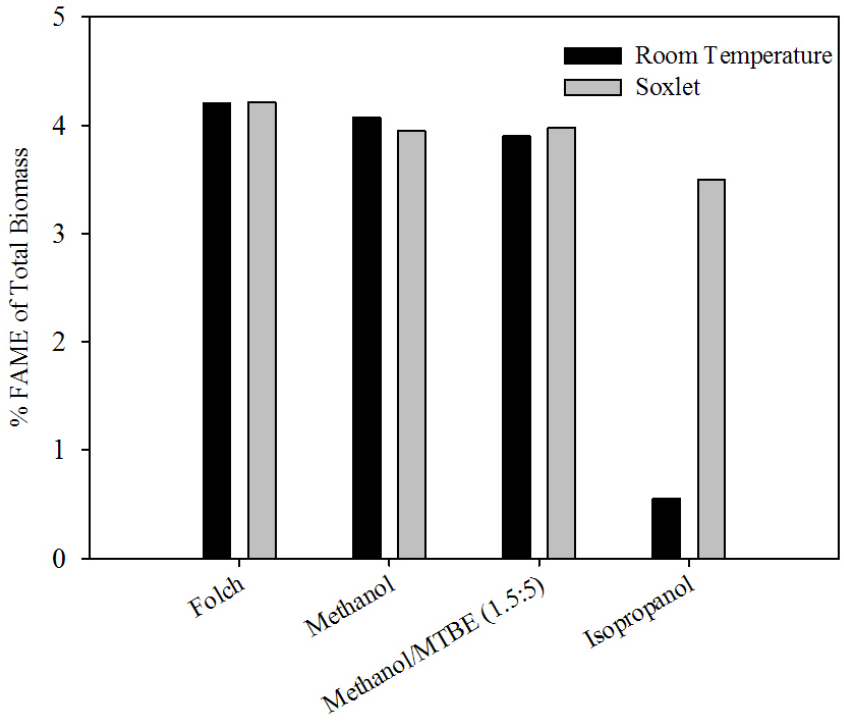

Figure 3.2. Comparison of regular extraction (room temperature) and Soxlet extraction (heated to 200^{o}C).

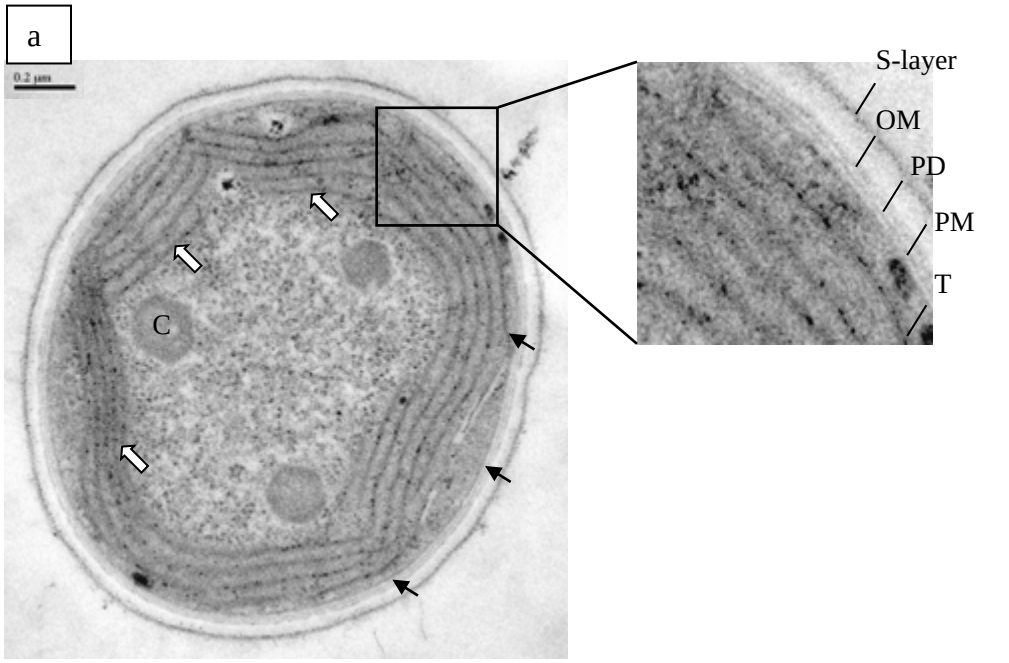
a
S-layer
OM
PD
PM
T
C

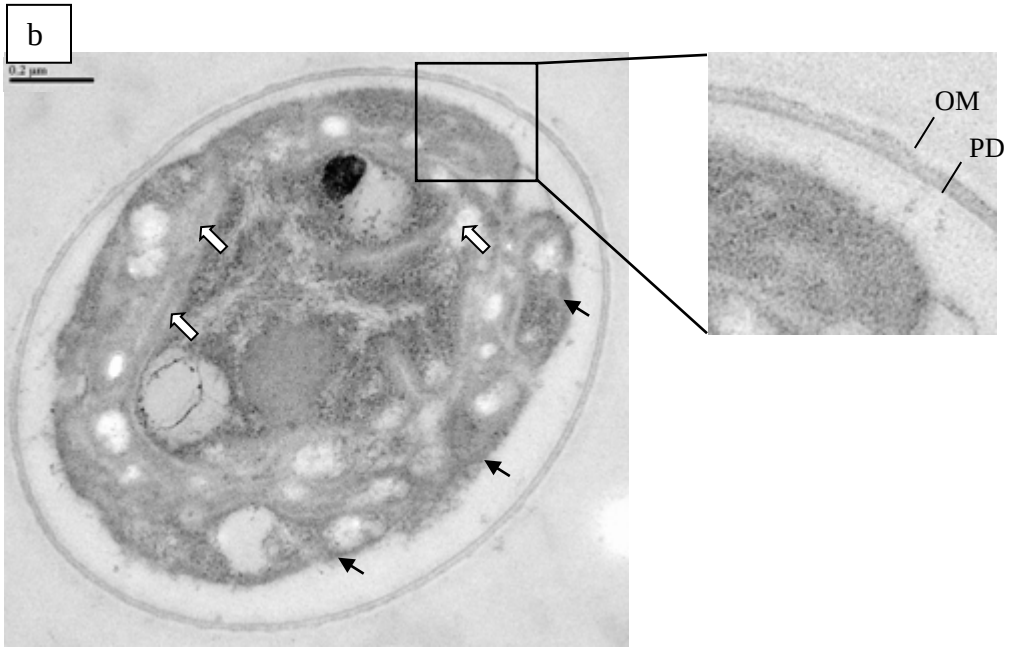
b
OM
PD

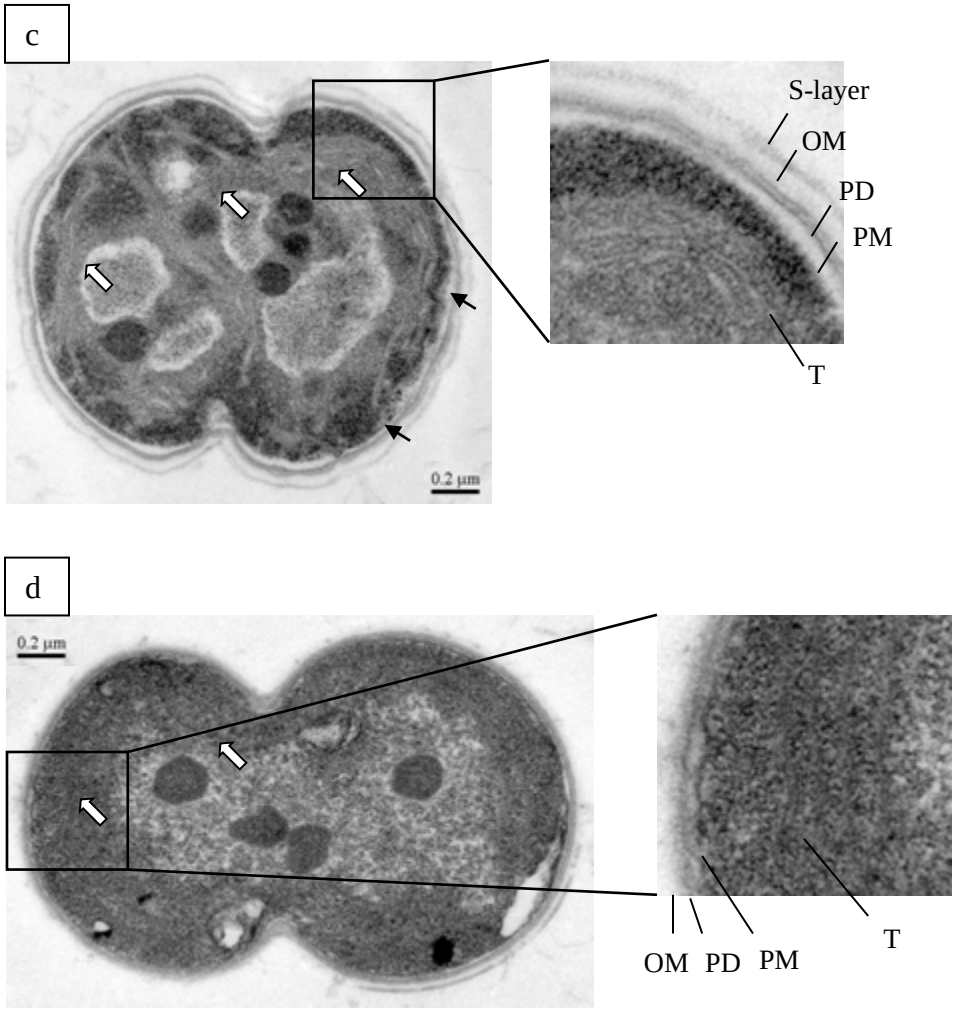

Figure 3.3. Comparison of an intact healthy cell with no extraction (***a***) and cell residual after Folch-method extraction (***b***), isopropanol extraction (***c***), and hexane extraction (***d***).

Black arrows show cytoplasm membrane. White arrows show disruption and loss of thylakoid membrane. OM: Outer membrane; PD: peptidoglycan layer; PM: plasma membrane; T: thylakoid membranes; C: carboxysome.

The similarity of chemical properties between solvent and solute also should be a factor that determines extraction efficiency. Figure 3.4 and Table 3.2 compare the dipole moment, solubility parameter, and polarity index of the solvents we tested with the values for the DAG and TAG. *Synechocystis* DAG have similar dipole moment (1.63 – 4.85 Debye vs. 1.62 Debye) and solubility parameter (20.04 – 23.10 $(J/cm^3)^{1/2}$ vs. 23.81 $(J/cm^3)^{1/2}$) as the chloroform + methanol solvents. The high polarity index value (4.65 – 5.66) of the chloroform + methanol solvents also demonstrates their stronger capability of dissolving much polar solutes like DAG. On the other hand, *n*-hexane, a typical non-polar solvent, has dipole moment and polarity index around 0, and this correlates to its inefficiency of extracting DAG from *Synechocystis*. Despite similarities in dipole moment and solubility parameter with DAG molecules, butanol and isopropanol were inefficient in lipid extraction from *Synechocystis* due to their lower polarity index value, which indicates their weaker ability of interacting with polar solutes than chloroform + methanol solvents.

The difference of extraction efficiency may also be attributed to hydrogen bonding associating with membrane lipids. The hydrogen bonding energies of DAG, which are 9.90 – 12.48 $(J/cm^3)^{1/2}$, are double to triple of those for TAG (4.90 $(J/cm^3)^{1/2}$) (Table 3.2). This stronger hydrogen bonding between membrane lipids and proteins may need to be disrupted during extraction (Cooney et al., 2009). According to Speight (2005), methanol interacts strongly with hydrogen bonds, while butanol, isopropanol, and hexane have little interaction with hydrogen bonds. This difference in ability to interact with hydrogen bonds also

could be one of the reasons of their vast differences in performance of extracting DAG from *Synechocystis*.

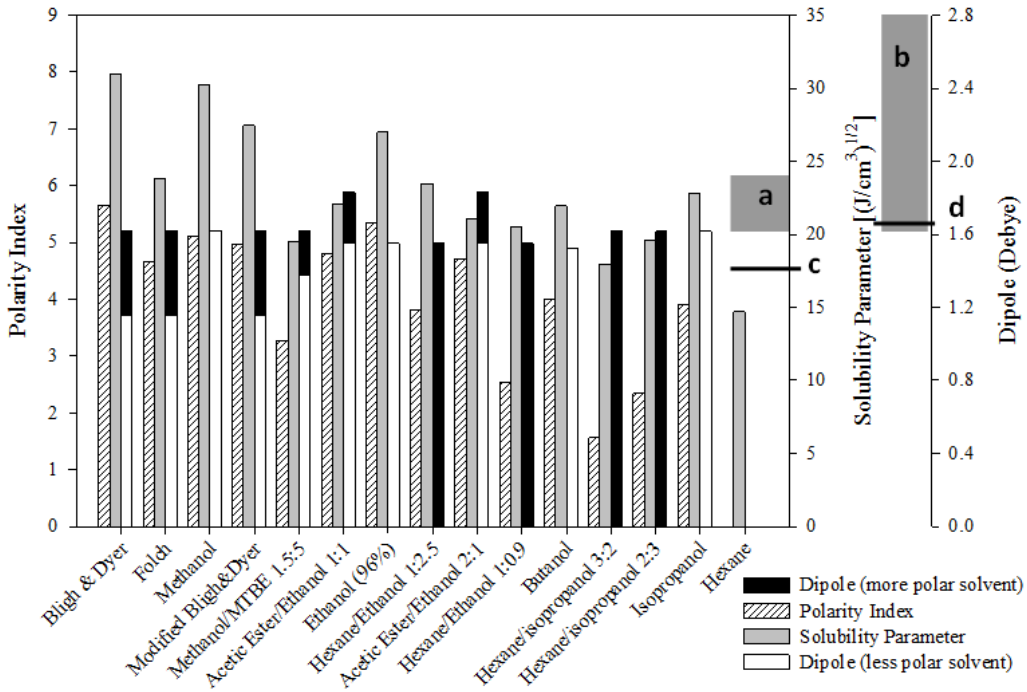

Figure 3.4. Comparison of dipole, solubility parameter, and polarity index of solvent systems, major DAG in *Synechocystis* PCC 6803, and TAG.
Area ***a*** and Line ***c*** are the solubility-parameter ranges of major DAG in *Synechocystis* and TAG, respectively. Area ***b*** and Line ***d*** are the dipole moment ranges of major DAG in *Synechocystis* and TAG, respectively.

Table 3.2. Chemical properties of solvents, DAG, and TAG

	Dipole moment (Debye)[a]	Solubility parameter $(J/cm^3)^{1/2}$ [b]	H-Bonding $(J/cm^3)^{1/2}$ [c]	Polarity index[d]	Log*P*[e]	Water solubility (%, pH 7, 25 °C)[f]	EPA toxicity[g]
Solvent							
Hexane	0	14.71	Poor	0	4	0.001	NA*
MTBE	1.373	15.14	NA	2.5	0.94	4.2	NA
Isopropanol	1.615	22.81	Poor	3.9	0.05	miscible	NA
Butanol	1.521	21.95	Poor	4	0.84	7.81	NA
Chloroform	1.155	18.79	NA	4.1	1.97	0.8	B2
Ethyl Acetate	1.831	18.06	Moderate	4.4	0.73	8.3	NA
Methanol	1.621	30.23	Strong	5.1	-0.74	1116	NA
Ethanol	1.55	26.12	Strong	5.2	-0.3	miscible	NA
DAG & TAG							
SQDG (C16:0;C16:0)	2.626	21.96	12.48	--	13.15	3.8	--
PG (C16:0;C16:0)	1.63	20.04	9.90	--	13.03	20	--
DGDG (C16:0;C18:3)	3.352	23.1	14.69	--	10.35	0.02	--
MGDG (C16:0;C18:3)	4.853	21.06	11.99	--	11.36	0.01	--
TAG (3*C16:0)	1.71	17.44	4.90	--	NA	NA	--

[a] calculated by Chem3D

[b, c] values for solvents were retrieved from Lange et al., 2005, values for DAG and TAG were calculated by Molecular Modeling Pro

[d] retrieved from Gupta et al., 1997, Snyder, 1974

[e, f] retrieved from Lange et al., 2005

[g] retrieved from Andersen et al., 2000

* None found in the literature.

Non-lipid materials, such as proteins, polysaccharides, and associated pigments, also may be extracted together with lipids, and this might interfere with fuel production or contaminate the final product. To understand the solvent specificity in extracting non-lipid compounds, we measured the dry weight of crude extract after solvent extraction and compared it against the lipid weight. The pure lipid weight was obtained from TLC separation of DAG groups followed by FAME measurement of each DAG group. Calculation of lipid from fatty acid (FAME result), which is shown in Table 3.3, is based on the concept that one mole DAG molecule has two moles of fatty acid groups. For a certain DAG group (SQDG, PG, MGDG or DGDG), although fatty acid group may differ, the non-fatty acid group is the same. The calculation result indicated that the ratio of fatty acids to lipids in *Synechocystis* was approximately 0.7. We then used this ratio to calculate the amount of lipids from the FAME results. The ratio of crude extract to total biomass and that of lipid to crude extract are shown in Figure 3.5. The crude extract constituted less than 20% of the total biomass with each solvent or solvent system. The actual lipid constituted 40 – 60% of the crude extract after Folch or Bligh & Dyer extraction. The less polar solvents, such as ethanol, isopropanol, and butanol, extracted less lipid (~30% of the crude extract), but more non-lipid material. Almost all extracted material from hexane extraction was non-lipid materials. The less-polar solvents have two disadvantages: lower lipid yield and extra purification to prevent negative effect of non-lipid impurities in the fuel product.

Table 3.3. Calculation of lipid (DAG) content from fatty acid (FA) concentration obtained from TLC separation and GC measurement

Lipid group	FA conc. (mg/L)	FA conc. (mM)	Lipid conc. (mM) (FA:lipid 2:1)	Non FA group conc. (mg/L)
SQDG	**178.45**	**0.657**	**0.328**	**84.37**
C16:0	153.16	0.567		$C_7H_{13}O_8S$
C16:1	10.72	0.040		(MW 257)
C18:1	9.59	0.032		
C18:2	4.97	0.017		
PG	**33.28**	**0.123**	**0.061**	**11.35**
C16:0	27.62	0.102		$C_4H_{10}O_6P$
C18:1	3.83	0.014		(MW 185)
C18:2	1.83	0.006		
DGDG	**63.38**	**0.232**	**0.116**	**41.20**
C16:0	52.90	0.196		$C_{13}H_{23}O_{11}$
C16:1	1.67	0.006		(MW 355)
C18:1	3.51	0.012		
C18:2	2.96	0.010		
MGDG	**241.70**	**0.889**	**0.445**	**85.80**
C16:0	208.74	0.773		$C_7H_{13}O_6$
C16:1	11.72	0.044		(MW 193)
C18:1	5.36	0.018		
C18:2	8.89	0.030		
C18:3	6.98	0.024		
Total	**516.80**			**222.72**
FA/Lipid	**0.70**			

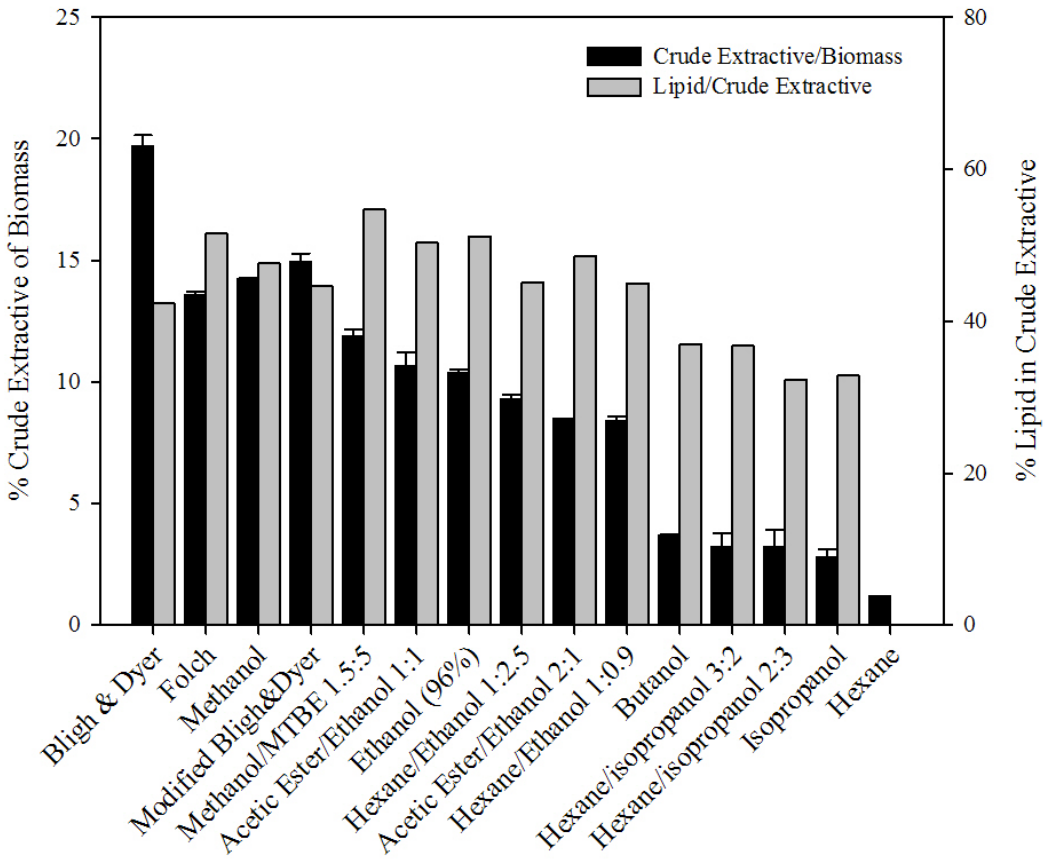

Figure 3.5. Percentage of extractable materials (wt. %) and lipid purity (wt. %) using different solvents and solvent systems.

The lipid content was calculated based on FAME-analysis results, as detailed in Table 3.3.

The fatty-acid compositions of five extracts are presented in Table 3.4, and a typical *Synechocystis* FAME chromatogram was shown in Figure 2.6. C16:0 (palmitoyl fatty acid group) was the predominant fatty acid group in *Synechocystis* PCC 6803, constituting about 60% of the total fatty acids (by wt.). Other abundant fatty acid groups included C16:1 (~9.5%), C18:0 (~1.2%), C18:1 (~2%), C18:2 (~9.8%), and C18:3 (~16.5%). Some other natural fatty acid groups – such as C16:2, C17:0, and C18:4 – were detected in trace amounts. The fatty-acid profiles extracted by Bligh & Dyer, Folch, methanol, MTBE or by direct transesterification were similar, even when the total amounts of lipid extracted differed. For diesel-fuel production, shorter chain and saturated fatty acids are preferred, as they have lower melting points and higher cetane numbers and are less prone to oxidation (Canakci, 2007). The dominance of C16:0 in *Synechocystis* makes it a good feedstock for diesel fuel production.

Table 3.4. Fatty acid profile in *Synechocystis* PCC 6803 extracted by different solvents and solvent systems

	Bligh & Dyer	Folch	Methanol	Direct Trans-esterification	Methanol/ MTBE
% wt. of total fatty acids					
C16:0	60.93 ± 0.02	61.52 ± 0.08	61.50 ± 0.09	60.55 ± 0.01	60.47 ± 0.30
C16:1	9.59 ± 0.00	9.51 ± 0.10	9.42 ± 0.00	9.85 ± 0.04	9.37 ± 0.06
C18:0	1.16 ± 0.03	1.03 ± 0.03	1.19 ± 0.00	1.26 ± 0.01	1.24 ± 0.01
C18:1	1.94 ± 0.16	1.96 ± 0.17	1.86 ± 0.15	1.96 ± 0.15	2.12 ± 0.01
C18:2	9.81 ± 0.03	9.62 ± 0.04	9.69 ± 0.00	9.75 ± 0.03	9.85 ± 0.07
C18:3	16.58 ± 0.08	16.36 ± 0.11	16.35 ± 0.05	16.63 ± 0.06	16.95 ± 0.14
% wt. of biomass					
C16:0	2.57 ± 0.00	2.58 ± 0.01	2.50 ± 0.00	2.40 ± 0.01	2.36 ± 0.02
C16:1	0.40 ± 0.00	0.40 ± 0.00	0.38 ± 0.00	0.39 ± 0.00	0.37 ± 0.00
C18:0	0.05 ± 0.00	0.04 ± 0.00	0.05 ± 0.00	0.05 ± 0.00	0.05 ± 0.00
C18:1	0.08 ± 0.01	0.08 ± 0.01	0.08 ± 0.01	0.08 ± 0.01	0.08 ± 0.00
C18:2	0.41 ± 0.00	0.40 ± 0.00	0.39 ± 0.00	0.39 ± 0.00	0.38 ± 0.00
C18:3	0.70 ± 0.00	0.69 ± 0.01	0.66 ± 0.00	0.66 ± 0.00	0.66 ± 0.00

3.4 Conclusions

The chloroform + methanol-based Folch and Bligh & Dyer methods were most efficient for DAG extraction from *Synechocystis* and can be considered as the “gold standards” for bench-scale analysis. Their superiority was due to their ability to penetrate and disrupt the cell membrane system, polarity being well matched to DAG, and high interaction with hydrogen bonds. Methanol plus MTBE and direct transesterification (with no pre-extraction) had only slightly lower recovery rates; due to their lower toxicity, they may be more appropriate for large-scale industrial processing, although direct transesterification requires more extensive removal of water and acid catalysis, both of which are difficult at large scale. Although efficient for TAG extraction, ethanol, isopropanol, butanol, acetic ester, hexane, and their combinations recovered less lipid and also extracted relatively more non-lipid impurities from *Synechocystis*. The dominance of C16:0 in *Synechocystis* lipids matches the technical specification for diesel fuel production.

4 Effects of Temperature Shifts on Growth Rate and Lipid Characteristics of *Synechocystis* sp. PCC6803 in a Bench-top Photobioreactor[*]

4.1 Introduction

Sustainable energy from cyanobacterial or algal lipids may provide a long-term solution for fossil fuel replacement and increasing concerns about global warming (Czucz et al., 2010; Ragauskas et al., 2006; Rittmann, 2008). Among the candidates, the cyanobacterium *Synechocystis* appears to have excellent potential for large-scale biomass production due to its fast growth rate, naturally high lipid content, ability to be genetically transformed, and robustness towards a wide range of environmental conditions (including salt concentration, pH, temperature, UV light, and carbon dioxide (CO_2) level) (Angermayr et al., 2009; Dismukes et al., 2008; Ogawa and Kaplan, 2003; Ohkawa et al., 2000; Vannela and Verma, 2006; Vermaas, 1996). Nevertheless, large-scale culturing of *Synechocystis* can be challenging when considering the inevitable large swings of outdoor ambient temperature and sunlight intensity. In sunny and arid regions, such as the southwestern United States, day-to-night temperature difference can be as much as 26ºC (47ºF) (Lee and Ho, 2010), and daily average temperature varies by 22°C (40°F) (http://www.weather.com/weather/climatology/daily/USAZ0166). In particular,

[*] This chapter was published as Sheng, J., Kim, H.W., Badalamenti, J.P., Zhou, C., Sridharakrishnan, S., Krajmalnik-Brown, R., Rittmann, B.E., Vannela, R. 2011. Effects of temperature shifts on growth rate and lipid characteristics of *Synechocystis* sp. PCC6803 in a bench-top photobioreactor. *Bioresource Technology*, **102**(24), 11218-11225.

the biomass specific growth rate and the quantity and quality of its lipids can be affected by these changes (Wada et al., 1994).

Light irradiance (LI), ambient temperature, pH, inorganic-C concentrations, and nutrient levels appear to be the most important growth factors for cyanobacteria (Kim et al., 2010). Temperature, in particular, affects the integrity of thylakoid membranes and the quality and quantity of the fatty acids attached to the glycerol backbone of membrane lipids (Murata, 1989). Typically, a temperature effect on the growth of cyanobacteria is related to the activity of photosystem II (PS II), in which the most rate-limiting photosynthetic electron-transport carrier, plastoquinone, and its associated lipid molecules are highly temperature sensitive (Berry and Bjorkman, 1980; Hirano et al., 1981; Wada and Murata, 1990). At temperatures above 40ºC, the most commonly observed effect is the inhibition of primary charge-separation activity of the PS II reaction center and inactivation of oxygen-evolving capability of PS II (i.e., dissociation of Mn^{2+} ions from the photocatalytic center), which leads to excessive production of radical oxygen species that cause peroxidation of polyunsaturated fatty acids and an undesirable non-equilibrium state within the membrane (Enami et al., 1994; Gombos et al., 1992; Klimov and Krasnovskii, 1981). On the other hand, at low temperature, the transition of thylakoid membranes from a liquid crystalline state to more of a gel structure causes damage to the photosynthetic apparatus (Murata, 1989). Temperature-induced changes in membrane permeability and fluidity are other immediate consequences of temperature stress that might cause injury to the cell (Chapman, 1975; Sung et al., 2003).

The change in the degree of unsaturation of fatty acid groups in cyanobacterial lipids is one of the important responses to temperature stress (Gombos et al., 1995; Murata and Wada, 1995). Cyanobacteria are reported to alter desaturation of membrane fatty acids by adding or deleting double bonds onto hydrocarbon chains to compensate for the changes in membrane fluidity and phase-transition temperature (Chapman, 1975). For example, addition of double bonds was reported when cyanobacteria were exposed to 22^{o}C (Wada et al., 1994). In addition, cyanobacteria optimize membrane barrier functions, permeability properties, the activities of membrane-bound enzymes, and signaling mechanisms in response to temperature changes.

The temperature-induced changes to biomass production, lipid quantity, and lipid quality are crucial for large-scale production of biofuels using cyanobacteria. The biomass and lipid production rates directly determine biofuel productivity and economic feasibility. Important lipid characteristics, such as the chain length and unsaturation, influence the quality of derived biofuel product in ways that affect engine performance, combustion characteristics, and gas emissions (Benjumea et al., 2011). In general, lipid unsaturation is an undesired property for a fuel feedstock (Canakci, 2007).

In this study, we systematically studied how the cyanobacterium *Synechocystis* sp. PCC6803 (PCC6803, in short) responds to low and high temperatures. We employed a precisely controlled non-axenic bench-top photobioreactor (BT-PBR) to comprehensively study specific growth rate, biomass productivity, and fatty acid quality and quantity in lipids. The results help

understand the physiological response of PCC6803 and its tolerance in response to drastic temperature shifts. This will be valuable when scaling up in the real application, such as to produce renewable feedstock for liquid transportation fuel.

A team of researchers carried out all aspects of the research. I took responsibility for routine culture maintenance and sampling, performing lipid analyses, interpreting the result, and writing the manuscript/chapter.

4.2 Materials and methods

4.2.1 Bench-top photobioreactor configuration and operation

The configuration of the bench-top PBR was described in detail by Kim et al. (2010) and is summarized briefly here. Figure 4.1 shows a schematic of the bench-top PBR system. The bench-top PBR system consisted of a vertical flat-plate rectangular body made of polymethyl methacrylate plastic and had a liquid working volume of 16 L. An outer-layer water jacket contained water circulating through a water bath (Thermo Scientific *Digital Plus*) for temperature control. A controlled mixture of air and CO_2 was sparged into the reactor through a commercially available gas diffuser at the bottom of the reactor. In addition to turbulence provided by gas bubbling, two liquid-circulation impellers (2-cm radius) on stainless steel bars were installed inside the reactor. Liquid inlet and drain ports were located at the top and bottom of the reactor, respectively, and an advanced 3-way port was used for sampling the reactor from the front panel.

Light panels on both sides each contained eight white-fluorescent lamps (Prolume F24T5/841/HO, Halco lighting technologies, GA) that generated

controlled light irradiance (LI) in the range of 3 to 209 W/m^2 (from each side) as photosynthetically active radiation (PAR). The average ambient LI in the laboratory was 3 W/m^2. The temperature inside the PBR was controlled by altering the water-jacket temperature through a computer-controlled feedback loop linked to a temperature probe located in the center of the PBR culture. Before inoculation, we sanitized the PBR with 0.04% NaOCl (190 mg/L as Cl_2) and 0.2% NaOH for 30 min, followed by two successive rinses with sterile deionized water.

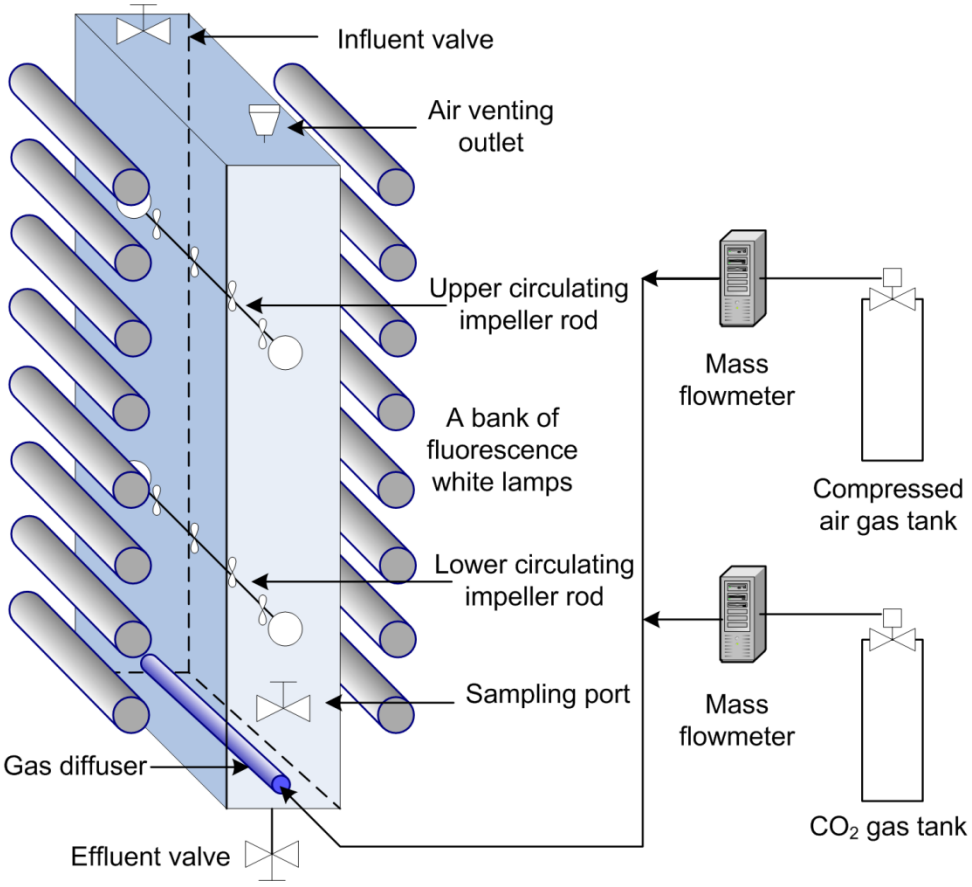

Figure 4.1. Schematic of the bench-scale photobioreactor system (Kim et al., 2010).

4.2.2 Inoculum and culture media

We obtained the mother inoculum of PCC6803 from Dr. W. F. J. Vermaas of the School of Life Sciences, Arizona State University. We maintained a mother inoculum in standard liquid BG-11 medium (Rippka et al., 1979) in a 150-mL Erlenmeyer flask sparged with filtered laboratory air. We used this initial culture to produce larger volumes of 20-L in carboys (Nalgene) sparged with filtered laboratory air at a temperature of 28ºC. For PBR inoculation, we utilized modified BG-11 growth medium with a higher P supply to eliminate phosphorus limitation. Each liter of the modified BG-11 medium contained 1.5 g $NaNO_3$, 200 mg $K_2HPO_4 \cdot 3H_2O$ (5X higher than standard recipe), 80 mg $MgSO_4 \cdot 7H_2O$, 36 mg $CaCl_2 \cdot 2H_2O$, 6 mg citric acid, 6 mg ferric ammonium citrate, 1 mg EDTA disodium salt, 20 mg Na_2CO_3, and 1 mL mixed trace metal solution. Each liter of trace metal solution contained 2.9 g H_3BO_3, 1.8 g $MnCl_2 \cdot 4H_2O$, 0.22 g $ZnSO_4 \cdot 7H_2O$, 0.39 g $Na_2MoO_4 \cdot 2H_2O$, 79 mg $CuSO_4 \cdot 5H_2O$, and 49 mg $Co(NO_3)_2 \cdot 6H_2O$. We autoclaved all culture media (121 ºC, 30 min) before use.

4.2.3 PBR inoculation and temperature experiment

We loaded the PBR with 12 L of modified BG-11 medium plus 4 L of exponential phase PCC6803 inoculum (from a carboy). We set the PBR LI at a constant 108 W/m^2 (total exposed light from both sides of the reactor), set the temperature at 30ºC, and used a flow rate of 10 L/hr of air enriched to 2.5% (v/v) CO_2. We also set the impeller speed at 200 rpm. Under these conditions, acclimation and growth of PCC6803 (prior to changing temperature) took place

for 4 days, yielding a biomass concentration of approximately 0.52 g/L dry weight (DW).

After acclimation at 30ºC, we systematically changed the PBR's temperature according to this program: 22ºC for 3 days, 33ºC for 4 days, 44ºC for 4 days, 33ºC for 10 days, 22ºC for 7 days, 18ºC for 7 days, and 30ºC for 8 days; Table 4.1 summarizes the temperature program, as well as key conditions for each temperature. When we carried out the temperature program, PBR operation was semi-continuous, with periodic harvest and recharge to maintain a biomass DW concentration between 200 and 500 mg/L. LI and gas flow rate were maintained constant during the experiment. We performed PBR sampling either three times per day (during the acclimation period) or four times per day (during semi-continuous operation). Samples were assayed for biomass DW, an array of chemical parameters, lipid quantity and composition, and bacterial-community composition. All chemical analyses were determined in duplicate after appropriate pretreatment and storage at 4°C, as needed.

4.2.4 Chemical analyses

We measured the optical density (OD) with a UV-Vis spectrophotometer (Cary 50 Bio, Varian Inc.) at a wavelength of 730 nm and converted it to DW using a calibration curve specifically determined for PCC6803. For the calibration, we determined the sample DW using total suspended solids (Method 2540D) in *Standard Methods* (American Public Health Association, 2005). Under semi-continuous operation, we calculated the biomass production rate (BPR) from the

daily harvest volume and DW concentration: BPR (g/L/d) = $X_{eff}\,Q_{eff}/V$; X_{eff} is the biomass DW concentration at particular harvesting event (g/L), Q_{eff} is the volume of the harvested (and recharged) liquid (L/d), and V is the reactor volume (16 L). We computed the daily-average specific growth rate (μ_{da} in d^{-1}) from μ_{da} (d^{-1}) = $X_{eff}\,Q_{eff}/(X_{ave}V)$; X_{ave} is the daily-average biomass concentration (Kim et al., 2011).

We measured the dissolved oxygen (DO) concentration in the PBR using an electrode (InPro6000, Mettler Toledo) located in the liquid near the top of PBR. We measured total carbon (TC), total organic carbon (TOC), and total inorganic carbon (C_i) using a TOC analyzer (TOC-V_{CSH}, Shimadzu Scientific Instruments) equipped with combustion catalytic oxidation/non-dispersive infrared (NDIR) gas analyzer (Kim et al., 2010). We calculated the speciation of C_i (i.e., $CO_{2(aq)}$, HCO_3^-, and CO_3^{2-} concentrations) in a sample following well-known equilibrium relationships among pH and the pK_as of the carbonate system (Snoeyink and Jenkins, 1980). We measured other inorganic nutrients — nitrate (NO_3^-), nitrite (NO_2^-), total phosphate (PO_4^{3-}), and sulfate (SO_4^{2-}) — by first filtering the sample through a 0.2-μm membrane filter (GD/X, Whatman) of polyvinylidene fluoride (PVDF) and then injecting the filtrate into an ion chromatograph (ICS-3000, Dionex) with an anion-exchange column (IonPac AS18, Dionex). The nutrient requirement for biomass synthesis was calculated using an empirical formula for PCC6803 ($C_{1.00}H_{1.62}O_{0.40}N_{0.22}P_{0.01}$) that we measured from dried biomass by using an elemental analyzer (2400 series II, PerkinElmer). The corresponding mass (gram) ratios are C : H : O : N : P : S : Ash = 49.8% : 6.7% : 26.8% : 12.5% : 1.5% : 0.7% : 2.7% (Kim et al., 2010).

4.2.5 Culture purity analyses

We routinely performed a culture-purity check by light microscopy observation and T-RFLP (terminal restriction fragment length polymorphism) analysis. Detailed analysis procedures are provided in section 4.5 Appendix for Chapter 4.

4.2.6 Lipid quantitation

We performed lipid extraction and quantitation as described by Sheng et al. (2011d). Briefly, we placed 15 mL of culture in a glass tube and centrifuged (Avanti J-26 XPI, Beckman Coulter) it at 2000 *g* for 15 min. After decanting the supernatant, we vortexed the pellet (VWR Vortex Mixer), extracted it by 3 mL Folch solvent (chloroform: methanol 2:1) for 24 h, filtered the solvent-lipid mixture through a 0.45-μm PTFE membrane, and evaporated the solvent completely under N_2. We transesterified the extracted lipids to fatty acid methyl esters (FAME) by acid catalysis (3 N methanolic HCl; Supelco, St. Louis, MO). The FAME was further extracted by hexane for gas chromatography (GC) measurement.

We injected FAME into a gas chromatography (Shimadzu GC 2010) equipped with Supelco SP 2380 capillary column (30 m × 0.25 mm × 0.20 μm) and flame ionization detector (FID) for FAME quantitation. GC operating conditions were: Split ratio 1:10; inject volume 1 μL; helium carrier gas with constant linear velocity 20 cm/s; H_2 40 mL/min, air 400 mL/min, make up gas

(helium) 30 mL/min; injector and detector temperature 240^{o}C; and oven temperature started at 140^{o}C for 1 min and increased at a rate of 4^{o}C/min to 220^{o}C. We identified individual peaks by comparing retention times with those of standard compounds and also re-confirmed them by GC-MS. We established the calibration curve for each FAME compound using the Supelco 37 Component FAME Mix standard (Supelco, St. Louis, MO) and quantified compound concentrations in samples by comparing peak areas with the standards.

4.3 Results and discussion

4.3.1 Initial acclimation

The PCC6803 inoculum first experienced a 4-day acclimation period under a constant LI of 108 W/m^2 and a temperature of 30°C. The biomass concentration increased from 0.11 to 0.52 g/L (DW), and the approximate average specific growth rate (μ_{da}) and BPR were 0.39 d^{-1} and 0.1 g/L/d, respectively, for the entire acclimation period.

4.3.2 Thermally induced changes in PCC6803 growth and BPR

Table 4.1 summarizes the results for semi-continuous PBR operation after acclimation. The initial temperature of 22ºC resulted in average μ_{da} and BPR of 0.68 d^{-1} and 0.26 g/L/d, respectively. Subsequently, we exposed the PBR to 33ºC for 4 days, and μ_{da} increased to an average of 0.79 d^{-1}, with the corresponding BPR being 0.28 g/L/d.

When the BT-PBR was exposed to 44ºC for 4 days, μ_{da} and BPR decreased by 27% and 29%, respectively, from the values at 33°C. PCC6803 biomass in the reactor showed pigment discoloration (turning light yellow from dark green) after a 3-day exposure to 44ºC, and the reactor showed thin biofilms on the reactor side plates. These responses indicated severe stress on PCC6803 resulting from relatively long-term heat shock by exposure to 44ºC. The high-temperature effects may have resulted to some degree from inactivation of the oxygen-evolving capability of PS II (Enami et al., 1994; Klimov and Krasnovskii, 1981).

When the temperature was returned to 33ºC for the next 10 days, PCC6803 did not fully return to its status before the heat shock at 44^{o}C (μ_{da} 0.57 d^{-1} vs. 0.79 d^{-1}, BPR 0.21 g/L/d vs. 0.28 g/L/d), but the culture recovered its normal dark-green color. Thus, PCC6803 could recover from the extreme temperature of 44^{o}C.

After PCC6803 was allowed to recover at 33ºC, we exposed the PBR to a lower temperature of 22ºC for 7 days. As a result, PBR performance declined, with μ_{da} and BPR dropping to 0.54 d^{-1} and 0.18 g/L/d, respectively. A further decrease in temperature to 18ºC resulted in drastic drop in μ_{da} and BPR to 0.27 d^{-1} and 0.08 g/L/d, respectively; these are 66% and 71% decreases, respectively, from the first 33^{o}C period (Days 3 – 7). This drastic decrease in PCC6803 growth rate suggests an irreversible damage on photochemical efficiency of PCC6803 at 18ºC temperature. The irreversible damage is evident because when the reactor was

exposed to 30°C for 8 days, μ_{da} and BPR only partially recovered to 0.31 d^{-1} and 0.11 d^{-1} g/L/d, respectively.

4.3.3 Inorganic nutrients

Figure 4.2 shows the C_i concentration, its speciation, and pH for the different temperatures. The C_i concentration was in the range of 36 – 66 mg C/L, and the pH was maintained between 7.5 and 9.0, making HCO_3^- the dominant form of C_i. The HCO_3^- concentration was sufficient to preclude C_i limitation (Kim et al., 2011).

Figure 4.3 shows the concentrations for P_i, N_i, and S_i throughout all experiments. In our previous research (Kim et al., 2010), we observed severe PCC6803 growth retardation due to insufficient availability of inorganic phosphate in standard BG-11. In this study, we provided 5-fold excess P_i, which led to the non-limiting concentration of P_i, close to 20 mg/L, throughout the run. N_i, and S_i also were well above rate-limiting levels throughout the experiment.

Table 4.1 shows that the nutrient utilization rates for C_i, N_i and P_i were reduced during 44°C, 22°C, and 18°C exposures due to lower values of μ_{da} and BPR (up to 77% decrease). Since the nutrient concentrations were not limiting at any time, the lower μ_{da}, BPR, and nutrient utilization rates were due to temperature stress.

Table 4.1. Daily average biomass concentration, BPR, μ_{da}, nutrient utilization rates, and final lipid production rate (LPR) of each temperature period with temperatures from 18 to 44°C at constant LI (108 W/m^2) and aeration (10 L/hr of 2.5% CO_2) in BT-PBR inoculated with PCC6803

Time period (d)	Days	temp. (^oC)	X_{ave} (mg/L)	μ_{da} (d^{-1})	BPR (g/L/d)	LPR (mg FAME/L/d)	Daily utilization rates (g/L/d)		
							C	N	P
0 - 3	3	22	375	0.68	0.26	10.6	0.128	0.032	0.004
3 - 7	4	33	353	0.79	0.28	12.9	0.139	0.035	0.004
7 -11	4	44	338	0.58	0.20	5.9	0.098	0.025	0.003
11 - 21	10	33	358	0.57	0.21	9.4	0.103	0.026	0.003
21 - 28	7	22	320	0.54	0.18	3.4	0.089	0.022	0.003
28 - 35	7	18	293	0.27	0.08	2.6	0.041	0.010	0.001
35 - 43	8	30	371	0.31	0.11	5.1	0.057	0.014	0.002

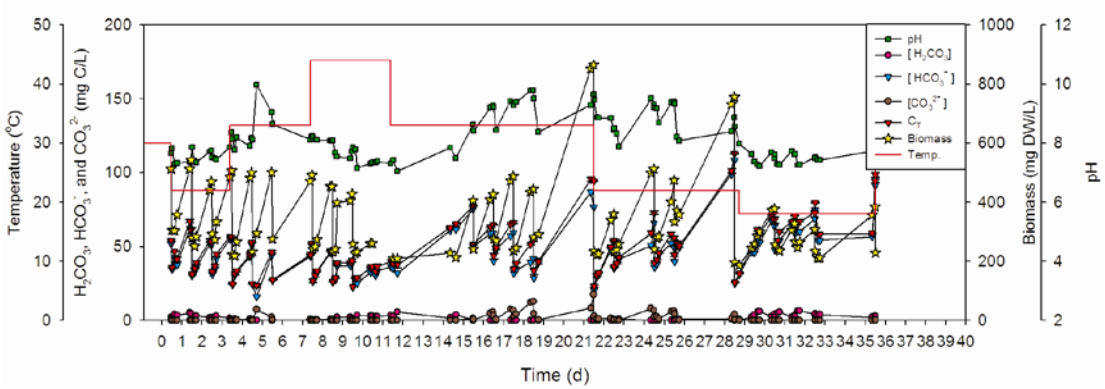

Figure 4.2. Dynamics of C_i species (H_2CO_3, HCO_3^-, and CO_3^{2-}), pH, and biomass during growth of PCC6803 exposed to different temperatures at constant LI (108 W/m^2) and aeration (10 L/hr of 2.5% CO_2) in the BT-PBR.

Inorganic C was present at a non-limiting concentration throughout the experiments.

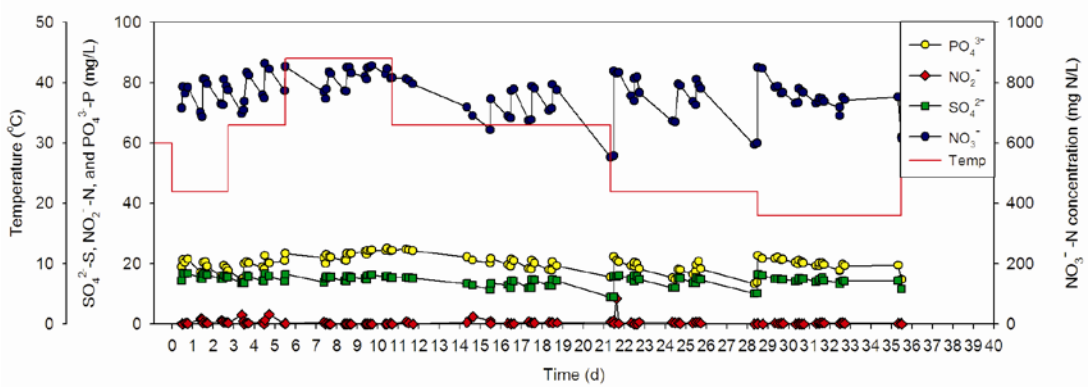

Figure 4.3. Dynamics of phosphate, sulfate, nitrate, and nitrite during growth of PCC6803 in response to different temperatures at constant LI (108 W/m^2) and aeration (10 L/hr of 2.5% CO_2) in the BT-PBR.

Each of N, S, and P was present at a non-limiting concentration throughout the experiments.

4.3.4 Dissolved oxygen (DO)

The DO concentration in a photobioreactor is an indicator of PS II activity and oxygen evolution. Figure 4.4 shows the DO concentrations in response to varying temperatures. The percentage saturation (compared to ambient air) is the ratio of the measured DO concentration divided by the saturated DO for the particular temperature. Clearly, the highest DO saturation occurred for the optimal temperatures of 33°C and 30°C. The percentage saturation declined during the low temperatures of 18°C and 22°C, and the decline was more pronounced at 44°C, indicating severe stress to PS II activity. These results support of the μ_{da} and BPR data reported in Table 1 and agree with other reports on temperature effects to PS II activity (Doucha and Livansky, 2006; Torzillo et al., 1984).

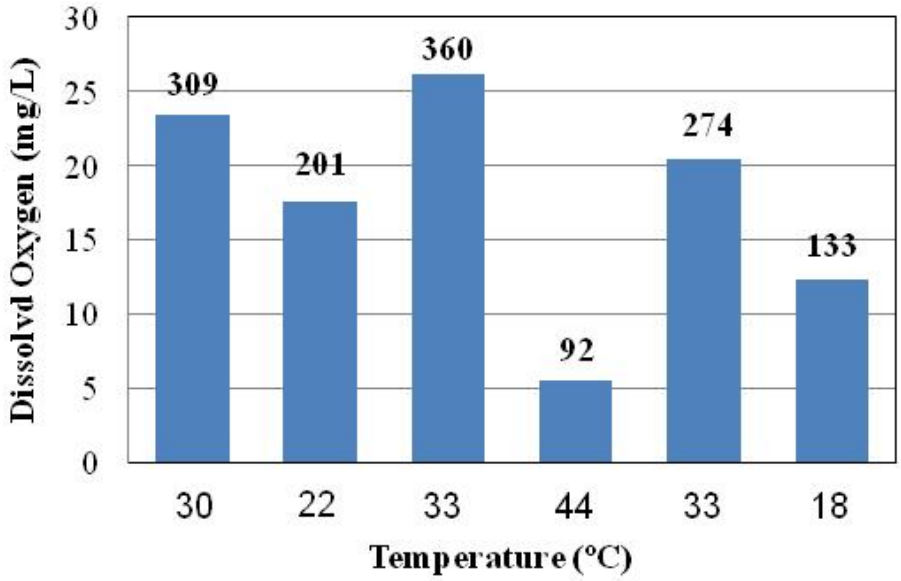

Figure 4.4. Average dissolved oxygen (DO) concentrations measured in the BT-PBR for different temperatures.
The numbers shown on the top of the bars are the temperature-adjusted % air saturation. The DO is most significantly super-saturated for the optimal temperatures of 30 and 33°C, confirming strong PS II activity. The poorest PS II activity is indicated for 44°C.

4.3.5 Thermally induced changes in lipid quantity

The temperature changes affected lipid production and composition. Figure 4.5 shows the percentage of each fatty acid group and total fatty acid (as FAME) normalized to the total DW of the biomass. The highest fatty acid content in the cells (~5%, w/w dry weight) always was found at 30 – 33^{o}C. Soon after returning to 33^{o}C from 44^{o}C (Days 11 – 21), the total amount of fatty acids in the cells returned back to their normal levels (compared with partial recovery of μ_{da} and BPR). A similar recovery also took place after returning the temperature from 18^{o}C to 30^{o}C (after Day 35). In contrast, growth at 22^{o}C showed ~20% suppression of lipid synthesis (to ~4% as dry biomass). An even more severe suppression of lipid synthesis (by 35% – 40%) occurred at high temperature (44^{o}C) and the lowest temperature (18^{o}C). The reduced rates of lipid synthesis may have resulted from the stress to PS II activity, as confirmed by DO measurements (Figure 4.4), which generate less available energy and reducing power (Blankenship, 2002).

A detailed look at the major fatty acids indicates that saturated and unsaturated fatty acids had different response to temperature stress. With high temperature stress (44^{o}C), all fatty acids, including saturated (e.g., C16:0, palmitoyl fatty acid group) and unsaturated (e.g., γ-C18:3), were suppressed. However, 22°C exposure led to more γ-C18:3 and α-C18:3, indicating that the 18-C unsaturated acids may have been produced as a response to low temperature. At the still lower temperature of 18^{o}C, all fatty acids except α-C18:3 were suppressed, indicating serious stress on the cells' ability to cope with extreme low temperature.

The stepwise decrease of C16:0 and almost all other fatty acids at 44°C and 18°C coincided with a decrease of lipid synthesis, μ_{da}, and BPR (as previously noted), confirming the severe stress on the growth and metabolism of PCC6803.

Figure 4.5 also shows the lipid production rates (LPR, as FAME, white square symbol), calculated from the combination of cellular lipid content and BPR; Table 4.1 compares the LPR at the end of each period to the BPR. The LPR in this study is comparable with LPRs reported by Chen et al. (2011). Although the LPR recovered at 33°C (during Days 3 – 7) after a short exposure to 22°C, a 4-d exposure to 44°C lowered the LPR from 12.9 mg/L/d (33°C) to 5.9 mg/L/d, a 55% decrease. The heat-shock effect appeared to be partially irreversible, as the subsequent 10-d growth at 33°C (Days 11 – 21) only recovered the lipid production rate to 72% of its best observed level in the first 33°C exposure (Days 3 – 7). After that, the LPR decreased stepwise with the exposure to 22°C to 18°C, at which point the LPR was only ~2.6 mg/L/d, an 80% loss compared with 33°C. Although the LPR increased to 5.1 mg/L/d after an 8-day period at 30°C from 18°C, it did not fully recover and only reached 39% of its best observed level in the first 33°C period (Days 3 – 7).

During exposure to non-optimal temperatures (44°C, 22°C, and 18°C), the BPR and cell lipid content were clearly suppressed, leading to drastic decreases in LPR. Quantitatively, the decline of BPR contributed more to the decrease of LPR. Although the μ_{da} and BPR results show that PCC6803 could tolerate severe temperature stress, the LPR results demonstrate that maintaining a temperature far

from its optimum resulted in severe loss of lipid production that could not be recovered.

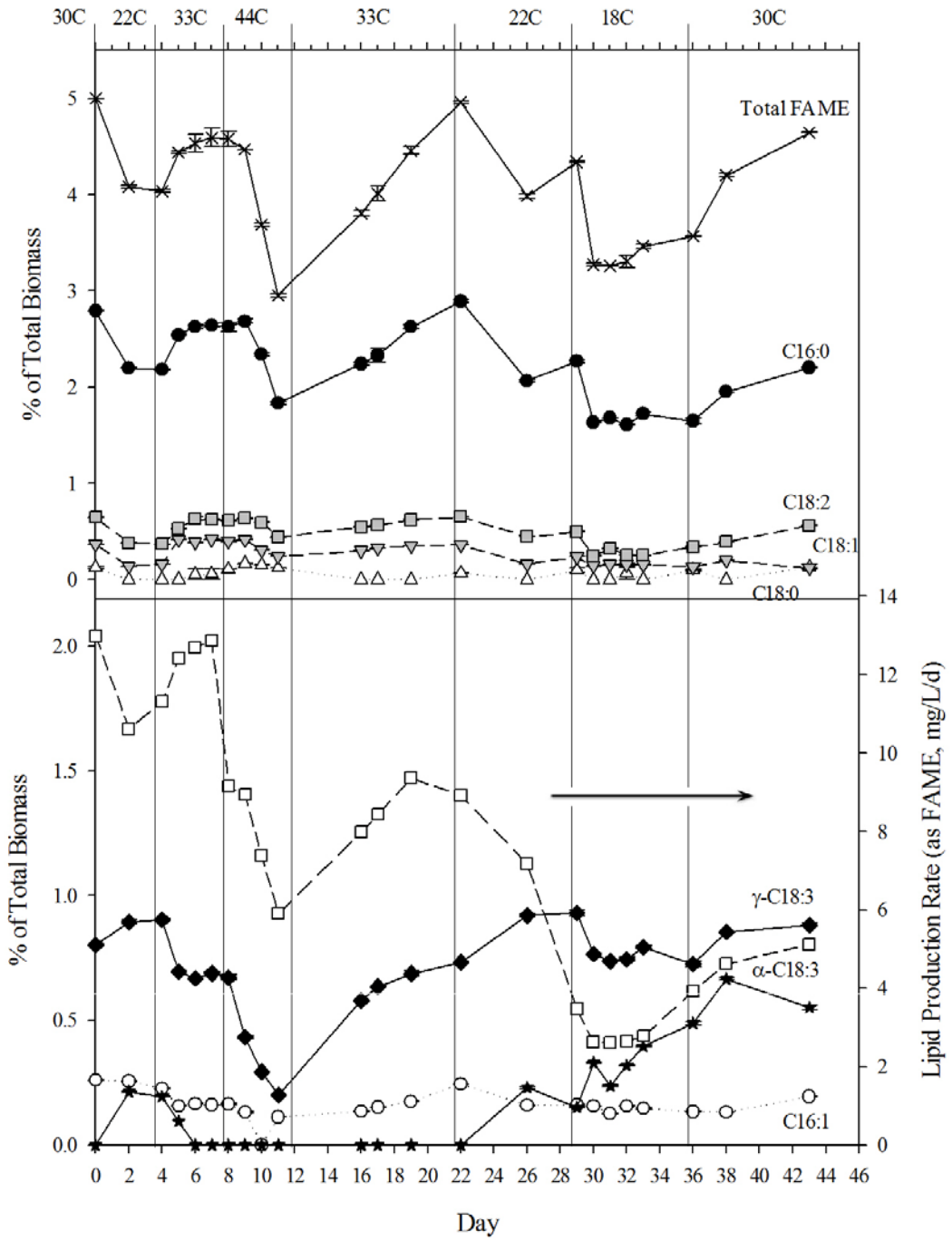

Figure 4.5. Percentage fraction of each fatty acid composition (as FAME) normalized to biomass (DW) of PCC6803 during temperature cycling in the BT-PBR.
The white squares represent the total lipid production rate (LPR, as FAME).

4.3.6 Thermally induced changes on lipid quality

Changes in lipid quality, such as different carbon chain length and degree of unsaturation, play an important role in tolerance towards temperature acclimation in phototrophic organisms (Gombos et al., 1992; Somerville and Browse, 1991). During PCC6803 initial growth at 30ºC, C16:0 was the predominant fatty acid group in its lipids, constituting about 56% of the total fatty acids (by weight). Other abundant fatty acids included C16:1 (5.2%), C18:0 (2.5%), C18:1 (7.4%), C18:2 (13%) and γ-C18:3 (16%). Some other natural fatty acids — such as C16:2, C17:0, and C18:4 — were detected only in trace amounts. The degree of unsaturation was 0.87. Unsaturation was mainly attributed by the C18 fatty acids such as C18:1, C18:2, and C18:3.

The lipid quality of PCC6803 (reported as a particular FAME/total FAME, w/w) for various temperature shifts is presented in Figure 4.6. All fatty acid species were suppressed at 44°C (as noted in Figure 4.5), probably due to heat-shock denaturation of PS II and destabilization of its associated lipid-protein interactions in the thylakoid membranes (Inoue et al., 2001). However, polyunsaturated fatty acid C18:3 decreased most (to 6.7%, C18:3/total fatty acids, w/w), which gave higher fractions for C16:0 (62%) and C18:2 (16%) and caused the level of unsaturation to decrease to 0.62 (white open squares in Figure 4.6). The much larger decrease of C18:3 suggests that it is more vulnerable to oxidative stress and damage during high temperature exposure (Gombos et al., 1992).

At 22^{o}C, γ-C18:3 became 22%, increasing the degree of unsaturation to 1.1 and bringing down the percentages of C16:0 (54%) and C18:2 (9.9%).

Another tri-unsaturated fatty acid, α-C18:3, which could not be detected at 30°C, appeared and reached 4.8% after exposure to 22ºC, as shown with the chromatogram in Figure 4.7. This observation was reproducible, as both stages at 22°C (Days 0 – 3 and Days 21 – 28) showed similar patterns. The over-production of γ-C18:3 and α-C18:3 appears to be a strategy to overcome the low-temperature-induced decrease of membrane fluidity and increase of the phase-transition temperature (Chapman, 1975; Wada et al., 1994; Wada and Murata, 1990).

As the temperature dropped to 18°C, temperature stress out-paced the ability of PCC6803 to adapt: C16:0, C18:1, C18:2, and γ-C18:3 declined, while the percent α-C18:3, which might be considered as an extreme response to severe low-temperature stress (Wada and Murata, 1990), climbed to 16%. The relative shifting of each fatty acid group brought the degree of unsaturation further to 1.29.

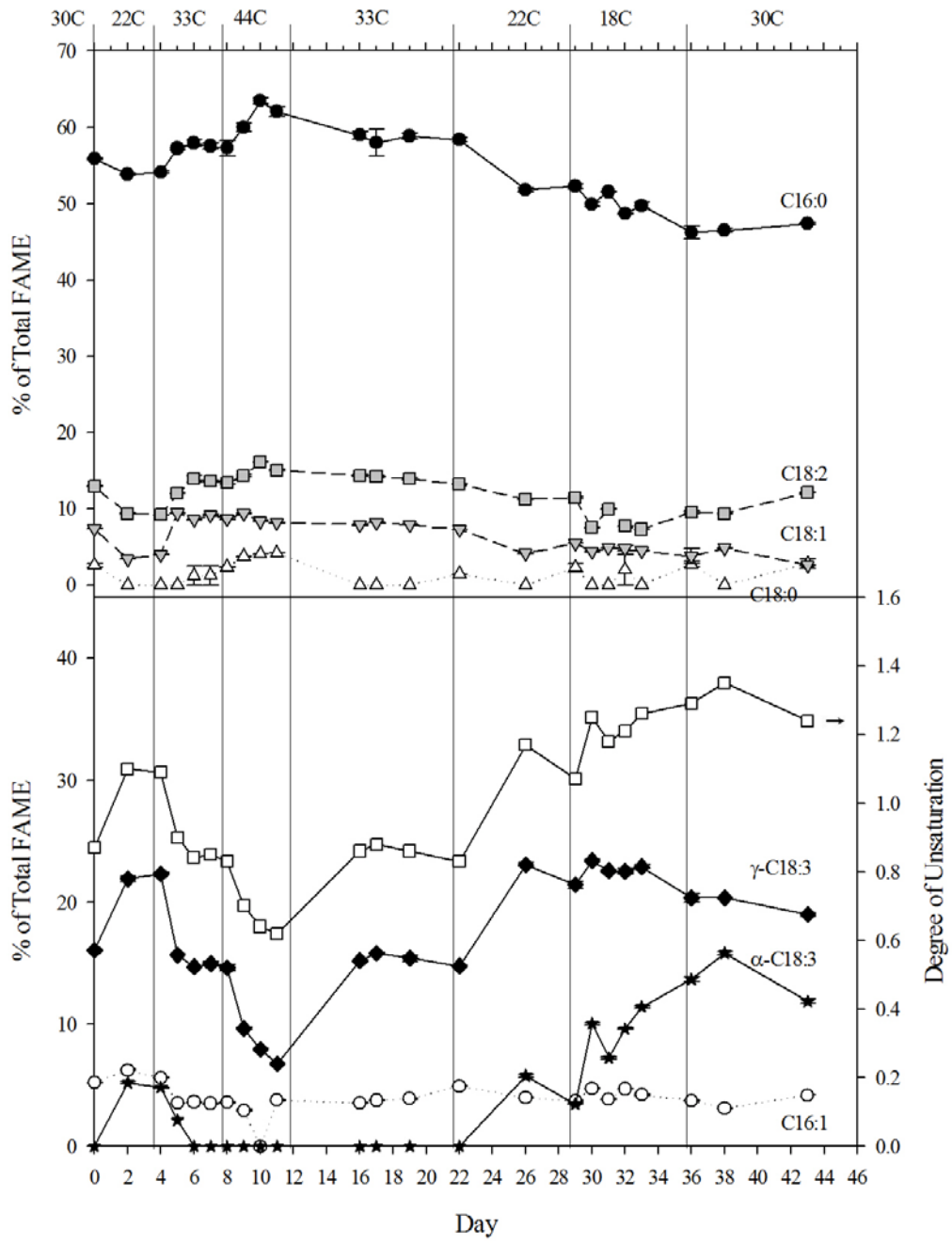

Figure 4.6. Fatty acid profile of PCC6803 during temperature changes in the BT-PBR.

Degree of unsaturated (white square symbol) = [1.0 (% monene) + 2.0 (% diene) + 3.0 (% triene) + 4.0 (% tetraenes) + 5.0 (% pentanes) + 6.0 (% hexane)]/100 (Feng and Johns, 1991).

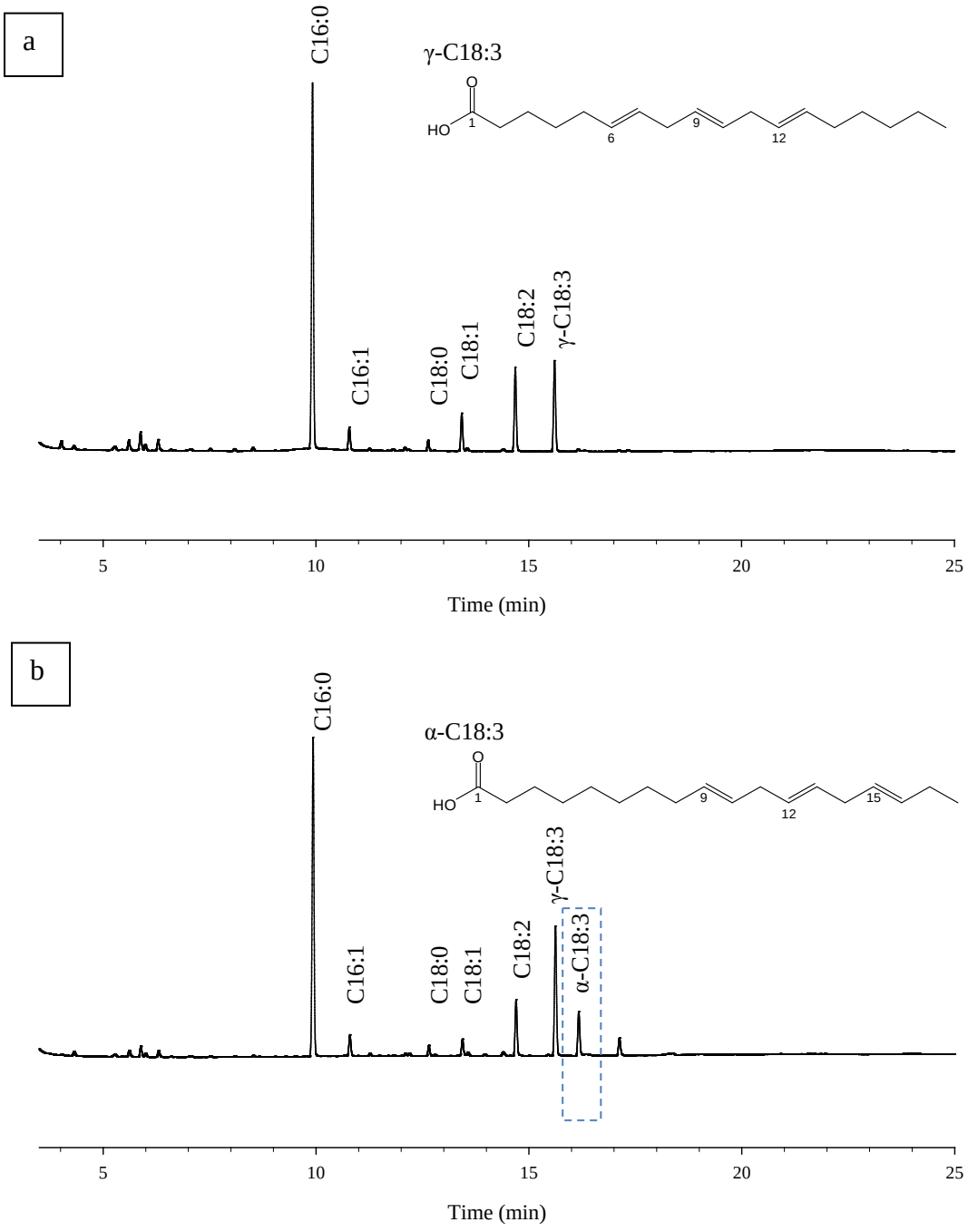

Figure 4.7. Comparison of GC chromatograms of (a) Day 19, 33^{o}C and (b) Day 31, 18^{o}C.

The peak of α-C18:3 was detectable only in the low-temperature sample before exposed to 18^{o}C (which led to a tailing effect in following recovery).

PCC6803 was able to tolerate the low-temperature stress by adding double bonds to fatty acids, resulting in reduction of saturated fatty acids of membrane lipids. However, irreversible damage caused by low-temperature stress resulted in a "tailing effect" on fatty acid production. Although the tri-unsaturated fatty acid α-C18:3 has not been documented before at 30ºC (Wada and Murata, 1990), its residual production by PCC6803 remained even after 7-day growth at 30ºC (Day 35 to 43 in Figure 4.6) following the exposure to 18ºC. Irreversible damage at 18^{o}C also is evidenced by the partial recovery of μ_{da}, BPR, and LPR after returning to 30^{o}C from 18^{o}C, as noted before.

In addition to causing a change in the degree of unsaturation, extremes in temperature altered the molar ratio of C16 and C18 significantly, as seen in Figure 4.8. Relatively more C16 was present at higher temperature, while C18 was more important at lower temperature. For biofuel production, shorter-chain and saturated fatty acids are preferred, as they have lower melting points, higher cetane numbers, fewer NO_x emissions, and better oxidative stability (Benjumea et al., 2011; Canakci, 2007). Although higher temperature led to desirable molar ratios of shorter-chain and saturated fatty acids, the suppression of LPR (noted above) made this temperature condition unfavorable for biofuel production. Lower temperatures were even more unfavorable, because they suppressed the LPR and also produced relatively more long-chain and unsaturated C18, which significantly deteriorate the quality of the fatty acids as fuel feedstock. The results indicate that high and low temperature extremes should be avoided in large-scale cultivation for biofuel production.

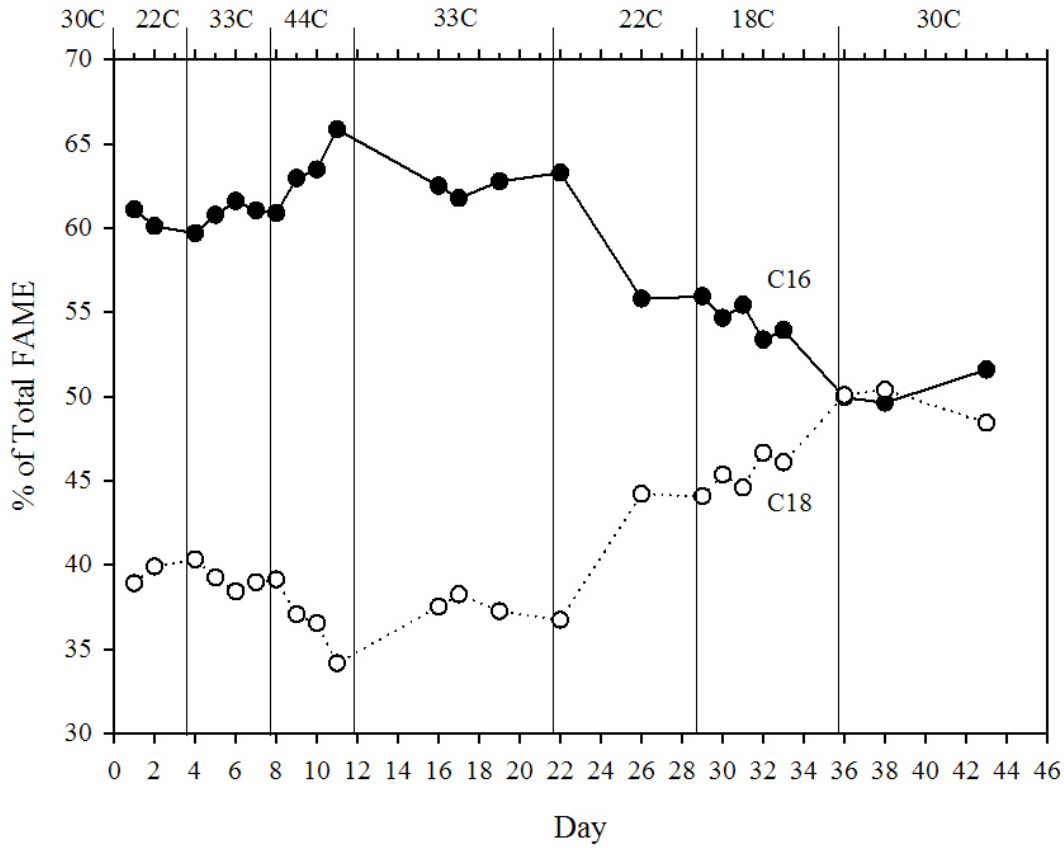

Figure 4.8. Relative molar percentages of C16 and C18 fatty acid (as FAME) to total measured FAME of PCC6803 during temperature shifts.

4.3.7 Microbial community assessment

Figure 4.9 in section 4.5 Appendix for Chapter 4 shows T-RFLP assays used to screen for bacteria other than PCC6803 (Liu et al., 1997). We found no evidence of non-PCC6803 bacteria over the duration of the experiments. Instead, the T-RFLP data show long-term maintenance of only the peak associated with PCC6803. Light microscopy also did not reveal any contamination with eukaryotes or bacteria having morphology different from PCC6803. Despite the severe stress of non-optimal temperatures (44^{o}C, 22^{o}C, and 18^{o}C), PCC6803 still dominated the microbial community. Thus, all observed changes in growth and fatty acid composition originated from PCC6803, not other microorganisms.

4.4 Conclusions

Temperature played an important role in biomass and lipid production rates of PCC6803. Higher temperature (44^{o}C) and lower temperatures (22°C and 18^{o}C) lowered the specific growth rate, lipid content, and, in combination, lipid production rate. Temperature also caused shifts in the degree of lipid unsaturation: 0.87 at 33^{o}C, 0.62 at 44^{o}C, and 1.29 at 18^{o}C. Although PCC6803 survived temperature stress and maintained its predominate position in the culture, it could not fully recover from long-term temperature stress. Thus, avoiding prolonged exposure to extreme temperature is crucial for using PCC6803 as feedstock for biofuel production.

4.5 Appendix for Chapter 4 — Culture purity check (microbial community assessment)

Light Microscopy. Liquid cultures (20 µl) were spotted onto glass microscope slides (VWR International, West Chester, PA) and observed with 1000X magnification using a phase contrast objective on a Zeiss light microscope. Grayscale images were captured using a CoolSnap ES camera.

DNA Isolation. Liquid samples (1 mL) were pelleted at 10,000 *g* for one minute. After the supernatant was removed, the cell pellets were stored immediately at -80°C. The pellets were resuspended in 200 µl lysis buffer (30 mM Tris·HCl, 10 mM EDTA, 200 mM sucrose; pH 8.2) and incubated at 65°C for 10 minutes. Lysozyme was added to a final concentration of 10 mg/mL, and samples were incubated at 37°C for 60 minutes, followed by addition of 1% (w/v) sodium dodecyl sulfate and additional incubation at 56°C for 10 minutes. After 25 µl proteinase K and 200 µl buffer AL (DNeasy Blood & Tissue Kit, Qiagen, Valencia, CA) were added, the lysates were further incubated at 56°C for 30 minutes. Subsequent steps for DNA preparation from lysates were performed with the DNeasy kit as described. The DNA concentration was measured using a NanoDrop spectrophotometer (NanoDrop Products, Wilmington, DE), and then the DNA was stored at -20°C.

PCR. Community DNA was normalized to 10 ng/µl before undergoing PCR amplification using universal primers targeting 16S rDNA of *Bacteria*. The forward primer 8F (5'-AGAGTTTGATCCTGGCTCAG) (Baker et al., 2003) and reverse primer 1392r (5'-ACGGGCGGTGTGTAC) (Dionisi et al., 2003) were

labeled at the 5' end with the fluorescent dyes HEX and FAM, respectively. PCRs were prepared containing 2.5 mM $MgCl_2$, 4 ng template DNA, 1x *Taq* PCR Master Mix (Qiagen), and 250 nM each primer in a 50 µl total reaction volume. Amplification was achieved using the following thermal profile: 94°C for 6 minutes, 30 cycles of 94°C for 45 seconds, 55°C for 45 seconds, and 72°C for 90 seconds, followed by a final extension at 72°C for 10 minutes. 10 ng Genomic DNA from a pure *Synechocystis* culture and 1 ng of *Synechocystis* 16S rDNA harbored in plasmid pCR4-TOPO (Invitrogen, Carlsbad, CA) served as separate positive controls for both PCR and T-RFLP. 10µl of PCR product were visualized on a 1% (w/v) agarose gel stained with ethidium bromide. The remainder was purified using the QiaQuick PCR Purification Kit (Qiagen) and DNA concentration was measured as described above. All procedures were conducted in darkness to prevent degradation of the primer-bound fluorescent dyes.

T-RFLP. Restriction digests were prepared containing 40 to 60 ng labeled PCR product, as described by the manufacturer (New England Biolabs, Ipswich, MA), using 2 units of either *Mse*I, *Hha*I, *Msp*I, or *Rsa*I in a total digest volume of 15 µl. Digests were incubated in the dark at 37°C for 3 hours followed by heat inactivation at 65°C for 20 minutes. 1 µl of each digest was added to 9 µl deionized formamide and GS500-ROX size standard (Applied Biosystems, Foster City, CA) and denatured at 95°C for 10 minutes prior to loading on an Applied Biosystems 3730 DNA analyzer with an injection time of 40 seconds. Data were analyzed using PeakScanner software v. 1.0 (Applied Biosystems).

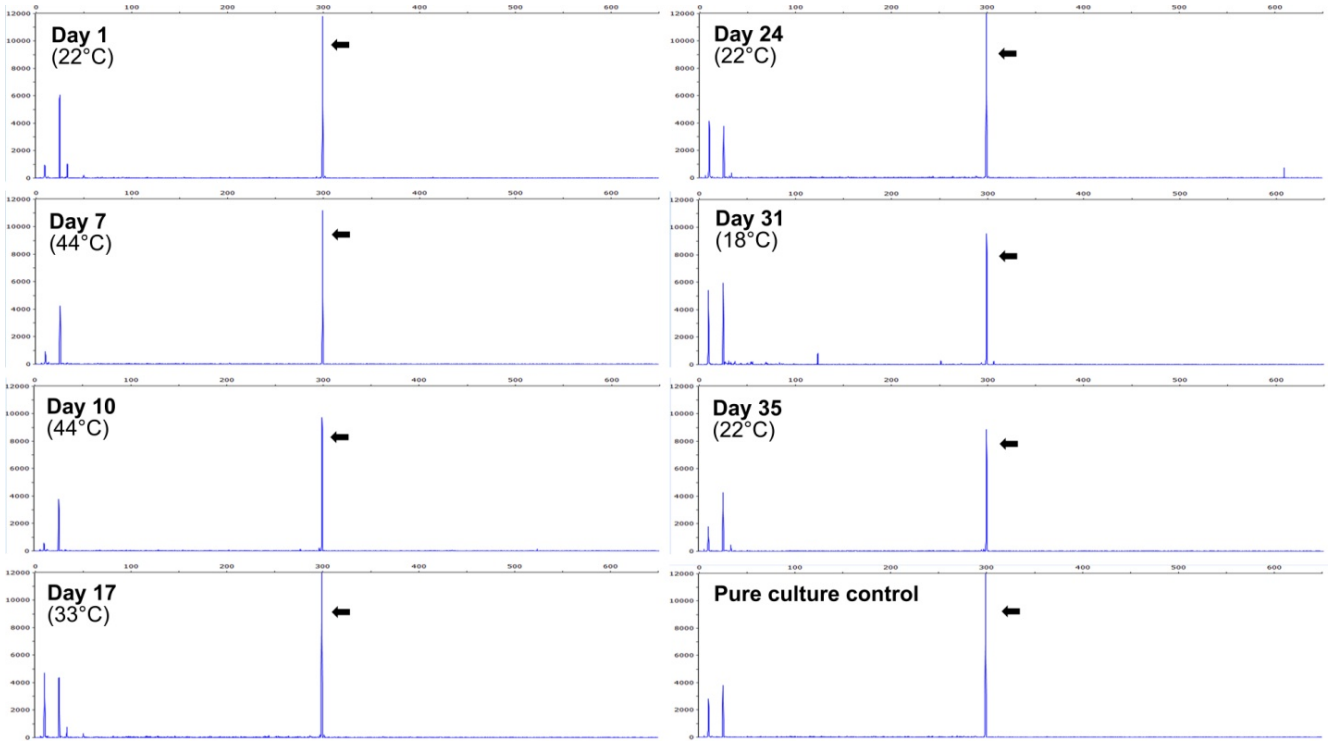

Figure 4.9. T-RFLP profiles of total bacterial 16S rDNA PCR products of *Synechocystis* PCC6803 culture in BT-PBR during exposure to different temperatures, as shown in Figure 4.2 and Figure 4.3.

These PCR products were digested with *Hha*I (blue; FAM fluorescence), where *Synechocystis* yields a peak at 300 bp (black arrows). Recurrent peaks < 30 bp result from residual labeled primer and can be ignored. These results demonstrate that PCC6803 was the dominant type of bacterium throughout the experiments.

5 Evaluation of Cell-disruption Effects of Pulsed-electric-field Treatment of *Synechocystis* PCC 6803[*]

5.1 Introduction

Concerns over the decline of worldwide petroleum production and global warming drive human society to seek more sustainable and carbon-neutral energy resources, including nonpetroleum-based transportation fuel (Czucz et al., 2010; Pinto et al., 2005; Ragauskas et al., 2006; Rittmann, 2008). Compared with traditional lipid feedstock, such as oil-rich vegetables and animal tissues, phototrophic microorganisms (algae and cyanobacteria) appear to be more suitable for large-scale production of nonpetroleum-based transportation fuel due to their high biomass and lipid production rates and minimal competition with the food supply for human society (Antoni et al., 2007; Chisti, 2007; Hu et al., 2008; Karaosmanoglu, 1999). Among the phototrophic microorganisms, the cyanobacterium *Synechocystis* PCC 6803 is an interesting candidate due to its rapid growth rate, environmental robustness, naturally high lipid content, and ability to be genetically transformed to direct its metabolism towards lipid production (Kim et al., 2010; Koksharova, 2010; Nakamura et al., 1998; Vermaas, 1996; Wada and Murata, 1989).

Most of the lipids in cyanobacteria are diacylglycerols (DAG) located in the photosynthetically active thylakoid membranes (Weier et al., 2005). In order

[*] This chapter was published as Sheng, J., Vannela, R., Rittmann, B.E. 2011. Evaluation of cell-disruption effects of pulsed-electric-field treatment of *Synechocystis* PCC 6803. *Environmental Science & Technology*, **45**(8), 3795-3802.

to retrieve these intracellular-membrane lipids more efficiently, cell disruption usually is required ahead of lipid extraction step (Cooney et al., 2009). However, disrupting cyanobacteria turns out to be a challenging task due to their unique cell structure. Being Gram-negative, cyanobacteria have a cell envelope consisting of a plasma membrane, peptidoglycan layer, outer membrane, and S-layer (Koksharova, 2010; Liberton et al., 2006). Despite the cyanobacteria's overall Gram-negative structure, the peptidoglycan layer and the outer membrane are considerably thicker than in most Gram-negative bacteria. The degree of cross-linking between peptidoglycan chains within the murein also is higher than in most other Gram-negative bacteria (Hoiczyk and Hansel, 2000). Thus, the peptidoglycan in cyanobacterium is similar to that of Gram-positive bacteria, and this makes cyanobacteria especially able to resist cell disruption and the penetration of organic solvents.

Recently, a cell-disruption approach that may be useful as pre-treatment of cyanobacteria before lipid extraction has been field-tested for making biomass more available for methanogenesis and denitrification (Lee et al., 2010a; Rittmann et al., 2008b; Salerno et al., 2009). Called Focused Pulsed (FP) technology (OpenCEL^{TM}, Glencoe, IL, http://www.opencel.com), it is an adaptation of the pulsed electric field (PEF) technology that has been used for food disinfection, sludge digestion, and oil extraction from plants (Guderjan et al., 2005; Kopplow et al., 2004; Min et al., 2007; Salerno et al., 2009). When a cell passes through the high-strength (~30 kV) and quickly changing (~2000 Hz) electric field, unequal electric charges are accumulated on dipolar molecules, such

as DAG in the cell membrane and peptidoglycan in the cell wall. When a critical potential value of the electric field is exceeded (usually 1 V for bacteria), the pressure on the membrane produced by the attractive forces of unequal electric charges is high enough to form irreversible pores in the membrane (Schoenbach et al., 2000). This mechanism is called “electroporation” (Hamilton and Sale, 1967; Weaver and Chizmadzhev, 1996), and the membrane also loses its intrinsic properties of electrical resistance, membrane potential, and barrier function (Somolinos et al., 2007).

Compared with traditional PEF, FP was optimized to generate more square waves, deliver more power (up to 500 kW), and control power delivery more precisely to enhance the disruption and break down of cellular membranes and cell walls. FP also was developed specifically for high treatment capacity of biomass slurries and with integrated automation to satisfy large-scale industrial application (Rittmann et al., 2008b; Zhang et al., 2009a). Information on the FP device can be found at http://www.opencel.com/pef_technology.shtml.

Because many factors can affect cell disruption when applying FP, the Treatment Intensity (*TI*) is utilized to combine the effects of electric field strength, pulse width, frequency, and hydraulic residence time (Lee et al., 2010a). *TI* is calculated by (Lee et al., 2010a; Salerno et al., 2009):

$$TI(\text{kWh/m}^3)=K\cdot\frac{V^2\cdot D\cdot f\cdot\sigma\cdot HRT}{L^2} \qquad (5.1)$$

where

V = applied voltage (V = J/C = kg-m^2/C-s^2)

D = pulse width (s/pulse)

f = pulse frequency (Hz = pulse/s)

σ = sample conductivity (S/m = s-C^2/kg-m^3)

L = distance between electrodes (m)

HRT = residence time of liquid culture in treatment chamber (s)

K = constant for unit conversion (2.78×10^{-7} kWh/J).

In this research, we disrupted *Synechocystis* PCC 6803 using FP technology prior to lipid extraction to make intracellular lipids more accessible by organic solvents. We evaluated the effect of FP on cell disruption by fluorescence staining, electron microscopy, and lipid extraction. We interpret the results in terms of the mechanisms of cell disruption and how they aid lipid recovery from *Synechocystis* biomass.

5.2 Materials and methods

5.2.1 Cell cultures

The growth and maintenance procedures for the *Synechocystis* PCC 6803 culture were described in Sheng et al. (2011d) and Kim et al. (2010). In brief, we scaled up the *Synechocystis* culture from plate colonies to a 250-mL flask, then to a 1-L flask, and finally to a 25-L transparent carboy (2251 Clearboy, NALGENE, Rochester, NY) with 20 L BG-11 medium (Rippka et al., 1979; van de Meene et al., 2006). We harvested biomass after 1- to 2-week growth in a carboy, when sufficient biomass was available.

5.2.2 FP treatment

We used an FP unit manufactured by OpenCEL for biomass treatment. We selected five treatment conditions (A-E) with various electric field strengths, pulse lengths, and treatment times. Table 5.1 summarizes *TI* values of the five treatment conditions. Prior to the treatment, we cleaned and disinfected the entire flow system by flushing 1% NaOCl bleach followed by sterilized DI water. We also adjusted the conductivity of the culture to a uniform value of 0.18 S/m by adding DI water, as needed. We used one batch of culture to perform all experiments reported here. Its concentration was approximately 2×10^8 CFU/mL (approximately 300 mg/L in dry weight), the pH was maintained at 8.0, and the temperature of input culture was maintained at 26^oC.

We collected treated culture at the outlet after treatment condition became stable, measured outlet temperature, and cooled the sample to room temperature immediately on ice to prevent any additional thermal effect. For condition E, the treated culture was recycled back once again to double the treatment time. For FP treatment at low inlet temperature, we first cooled the culture to 16^oC in a 4^oC cold room over 10 h with constant agitation by air to maintain its growth, and we followed the same procedure as condition D. We performed the control experiment by passing the same culture through the FP system under the same conditions, but without an electric field. All experiments reported here were performed in duplicate or triplicate to confirm the observation of each experiment.

5.2.3 Heat-only treatment

In order to separate the thermal effect from the FP effect, we conducted experiments by heating the culture without exposure to FP. We used approximately 5 mL of culture in a capped glass tube and heated it in a water bath separately to the same outlet temperature of each FP treatment (as in Table 5.1). The water bath temperature was 5^{o}C higher than each target temperature to reach the target temperature within 10 min (versus less than one second with FP), and the samples were taken out of water bath immediately after target temperature was reached. After heating, we put the samples in ice immediately to cool them to room temperature (26^{o}C) within 5 minutes.

5.2.4 Evaluation of cell disruption

Dry weight, SCOD, and cell viability tests. We measured dry weight of biomass by using total suspended solids (Method 2540D in *Standard Methods* (American Public Health Association, 2005)). We filtered the culture sample through a GF/C membrane (Whatman) and dried the membrane at 105^{o}C overnight. Soluble chemical oxygen demand (SCOD) was analyzed by closed reflux colorimetric method (Method 5220D in *Standard Methods* (American Public Health Association, 2005)). Prior to the measurement, culture sample was filtered through a 0.2-μm membrane filter (GD/X, Whatman). We also used culture-based techniques to test the viability of cells under treated versus control conditions. We diluted the culture (before and after treatment), inoculated it onto BG-11 plates, incubated the plates in the light incubator (Percival Scientific, Inc.)

at 30^{o}C for 4 to 5 days, and counted the number of CFU per milliliter to determine the inactivation rate after treatment.

SYTOX Green staining. We used the fluorescence dye SYTOX Green (Invitrogen, Carlsbad, CA) to label damaged and dead cells. We prepared and used stock solution of SYTOX Green according to the instructions provided by manufacturer. Prior to mixing with SYTOX Green solution, we concentrated the cells by centrifugation at 13,000 *g* for 2 min and re-suspended them in DI water (pH 7.0) twice to eliminate interferences from BG-11 medium.

We observed fluorescently stained cells using an Olympus BX61 fluorescence microscope equipped with a DP70 camera. We loaded stained sample to a slide coated with 2% agarose in BG-11 (Huang et al., 2002) and used bright-field microscopy to determine the total number of cells in a given field. Lysed cells with SYTOX Green emission were detected using an FITC filter (ex. 460 – 505 nm, em. 510 – 550 nm). Red auto-fluorescence emission from *Synechocystis* phycocyanin and chlorophyll were visualized using a CY5 filter (ex. 605 – 655 nm, em. 670 – 720 nm). We obtained and post-adjusted images with DP-BSW software (Olympus).

Flow cytometry. We also performed flow cytometry measurement (FCM) of SYTOX Green-stained samples using a Beckman Coulter FC 500 flow cytometer. Excitation was done with an air-cooled 20-mW argon ion laser at 488 nm. The fluorescence emission of SYTOX was detected using a 510 – 550 nm FITC filter. We used the bacterial size gate (0.5 – 3 μm) for prescreening and counted 10,000 events for each sample.

Transmission Electron Microscopy (TEM) Observation. We initially fixed the cells in 2% glutaraldehyde in 50 mM $NaPO_4$ at pH 7.2, and then we post-fixed them with 1% osmium tetroxide in the same buffer. Following acetone dehydration, we infiltrated the cells and embedded them in Spurr's epoxy resin polymerized at 60°C for 36 h. We cut 60-nm sections and post-stained them in uranyl acetate and lead citrate (van de Meene et al., 2006). Images were generated on a Philips CM12 TEM operated at 80 kV with a Gatan model 791 camera.

5.2.5 Lipid extraction and quantification

We performed lipid extraction and quantification according to Sheng et al. (2011d). Briefly, we used 100 mL of each sample for lipid extraction and quantification. We collected suspended biomass by centrifuging at 2000 *g* for 15 min, followed by a filtration of the supernatant through a 0.2-μm regenerated cellulous membrane (Whatman). We combined the filter-collected biomass with the pellet for lipid extraction by isopropanol (Sheng et al., 2011d). We investigated three solvent/wet biomass ratios (v/v): 5 (low solvent usage), 10 (moderate), and 70 (extra solvent) (Folch et al., 1957; Sheng et al., 2011d). We calculated the volume of wet biomass pellet from the biomass concentration by assuming 80% water content of wet pellet, which we calculated from weights and densities of biomass and water. After extraction, we filtered the solvent-lipid mixture through a 0.45-μm PTFE membrane (Whatman) and evaporated the solvent completely under N_2. Then, we transesterified the lipids to fatty acid methyl esters (FAME) by acid catalysis and injected the FAME into a gas

chromatograph (Shimadzu GC 2010) equipped with Supelco SP 2380 capillary column (30 m × 0.25 mm × 0.20 μm) and flame ionization detector (FID) for FAME quantification by a modification (Sheng et al., 2011d) of a method by Liu et al. (2005).

5.3 Results and discussion

5.3.1 FP treatment with room inlet temperature

Table 5.1 compares the treatment results for conditions A through E. The outlet temperature increased by 10 to 28°C, with an almost linear relationship to *TI* from condition A to D. Wouters et al. (1999) reported a similar trend. For condition E, we cooled the culture after the first run, which is why the increase did not follow the linear projection. When the temperature exceeded 50^{o}C (condition E), the color of the outlet culture turned to yellowish-green from dark green (native color), indicating denaturation of phycocyanin and chlorophyll pigments in the *Synechocystis* cells. The dry-weight measurement also showed small biomass loss that correlated to *TI*. A dry weight loss of 9.4 ± 0.1% was observed with the most severe treatment condition (E). Dry weight loss indicates that some cells were severely disrupted to cell fragments smaller than the pore size of glass-fiber filter (1.2 μm) or that some soluble components were released into the medium (Salerno et al., 2009; Wouters et al., 2001). The release of soluble components also was confirmed by an increasing trend of SCOD that correlated to *TI*, which reached a 12.3 ± 0.0% increase of SCOD with condition E.

Table 5.1. FP treatment conditions and outputs

	A	**B**	**C**	**D**	**E**
Treatment intensity (kWh/m^3)	17.9	23.3	29.2	35.8	71.7
Outflow temperature (^oC)*	36	40	43	46	54
Culture appearance	Dark green	Dark green	Dark green	Dark green	Yellowish-green
Dry weight loss (%)**	1.37±0.02	2.05±0.02	2.05±0.00	6.16±0.09	9.44±0.10
SCOD increase (%)***	1.64±0.82	1.22±0.41	4.92±0.00	4.92±0.00	12.30±0.00
Log Reduction = -Log(N_t/N_0)****	0.0088	0.16	2	> 5	> 7

* Inflow temperature 26^{o}C

** Biomass was collected by GF/C membrane

*** SCOD was measured after filtering by 0.2-μm membrane filter

**** FP-treated culture was spread on BG-11 plate and counted by colonies; N_t, number of survivors after treatment; N_0, number of cells before treatment.

The more severe FP treatments also inactivated the *Synechocystis* cells. Although inactivation was not obvious with condition A, more than 5-log and 7-log reductions occurred with conditions D and E, respectively.

Disruption of the cell membranes was visualized by the uptake of SYTOX Green dye. Due to its large molecular size, SYTOX Green dye cannot penetrate an intact cell membrane; thus, it will not label healthy cells. However, when the cell membrane is damaged, the SYTOX Green dye can penetrate into the cell and combine with intracellular DNA so that the cell emits green fluorescence light. FCM results are shown in Figure 5.1, with the X-axis being SYTOX Green emission intensity and Y-axis the cell count with a given intensity. 92% of cells in the non-treated control had SYTOX Green emission under 30 Fluorescence Intensity Units (FIU), which also is confirmed by fluorescence microscopy. As FP treatment became more intense, the peak of fluorescence intensity shifted to higher range of FIU, indicating more disruption of membrane integrity; a similar observation also was reported for *E. coli* (Unal et al., 2002). Conditions D and E had 71% and 87% of the cells with a SYTOX Green emission higher than 30 FIU. It should be noted FCM may underestimate the actual percent of FP-treated cells that had membrane disruption, because cell fragments smaller than the bacterial-size were not counted.

TEM images of the cells before and after FP treatment, shown in Figure 5.2, illuminate the morphological impacts on disrupted cells. Compared to a non-treated healthy cell (Figure 5.2a), the FP-treated cell (condition D, Figure 5.2b) showed obvious disorder of the membrane structure. FP treatment severely

disorganized the intracellular thylakoid membranes (white arrows), and other cell organelles, such as the carboxysomes (symbol C), also were destroyed. Although FP treatment also compromised the plasma membrane and cell wall, as indicated by the penetration of SYTOX Green (Figure 5.1), those changes are not easily interpreted in TEM images.

Severe treatment conditions D and E caused some cells to disintegrate into fragments, as shown in Figure 5.2c. Using a wider field under lower magnification, we estimated that about 10% of the cells were disintegrated like the one in Figure 5.2c with treatment condition D. The fragmentation in these treatment conditions correlates to the observation of significant biomass loss (Table 5.1).

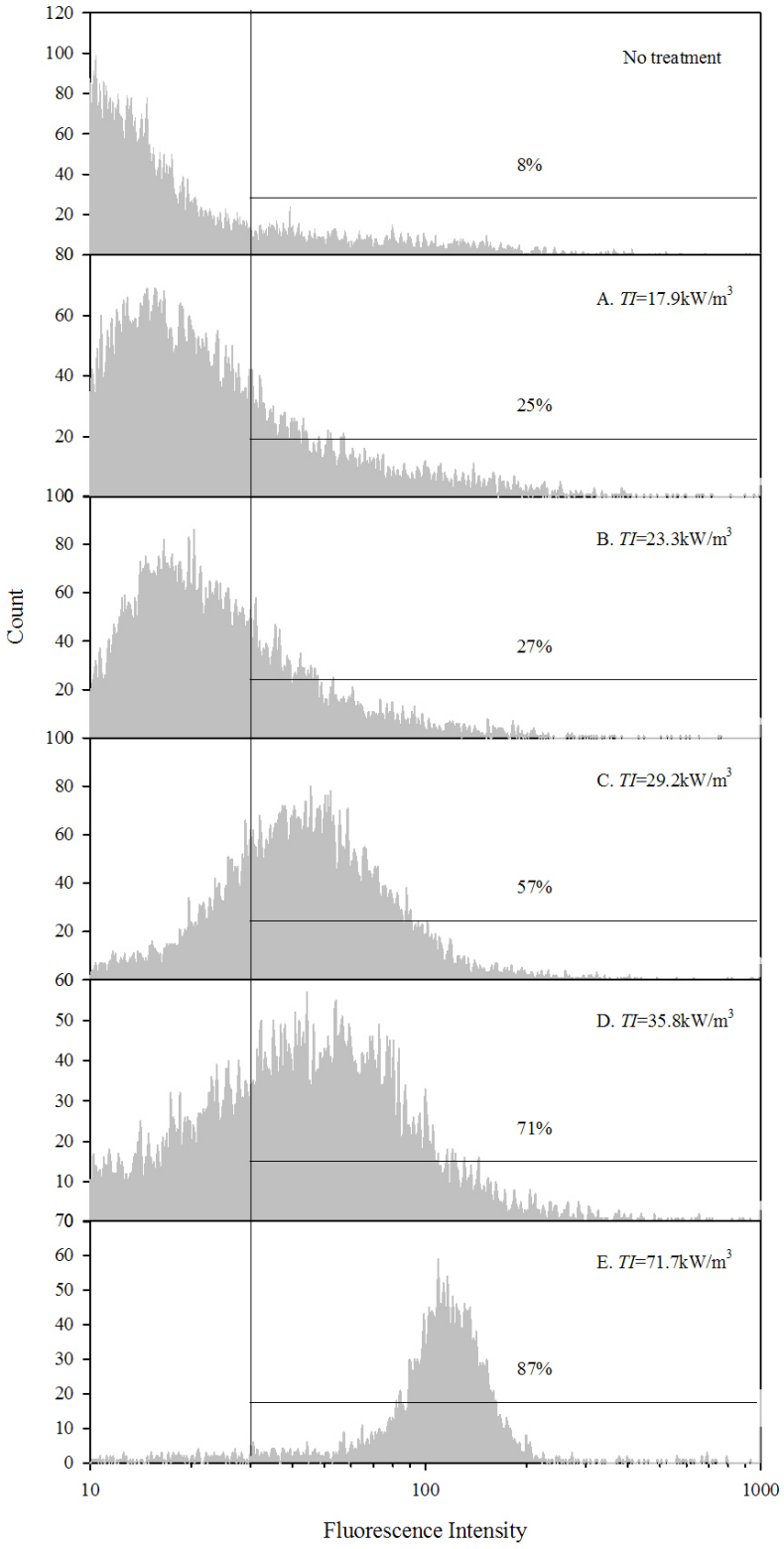

Figure 5.1. FCM of SYTOX Green staining of non-treated and FP-treated samples.

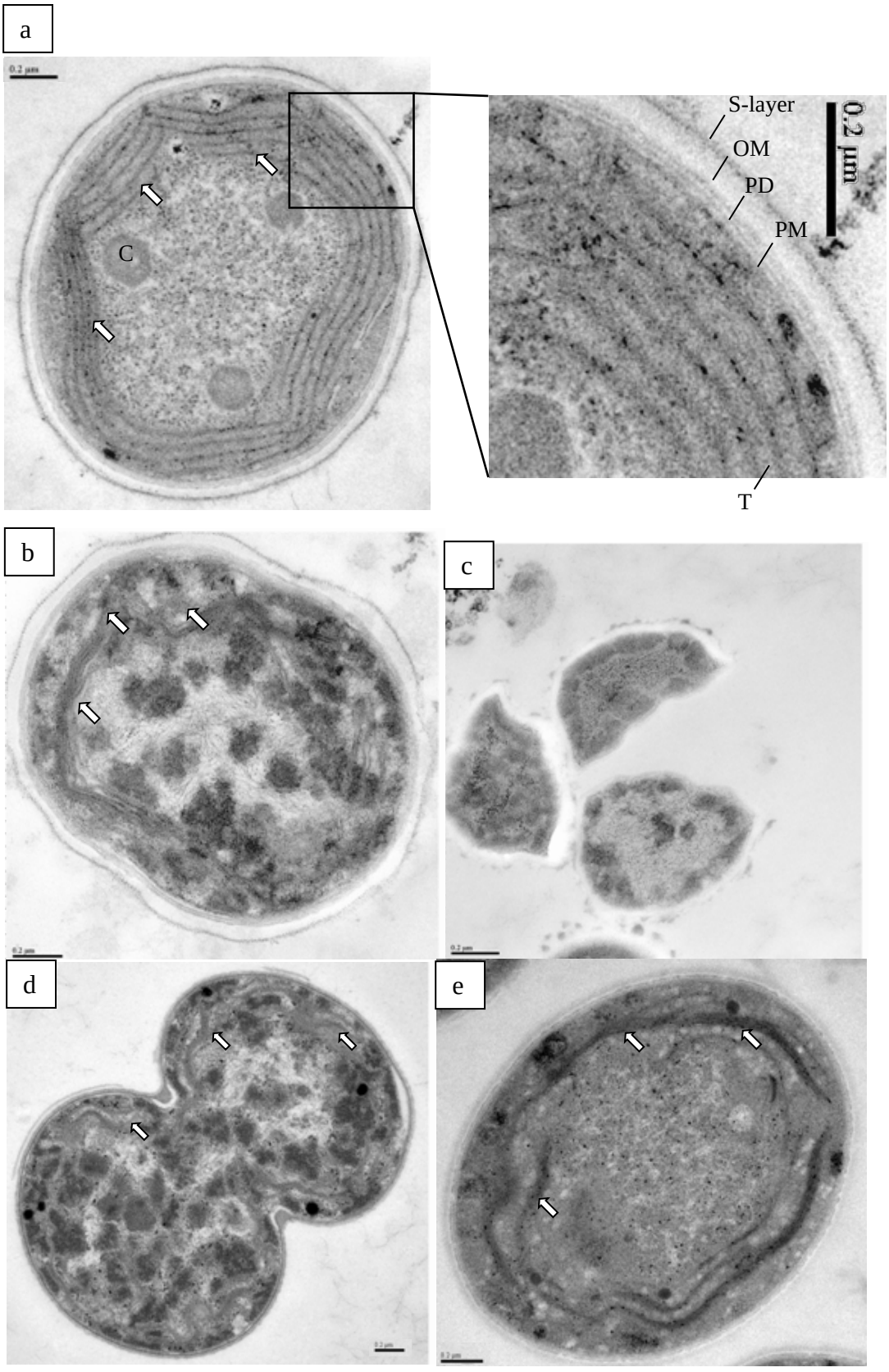
a
C
S-layer
OM
PD
PM
0.2 µm
T
b
c
d
e

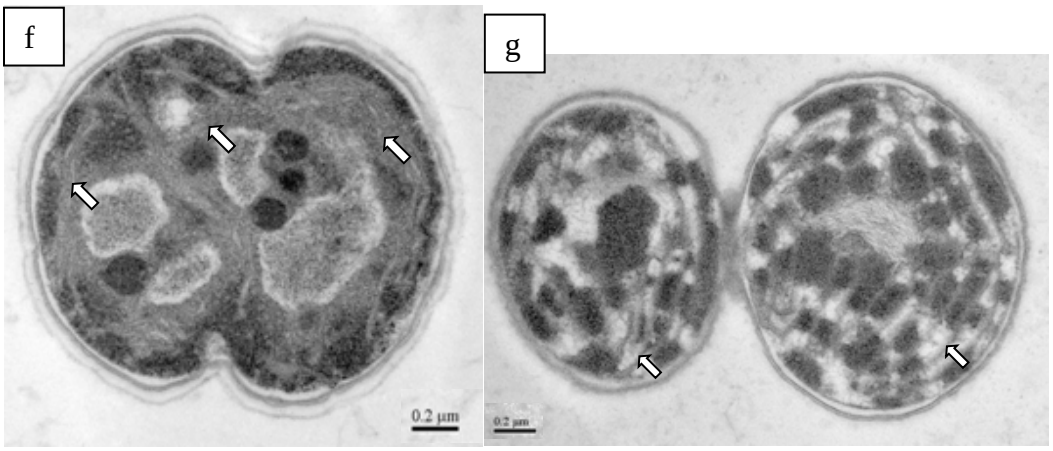

Figure 5.2. TEM images of non-treated and FP-treated cells under different conditions.

a. non-treated cell; FP-treated cells under condition A and B and heat-treated samples (up to 46^{o}C) showed similar shapes.

b. FP-treated cell under condition D; FP-treated cells under condition C and E showed similar shapes.

c. complete breakdown of a cell under FP treatment condition D; FP-treated cells under condition E showed similar shapes.

d. heat-treated cell at 54^{o}C.

e. low inlet temperature (inlet, 16^{o}C; outlet, 36^{o}C) FP-treated (condition D) cell.

f. non-treated cell, after direct isopropanol extraction.

g. FP-treated (condition D) cell, followed by isopropanol extraction.

White arrows show disruption and loss of thylakoid membrane. OM: Outer membrane; PD: peptidoglycan layer; PM: plasma membrane; T: thylakoid membranes; C: carboxysome. Scale bars in all figures represent 0.2 µm.

5.3.2 Heat-only treatment

One mechanism of cell disruption during FP treatment is electroporation, as the buildup of electrical charge on the dielectric lipid membrane causes disruption and, further, irreversible breakdown of the membrane. However, FP treatment also causes a significant temperature increase (Table 5.1), which also may be a cause of cell disruption. When we conducted heating-only experiments, we saw no significant biomass loss, compared to more than 5% loss in FP treatment condition D and E (Table 5.1). Thus, thermal denaturation was not severe enough to break up cells. Samples with heat-only treatment also were spread on BG-11 plates. A 2-log reduction was observed when the temperature was increased up to 46^{o}C, but this was much less than the > 5-log inactivation with FP treatment to 46°C (condition D, Table 5.1).

Comparison of plasma-membrane damage by FP treatment and heat-only treatment was further investigated using fluorescence microscopy. Figure 5.3 shows bright field, SYTOX Green emission, and auto-fluorescence of cells after various treatment conditions. Compared with non-treated cells (Figure 5.3a), FP-treated cells under condition E (Figure 5.3b) showed strong SYTOX Green emission. A similar uptake of SYTOX Green among the majority of the cells also took place after condition D, showing severe damage towards the plasma membrane. However, heat-only treatment to the same outlet temperature (46^{o}C) with FP treatment-condition D showed only a few cells stained by SYTOX Green, and the green emission was dim, indicating mild damage of cell membranes (Figure 5.3c and d). More cells and much brighter SYTOX Green emission were

observed after heat-only treatment to 54^{o}C (Figure 5.3e), indicating more intensive damage to the cell membrane. However, when we observed the FP-treated cells under a bright field (Figure 5.3f), only a portion of the cells was stained by SYTOX Green (green arrows), compared with staining of almost all cells after FP treatment (Figure 5.3b). Although thermal denaturation generated some damage to the plasma membrane, most of the disruption of the plasma membrane and cell wall came from the electric field of FP treatment.

We also observed denaturation of photosynthetic pigments by using fluorescence microscopy. We saw no red auto-fluorescence in FP-treated cells for condition E (54^{o}C, Figure 5.3b), although the cells retained auto-fluorescence with FP-treatment-condition D (46^{o}C). This disappearance of auto-fluorescence correlated to the change in the color of the culture from dark green to yellowish green after FP treatment, confirming the denaturation of phycocyanin and chlorophyll pigments. We saw similar patterns with heat-only treatment. The cells still retained auto-fluorescence emission when heated to 46^{o}C (Figure 5.3d), but no cell emitted red auto-fluorescence after the temperature reached 54^{o}C (Figure 5.3e). These similar observations indicate that the destruction of photosynthetic pigments can be attributed to thermal denaturation.

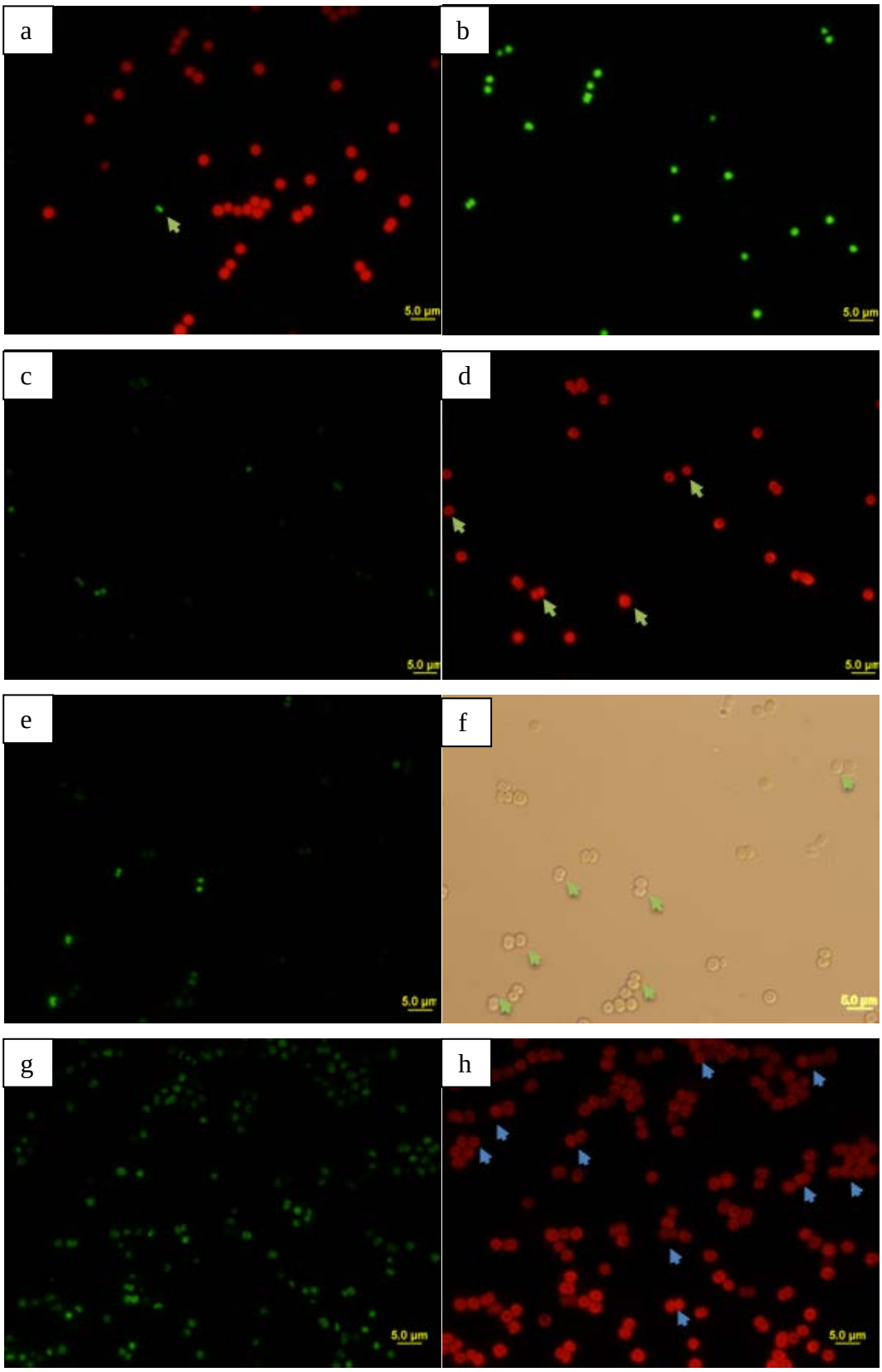
a
b
c
d
e
f
g
h
5.0 µm

Figure 5.3. Fluorescence-microscopy images of non-treated and FP-treated cells under different conditions:

a. combination of SYTOX Green emission (green) and auto-fluorescence (red) of non-treated cells.

b. SYTOX Green emission of FP-treated cells (condition E); no red auto-fluorescence emission was detected.

c and ***d.*** SYTOX Green and auto-fluorescence emission of heat-treated cells (46^{o}C).

e and ***f.*** SYTOX Green emission and light field of heat-treated cells (54^{o}C); no red auto-fluorescence emission was detected.

g and ***h.*** SYTOX Green and auto-fluorescence emission of low inlet temperature FP-treated cells (inlet 16^{o}C, outlet 36^{o}C, condition D).

Green arrows point to SYTOX Green stained cells. Blue arrows point to non-SYTOX stained cells.

Using TEM, we observed morphological changes from heat treatment, but they were less severe that with FP treatment. While most cells heated to 46°C maintained the well-organized structure of Figure 5.2a, heat treatment to 54^{o}C (Figure 5.2d) caused significant destruction of thylakoid membranes and cell organelles. However, no complete disruption, like Figure 5.2c, ever occurred in heat-only treatment. While FP treatment did have a synergistic relationship with the temperature increase of the medium, the forces associated with the electric field caused the complete breakdown of the plasma membrane and cell wall and the release of intracellular components.

5.3.3 FP treatment with lower inlet temperature

The separation of the heat effect from electric forces is further revealed by treatment with the same FP treatment intensity (condition D), but lower inlet temperature (16^{o}C vs. room temperature 26^{o}C). The outlet temperature after treatment was 36^{o}C. After treatment, most cells were still viable on BG-11 plates, and cells still retained their auto-fluorescence emission (Figure 5.3h), which confirmed that most inactivation and destruction of pigments came from the heat effect. No significant biomass loss was observed. However, membrane damage with FP treatment was similar for inlet room temperature and lower inlet temperature: TEM observation showed that similar disordering of the thylakoid membrane occurred after FP treatment for both temperatures (Figure 5.2b vs. Figure 5.2e). Since thylakoid membranes can act as dielectrics that build up electrical charge during FP treatment, the destruction of the thylakoid membrane

at lower temperature resulted from electric force rather than thermal denaturation. Fluorescence microscopy also revealed that most cells were stained by SYTOX Green (Figure 5.3g), but the SYTOX emission was not as bright as that with inlet room temperature (26^{o}C). These results confirm that, although destruction of auto-fluorescence compounds resulted from thermal denaturation due to a high outlet temperature, electrical forces were dominant in cell disruption. They also confirm that inlet temperature had a synergistic relationship with FP treatment, as higher inlet temperature enhanced cell damage under the same FP treatment intensity.

5.3.4 Lipid extraction

Due to cell disruption effects during FP treatment, intracellular lipids could be extracted more efficiently by the low-toxicity solvent isopropanol, particularly with a low solvent/wet biomass ratio. Figure 5.2f and g compare TEM images of cell residuals after isopropanol extraction with and without FP pre-treatment. With direct extraction, isopropanol did not efficiently break down intracellular thylakoid membranes, as shown by white arrows in Figure 5.2f. However, the extraction of FP-treated biomass (condition D) presented only a few residuals of damaged thylakoid membranes after isopropanol extraction (Figure 5.2g). This difference supports that the intracellular lipids that attached to the thylakoid membranes became more available for solvent extraction after FP treatment.

Figure 5.4 shows the lipid-extraction results (as FAME) by isopropanol with solvent/wet biomass ratios (v/v) of 5, 10, and 70. Lipid profiles did not change after FP treatment, indicating that FP did not destroy or alter the lipids. Using more solvent increased lipid recovery, as expected, but FP treatment also allowed more recovery for the lower solvent/wet biomass ratios. Compared to the control with no FP treatment, FP treatment boosted lipid recovery by 25 to 75% with the low solvent/wet biomass ratio of 5. The best recovery with the solvent/wet biomass ratio of 5 — condition A, 3.03% (wt. % FAME/biomass) — was better that the control at a ratio of 10 and only 20% less than the control for the very high ratio of 70. This enhancement by FP may be attributable to the fact that cells disrupted by FP treatment produced a less resistant barrier towards intrusion of organic solvent and a biomass pellet after centrifugation that could be more homogeneously mixed with organic solvent.

Lipid recovery declined as the FP treatment intensity became larger; this probably resulted from the slight biomass loss with larger *TI* (Table 5.1). Since the extraction procedure was performed only on the biomass solids, a loss of biomass solids should have diverted lipids from being extracted. In summary, the benefit of cell disruption by FP was maximized when solvent use and FP treatment intensity were at their lowest levels. These are promising results for lowering the costs and environmental effects of the solvent-based extraction step.

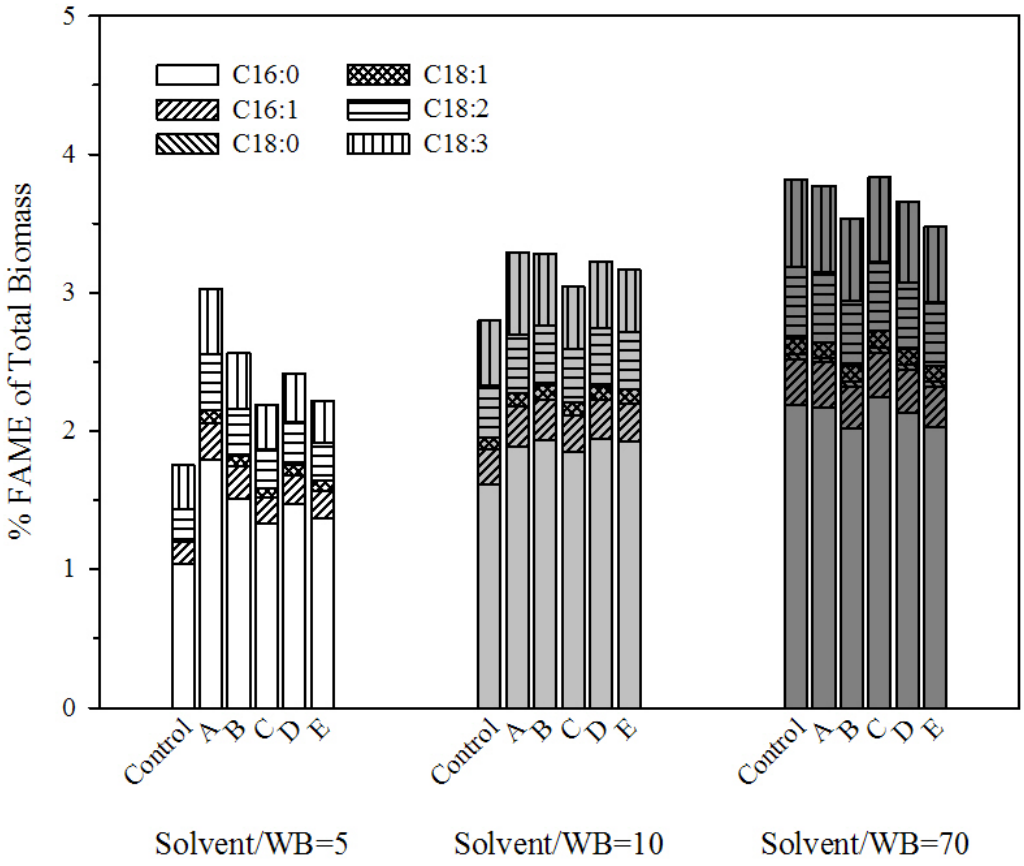

Figure 5.4. Lipid recovery (as FAME) by isopropanol extraction after FP treatment.

WB: wet biomass; A-E are different FP treatment conditions as present in Table 5.1.

5.4 Summary

Table 5.2 summarizes the main effects caused by electrical forces and temperature effects during FP treatment of *Synechocystis* PCC 6803. Whereas heat treatment destroyed auto-fluorescence and inactivated the cells, the electric field of FP (particularly for $TI > 35$ kWh/m^3) damaged the cell wall and the plasma and thylakoid membranes; fragmented cells; and enhanced the effectiveness by which isopropanol extracted intracellular lipids.

A sophisticated cost-benefit model is beyond the scope of this research. However, a brief calculation is presented here. Considering the use of FP at condition A (18 kW/m^3) for the treatment of concentrated biomass slurry of 30 kg/m^3 and a flow rate of 0.2 L/s, the total energy required for FP treatment will be 3 MJ/kg. The heating value of biomass can be estimated as 25 MJ/kg (Franco and Giannini, 2005). By this calculation, FP treatment can be economically feasible. A more concentrated biomass slurry and a higher treatment speed (i.e., higher flow rate) will further reduce the energy cost per kg biomass of FP treatment.

Table 5.2. Comparison of FP treatment (symbol ●) and heat-only treatment (symbol □)

	Control	**A**	**B**	**C**	**D**	**E**
FP Treatment intensity (kWh/m^3)	0	17.9	23.3	29.2	35.8	71.7
Outlet temperature (^oC)	26	36	40	43	46	54
Dry weight loss > 5%					●	●
Inactivation > 2-log				●	●	●
					□	□
Destruction of thylakoid membrane and cell organelle				●	●	●
						□
Disappearance of auto-fluorescence						●
						□
SYTOX Green uptake > 50%				●	●	●
Lipids (as FAME/biomass, wt.%) extracted by isopropanol with the low solvent: wet biomass ratio of 5	1.76	3.03	2.56	2.19	2.42	2.22

6 Disruption of *Synechocystis* PCC 6803 for Lipid Extraction[*]

6.1 Introduction

Renewable and carbon-neutral energy resources are becoming more essential for the sustainable development of our society (Campbell et al., 2009; Karaosmanoglu, 1999; Ragauskas et al., 2006; Rittmann, 2008). Among all possibilities, biofuel from phototrophic microorganisms — algae and cyanobacteria — appears to be promising due to their capability of massive cultivation, minimal competition with the food and water supply, and close zero net-carbon emission for the whole life cycle (Chisti, 2007; Hu et al., 2008). In particular, the, Gram-negative cyanobacterium *Synechocystis* PCC 6803 has gained attraction due to its physiological robustness and ability to be genetically transformed (Angermayr et al., 2009; Ikeuchi and Tabata, 2001; Koksharova, 2010; Vermaas, 1996).

Synechocystis's intracellular lipids and their fatty acids typically are the target feedstock for production of biofuel (Weier et al., 2005). The lipids normally are extracted by solvents (Sheng et al., 2011d). Before reaching lipids located in thylakoid membranes, organic solvents have to penetrate multiple barriers: the S-layer, outer membrane, peptidoglycan layer, and plasma membrane (Gombos et al., 1992; Liberton et al., 2006; Mullineaux, 1999; Sarcina et al., 2003; Zsiros et

[*] This chapter was presented at *8th IWA Leading-Edge Conference on Water and Wastewater Technologies* (Amsterdam, The Netherlands, 2011) and was accepted for publication as Sheng, J., Vannela, R., Rittmann, B.E. 2011. Disruption of *Synechocystis* PCC 6803 for lipid extraction. *Water Science and Technology*, DOI: 10.2166/wst.2011.879.

al., 2002). It may be necessary to disrupt the cells so that lipid extraction is efficient enough to make the process economically feasible (Cooney et al., 2009).

Cell-disruption methods can be categorized into physical, chemical, and enzymatic (Chisti and Mooyoung, 1986; Middelberg, 1995). Physical disruption techniques currently are more common for large-scale application due to their advantages of continuous operation, low costs, and relatively easy operation and maintenance (Middelberg, 1995). Table 6.1 summarizes key features of some typical physical-disruption techniques.

In this work, we attempted to disrupt *Synechocystis* PCC 6803 using seven cell-disruption techniques to make intracellular lipids more accessible by organic solvents prior to lipid extraction: autoclaving, bead beating, freeze drying, French press, microwave, pulsed electric fields (PEF), and ultrasound. We interpret the results in terms of cell disruption effects, mechanisms of disruption, and the degree to which they aid in lipid recovery from *Synechocystis* biomass.

Table 6.1. Mechanisms of typical physical cell-disruption methods

Methods	Description and Mechanisms	References
Autoclaving	Weakens and breaks chemical bonds within the cell wall or membrane of microorganisms. Shown to disrupt the outer membrane of *E. coli* to release periplasmic proteins (50 – 55^{o}C) and cytoplasmic proteins (90^{o}C).	Katsui et al. (1982); Middelberg (1995)
Bead beating	Disrupts cells with physical mechanisms such as collision with beads, compaction, or shearing action. The strength-providing components of the cell wall are torn up during the milling.	Ferrera et al. (2010)
Freeze drying	Improves solvation and penetration of the solvent by reducing the solvent dilution effect and water effect.	Hagerthey et al. (2006)
French press	Disrupts cells by mechanical force and pressure press when the cells pass through a very small size pore under very high pressure.	van der Staay and Staehelin (1994)
Microwave	Depends on dielectric heating. Promotes the rotation of molecular dipoles so as to disrupt weak hydrogen bonds. The movement of dissolved ions increases solvent penetration into the matrix and facilitates analyte solvation.	Cravotto et al. (2008); Metcalf and Codd (2000); Rasmussen et al. (2008)
PEF	Generates unequal electric charges that accumulate on dipolar molecules when a cell passes through the high-strength and quickly changing electric field. The pressure on the membrane produced by the attractive forces of unequal electric charges leads to the formation of irreversible pores in the membrane, and the membrane also loses its intrinsic properties of electrical resistance, membrane potential, and barrier function.	Guderjan et al. (2005); Rittmann et al. (2008b); Sheng et al. (2011c)
Ultrasound	Includes a metal probe (direct) or sonicator bath (indirect) to generate high-frequency (typically 2 – 50 kHz) oscillations that causes localized intense sonic pressure waves, resulting in cavitation and impaction. Increases the porosity and permeability of cell membrane and promotes the release of intracellular compounds. Considerable heat and free radicals that might react with biomolecules are also generated during sonication.	Liberton et al. (2006); Zhang et al. (2007)

6.2 Materials and methods

6.2.1 Cell growth and harvest

The methods of growth and harvest of *Synechocystis* PCC 6803 are the same as in Sheng et al. (2011d) and Kim et al. (2010). In brief, we grew *Synechocystis* on sterile BG-11 plates, transferred the colonies to a 250-mL flask, and then transferred the culture into a 25-L transparent carboy (2251 Clearboy, NALGENE, Rochester, NY) holding 20 L of BG-11 medium (Rippka et al., 1979; van de Meene et al., 2006). After about 2 weeks, we harvested biomass by concentrating the culture from 370 mg/L to 20,600 mg/L (dry wt.) using a Millipore Pellicon membrane module (0.45 μm) (Lee et al., 1998; Matyash et al., 2008). For PEF treatment, we used non-concentrated culture as the treatment required large volume of culture. We used the same batch of culture for all the experiments in this study.

6.2.2 Cell disruption

We used the conditions in Table 6.2 for autoclaving, bead beating, freeze drying, French press, microwave, PEF, and ultrasound. For microwave, PEF, and ultrasound, which generate heat, we performed controlled-temperature (maintaining at room temperature with ice during treatment) and no temperature control (final temperature reported in Table 6.2). A typical bead-beating treatment always required temperature control. All experiments were performed in duplicate.

Table 6.2. Experimental conditions for the disruption treatments

Methods	Conditions
Autoclaving	121^{o}C, 15 min
Bead Beating	1 mL culture + 0.2 mL 0.1-mm glass beads. 30 s on, 30 s pause, 3-min total treatment time. Cooled by ice, maintained at room temperature (26^{o}C)
Freeze Drying	Freeze dried to powder under 4.5 Pa, -48^{o}C for 1 d
French Press	2600 psi (gauge reading), mid speed
Microwave w/o temperature control	1.4 kW, 1-min treatment time. Final temperature 57^{o}C
Microwave with temperature control	1.4 kW, 30 s on, 30 s pause, 3-min treatment time, maintained at room temperature (26^{o}C)
PEF w/o temperature control	Treatment intensity 36 kWh/m^{3}, Final temperature 46^{o}C
PEF with temperature control	Treatment intensity 36 kWh/m^{3}, Final temperature 36^{o}C
Ultrasound w/o temperature control	2 kW, 3-min treatment time. Final temperature 52^{o}C
Ultrasound with temperature control	2 kW, 30 s on, 30 s pause, 15-min treatment time. Cooled by ice, maintain at room temperature (26^{o}C)

6.2.3 Evaluation of cell damage

We measured dry weight as total suspended solids (Method 2540D in *Standard Methods* (American Public Health Association, 2005)) by filtering the culture sample through a GF/C membrane (Whatman) and drying the membrane overnight at 105^{o}C. In order to measure released cell materials, we filtered the culture sample through a 0.2-μm membrane filter (GD/X, Whatman) and analyzed soluble chemical oxygen demand (SCOD) by the closed reflux colorimetric method (Method 5220D in *Standard Methods* (American Public Health Association, 2005)).

Transmission Electron Microscopy (TEM) provided detailed information about morphological changes after cell-disruption treatment. For sample pretreatment, we fixed the cells in 2% glutaraldehyde in 50 mM $NaPO_4$ at pH 7.2 and then post-fixed them with 1% osmium tetroxide in the same buffer. After acetone dehydration, we infiltrated the cells and embedded them in Spurr's epoxy resin polymerized at 60°C for 36 h. We then cut 60-nm sections and post-stained them in uranyl acetate and lead citrate (van de Meene et al., 2006). We observed specimen under a Philips CM12 TEM operated at 80 kV equipped with a Gatan model 791 camera.

6.2.4 Lipid extraction and analysis

We performed lipid extraction by the Folch method (Folch et al., 1957) with certain modification. Briefly, we took 0.15 mL of concentrated culture (after a cell-disruption treatment) and mixed it with 3 mL of solvent (chloroform:

methanol = 2:1, v/v) for total lipid extraction. We vortexed (VWR Vortex Mixer) the mixture for 24 h at room temperature and then filtered the solvent-biomass mixture through a 0.45-μm PTFE membrane (Whatman). We evaporated the filtrate completely under N_2 (Labconco RapVap N_2 evaporation system) to eliminate residual solvent, maintaining the evaporation temperature below 60^{o}C to prevent lipid loss (Cantrell and Walker, 2009).

In order to measure released lipids after cell disruption, we first measured suspended solid lipids (SS lipids) by filtering sample by 0.2-μm regenerated-cellulous membrane (Whatman) and exacting the solids as noted above. Then, we subtracted SS lipids from total lipids to calculate released lipids.

We performed lipid analysis according to Sheng et al. (2011d). We transesterified the lipids to fatty acid methyl esters (FAME) by acid catalysis and measured the FAME by a gas chromatograph (Shimadzu GC 2010) equipped with Supelco SP 2380 capillary column (30 m × 0.25 mm × 0.20 μm) and flame ionization detector (FID) for quantification. FAME quantification provides information about the fatty acids in lipids, the parts that are used for biofuel production.

6.3 Results and discussion

6.3.1 Cell morphological changes

Figure 6.1 shows morphological changes to *Synechocystis* cells based on TEM before and after cell-disruption treatments. Before cell disruption (Figure 6.1a), *Synechocystis* cells had distinct cell envelope, plasma membrane (black

arrows), and internal thylakoid membranes (white arrows). The different cell-disruption treatments resulted in distinct morphological changes (Figure 6.1b – i). High pressure during French press treatment (Figure 6.1b) brought about complete breakdown of the cell envelope. Most observed cell debris was cell wall and membrane, as most released debris from the cytoplasm was not collected during centrifugation prior to TEM. However, remaining fragments of thylakoid membrane still showed a well-aligned shape (white arrows); thus, the main effect of French press was mechanical disruption of the cell's integrity, but not chemical dissociation of membrane. Similarly, the compaction and shearing forces from bead beating (Figure 6.1c) resulted in significant disruption of the cell envelope such as S-layer, outer membrane, and cell wall (black arrows show all types). The shape of cell also was changed from smooth round to irregular shapes as a result of grinding. In contrast to the French press (Figure 6.1b), the cell was not completely disrupted, suggesting that the mechanical forces during bead-beating were less intense than those of the French press.

The sonic pressures and shear forces in ultrasonication (Figure 6.1d) also resulted in disruption of the cell envelope (black arrows), but the released heat and free radicals associated with ultrasonication also may have oxidized or thermally denatured membrane lipids, even though this type of damage may not be clearly depicted from a TEM image. The combination of heat and the electric field in PEF treatment (Figure 6.1e) destroyed the cell envelope and plasma membrane (black arrows show both), but also disordered the intracellular thylakoid membranes (white arrows).

Even with strict temperature control (no temperature increase), microwave treatment (Figure 6.1f) destroyed the intracellular thylakoid membranes (white arrows). This result may be explained by microwave's local thermal effect, as described in Table 1, since the bulk temperature was controlled and some thylakoid membrane residuals still can be seen. When the temperature was not controlled (Figure 6.1g), the destruction of intracellular materials became more severe.

After treatment by autoclaving (Figure 6.1h), intracellular thylakoid membranes were completely destroyed. In contrast, freeze-drying (Figure 6.1i) did not show much morphological change.

The complete disruption and the release of cell materials also are confirmed by SCOD measurement, as shown in Table 6.3. When compared to total COD of biomass (29,700 mg/L), 32.2 ± 0.8% of all cell materials was released after French press treatment, which correlates with the complete disruption showed in Figure 6.1b. The release of cell materials (increase of SCOD) was 29.8 ± 0.6% after ultrasound (w/o temperature control) and 29.2 ± 0.2% after autoclaving. Release of cell materials was less significant after other cell-disruption treatments. Heat clearly enhanced the release of cell materials as more SCOD increase was observed after ultrasound, microwave, and PEF without temperature than those conditions with temperature control.

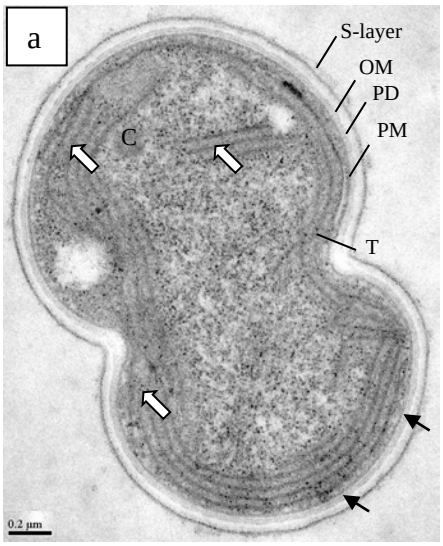
a
S-layer
OM
PD
PM
C
T
0.2 µm

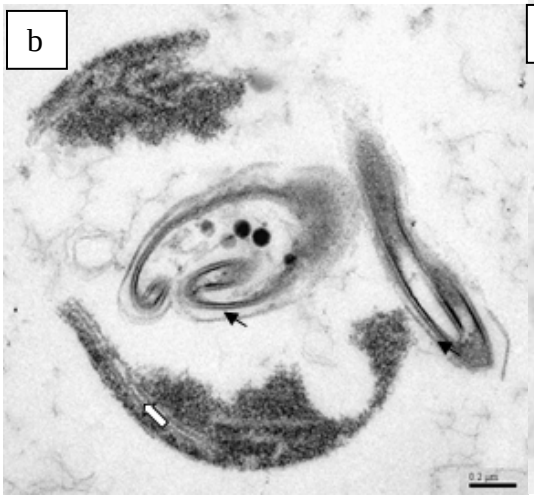
b

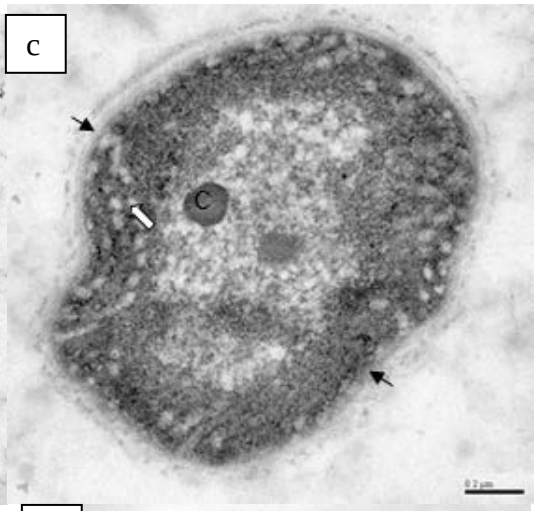
c
C

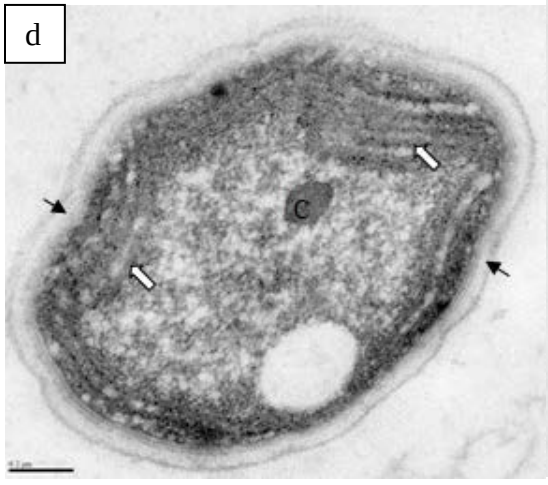
d
C

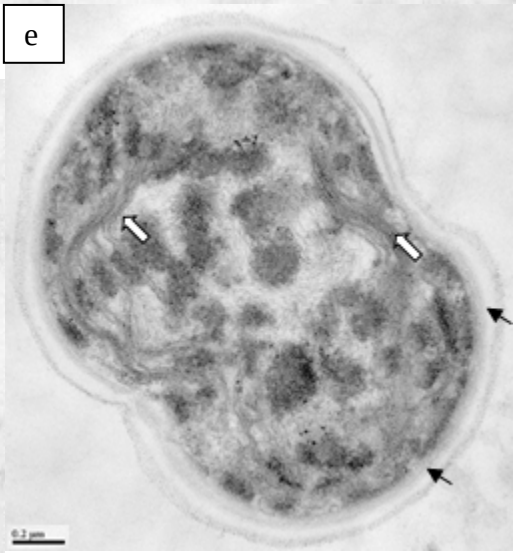
e

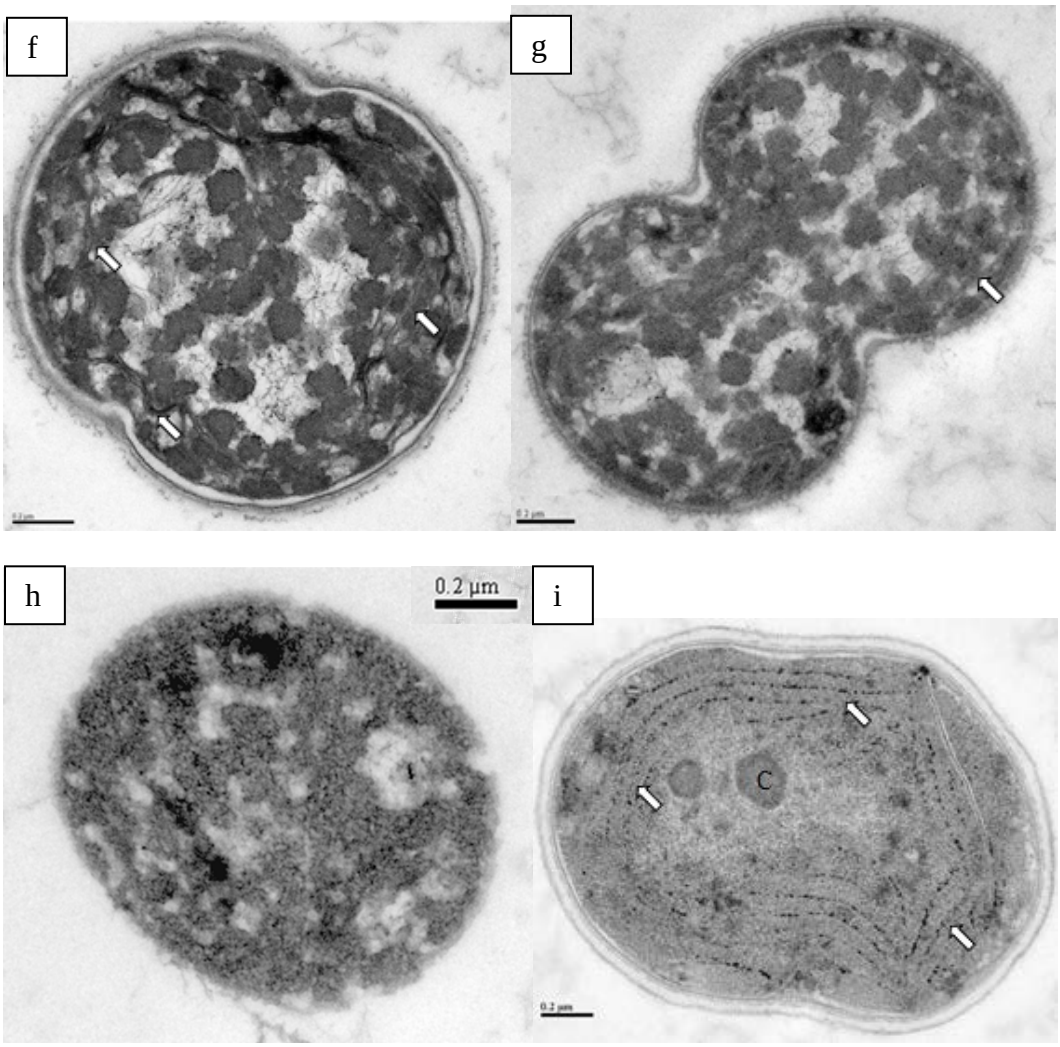

Figure 6.1. TEM observation of ***a.*** an intact healthy *Synechocystis* cell with no cell disruption; ***b.*** after French press; ***c.*** after bead beating; ***d.*** after ultrasound w/o temperature control; ***e.*** after PEF w/o temperature control; ***f.*** after microwave with temperature control; ***g.*** after microwave w/o temperature control; ***h.*** after autoclaving; and ***i.*** after freeze drying.

Black arrows show the cell envelope (S-layer, outer membrane, and cell wall) and cytoplasm membrane. White arrows show thylakoid membranes. OM, Outer membrane; PD, peptidoglycan layer; PM, plasma membrane; T, thylakoid membranes; and C, carboxysome. Scale bars in all figures represent 0.2 µm.

Table 6.3. Increase of SCOD (compare with non-disrupted control) after cell-disruption treatment

Sample	SCOD increase
Control	0.0%
French press	32.2 ± 0.8%
Ultrasound (w/o temperature control)	29.8 ± 0.6%
Autoclaving	29.2 ± 0.2%
Microwave (w/o temperature control)	14.5 ± 0.3%
Ultrasound (with temperature control)	6.7 ± 0.1%
Microwave (with temperature control)	4.4 ± 0.1%
PEF (w/o temperature control)	4.9 ± 0.0%
Bead beating	2.4 ± 0.1%
PEF (with temperature control)	1.4 ± 0.0%

Figure 6.2 shows the color of filtrates before and after each disruption treatment. After filtration, the no-treatment control was clear, indicating minimal release of cell materials. Filtrates of other samples showed different colors, indicative of the release of different pigments. Filtrate of the French-press-treated sample (FP) was dark green and oily, which indicated existence of lipids in solution. Microwave treated samples (MW and MWH, with temperature control and w/o temperature control) showed the lightest color among all samples, which was correlated with lower cell-material release. The yellow or yellow-green color of filtrates after autoclaving (AC), microwave (MW and MWH), and ultrasound w/o temperature control (USH) might indicate the thermal denaturation of chlorophyll or release of xanthophyll. The blue color of the filtrate after bead beating (BB) may be attributed to the release of phycobilin.

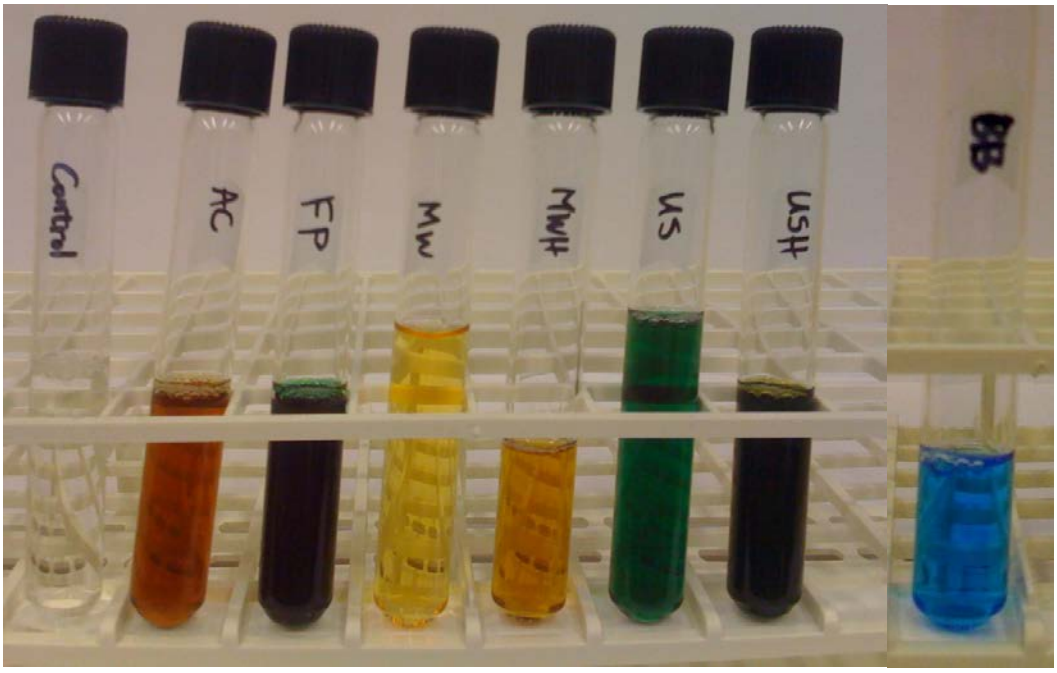

Figure 6.2. Colors of filtrates after cell-disruption treatment.

AC — Autoclaving; FP — French press; MW — Microwave (with temperature control); MWH — Microwave (w/o temperature control); US — Ultrasound (with temperature control); USH — Ultrasound (w/o temperature control); BB — Bead beating.

6.3.2 Lipid analysis

Figure 6.3 and Table 6.4 compare total extracted lipids (as FAME) before and after the different cell-disruption treatments. In term of total lipid extraction (as total FAME, black bars), most disruption treatments showed an increase of lipid recovery over the non-treated biomass (control). Among all methods tested, microwave (w/o temperature control) appeared to give the highest enhancement to lipid extraction (13% increase), following by autoclaving (12% increase), ultrasound (w/o temperature control, 10% increase), and PEF (with temperature control, 9% increase). Comparing temperature-controlled microwave and ultrasound with non-temperature controlled, heat helped enhance extraction while also shortening the extraction time. The non-temperature-controlled PEF yielded lower lipid (as FAME) recovery because non-concentrated culture was used for PEF treatment, so released lipids after cell disruption could not be recovered (total FAME not available). Although the French press and bead beating severely disrupt the cell envelope, they, like freeze drying, did not significantly enhance lipid extraction. It seems that the dissociation of chemical structure was more important for the enhancement of lipid recovery than simple mechanical forces.

Table 6.4 also shows detailed fatty acid profile (individual FAME/total FAME) of the total extracted lipids. Although significant enhancement of lipid recovery was observed for microwave, autoclave, ultrasound, and PEF, no significant changes of fatty acid profile was observed among treated samples and non-treated control. It seems this enhancement did not target to specific lipid species.

Released lipids after treatment can be calculated from total lipid (total FAME) – suspended lipid (SS FAME) (black bar – grey bar) in Figure 6.3 and Table 6.5. No SS FAME value is available for freeze drying, because all the cell mass was freeze dried and, therefore, counted as total FAME during the treatment. Autoclaving, French press, and ultrasound treatment caused significant release of lipid into the medium. For example, 35.1 ± 0.1% of total lipids was released after French-press treatment, 31.8 ± 0.1% after autoclaving, and 27.8 ± 0.1% after ultrasound (w/o temperature control). Release of cell materials correlated with signs of cell disruption, as previously noted from TEM observation, SCOD, and filtrate colors. The release of lipids was not significant after microwave and bead beating treatments. Table 6.5 also shows detailed fatty acid profile of the SS lipids. No significant change of fatty acid profile was observed among treated samples and non-treated control. The release of lipids did not target to specific lipid species.

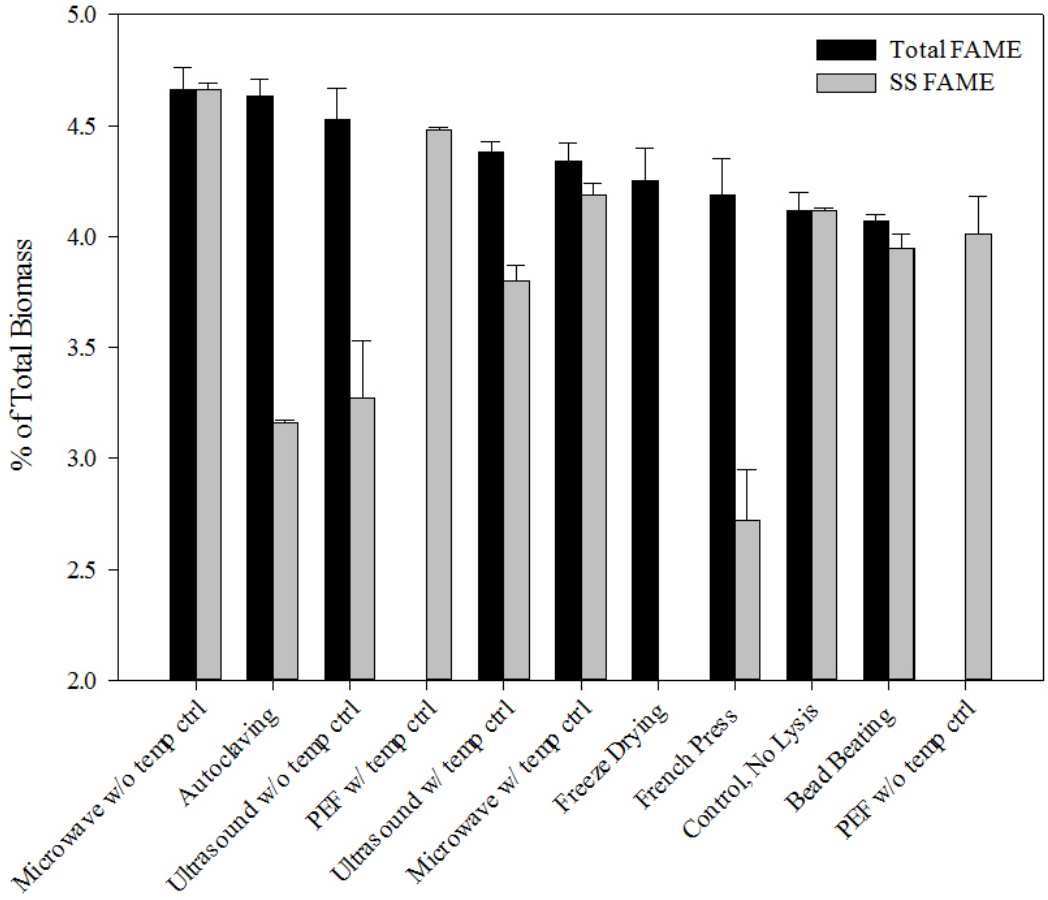

Figure 6.3. Percent FAME of total biomass (dry wt. %) after different cell disruption treatments following total-lipid (total FAME) and suspended-lipid (SS FAME) extractions from *Synechocystis* PCC 6803.

No total FAME value is available for PEF; SS FAME is not possible after freeze drying.

Table 6.4. Extracted total lipid recovery (as FAME) after cell-lysis treatment

Sample	Fatty acid profile (% Individual FAME/total FAME)						FAME (%)**	Lipid Incr. (%)
	C16:0	C16:1	C18:0	C18:1	C18:2	C18:3		
Control	55.3	8.1	4.4	2.8	12.4	17.1	4.12 ± 0.08	----
MWH*	56.0	8.6	1.8	2.7	13.0	18.0	4.66 ± 0.10	+13.1
AC	55.8	8.3	3.0	2.6	12.7	17.5	4.63 ± 0.08	+12.4
USH	56.0	8.5	2.2	2.6	12.9	17.7	4.53 ± 0.14	+10.0
US	55.8	8.5	2.6	2.7	12.9	17.7	4.38 ± 0.05	+6.3
MW	55.8	8.4	2.9	2.7	12.7	17.5	4.34 ± 0.08	+5.3
FD	56.2	8.5	2.7	2.7	12.6	17.2	4.25 ± 0.15	+3.2
FP	55.9	8.4	2.6	2.8	12.7	17.6	4.19 ± 0.16	+1.7
BB	55.7	8.7	1.9	2.7	13.1	17.9	4.07 ± 0.03	-1.2

* MWH — Microwave (w/o temperature control); AC — Autoclaving; USH — Ultrasound (w/o temperature control); US — Ultrasound (with temperature control); MW — Microwave (with temperature control); FD — Freeze drying; FP — French press; BB — Bead beating

** Percentage FAME of total biomass (dry wt. %).

Table 6.5. Suspended solid lipid recovery and calculation of lipid release after cell-lysis treatment

Sample	**Fatty acid profile (% Individual FAME/total FAME)**						**FAME (%)****	**Lipid release (%)**
	C16:0	**C16:1**	**C18:0**	**C18:1**	**C18:2**	**C18:3**		
Control	55.8	8.4	2.5	2.7	12.8	17.8	4.12 ± 0.01	0.0
FP*	55.2	8.4	3.4	3.1	12.7	17.3	2.72 ± 0.23	35.1
AC	55.4	8.2	3.0	3.0	12.9	17.5	3.16 ± 0.01	31.8
USH	56.3	8.5	2.4	3.4	12.7	16.6	3.27 ± 0.26	27.8
US	55.5	8.6	2.5	2.8	12.9	17.6	3.80 ± 0.07	13.2
BB	55.8	8.6	1.9	2.8	13.0	17.8	3.95 ± 0.06	3.0
MW	55.8	8.6	2.4	2.8	12.9	17.6	4.19 ± 0.05	3.5
MWH	56.1	8.5	1.7	2.7	13.1	17.9	4.66 ± 0.03	0.0
FD	--***	--	--	--	--	--	--	--

* FP — French press; AC — Autoclaving; USH — Ultrasound (w/o temperature control); US — Ultrasound (with temperature control); BB — Bead beating; MW — Microwave (with temperature control); MWH — Microwave (w/o temperature control); FD — Freeze drying

** Percentage FAME of total biomass (dry wt. %)

** Not available.

6.4 Conclusions

The cost of downstream processing of biomass comes from two major steps: cell disruption and lipid extraction. In order to be cost effective in the cell-disruption step, the energy input should be minimized. For lipid extraction, keeping the lipid with the suspended phase, not in the liquid medium, is preferred to minimize solvent usage and to be able to recycle medium. In this light, microwave and PEF (with temperature control) seem to be the best suited techniques for large-scale cell disruption, because they provide enhanced lipid recovery (9 – 13%) while retaining most lipids in the suspended phase. Autoclaving, bead beating, freeze drying, French press, and ultrasound may not be as well suited to large-scale application, because they yield an insignificant enhancement of lipid extraction, a release of the lipids to medium, or both.

7 Behavior of Excreted Free Fatty Acids from Mutant-type *Synechocystis*

7.1 Introduction

A recent breakthrough through genetic modification allows mutant-type *Synechocystis* to produce and excrete free fatty acids (FFA), typically C12 through C18 (Kaczmarzyk and Fulda, 2010; Liu et al., 2011b). The excreted FFA can be further decarboxylated to long-chain alkanes, generally known as renewable diesel, with a composition similar to petroleum diesel and potentially useful as jet fuel (Knothe, 2010). Compared with intracellular lipids from wild-type *Synechocystis*, excreted FFA not only avoids energy-consuming dewatering, cell disruption, and biomass extraction, but also simplifies the conversion process to usable energy. The alkane-based renewable diesel has several advantages to fatty-acid-methyl-ester (FAME)-based biodiesel, including the ability to use existing refinery and distribution infrastructure, a very high cetane number, a lower cloud point, greater stability, and lower nitrogen oxides (NO_x) and hydrocarbons (HC) exhaust emissions (Knothe, 2010; Kubicková et al., 2005).

Large-scale production of excreted FFA from mutant-type *Synechocystis* presents significant technical challenges. First, under certain conditions, the modified gene of mutant-type *Synechocystis* may be unstable in mass production, which leads to the loss of FFA-producing capability. Second, mutant-type *Synechocystis* also may yield its domination to wild-type *Synechocystis* or contaminant phototrophs due to its slower growth rate. Third, the solubility of FFA in aqueous phase is limited and is drastically reduced at neutral or acidic pH.

For example, the solubility of lauric acid (C12:0) at pH = 6 is two orders of magnitude lower than that at pH = 8 (10^{-4} vs. 10^{-2} mol/L) (Nyren and Back, 1958). The FFA can also combine with divalent cations, such as Ca^{2+} to form calcium soap scum or lime soap (Graham and Sackman, 1983; Owen et al., 1995), which usually has 10-times lower solubility than its corresponding FFA (Yoke, 1958). The insoluble precipitates of FFA and FFA salts can attach and accumulate on the walls of a photobioreactor (PBR), which adds difficulty to harvesting the FFA (Vorum and Brodersen, 1994). Fourth, dissolved FFA appears to be an excellent food for FFA scavengers, such as heterotrophic bacteria, that may biodegrade the FFA and reduce the FFA yield (Ding and Sun, 2005; Klein et al., 1971; Novak and Kraus, 1973; Sousa et al., 2009). In this chapter, I focus on the challenges from precipitation and biodegradation.

Several strategies may be useful to overcome the loss of FFA by precipitation and biodegradation. Addition of EDTA, a potent chelator of divalent cations (especially calcium), may help solubilize fatty acids complexed to calcium (Owen et al., 1995). Because *Synechocystis* is reported to tolerate high pH (pH > 10) (Lopez-Archilla et al., 2004; Summerfield and Sherman, 2008; Zhang et al., 2009b), a high pH (pH = 10 – 11 vs. 8 – 9) increases the FFA solubility and also prevents precipitation of calcium soap scum, because other Ca^{2+} precipitates, such as $Ca(OH)_2$ or $CaCO_3$, form preferentially at high pH. High pH also may selectively inhibit the growth of heterotrophic bacteria and their uptake of FFA, as reported in the literature (Galbraith and Miller, 1973; Meseck, 2007).

Other strategies also may help prevent FFA loss. Rapid harvest of FFA by an adsorptive resin may sequester FFA from FFA scavengers. Two types of polymeric resins, ion-exchange or hydrophobic, can be considered (Levario et al., 2011; Nielsen et al., 2010; Nielsen and Prather, 2009). Routine harvest of resin with adsorbed FFA may be required to maintain a low enough FFA concentration to prevent significant accumulation of FFA scavengers in the suspension or on the outer surface of the resin. Sterilizing the PBR and addition of antibiotic agents also can help inhibit the growth of FFA scavengers, while maintaining a culture dominated by FFA-excreting mutant-type *Synechocystis*.

It is important that the conditions imposed to minimize FFA precipitation and biodegradation also be suitable for a high FFA production rate (FPR) by mutant-type *Synechocystis*. For example, it would be self-defeating if high pH inhibited mutant-type *Synechocystis* cells or their FFA production and excretion; a FFA-loss-prevention strategy that has these negative effects must be avoided.

In this study, I first monitored non-steady-state FFA production and loss in several growth conditions and scales. Based on those results, I discuss and document FFA loss by precipitation and biodegradation by heterotrophic bacteria. I then evaluate potential solutions (i.e., high pH, resin adsorption, and sterilization techniques) and their net effects on preventing FFA loss.

I designed, performed, and interpreted most of the experiments presented in this chapter; however, members of the PBR Research Team performed some parts of the experiments in this chapter. My work focused on routine sampling; FFA elution, extraction, and analysis; interpreting data; and writing the

manuscript. For experiments with bench-top photobioreactors (BT-PBR) and single-tube roof-top photobioreactors (ST-PBR), other important contributions were by Dr. Ravi Vannela (coordinating all experiments); Joshua McIlwain and Cody Anderson (inoculation and maintenance); Binh Nguyen, Christopher Bremer, and Swathi Sridharakrishnan (inoculum and medium); Dr. Hyun Woo Kim (chemical analysis); Chao Zhou (water chemistry model); Alexander Zevin (T-RFLP, terminal restriction fragment length polymorphism); Dr. David Nielsen's laboratory (selecting resins and developing FFA-elution methods); and Dr. Robert W. Roberson's laboratory (light microscopy). The high-pH experiments were collaborations between Joshua McIlwain and me, with support from Alexander Zevin (T-RFLP) and Dr. Robert W. Roberson's lab (light microscopy).

7.2 Materials and methods

7.2.1 Cell culture

We obtained the mother inoculum of mutant-type *Synechocystis* TE/Δ*slr1609* (TE/Δ*slr1609* for short) from Dr. W. F. J. Vermaas of the School of Life Sciences, Arizona State University. In brief, TE/Δ*slr1609* was constructed by expressing California Bay acyl-ACP thioesterase (TE) in a background strain with over-expressed AccABCD and PAP, yielding the TE strain. The insertion of TE helps the excretion of FFA, while the over expression of AccABCD increases the production of FFA. Then, *slr1609* was knocked out by insertion of a chloramphenicol resistance cassette to reduce the utilization of produced FFA.

The typical profile of excreted FFA by TE/Δ*slr1609* is shown in Figure 2.8a in Chapter 2. The major FFA species is lauric acid (C12:0, > 90% wt.), with myristic acid (C14:0, < 10% wt.) and palmitic acid (C16:0) detectable. Other FFA species – C8:0, C10:0, C16:1, C18:0, C18:2, C18:3 – occur in trace amounts.

We maintained the pure strains on sterile BG-11 plates with 10-mM TES-NaOH (pH 8.0) (TES is N-tris(hydroxymethyl)methyl-2- aminoethanesulfonic acid), 1.5% agar, and 0.3% sodium thiosulfate (Rippka et al., 1979; van de Meene et al., 2006). We collected and transferred colonies to a 250-mL autoclaved flask containing 100 mL sterile BG-11 medium and allowed cells to grow for 4 to 5 d at a light irradiance (LI) of 100 µmol photons/m^2-s and a constant temperature of 30^{o}C.

7.2.2 Cell growth and scaling

We transferred and scaled up the inoculum to a bigger flask, carboy, commercial wave bioreactor (GE Healthcare Life Sciences), and BT-PBR or ST-PBR for the experiments described below.

The bigger flask was a 1-L autoclaved flask containing 500 mL sterile BG-11 medium. We sparged air (2 – 5 LPM) through a bacterial air vent filter (Pall Life Sciences) into the flask to provide CO_2 and grew the cells at a constant LI of 300 µmol photons/m^2-s and room temperature of 26^{o}C.

We also scaled the culture to 20-L carboys (Nalgene) that were sparged with filtered laboratory air at room temperature of 26^{o}C. We provided a constant

LI of 300 µmol photons/m^2-s on the side by light panels with white-fluorescent lamps.

When further scaled up to 16-L (working volume) BT-PBR, we used the BT-PBR with the same configuration as that described in section 4.2.1 of Chapter 4. We set the computer-controlled temperature to 30^{o}C and total LI to 108 W/m^2 (≈500 µmol photons/m^2-s), and we used a flow rate of 10 L/hr of air enriched to 2.5% (v/v) CO_2. We also set the impeller speed at 200 rpm to provide sufficient agitation.

We also used a 10-ft long and 6-in diameter ST-PBR with total volume in tube 75 L (working volume 65 L). A 20-L harvest tank (working volume 15 L) was attached to the ST-PBR. Cells growing in the ST-PBR were exposed to ambient LI, as discussed in section 1.3.1 of Chapter 1. We controlled the temperature by circulating water flowing through the water jacket around the tube and sparged air at a flow rate of 3 to 35 LPM with 0.1 – 5% CO_2 into the reactor, as needed.

In order to provide a sterilized environment with minimal perturbation from sampling activities, we investigated a commercially available wave bioreactor from GE Healthcare Life Sciences (http://www.gelifesciences.com/aptrix/upp01077.nsf/content/wave_bioreactor_home). This sterilized and disposable bioreactor is made by transparent plastic with preset aeration and sampling ports. We grew 1 L of culture in a 2-L wave bioreactor and shook the reactor on a VWR standard analog shaker. We used the same LI, and temperature conditions as those of bigger flask noted above. The air

sparging was 1 LPM. We also added 5 mg/L antibiotics — spectinomycin — into the BG-11 medium, as it is reported to inhibit heterotrophic bacteria while having minimal impact on mutant-type *Synechocystis* (Carter et al., 2000; Hirani et al., 2001).

7.2.3 pH control

In order to stabilize the pH of the culture, we dosed 25 to 35 mM of the commonly used organic buffer CAPS (3-(Cyclohexylamino)-1-propanesulfonic acid) to provide buffer capacity for pH in the range of 9.7 – 11.1 (Summerfield and Sherman, 2008; Zhang et al., 2009b). We then titrated with 1 M NaOH or 0.5 M H_2SO_4 to obtain the desired pH value. We filtered CAPS, NaOH, and H_2SO_4 solutions through 0.2-μm Acrodics syringe filter membrane (Pall Life Sciences) to avoid bacterial contamination.

7.2.4 FFA harvest by resin

In some BT-PBR and ST-PBR experiments, we added adsorptive resin for the purpose of rapidly harvesting FFA. We attached a resin column containing ion exchange resin Lewatit® MP-64 (Sigma-Aldrich) to the BT-PBR. Culture was circulated by pump between the BT-PBR and the resin column so that FFA could be adsorbed from the medium. We also dosed 150 to 500 g hydrophobic polymeric resin DOWEX™ OPTIPORE™ L493 (Dow Chemical) to the harvest tank attaching to the ST-PBR. Resin particles were well mixed with the culture inflow from the single tube and were well separated by filtration system from the

outflow to retain the resin in the harvest tank. We regularly sampled or replaced resin to assay for FFA. We decanted aqueous medium and eluted FFA from the resin by methanol. The mixture of methanol and FFA was injected to gas chromatography (GC) for FFA measurement and compared the results with pre-defined elution curve to calculate the amount of FFA on the resin (Levario et al., 2011).

7.2.5 Culture purity check

In order to check the purity of the culture, we used the fluorescence dye SYTO 9 (Invitrogen, Carlsbad, CA) to label all bacteria. Non-*Synechocystis* cells show only SYTO 9 green emission, but not red auto-fluorescence characteristic of *Synechocystis*. We prepared and used stock solution of SYTO 9 according to the manufacturer's instruction. Prior to mixing with SYTO 9 solution, we concentrated the cells by centrifugation at 13,000 *g* for 2 min and re-suspended them in DI water (pH 7.0) twice to eliminate interferences from BG-11 medium.

We observed staining results with an Olympus BX61 fluorescence microscope with a DP70 camera. We loaded stained sample to a slide coated with 2% agarose in BG-11 (Huang et al., 2002). Total bacteria with SYTO 9 Green emission were detected using a FITC filter (ex. 460 – 505 nm, em. 510 – 550 nm). Red auto-fluorescence emission from *Synechocystis* phycocyanin and chlorophyll was detected using a CY5 filter (ex. 605 – 655 nm, em. 670 – 720 nm). We obtained and post-adjusted images with DP-BSW software (Olympus).

We also maintained regular check of culture purity by light microscopy and T-RFLP. Methods for light microscopy and T-RFLP are presented in detail in section 4.5 of Chapter 4.

7.2.6 FFA sampling and extraction

To sample and extract excreted FFA by TE/Δ*slr1609*, we first shook the whole culture by hand to achieve a homogeneous distribution of FFA; we also took enough liquid culture samples (usually more than 10 mL). This sampling method is sufficient to get good representation of the FFA production by the culture, even in the presence of FFA precipitation. In BT-PBRs and RT-PBRs, where ideal homogeneousness cannot be achieved, the sampling of FFA may have a negative bias due to FFA precipitation. We then took a 1-mL sample and added 20 µL of 0.5 M EDTA to retrieve any precipitated FFA (mainly calcium or magnesium fatty acid salts) back to the dissolved phase. We centrifuged the sample at 13,000*g* for 2 min to remove biomass, transferred supernatant into an 8-mL glass tube, and adjusted the pH and ionic strength by adding 80 µL of 50% H_2SO_4 and 0.05 g NaCl. We then added 2 mL hexane, vortexed (VWR Vortex Mixer), and centrifuged the samples at 1,900*g* for 5 min to separate the aqueous and hexane layers. In order to have the FFA concentration fall into the linear range of calibration curve, we resized the volume of hexane/FFA mixture before injecting into GC, if necessary.

7.2.7 FFA measurement

We identified and quantified FFA using a GC equipped with a Supelco Nukol capillary column (30 m × 0.53 mm × 0.50 μm) and a flame ionization detector (FID). The operating conditions were as follows: Split ratio 1:10; inject volume 1μL; helium carrier gas with constant flow rate 30 mL/min; H_2 40 mL/min, air 400 mL/min, make up gas (helium) 5 mL/min; injector and detector temperature 250^{o}C; and oven temperature started at 100^{o}C and increased at rate of 10^{o}C/min to 220^{o}C and hold for 5 min.

7.3 Results and discussion

7.3.1 Evidence of FFA loss in culture scaling

Batch growth in flask. We performed batch growth of TE/Δ*slr1609* in a flask (culture volume 500 mL). Figure 7.1 shows the monitoring of biomass, FFA (mainly C12:0, > 90% wt.), and pH. After 5 days of acclimation, the flask culture showed exponential growth of biomass and continuous production and excretion of FFA from Day 6 to Day 16. The average biomass growth rate (BPR) and specific growth rate (μ) were 103 mg/L/d and 0.2 d^{-1}, respectively. The best net FFA production rate (nFPR) was 10 mg/L/d, with the average nFPR being 7.6 mg/L/d for Days 6 – 14. In order to calculate electron-equivalent flow to FFA, we assumed (1) the same composition of TE/Δ*slr1609* biomass as with wild-type *Synechocystis* biomass, and (2) all excreted FFA was C12:0. Then, the electron equivalent of biomass was 0.18 e^{-} eq/g from Table 1.3 of Chapter 1, and the electron equivalent of FFA was 0.34 e^{-} eq/g from the similar calculation to

equations (1.1) and (1.2) of Chapter 1. As a result, ~12% of electrons were located in FFA, with the other ~88% in biomass.

We recharged with fresh medium (~100 mL) on Day 16 to overcome volume loss from sampling. The dilution during recharge reduced the biomass and FFA concentrations. After fresh medium was added, growth of biomass and FFA continued until Day 22, when a drastic decrease of FFA was observed, even though the biomass was still growing. FFA completely disappeared within 2 days. Reasons for the FFA loss in experiments presented in this section are discussed in detail in section 7.3.2.

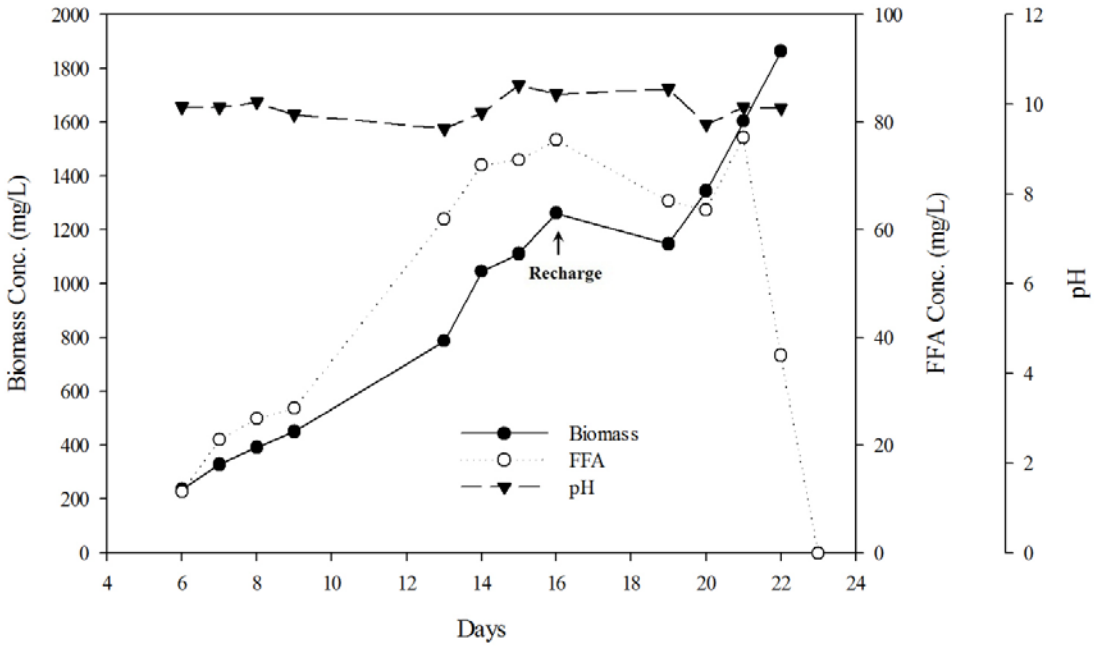

Figure 7.1. Batch growth of TE/Δ*slr1609* and concomitant production of FFA in a flask.

Batch growth in carboy and BT-PBR. We observed similar FFA loss in carboy and BT-PBR experiments. Figure 7.2 shows monitoring results for biomass, FFA, and pH during batch growth of TE/Δ*slr*1609 in a 20-L carboy. Due to light limitation, the growth rate of *Synechocystis* in the carboy was slower than in the flask (Figure 7.1). The average BPR and μ were 16 mg/L/d and 0.07 d^{-1}, respectively (vs. 103 mg/L/d and 0.2 d^{-1} in Figure 7.1). FFA accumulated from Day 7 to Day 14, with average nFPR of 0.3 mg/L/d. The electron-equivalent flow to FFA in the carboy was ~3.4%, significantly less than that in the flask (~12%), showing either that FFA was produced more slowly or consumed in the carboy. The FFA concentration declined after 14 days and was completely consumed by Day 23.

FFA loss became more prominent when further scaling up the TE/Δ*slr1609* culture. Figure 7.3 shows batch growth of TE/Δ*slr1609* in a BT-PBR. The FFA concentration increased during the first two days, but sharply decreased on Day 3, even though biomass sustained growth for the rest of the experiment. The decrease of FFA correlated with the appearance of non-*Synechocystis* bacteria by light-microscopy, as discussed in section 7.3.2.

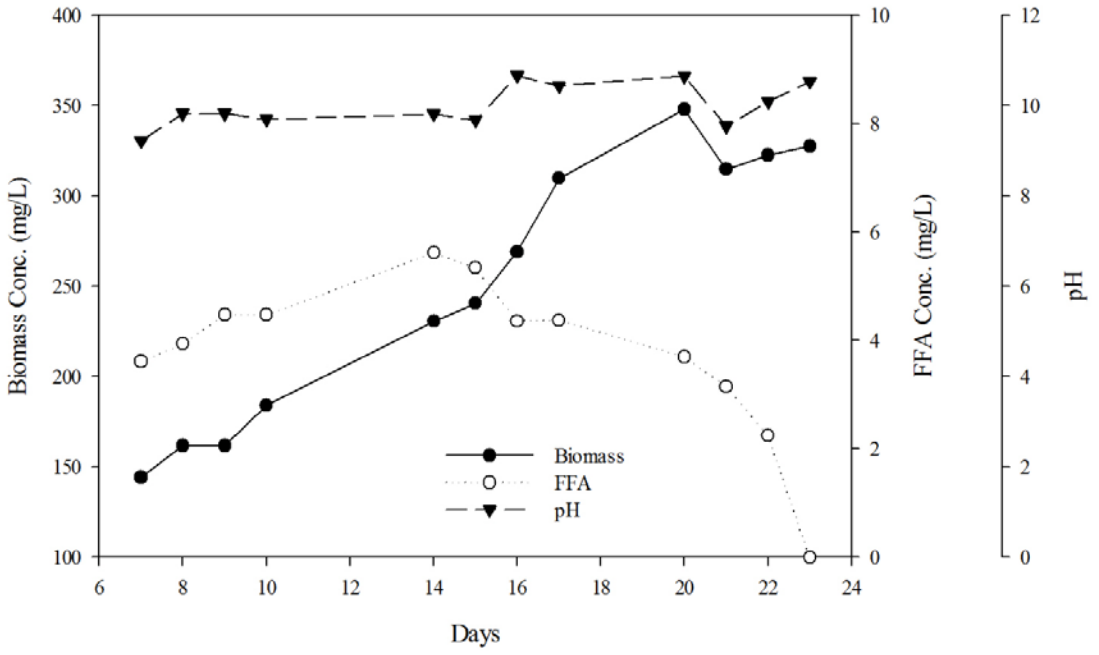

Figure 7.2. Batch growth of TE/Δ*slr1609* and production of FFA in a carboy.

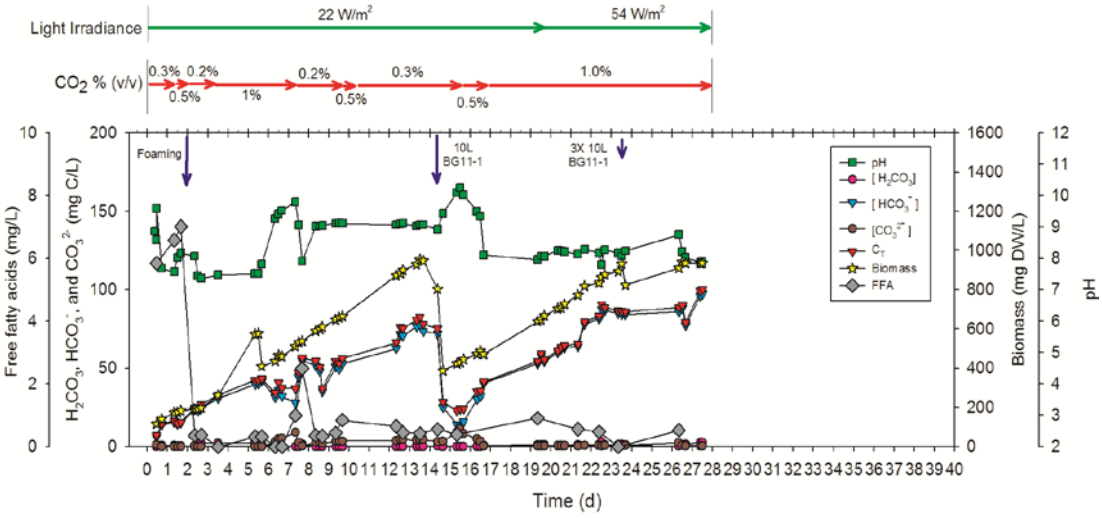

Figure 7.3. Batch growth of TE/Δ*slr1609* and production of FFA in a BT-PBR without resin. A recharge was performed on Day 15.

7.3.2 Possible reasons for FFA loss

Sharp declines in the FFA concentration occurred with batch growth of *Synechocystis* in a flask, a carboy, and a BT-PBR. Possible mechanisms for FFA loss are precipitation and biodegradation.

Evidence for chemical precipitation. Precipitation of FFA can occur under certain conditions. First, the solubility of FFA is particularly limited when pH < 8. For example, the solubility of C12:0 at pH = 6 is two orders of magnitude lower than that at pH = 8 (Nyren and Back, 1958). Second, the FFA anion can combine with cations such as Ca^{2+} to form the precipitate $[CH_3(CH_2)_{10}COO]_2Ca$ (Graham and Sackman, 1983; Owen et al., 1995), which is commonly called soap scum or lime soap. Figure 7.4 shows results from a water-chemistry model that describes the behavior of the $[CH_3(CH_2)_{10}COO]_2Ca$ precipitate with pH. The model indicates that the formation of $[CH_3(CH_2)_{10}COO]_2Ca$ can occur for pH between pH 4 and pH 9 when the total Ca^{2+} concentration is 10 mg/L (regular Ca^{2+} in BG-11, purple line in Figure 7.4). This pH range of C12:0 precipitation can be even wider if more Ca^{2+} is present in the medium (e.g., with unsoftened tap water, blue and red line in Figure 7.4). Although ~8 mg/L Mg^{2+} also is present in BG-11, its precipitation effect with FFA is much less than that of Ca^{2+}, as indicated by the model. Other cations that can co-precipitate with FFA are in trace amounts at least one magnitude lower than that of Ca^{2+} and Mg^{2+}. A detailed discussion about the water-chemistry model is beyond the scope of this dissertation and is provided elsewhere by Chao Zhou.

Figure 7.5 shows the results of chemical precipitation after adding C12:0 into sterilized BG-11 medium (pH ~7, Ca^{2+} ~10 mg/L). We maintained the sterilized condition throughout the experiment to rule out biodegradation. The initial concentration of C12:0 was around 50 mg/L, similar to the range of concentration of excreted FFA by TE/Δ*slr1609*. The normal EDTA concentration in BG-11 medium is 0.0028 mM, which allowed about 65% of the added C12:0 to be precipitated within 2 d (black circle symbol), similar to the model prediction in Figure 7.4 (~60% precipitation as $[CH_3(CH_2)_{10}COO]_2Ca$). After 2 d, the concentration of C12:0 became stable. Addition of more EDTA to the medium (dashed and dotted lines in Figure 7.5) prevented chemical precipitation of C12:0, as EDTA strongly associated with Ca^{2+}, dissociating Ca^{2+} from C12:0. An EDTA concentration of 2 mM limited laurate precipitation to ~10%, and 3 mM EDTA almost totally prevented precipitation of C12:0. However, other evidence shows that EDTA cannot be used at mM concentrations in the TE/Δ*slr1609* culture, as it is severely toxic to TE/Δ*slr1609* (data not shown).

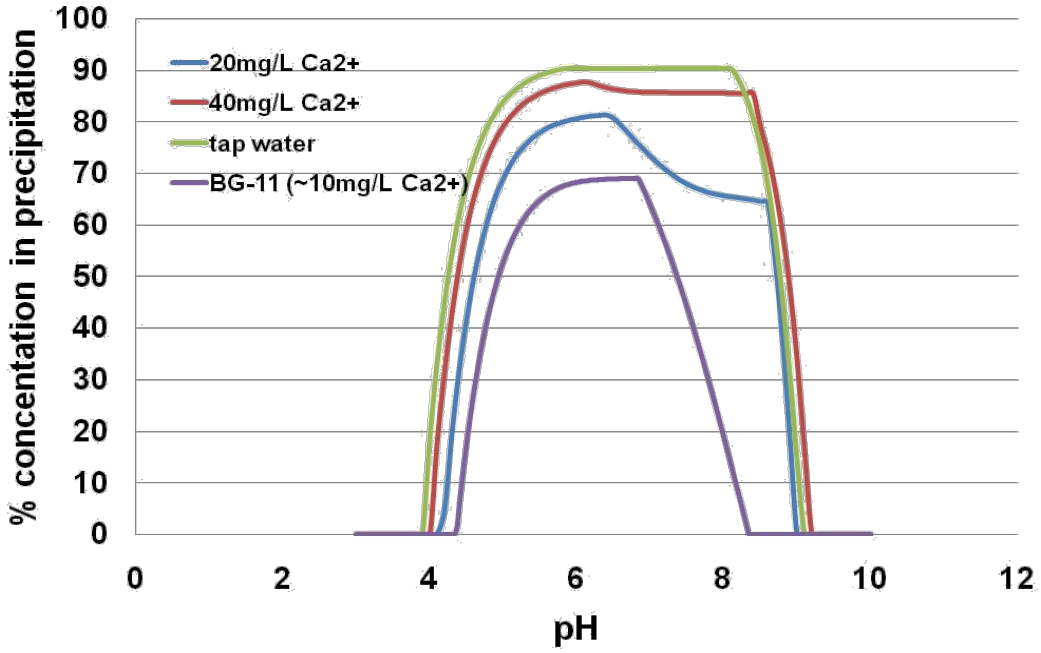

Figure 7.4. Modeling of formation of $[CH_3(CH_2)_{10}COO]_2Ca$ precipitate based on pH and Ca^{2+} concentration (initial C12:0 concentration 50 mg/L (100%)).

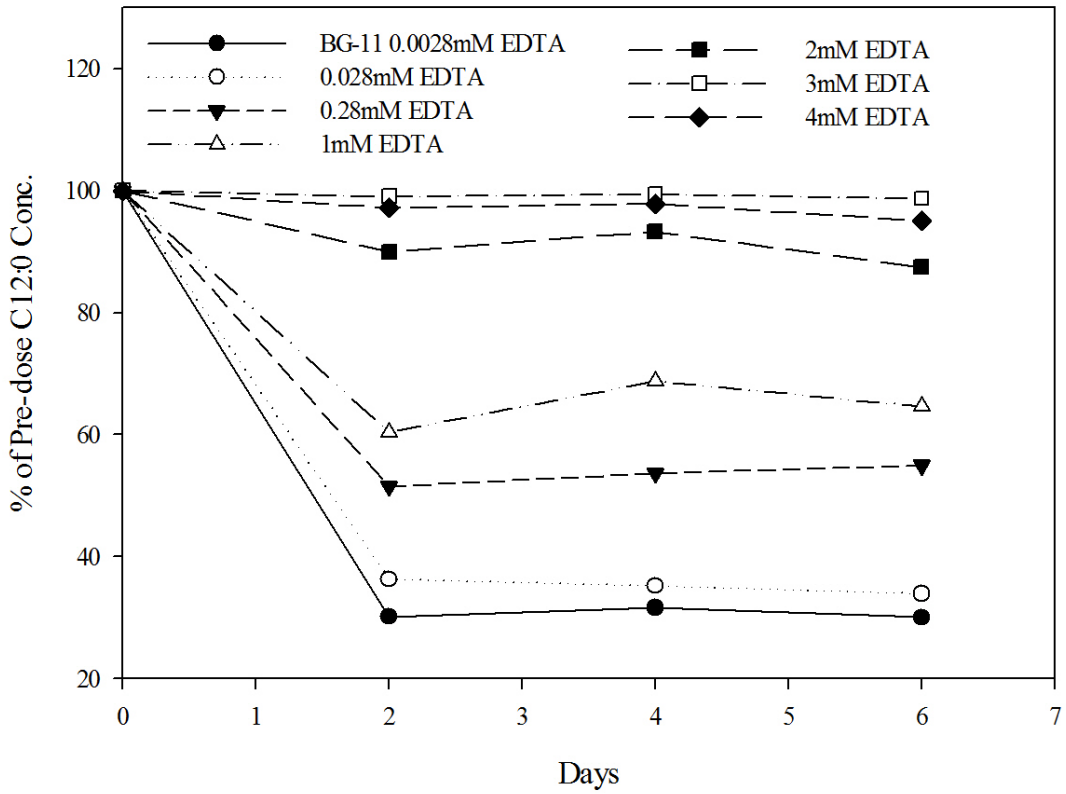

Figure 7.5. Chemical precipitation of ~50 mg/L (100%) of C12:0 in BG-11 with different EDTA concentrations.

An EDTA concentration ≥ 2 mM nearly prevented precipitation of C12:0 with 10 mg/L of Ca^{2+}.

Evidence for biodegradation. When scaling up mutant-type *Synechocystis* culture, we identified heterotrophic bacteria, algae, and protozoa by fluorescence and light microscopy. Figure 7.6 shows example microscopy observations of the mother culture and scaled-up cultures (from flask, carboy, BT-PBR, or ST-PBR). Figure 7.6a and b are cultures stained by SYTO 9 and observed under fluorescence microscope. SYTO 9 can stain all bacteria and emit green fluorescence, while *Synechocystis* also emits red auto-fluorescence. After staining, non-*Synechocystis* bacteria can be detected by having only green fluorescence. The mother culture (Figure 7.6a) had undetectable non-*Synechocystis* bacteria: No non-*Synechocystis* bacteria were observed in fields containing ~500 *Synechocystis* cells. In contrast, scaled-up cultures from a BT-PBR (Figure 7.3) showed significant non-*Synechocystis* bacteria (Figure 7.6b). Staining results similar to Figure 7.6b also were observed in flask (Figure 7.1), carboy (Figure 7.2), and ST-PBR cultures after FFA loss was observed. The cell count indicated that non-*Synechocystis* bacteria accounted for 10 to 50% of total cell counts in significantly contaminated cultures.

The percentage of non-*Synechocystis* bacteria in total cell count can be converted to a percentage based on dry biomass. Assuming a density of 530 fg/μm^3 (dry mass) and a diameter of 2 μm for a *Synechocystis* cell, the dry weight of one *Synechocystis* cell is approximately 2.2×10^{-12} g. For heterotrophic bacteria of the size shown in the photomicrographs, the dry weight is approximately 3×10^{-13} g per cell (Mahlmann et al., 2008; Sundararaj and Guo, 2008). Thus, one *Synechocystis* cell has mass ~7-fold larger than for a heterotroph

cell. Thus, 10 to 50% of non-*Synechocystis* bacteria in total cell count accounts for 1.3 to 7% in terms of dry biomass.

Using light microscopy, we observed non-*Synechocystis* bacteria (Figure 7.6c), algae (Figure 7.6d), and protozoa (Figure 7.6e) in several batches from a BT-PBR or a ST-PBR. The non-*Synechocystis* microorganisms are easily distinguished from *Synechocystis* by their sizes or shapes. Compared with wild-type *Synechocystis* cultures, the non-*Synechocystis* microorganisms are more common and more abundant in the TE/Δ*slr1609* culture (Sheng et al., 2011a). Thus, non-*Synechocystis* microorganisms seem to be boosted by the excreted FFA from TE/Δ*slr1609*.

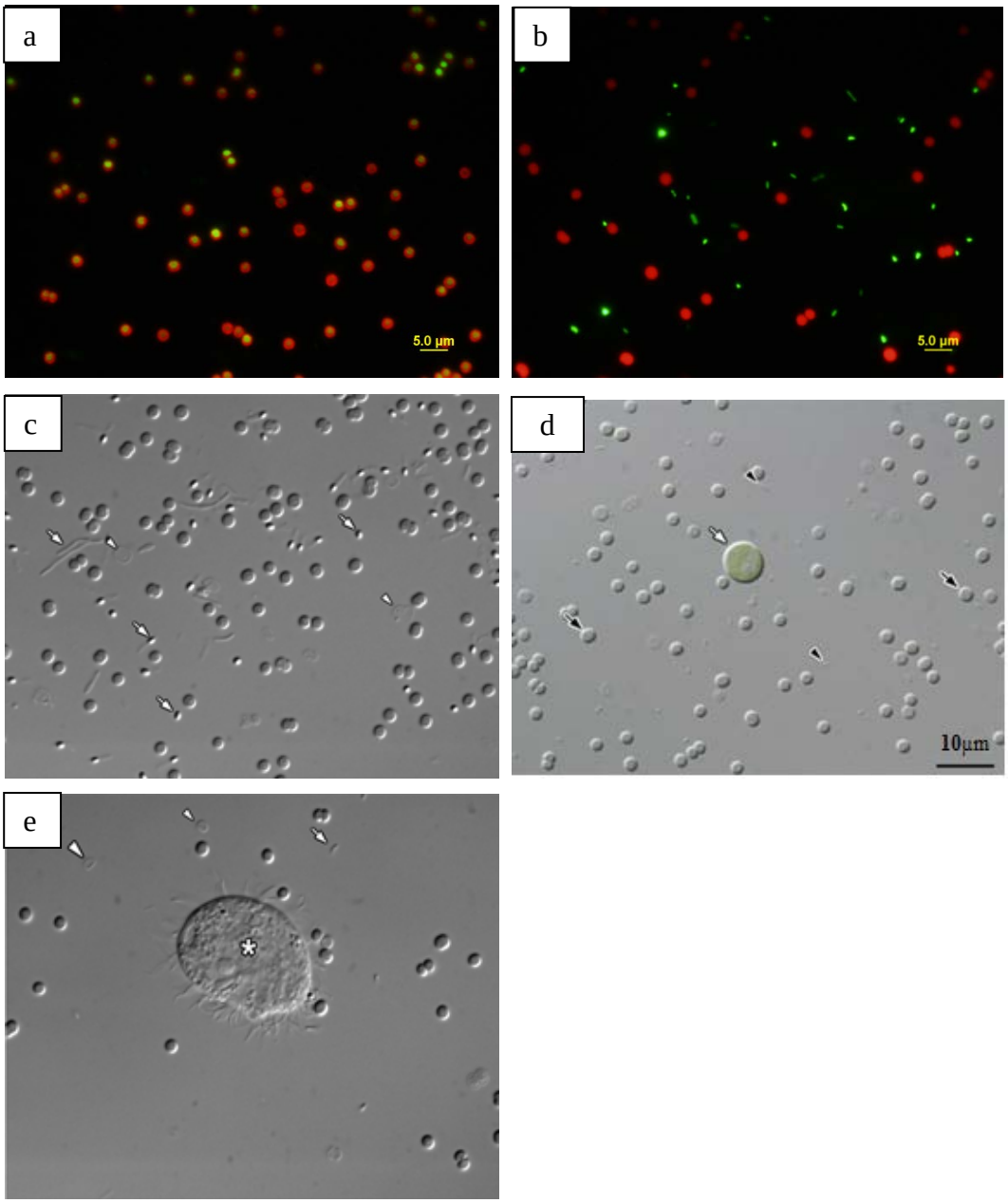

Figure 7.6. Fluorescence and light microscopy observations of TE/Δ*slr1609* cultures.
a. SYTO 9 staining and auto-fluorescence of mother culture. All cells show red auto-fluorescence and green SYTO 9 emission; they are confirmed to be *Synechocystis*. ***b.*** SYTO 9 staining and auto-fluorescence of a BT-PBR culture. non-*Synechocystis* bacteria only show green SYTO 9 emission (no red auto-fluorescence. ***c.*** non-*Synechocystis* bacteria (white arrows) under light microscopy. ***d.*** algae (white arrow). ***e.*** protozoa (white asterisk). ***c*** – ***e*** are from a ST-PBR.

In order to test biodegradation of FFA by non-*Synechocystis* microorganisms, we pre-dosed ~50 mg/L of C12:0 to sterilized BG-11 medium at pH ~7 and with all other conditions similar to bigger flask conditions. We used 100X EDTA (0.28 mM) to increase the solubility of C12:0 in the medium without introducing severe inhibition to the cells. Figure 7.7 shows the fates of soluble C12:0 under different conditions. At room temperature (26^{o}C), chemical precipitation of C12:0 was complete within 2 d, with about 50% C12:0 precipitated (black circle symbol in Figure 7.7), which is similar to Figure 7.5. After filtering out FFA precipitates by 0.2-μm Acrodics syringe filter membrane (Pall Life Sciences), we performed parallel experiments with a dose of ~120 mg/L pure TE/Δ*slr1609* culture and a contaminated culture from a BT-PBR with an initial concentration of heterotrophic bacteria ~5% of total cells from cell count under light microscopy (corresponding to ~0.7% in dry weight). When no culture was dosed, the concentration of C12:0 was stable for the rest of the experiment, indicating no biodegradation (black circle symbol in Figure 7.7). Because no non-*Synechocystis* microorganisms were present in the pure-culture-dosed batch, we observed a sustained net production of FFA by TE/Δ*slr1609* (white circle symbol). The nFPR was 14 mg/L/d, BPR was 120 mg/L/d, μ was 0.6 d^{-1}, and the electron flow was 18% to FFA; all these values are similar to or slightly higher than those in Figure 7.1. In contrast, we saw a continuous decrease of C12:0 in the PBR-culture-dosed batch (black triangle symbol), indicating FFA biodegradation by FFA scavengers in the BT-PBR culture, even though the BPR was similar to that of pure culture. The FFA consumption rate was 21 mg/L/d, which indicates that

the FFA scavengers consumed C12:0 at a rate ~1.5 times greater than TE/Δ*slr1609* biomass produced it. From this comparison, we can see that FFA biodegradation poses a serious risk when the initial scavenger biomass is only ~0.7% of the TE/Δ*slr1609* biomass.

We performed a similar experiment at 4^{o}C. Compared with room temperature, low temperature decreased the rate of chemical precipitation (white triangle symbol) and deactivated biodegradation (black square symbol), as both culture-dosed and non-culture-dosed media showed similar patterns of C12:0 loss. This observation further confirms the biodegradation of FFA by FFA scavengers at room temperature. It also suggests that the impact of scavenging may be more important for higher temperatures, a factor that needs to be explored.

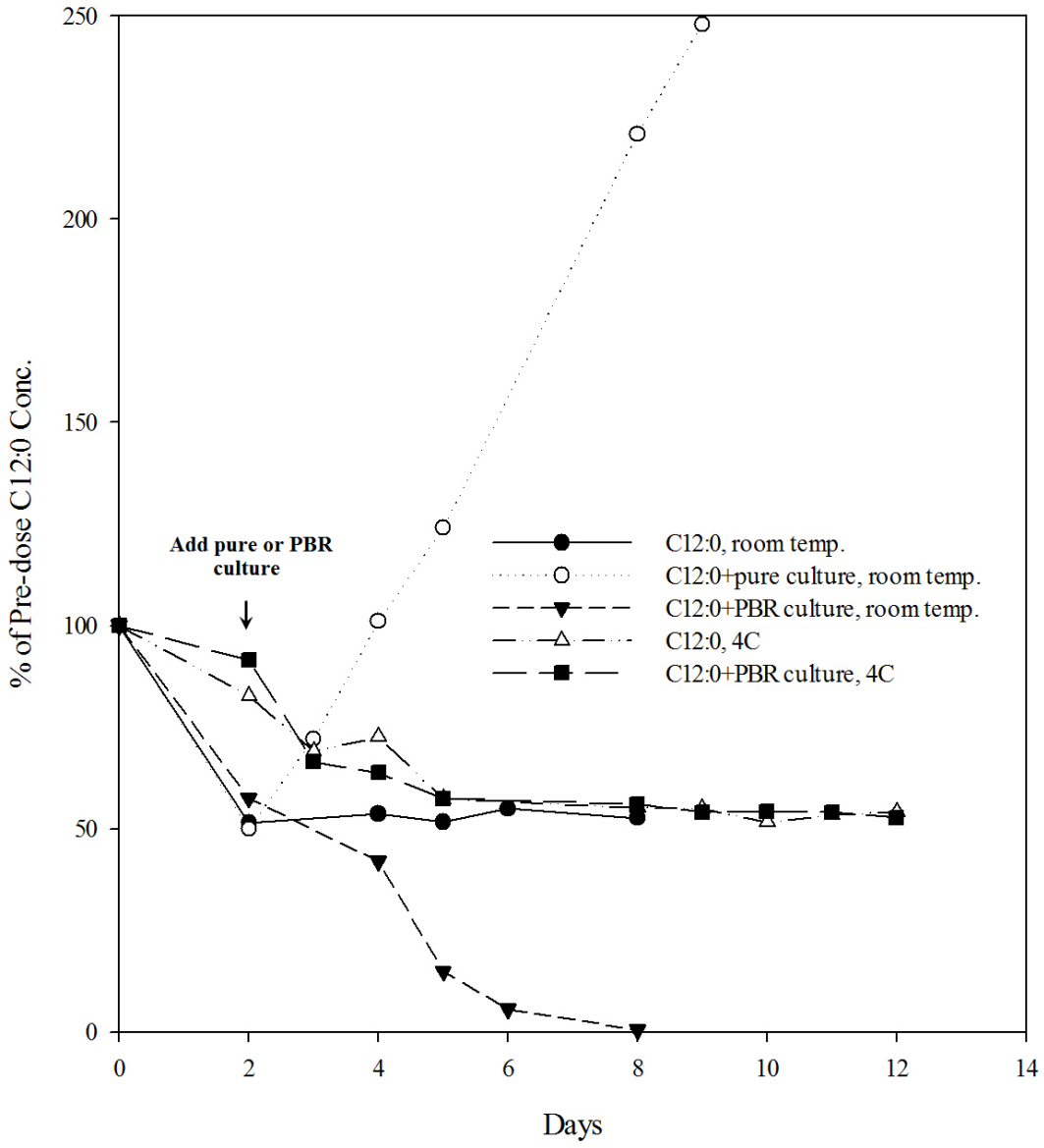

Figure 7.7. Chemical precipitation and biodegradation of C12:0 at room temperature (26 °C) or 4°C.

Initial concentration of C12:0 was ~50 mg/L (100%). 0.28 mM EDTA was dose to increase FFA solubility. FFA precipitation was filtered out by 0.2-µm Acrodics syringe filter membrane (Pall Life Sciences), and pure culture or BT-PBR culture (TE/Δ*slr1609*) was dosed in some flasks on Day 2. Initial TE/Δ*slr1609* biomass concentration was ~120 mg/L and initial concentration of heterotrophic bacteria in PBR culture was ~5% of total cell count (~0.7% of dry weight).

7.3.3 Possible solutions for overcoming FFA loss — High pH

Besides increasing FFA solubility, as indicated by Figure 7.4, high pH (pH > 10) probably also inhibits growth of FFA scavengers (Galbraith and Miller, 1973; Meseck, 2007). We observed inhibition of FFA scavengers by high pH in a BT-PBR experiment, as showed in Figure 7.8. Before Day 17, no FFA was detected due to the significant contamination by FFA scavengers (~30% of total cells and ~4% of dry weight). On Day 17, the pH increased from ~9 to ~12 due to a sharp lowering of the CO_2-supply rate (Figure 7.8a). The pH increase led to immediate net production of FFA at a nFPR of ~5 mg/L/d. When a new resin column (ion exchange resin Lewatit® MP-64, Sigma-Aldrich) was installed, all of the 120 mg FFA in the medium was adsorbed in 2 days. The net FFA production correlated with a decrease of non-*Synechocystis* bacteria confirmed by light microscopy (Figure 7.8b) and T-RFLP; the non-*Synechocystis* bacteria decreased to about ~3% of the cell numbers and ~0.4% of the dry weight. However, a long exposure to pH ~12 (4 d) appears to have been lethal to *Synechocystis*, as the culture eventually died on Day 25. Thus, a more precise pH-adjustment scheme is required to use a high-pH strategy for overcoming FFA loss.

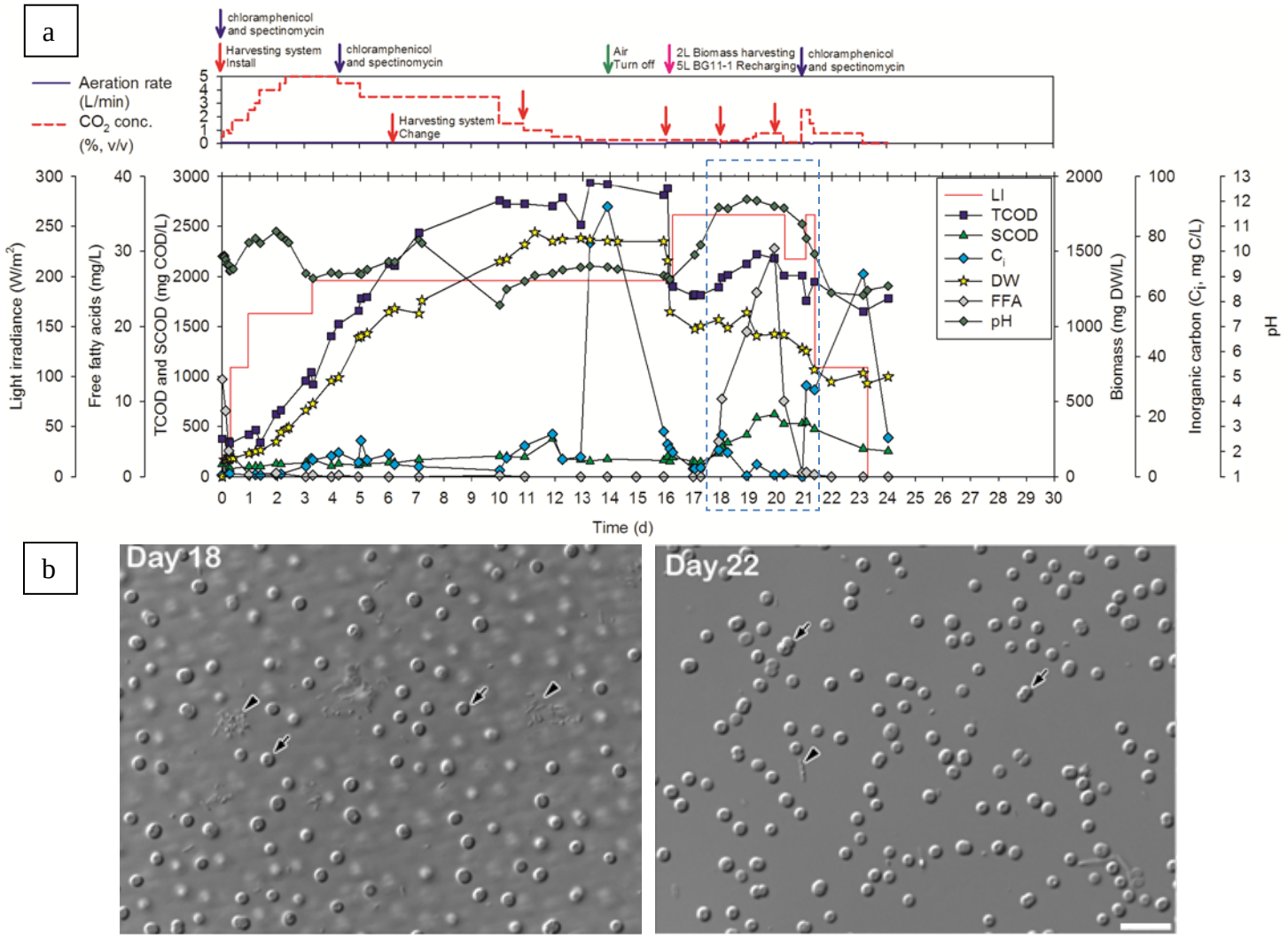
a
chloramphenicol and spectinomycin
Harvesting system Install
chloramphenicol and spectinomycin
Air Turn off
2L Biomass harvesting 5L BG11-1 Recharging
chloramphenicol and spectinomycin
Aeration rate (L/min)
CO2 conc. (%, v/v)
Harvesting system Change
Light irradiance (W/m2)
Free fatty acids (mg/L)
TCOD and SCOD (mg COD/L)
Biomass (mg DW/L)
Inorganic carbon (Ci, mg C/L)
pH
LI
TCOD
SCOD
Ci
DW
FFA
pH
Time (d)
b
Day 18
Day 22

Figure 7.8. Growth and activity of TE/Δ*slr1609* in a BT-PBR.

a. performance monitoring. A resin column (MP-64) was attached to the reactor up to Day 17, but was taken off from Days 17 to 20. No FFA was eluted from resin between Days 2 to 17, indicating no net FFA production during those days. Increased pH after Day 17 showed a rise in FFA concentration, and a new resin column was installed on Day 20; its adsorption of FFA was a major cause for the rapid loss of FFA between Day 20 and 21. Approximately 120 mg of FFA was recovered from the resin installed on Day 20 and removed on Day 22. ***b.*** the inhibition of heterotrophic bacteria after high pH is confirmed by light microscopy (Day 18 vs. Day 22). *Synechocystis* cells are shown with black arrows and heterotrophic bacteria with black arrowheads. Scale bar = 7 μm.

We used the organic buffer CAPS to provide buffer capacity to flasks containing 500 mL TE/Δ*slr1609* culture. Figure 7.9 shows the impact of CAPS (without pH adjustment) on TE/Δ*slr1609* at different concentrations (25 – 40 mM). A dose of up to 40 mM CAPS showed no significant inhibition to TE/Δ*slr1609* (Figure 7.9a), with BPR and μ similar to that in Figure 7.1. However, a higher concentration of CAPS provided a higher buffer capacity that restrained the pH variation (Figure 7.9b).

We then used 25 mM CAPS titrated by NaOH or H_2SO_4 to adjust the initial pH of pure cultures of TE/Δ*slr1609* to 5 target pH levels: 9, 9.5, 10, 10.5, and 11. Figure 7.10 shows the response of TE/Δ*slr1609* to the pH adjustment, including biomass production and FFA excretion. Initial pH ~11 (black square symbol in Figure 7.10) appears to have been lethal to low-density TE/Δ*slr1609* culture. Due to the poor growth of the culture, we did not further adjust the pH to the culture under this condition, but let the pH adjust depending on the initial alkalinity and the level of photosynthesis. TE/Δ*slr1609* culture exposed to initial pH ~11 grew more slowly at first and eventually died by 5 d; FFA production also was the least for this experiment. Initial pH ~10.5 (white triangle symbol) also showed some inhibition effects on low-density TE/Δ*slr1609*, but not as severe as for pH ~11. As a result, we adjusted the pH less frequently to alleviate the adverse effect of pH ~10.5.

In contrast, initial pH from 9 to 10 gave sustained growth of TE/Δ*slr1609* and continuous excretion of FFA. A daily pH adjustment achieved pH stabilization within ±0.5 pH units. The best BPR (~62 mg/L/d) and nFPR (~8.1

mg/L/d), which occurred at initial pH ~10 (black triangle symbol), were slightly lower than that in above-noted flask experiments (Figure 7.1 and Figure 7.9). Not shown in Figure 7.10 is that TE/Δ*slr1609* was able to maintain its growth and FFA production at these rates with pH ~10 for 20 d.

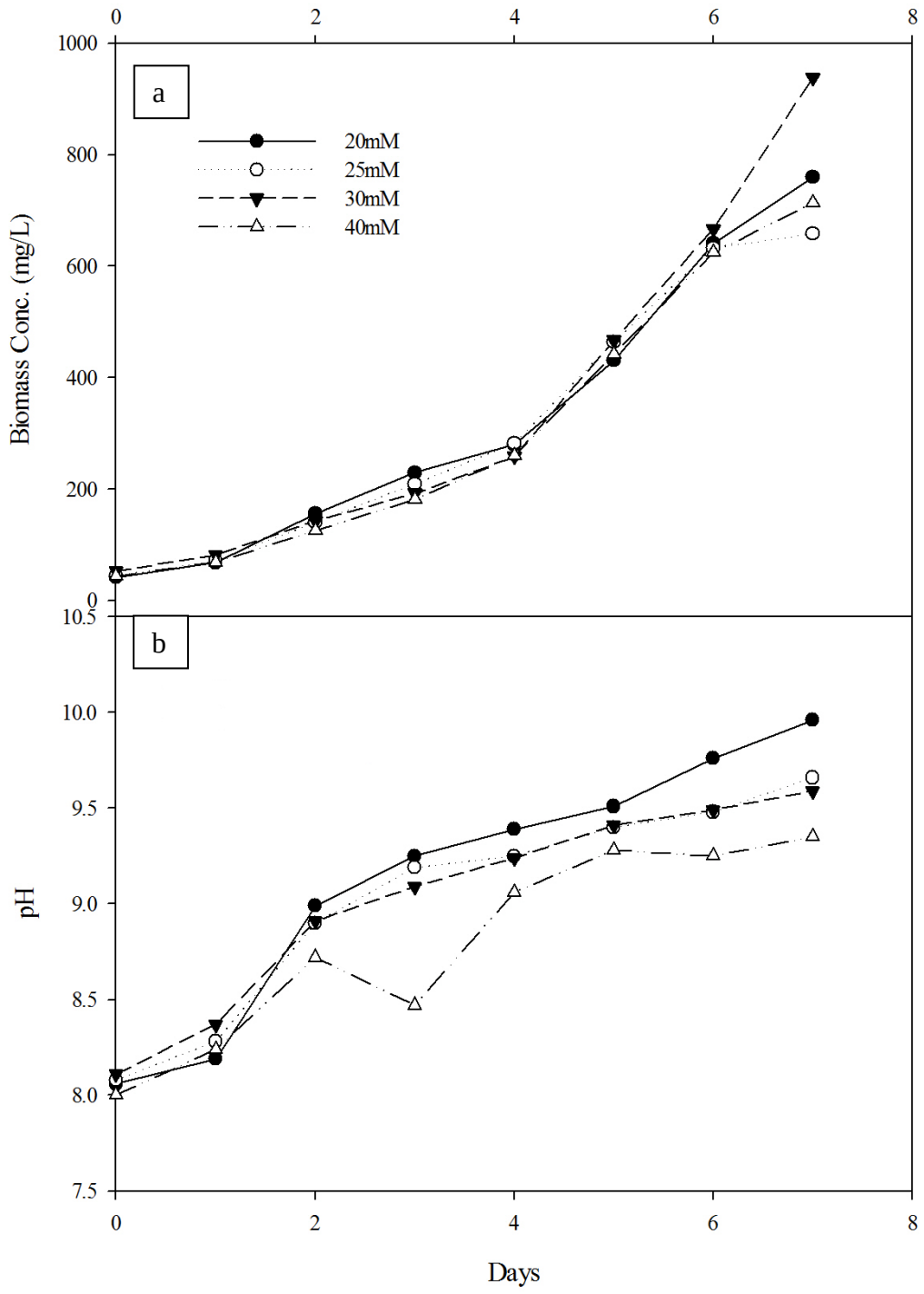

Figure 7.9. Addition of organic buffer CAPS at different concentration levels to TE/Δ*slr1609* culture.

a. biomass concentration. ***b.*** pH of the culture.

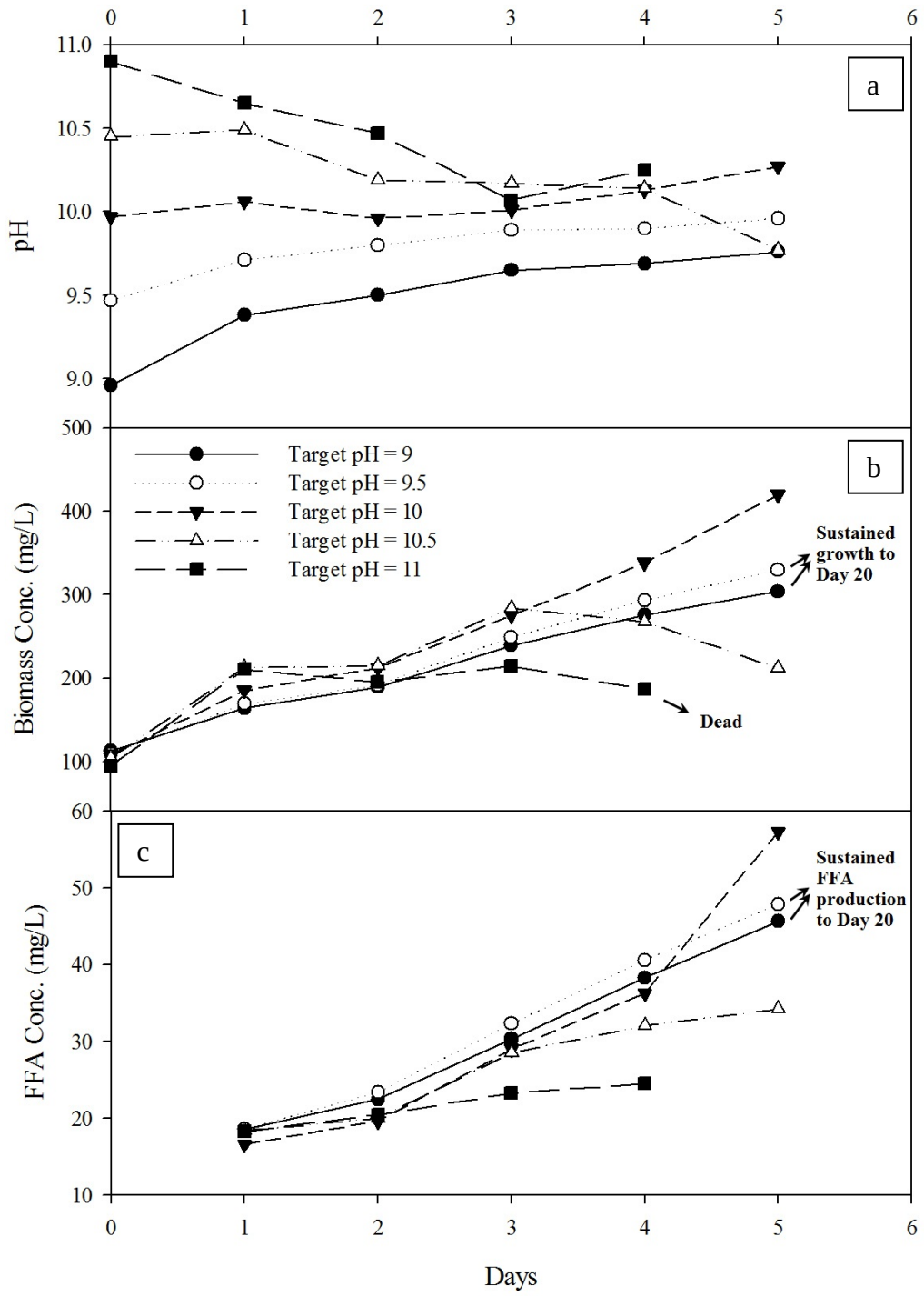

Figure 7.10. Effects of initial pH (range of 9 to 11 with 25 mM CAPS) on TE/Δ*slr1609* culture.

a. pH of the culture. ***b.*** biomass concentration. ***c.*** FFA concentration.

Using CAPS as a pH-control method, we tested the high-pH strategy to overcome FFA loss by scavengers. Figure 7.11 shows a flask experiment with 500 mL TE/Δ*slr1609* culture. The pH was initially adjusted to 9.5 – 9.8 by 35 mM CAPS + NaOH/H_2SO_4. As noted in Figure 7.4, FFA precipitation could not occur at this condition. We observed positive nFPR in the first 2 d. After 2 d, airborne heterotrophic bacteria were introduced into the flask. The presence of FFA scavengers was confirmed by the FFA loss after air exposure and light microscopy observation. By Day 8, the non-*Synechocystis* bacteria were ~40% by cell number and ~6% by dry weight under light microscopy. On Day 8, we adjusted pH to 10.6 – 10.9 by adding NaOH. We observed an immediate increase of FFA after the pH adjustment, and net FFA production was similar with the results after a pH increase in a BT-PBR (Figure 7.8), but with a much higher nFPR (25 mg/L/d). The non-*Synechocystis* bacteria had been reduced to ~5% by cell number and ~0.7% by dry weight under light microscopy. Significant net FFA production and a decrease of non-*Synechocystis* bacteria suggest that the FFA scavengers were substantially inhibited at pH > 10.5, which appeared to be the main mechanism for regaining a positive nFPR. Also, the high-density TE/Δ*slr1609* culture could endure the higher pH and continue growing at the same BPR (99 mg/L/d) as before the pH increase. These results suggest that a temporary increase of the pH to > 10.5 in a high density TE/Δ*slr1609* culture (> 600 mg/L) may help reduce FFA scavengers and restore net FFA production by TE/Δ*slr1609*. Further work is needed to define the optimal duration of pH > 10.5.

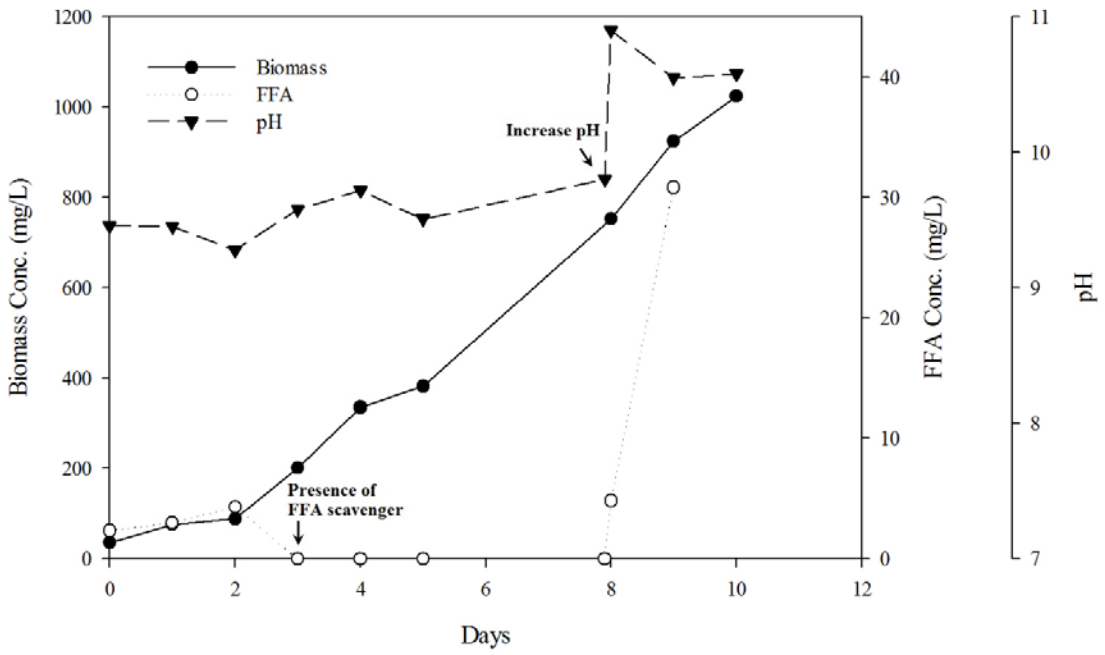

Figure 7.11. Applying a high-pH strategy for overcoming FFA loss in a flask. 35 mM CAPS + $NaOH/H_2SO_4$ was use to for pH control. Contamination with airborne heterotrophic bacteria was confirmed by light microscopy from Day 3 to Day 8. The pH was increased to 10.6 – 10.9 on Day 8.

7.3.4 Possible solutions for overcoming FFA loss — Resin adsorption and sterilization technique

We grew several batches of TE/Δ*slr1609* culture in an ST-PBR with or without adsorptive resin. The pH was maintained at 8.1 – 10.5. Figure 7.12 shows the monitoring of total FFA in mg in the reactor, which allows us to compare directly the fate of FFA in all experiments. Significant scavenging happened within the first day in the ST-PBR. When no resin was dosed (Line a in Figure 7.12), FFA increased only in the first several hours, but the FFA concentration decreased sharply within 1 d with a FFA degradation rate of ~3.3 mg/L/d. A dose of hydrophobic polymeric resin (DOWEX^{TM} OPTIPORE^{TM} L493, Dow Chemical) slowed consumption of FFA by FFA scavengers (Line b and c in Figure 7.12), as all FFA was adsorbed onto the resin (no FFA remained in the medium, data not shown). Based on the accumulation of FFA on the resin, nFPR ranged from 0.6 to 0.8 mg/L/d for the first 1 to 2 d. However, if resin replacement was not performed, biodegradation of adsorbed FFA took place (Line b in Figure 7.12), and all adsorbed FFA was consumed within 6 to 8 d, with a FFA degradation rate of ~1 mg/L/d. Regular replacement of resin, e.g., within 4 d (Line c in Figure 7.12) was helpful, as it reduced FFA loss on the resin to ~0.8 mg/L/d. Compared with the frequency of resin replacement, the dose amount of resin seemed to be less important, as 150 g resin was sufficient to adsorb all FFA from the 65-L culture (Line c in Figure 7.12).

Even though resin adsorption of FFA could slow down biodegradation of FFA in ST-PBR, it alone did not guarantee sustained net production of FFA,

perhaps because of the consumption of FFA during the hydraulic travel time between FFA production in the PBR and FFA adsorption in the tube and mix tank. Thus, a more sophisticated strategy is required, such as using a more rigorous cleaning and sterilization procedures, increasing the pH, and putting the resin directly into the PBR.

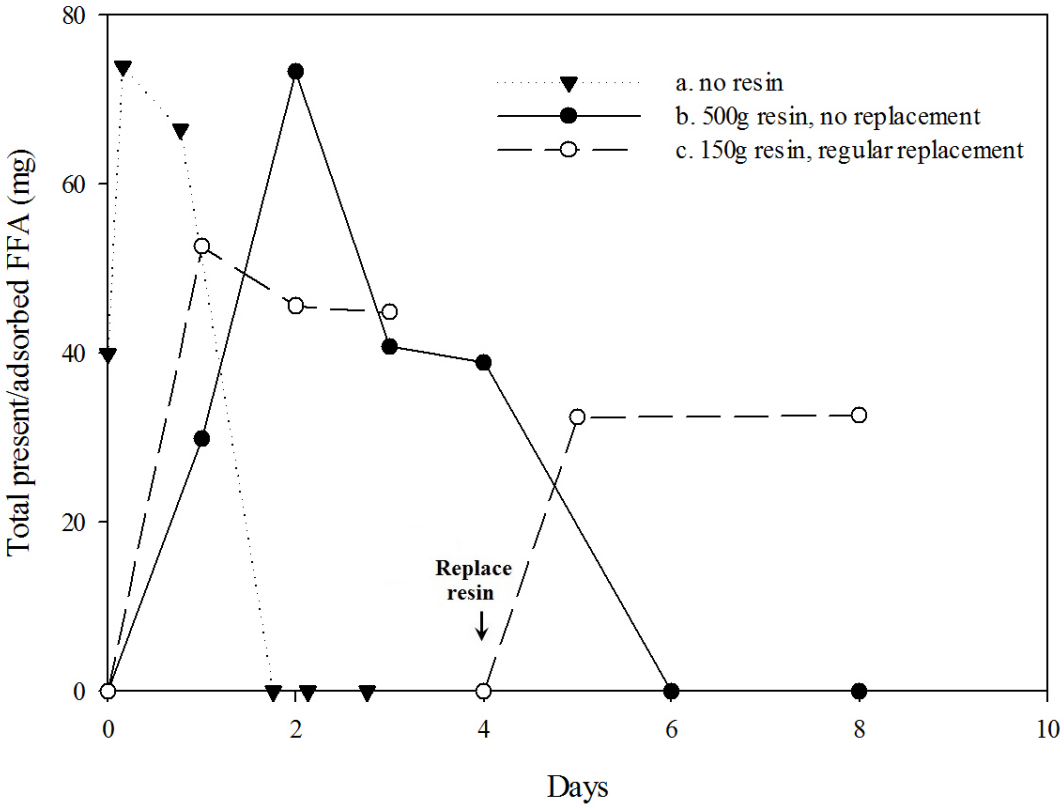

Figure 7.12. FFA net production by TE/Δ*slr1609* and adsorption on DOWEX™ OPTIPORE™ L493 hydrophobic resin in an ST-PBR that contain heterotrophic bacteria (about 10 – 50% in total cells according to light microscopy).

We tested reactor sterilization by using a commercially available wave bioreactor (GE Healthcare Life Sciences), also with an initial 5 mg/L dose of the antibiotic spectinomycin. Figure 7.13 shows sustained increases of TE/Δ*slr1609* biomass and excreted FFA over 15 days. The average BPR and average nFPR were 88 mg/L/d and 11 mg/L/d, respectively, similar to values obtained in flask conditions. The results support the value of preventing contamination when scaling up a TE/Δ*slr1609* culture. The absence of FFA scavengers was confirmed by the culture-purity check by light microscopy. To take more advantage of wave bioreactors for scaled-up production, we can obtain larger wave bioreactors (up to 500 L)

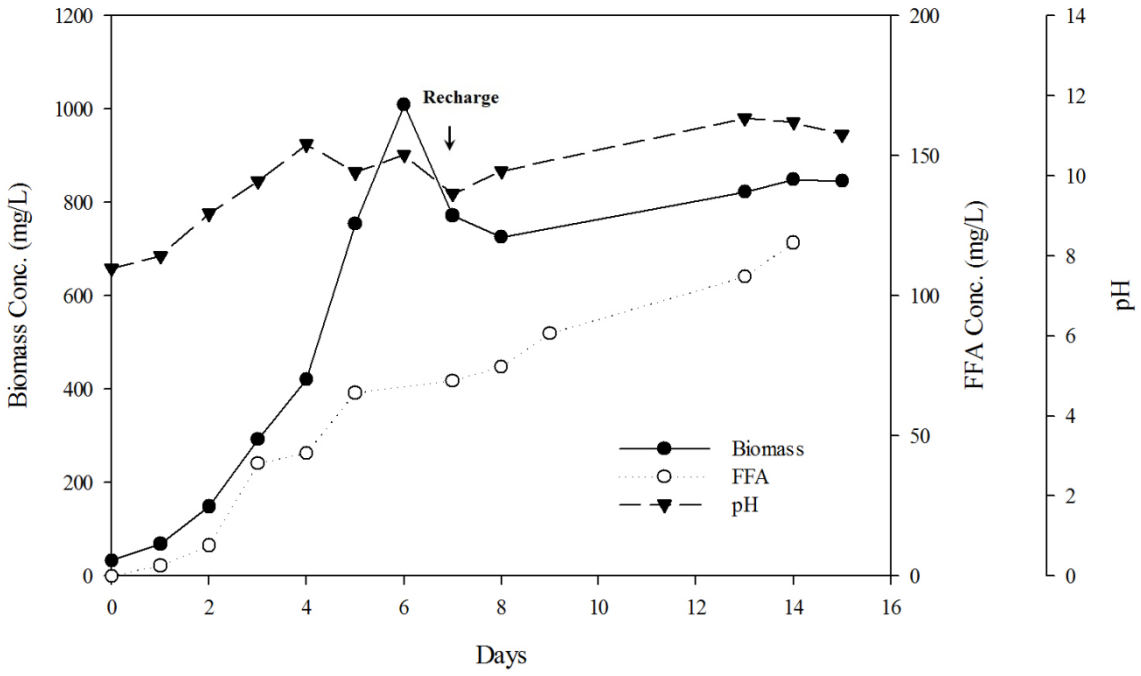

Figure 7.13. Batch growth of TE/Δ*slr1609* and production of FFA in a 1-L wave bioreactor (GE Healthcare Life Sciences) with 5 mg/L antibiotic spectinomycin. A recharge was performed on Day 7.

7.4 Conclusions

I summarize the kinetic results of experiments presented in this chapter in Table 7.1. Mutant-type *Synechocystis* TE/Δ*slr1609* can excrete FFA (mainly C12:0) into the medium. We observed higher BPR (90 – 120 mg/L/d) and nFPR (7.6 – 14 mg/L/d) in flasks, probably due to good light penetration and our ability to maintain a pure culture. We saw the most significant FFA consumption rates (0.8 – 21 mg/L/d) when we scaled up production to PBRs or expressly added FFA scavengers to flasks. Consistent with these findings, the best nFPR only occurred in conditions in which FFA scavenger were not significant. Thus, while FFA precipitation can occur, the more serious loss was from non-*Synechocystis* microorganisms (FFA scavengers). FFA consumption by FFA scavengers could outpace the nFPR, even when the initial concentration of FFA scavengers was only ~5% of total cells (~0.7% of dry weight).

We identified three strategies to overcome FFA loss by biodegradation: a temporary increase of pH, rapid FFA adsorption by resin, and sterilization technique.

Temporary high pH (> 10.5) could inhibit FFA consumption without incurring a large decrease in BPR and FPR in high-density culture (> 600 mg/L); the net result was the largest nFPR of all studies, ~25 mg/L/d. How long to maintain pH > 10.5 to balance control of FFA scavengers with harm to mutant *Synechocystis* remains to be investigated.

Adsorptive resin can slow down the FFA consumption rate by outcompeting the FFA scavengers. We observed a positive nFPR even in a highly

contaminated culture in ST-PBR. A regular replacement of resin (e.g., 4 d) is important to prevent further FFA loss on the resin. More controlled experiments are recommended to further investigate this strategy.

The use of sterilized bioreactor and antibiotics also can help prevent intrusion and growth of FFA scavengers. The advantage of sterilization techniques is to “kill the contamination in the cradle”. It also minimizes cross contamination during operation (e.g., sampling). Finding means to sterilize large-scale photobioreactors for scaling up has merit.

In summary, the research in this chapter provides fundamental advancement towards understanding FFA net productivity by mutant-type *Synechocystis* and practical advancements through the strategy of improving FFA net production in large-scale application.

Table 7.1. Summary of experiments presented in Chapter 7

Figure and symbol		Reactor type	Specific condition	pH	Temp. (°C)	BPR (mg/L/d)	nFPR (mg/L/d)	FFA consumption rate (mg/L/d)*
Fig.7.1		Flask	Apparently a pure culture	9.5–10.4	26	103 (on Days 6–16)	7.6 (on Days 6–14)	--***
Fig.7.2		Carboy	Contaminated after 15 d	9.2–10.6	26	16 (on Days 7–20)	0.3 (on Days 7–14)	--
Fig.7.3		BT-PBR	Contaminated after 2 d	8–10	30	65	--	--
Fig.7.7	white circle	Flask	Pure culture	9.6–10.4	26	120	14	--
	black triangle	Flask	PBR culture (5% contamination**)	--	26	120	--	21
	black square	Flask	PBR culture (5% contamination**)	--	4	--	--	0
Fig.7.9	black circle	Flask	CAPS 20 mM	8–10	26	103	--	--
	white circle	Flask	CAPS 25 mM	8–9.7	26	88	--	--
	black triangle	Flask	CAPS 30 mM	8–9.6	26	126	--	--
	white triangle	Flask	CAPS 40 mM	8–9.4	26	96	--	--
Fig.7.10	black circle	Flask	CAPS 25 mM; Target pH = 9	9–9.5	26	38	5.4	--
	white circle	Flask	CAPS 25 mM; Target pH = 9.5	9.5–10	26	44	5.9	--
	black triangle	Flask	CAPS 25 mM; Target pH = 10	10–10.3	26	62	8.1	--
	white triangle	Flask	CAPS 25 mM; Target pH = 10.5	10.5–10.2	26	60 (on Days 0–3)	3.2	--
	black square	Flask	CAPS 25 mM; Target pH = 11	10.9–10.3	26	--	1.6 (on Days 0–4)	--

Table 7.1 (continued)

Figure and symbol		Reactor type	Specific condition	pH	Temp. (°C)	BPR (mg/L/d)	nFPR (mg/L/d)	FFA consumption rate (mg/L/d)
Fig.7.11		Flask	CAPS 35 mM; heterotrophic contamination introduced on Day 2; pH increased to 10.5–11 on Day 8	9.5–9.8 (Days 0–7) 10.6–10.9 (after Day 8)	26	99	25 (after Day 8)	10 (on Days 2–8)
Fig.7.12	a	ST-PBR		8.1–8.7	--	--	3.3 (on Hours 0–3)	4.1
	b	ST-PBR	500g resin, no replacement	8.8–10.5	27–33	53	0.6 (on Days 0–2)	1.0
	c	ST-PBR	150g resin, regular replacement	8.3–10.1	25–36	25	0.8 (on Day 1)	0.8
Fig.7.13		Wave bioreactor	5 mg/L antibiotic spectinomycin	7.7–11.4	26	88	11	--

* FFA consumption rate (mg/L/d) = observed FFA decrease rate + FFA production rate

** Percentage of non-*Synechocystis* bacteria in total cell counts

*** Not available.

8 Summary and Significance

Biofuel production from cyanobacterium *Synechocystis* is still in its youth, and it will take years for this technology to mature in industrial scale. In order to accelerate its commercialization, several technical challenges should be resolved. Desired technical advancement includes high productivity, low operation cost, and minimal negative environment effects. Similar to other applied science research, research in this area should encompass broad, yet deep advancements in the scientific knowledge that underpins the technology and also engineering advancements toward real applications. My dissertation contributed several progresses to the principles and the applications of biofuel production from *Synechocystis*.

My studies especially focus on the downstream side of the biofuel production from *Synechocystis*, including culture growth, lipid/FFA harvest, and post-treatment. I emphasize factors key to scaling-up and real engineering application, as well as providing deep discussions about the scientific foundations of the topics. This combination of principles and applications is a core value of my dissertation, and my published work already has been recognized by peer researchers.

As illustrated in Figure 1.9 in Chapter 1, the downstream processing depends on the target component. For this reason, my dissertation can be separated into two parts by their different target components: Part I — targeting intracellular lipids (Chapter 1-6, Objective 1-4) and Part II — targeting excreted

FFA (Chapter 2 and 7, Objective 1 and 5). Part I provides step-by-step research of the downstream processing of lipids. Research in Part II focuses on several important issues that may be encountered in the real application when harvesting excreted FFA.

Part I of my dissertation — on intracellular lipid as the target component — starts with a thermodynamic model (Chapter 1) for the calculation of biomass and biofuel (i.e., biodiesel) productivities of *Synechocystis*. The model predicts that diesel-feedstock productivity can be 20 – 70 times larger than with oil-rich plants when using *Synechocystis*. This model provides an alternative method of calculating biomass and biofuel productivities from *Synechocystis* and supports the statement that *Synechocystis* is an optimal source for biofuel production.

I then lay down the analytical methods for the quantification of target compounds — lipids and FFA (Chapter 2). The accuracy of the analytical methods guarantees the trustworthiness of the data presented in following chapters. Based on the accurate analytical methods, I further screen out the best lipid extraction methods for small-scale analysis and large-scale application. I demonstrate that the chloroform + methanol-based Folch and Bligh & Dyer methods can be used as “gold standards” for small-scale analysis due to their efficient penetration of the cell membrane system, higher polarity, and stronger interaction with hydrogen bonds. I also demonstrate that methanol, MTBE, or direct transesterification can be considered for large-scale lipid extraction due to their minimal lipid loss and less toxicity. This work not only provides reliable

lipid-extraction method for following researches, but also sheds light on large-scale application.

With reliable lipid extraction and analytical methods in hand, I further study the effects of growth conditions (especially temperature) on cell growth and lipid characteristics of *Synechocystis*, a collaboration among a group of researchers (Chapter 4). We demonstrate that long-term exposure to non-optimal temperature not only severely inhibits the biomass production rate and lipid production rate, but also triggers changes in the fatty acid profile and, as a result, changes in the quality of final biofuel product. We perform experiments in a bench-top photobioreactor and emphasize the implications to massive production in real application.

Cell disruption typically is required after biomass harvest, but before lipid extraction; this step is discussed in Chapter 5 and 6. In Chapter 5, I demonstrate the feasibility of using the Focused-Pulsed (FP) technique to disrupt *Synechocystis* cells and facilitate lipid extraction. This is world-first research on this specific application of FP. I not only show the treatment results under different conditions, but also explain the two underlying mechanisms — heat and electric-field effects. The electric-field effect is much more significant for disrupting the cells for enhanced lipid extraction. This work contributes to engineering application and scientific understanding of the FP technique when the goal is lipid extraction from cyanobacteria.

Chapter 6 investigates a wide range of cell-disruption techniques. Similar to Chapter 5, the research in Chapter 6 provides insight for scientific principles

and engineering applications. I demonstrate different effects of cell-disruption techniques on cell morphology and lipid extraction. Together with Chapter 5, the research in Chapter 6 demonstrates that FP and microwave are the best candidates for the large-scale cell disruption for lipid recovery.

The major studies of Part II are in Chapter 7, although studies on analytical methods are in Chapter 2. Part II mainly focuses on characterizing one major concern when excreted FFA from mutant-type *Synechocystis* is the goal — FFA loss — and possible solutions when scaling up FFA production. I demonstrate two mechanisms of FFA loss — chemical precipitation and biodegradation by FFA scavengers, with FFA scavenging being far more important. Possible solutions to overcome FFA loss include high pH, rapid resin adsorption, and better sterilization. High pH can inhibit FFA scavengers; thus, it boosts net FFA productivity. FFA adsorption by resin can retrieve FFA from a highly contaminated culture, where FFA consumption rate outpaces FFA production rate if no adsorptive resin attached. Sterilized bioreactor can prevent contamination from the very beginning and during the operation; it also has the potential usage for scaling up. This research provides fundamental advancement towards understanding FFA net productivity by mutant-type *Synechocystis* and practical advancement on the strategy of improving FFA net production in large-scale application.

As previously discussed in section 7.1 of Chapter 7, FFA-oriented biofuel production from mutant-type *Synechocystis* has certain advantages over lipid-oriented biofuel production technique. First, FFA can be converted fairly easily to

a much more valuable form of biofuel than lipids; second, the production and excretion of FFA by mutant-type *Synechocystis* can simplify the downstream processing and reduce the processing cost. For these reasons, FFA-oriented biofuel production deserves more attention and effort toward its technical advancement. One giant leap towards the maturity of FFA-oriented technique will be the success of a much stricter control of pure culture in the large scale to prevent biodegradation of the FFA product by FFA scavengers. Studies on lipid-oriented biofuel production also have the merit, especially for the recovery of intracellular lipids from old mutant-type *Synechocystis* cells that stop producing FFA; this provides additional productivity and benefits for a FFA-based system.

From the foundation laid out in my dissertation, I envision three areas of future research that are needed to advance the principles and applications for using *Synechocystis* to produce renewable and carbon-neutral biofuels. First, upstream research on genetic mutation of *Synechocystis* is required. Preferred genetic advancement includes: (1) modification of target compounds so that they are more suitable for biofuel production, such as by requiring less downstream treatment; (2) enhancement of feedstock productivity; and (3) stability, reliability, and robustness in large-scale application, particularly when the pH and temperature are high. Second, scalability plays the inevitable key role in the commercialization of a biofuel. Conceptualization, screening, and testing of innovative processing techniques are needed to achieve high net productivity, low operation cost, and minimal negative environment effects. Third, economic feasibility analysis and life cycle assessment, such as the evaluations of costs vs.

profits, energy and water usage, and environmental impact, will give the panoramic view of the commercial application of biofuel production needed for attracting government or private investment funds.

WORKS CITED

Afi, L., Metzger, P., Largeau, C., Connan, J., Berkaloff, C., Rousseau, B. 1996. Bacterial degradation of green microalgae: Incubation of *Chlorella emersonii* and *Chlorella vulgaris* with *Pseudomonas oleovorans* and *Flavobacterium aquatile*. *Organic Geochemistry*, **25**(1-2), 117-130.

American Oil Chemists' Society. 1992. *Official methods and recommended practices of the American Oil Chemists' Society*. AOCS, Champaign.

American Public Health Association. 2005. *Standard methods for the examination of water and wastewater*. *21st ed*, Washington DC.

American Society for Testing and Materials. 2009. *Annual book of ASTM standards*. ASTM International, West Conshohocken.

Andersen, M.E., Meek, M.E., Boorman, G.A., Brusick, D.J., Cohen, S.M., Dragan, Y.P., Frederick, C.B., Goodman, J.I., Hard, G.C., O'Flaherty, E.J., Robinson, D.E. 2000. Lessons learned in applying the US EPA proposed cancer guidelines to specific compounds. *Toxicological Sciences*, **53**(2), 159-172.

Angermayr, S.A., Hellingwerf, K.J., Lindblad, P., de Mattos, M.J.T. 2009. Energy biotechnology with cyanobacteria. *Current Opinion in Biotechnology*, **20**(3), 257-263.

Antoni, D., Zverlov, V.V., Schwarz, W.H. 2007. Biofuels from microbes. *Applied Microbiology and Biotechnology*, **77**(1), 23-35.

Aseeva, E., Ossenbuhl, F., Eichacker, L.A., Wanner, G., Soll, J., Vothknecht, U.C. 2004. Complex formation of Vipp1 depends on its alpha-helical PspA-like domain. *Journal of Biological Chemistry*, **279**(34), 35535-35541.

Baker, G.C., Smith, J.J., Cowan, D.A. 2003. Review and re-analysis of domain-specific 16S primers. *Journal of Microbiological Methods*, **55**(3), 541-555.

Balogi, Z., Torok, Z., Balogh, G., Josvay, K., Shigapova, N., Vierling, E., Vigh, L., Horvath, L. 2005. "Heat shock lipid" in cyanobacteria during

heat/light-acclimation. *Archives of Biochemistry and Biophysics*, **436**(2), 346-354.

Belarbi, E.H., Molina, E., Chisti, Y. 2000. A process for high yield and scaleable recovery of high purity eicosapentaenoic acid esters from microalgae and fish oil. *Enzyme and Microbial Technology*, **26**(7), 516-529.

Benjumea, P., Agudelo, J.R., Agudelo, A.F. 2011. Effect of the degree of unsaturation of biodiesel fuels on engine performance, combustion characteristics, and emissions. *Energy & Fuels*, **25**, 77-85.

Berry, J., Bjorkman, O. 1980. Photosynthetic response and adaptation to temperature in higher-plants. *Annual Review of Plant Physiology and Plant Molecular Biology*, **31**, 491-543.

Blankenship, R.E. 2002. *Molecular mechanisms of photosynthesis*. Blackwell Science, Oxford; Malden, MA.

Bligh, E.G., Dyer, W.J. 1959. A rapid method of total lipid extraction and purification. *Canadian Journal of Biochemistry and Physiology*, **37**(8), 911-917.

Brondz, I. 2002. Development of fatty acid analysis by high-performance liquid chromatography, gas chromatography, and related techniques. *Analytica Chimica Acta*, **465**(1-2), 1-37.

Brown, J.H., Burnside, W.R., Davidson, A.D., DeLong, J.P., Dunn, W.C., Hamilton, M.J., Mercado-Silva, N., Nekola, J.C., Okie, J.G., Woodruff, W.H., Zuo, W.Y. 2011. Energetic limits to economic growth. *BioScience*, **61**(1), 19-26.

Byers, J.A. 2003. Solvent polarity and miscibility. http://www.chemical-ecology.net/java/solvents.htm.

Campbell, J.E., Lobell, D.B., Field, C.B. 2009. Greater transportation energy and GHG offsets from bioelectricity than ethanol. *Science*, **324**(5930), 1055-1057.

Canakci, M. 2007. The potential of restaurant waste lipids as biodiesel feedstocks. *Bioresource Technology*, **98**(1), 183-190.

Cantrell, K.B., Walker, T.H. 2009. Influence of temperature on growth and peak oil biosynthesis in a carbon-limited medium by *Pythium irregulare*. *Journal of the American Oil Chemists' Society*, **86**(8), 791-797.

Carter, A.P., Clemons, W.M., Brodersen, D.E., Morgan-Warren, R.J., Wimberly, B.T., Ramakrishnan, V. 2000. Functional insights from the structure of the 30S ribosomal subunit and its interactions with antibiotics. *Nature*, **407**(6802), 340-348.

Carvalho, A.P., Malcata, F.X. 2005. Preparation of fatty acid methyl esters for gas-chromatographic analysis of marine lipids: Insight studies. *Journal of Agricultural and Food Chemistry*, **53**(13), 5049-5059.

Carvalho, A.P., Meireles, L.A., Malcata, F.X. 2006. Microalgal reactors: A review of enclosed system designs and performances. *Biotechnology Progress*, **22**(6), 1490-1506.

Casadevall, A., Nicola, A.M., Frases, S. 2009. Lipophilic dye staining of *Cryptococcus neoformans* extracellular vesicles and capsule. *Eukaryotic Cell*, **8**(9), 1373-1380.

Cason, J., Sumrell, G. 1951. Branched-chain fatty acids. XVIII. Ultraviolet absorption spectra of saturated branched-chain acids. *The Journal of Organic Chemistry*, **16**(7), 1177-1180.

Chapman, D. 1975. Phase-transitions and fluidity characteristics of lipids and cell-membranes. *Quarterly Reviews of Biophysics*, **8**(2), 185-235.

Chen, C.-Y., Yeh, K.-L., Aisyah, R., Lee, D.-J., Chang, J.-S. 2011. Cultivation, photobioreactor design and harvesting of microalgae for biodiesel production: A critical review. *Bioresource Technology*, **102**(1), 71-81.

Chisti, Y. 2007. Biodiesel from microalgae. *Biotechnology Advances*, **25**(3), 294-306.

Chisti, Y., Mooyoung, M. 1986. Disruption of microbial-cells for intracellular products. *Enzyme and Microbial Technology*, **8**(4), 194-204.

Christie, W.W. 1993. Preparation of lipid extracts from tissues. in: *Advances in Lipid Methodology - Two*, Oily Press. Dundee, pp. 195-213.

Christie, W.W. 1986. Separation of lipid classes by high-performance liquid-chromatography with the mass detector. *Journal of Chromatography*, **361**, 396-399.

Cooney, M., Young, G., Nagle, N. 2009. Extraction of bio-oils from microalgae. *Separation and Purification Reviews*, **38**(4), 291-325.

Couto, R.M., Simoes, P.C., Reis, A., Da Silva, T.L., Martins, V.H., Sanchez-Vicente, Y. 2010. Supercritical fluid extraction of lipids from the heterotrophic microalga *Crypthecodinium cohnii*. *Engineering in Life Sciences*, **10**(2), 158-164.

Cravotto, G., Boffa, L., Mantegna, S., Perego, P., Avogadro, M., Cintas, P. 2008. Improved extraction of vegetable oils under high-intensity ultrasound and/or microwaves. *Ultrasonics Sonochemistry*, **15**(5), 898-902.

Czucz, B., Gathman, J.P., McPherson, G.R. 2010. The impending peak and decline of petroleum production: an underestimated challenge for conservation of ecological integrity. *Conservation Biology*, **24**(4), 948-956.

Ding, H., Sun, M.-Y. 2005. Biochemical degradation of algal fatty acids in oxic and anoxic sediment-seawater interface systems: effects of structural association and relative roles of aerobic and anaerobic bacteria. *Marine Chemistry*, **93**(1), 1-19.

Dionisi, H.M., Harms, G., Layton, A.C., Gregory, I.R., Parker, J., Hawkins, S.A., Robinson, K.G., Sayler, G.S. 2003. Power analysis for real-time PCR quantification of genes in activated sludge and analysis of the variability introduced by DNA extraction. *Applied and Environmental Microbiology*, **69**(11), 6597-6604.

Dismukes, G.C., Carrieri, D., Bennette, N., Ananyev, G.M., Posewitz, M.C. 2008. Aquatic phototrophs: efficient alternatives to land-based crops for biofuels. *Current Opinion in Biotechnology*, **19**(3), 235-240.

Doucha, J., Livansky, K. 2006. Productivity, CO_2/O_2 exchange and hydraulics in outdoor open high density microalgal (*Chlorella* sp.) photobioreactors operated in a Middle and Southern European climate. *Journal of Applied Phycology*, **18**(6), 811-826.

Enami, I., Kitamura, M., Tomo, T., Isokawa, Y., Ohta, H., Katoh, S. 1994. Is the primary cause of thermal inactivation of oxygen evolution in spinach PS-II membranes release of the extrinsic 33 kDa protein or of Mn? *Biochimica et Biophysica Acta-Bioenergetics*, **1186**(1-2), 52-58.

Fajardo, A.R., Cerdan, L.E., Medina, A.R., Fernandez, F.G.A., Moreno, P.A.G., Grima, E.M. 2007. Lipid extraction from the microalga *Phaeodactylum tricornutum*. *European Journal of Lipid Science and Technology*, **109**(2), 120-126.

Feng, C., Johns, M.R. 1991. Effect of C/N ratio and aeration on the fatty-acid composition of heterotrophic *Chlorella Sorokiniana*. *Journal of Applied Phycology*, **3**(3), 203-209.

Ferrera, I., Massana, R., Balague, V., Pedros-Alio, C., Sanchez, O., Mas, J. 2010. Evaluation of DNA extraction methods from complex phototrophic biofilms. *Biofouling*, **26**(3), 349-357.

Foglia, T.A., Jones, K.C., Nunez, A., Phillips, J.G., Mittelbach, M. 2004. Comparison of chromatographic methods for the determination of bound glycerol in biodiesel. *Chromatographia*, **60**(5-6), 305-311.

Folch, J., Lees, M., Stanley, G.H.S. 1957. A simple method for the isolation and purification of total lipids from animal tissues. *Journal of Biological Chemistry*, **226**(1), 497-509.

Franco, A., Giannini, N. 2005. Perspectives for the use of biomass as fuel in combined cycle power plants. *International Journal of Thermal Sciences*, **44**(2), 163-177.

Gabashvili, I.S., Menikh, A., Segui, J., Fragata, M. 1998. Protein structure of photosystem II studied by FTIR spectroscopy. Effect of digalactosyldiacylglycerol on the tyrosine side chain residues. *Journal of Molecular Structure*, **444**(1-3), 123-133.

Galbraith, H., Miller, T.B. 1973. Effect of metal cations and pH on antibacterial activity and uptake of long-chain fatty-acids. *Journal of Applied Bacteriology*, **36**(4), 635-646.

Gombos, Z., Hideg, E., Zsiros, O., Wada, H., Murata, N. 1995. The role of lipid desaturation in protection mechanism against temperature stresses. *Acta Phytopathologica et Entomologica Hungarica*, **30**(1-2), 89-92.

Gombos, Z., Wada, H., Murata, N. 1992. Unsaturation of fatty-acids in membrane-lipids enhances tolerance of the cyanobacterium *Synechocystis* PCC6803 to low-temperature photoinhibition. *Proceedings of the National Academy of Sciences of the United States of America*, **89**(20), 9959-9963.

Graham, D.Y., Sackman, J.W. 1983. Solubility of calcium soaps of long-chain fatty-acids in simulated intestinal environment. *Digestive Diseases and Sciences*, **28**(8), 733-736.

Greenspan, P., Mayer, E.P., Fowler, S.D. 1985. Nile red - a selective fluorescent stain for intracellular lipid droplets. *Journal of Cell Biology*, **100**(3), 965-973.

Guderjan, M., Topfl, S., Angersbach, A., Knorr, D. 2005. Impact of pulsed electric field treatment on the recovery and quality of plant oils. *Journal of Food Engineering*, **67**(3), 281-287.

Gupta, M.N., Batra, R., Tyagi, R., Sharma, A. 1997. Polarity index: The guiding solvent parameter for enzyme stability in aqueous-organic cosolvent mixtures. *Biotechnology Progress*, **13**(3), 284-288.

Hagerthey, S.E., Louda, J.W., Mongkronsri, P. 2006. Evaluation of pigment extraction methods and a recommended protocol for periphyton chlorophyll a determination and chemotaxonomic assessment. *Journal of Phycology*, **42**(5), 1125-1136.

Hamilton, W.A., Sale, A.J.H. 1967. Effects of high electric fields on microorganisms. 2. Mechanism of action of lethal effect. *Biochimica et Biophysica Acta*, **148**(3), 789-800.

Han, X.L., Gross, R.W. 2005. Shotgun lipidomics: Electrospray ionization mass spectrometric analysis and quantitation of cellular lipidomes directly from crude extracts of biological samples. *Mass Spectrometry Reviews*, **24**(3), 367-412.

Hansen, C.M., Erickson, A.E. 1969. Use of asphalt to increase water-holding capacity of droughty sand soils. *Industrial & Engineering Chemistry Product Research and Development*, **8**(3), 256-259.

Hirani, T.A., Suzuki, I., Murata, N., Hayashi, H., Eaton-Rye, J.J. 2001. Characterization of a two-component signal transduction system involved in the induction of alkaline phosphatase under phosphate-limiting conditions in Synechocystis sp PCC 6803. *Plant Molecular Biology*, **45**(2), 133-144.

Hirano, M., Satoh, K., Katoh, S. 1981. The effect on photosynthetic electron-transport of temperature-dependent changes in the fluidity of the thylakoid membrane in a thermophilic blue-green-alga. *Biochimica et Biophysica Acta*, **635**(3), 476-487.

Hoiczyk, E., Hansel, A. 2000. Cyanobacterial cell walls: News from an unusual prokaryotic envelope. *Journal of Bacteriology*, **182**(5), 1191-1199.

Hu, Q., Sommerfeld, M., Jarvis, E., Ghirardi, M., Posewitz, M., Seibert, M., Darzins, A. 2008. Microalgal triacylglycerols as feedstocks for biofuel production: perspectives and advances. *Plant Journal*, **54**(4), 621-639.

Huang, G.H., Chen, F., Wei, D., Zhang, X.W., Chen, G. 2010. Biodiesel production by microalgal biotechnology. *Applied Energy*, **87**(1), 38-46.

Huang, J.J., Kolodny, N.H., Redfearn, J.T., Allen, M.M. 2002. The acid stress response of the cyanobacterium *Synechocystis* sp strain PCC 6308. *Archives of Microbiology*, **177**(6), 486-493.

Huber, G.W., Iborra, S., Corma, A. 2006. Synthesis of transportation fuels from biomass: Chemistry, catalysts, and engineering. *Chemical Reviews*, **106**(9), 4044-4098.

Ikeuchi, M., Tabata, S. 2001. *Synechocystis* sp PCC 6803 - a useful tool in the study of the genetics of cyanobacteria. *Photosynthesis Research*, **70**(1), 73-83.

Inoue, N., Taira, Y., Emi, T., Yamane, Y., Kashino, Y., Koike, H., Satoh, K. 2001. Acclimation to the growth temperature and the high-temperature effects on photosystem II and plasma membranes in a mesophilic cyanobacterium, *Synechocystis* sp PCC6803. *Plant and Cell Physiology*, **42**(10), 1140-1148.

Intergovernmental Panel on Climate Change (IPCC). 2007. Climate change 2007: Synthesis report, United Nations. New York.

International Energy Agency. 2010. World energy outlook. http://www.iea.org/weo/.

International Union of Pure and Applied Chemistry (IUPAC). 1992. *Standard methods for the analysis of oils, fats and derivatives*. *7th ed*. Pergamon Press, Oxford.

Iverson, S.J., Lang, S.L.C., Cooper, M.H. 2001. Comparison of the Bligh and Dyer and Folch methods for total lipid determination in a broad range of marine tissue. *Lipids*, **36**(11), 1283-1287.

Kaczmarzyk, D., Fulda, M. 2010. Fatty acid activation in cyanobacteria mediated by acyl-acyl carrier protein synthetase enables fatty acid recycling. *Plant Physiology*, **152**(3), 1598-1610.

Kaneko, T., Sato, S., Kotani, H., Tanaka, A., Asamizu, E., Nakamura, Y., Miyajima, N., Hirosawa, M., Sugiura, M., Sasamoto, S., Kimura, T., Hosouchi, T., Matsuno, A., Muraki, A., Nakazaki, N., Naruo, K., Okumura, S., Shimpo, S., Takeuchi, C., Wada, T., Watanabe, A., Yamada, M., Yasuda, M., Tabata, S. 1996. Sequence analysis of the genome of the unicellular cyanobacterium *Synechocystis* sp. strain PCC6803. II. Sequence determination of the entire genome and assignment of potential protein-coding regions. *DNA Res*, **3**(3), 109-36.

Karaosmanoglu, F. 1999. Vegetable oil fuels: A review. *Energy Sources*, **21**(3), 221-231.

Katsui, N., Tsuchido, T., Hiramatsu, R., Fujikawa, S., Takano, M., Shibasaki, I. 1982. Heat-induced blebbing and vesiculation of the outer-membrane of *Escherichia coli*. *Journal of Bacteriology*, **151**(3), 1523-1531.

Kebede, E., Ahlgren, G. 1996. Optimum growth conditions and light utilization efficiency of *Spirulina platensis* (= *Arthrospira fusiformis*) (Cyanophyta) from Lake Chitu, Ethiopia. *Hydrobiologia*, **332(**2), 99-109.

Kim, H.W., Vannela, R., Zhou, C., Harto, C., Rittmann, B.E. 2010. Photoautotrophic nutrient utilization and limitation during semi-continuous growth of *Synechocystis* sp PCC6803. *Biotechnology and Bioengineering*, **106**(4), 553-563.

Kim, H.W., Vannela, R., Zhou, C., Rittmann, B.E. 2011. Nutrient acquisition and limitation for the photoautotrophic growth of *Synechocystis* sp. PCC6803 as a renewable biomass source. *Biotechnology and Bioengineering*, **108**(2), 277-285.

Klein, K., Steinberg, R., Fiethen, B., Overath, P. 1971. Fatty acid degradation in *Escherichia coli*. *European Journal of Biochemistry*, **19**(3), 442-450.

Klimov, V.V., Krasnovskii, A.A. 1981. Pheophytin as the primary electron-acceptor in Photosystem II reaction centers. *Photosynthetica*, **15**(4), 592-609.

Knothe, G. 2006. Analyzing biodiesel: Standards and other methods. *Journal of the American Oil Chemists' Society*, **83**(10), 823-833.

Knothe, G. 2010. Biodiesel and renewable diesel: A comparison. *Progress in Energy and Combustion Science*, **36**(3), 364-373.

Knothe, G., Van Gerpen, J., Krahl, J. 2005. *The biodiesel handbook*. AOCS Press, Urbana, IL.

Koksharova, O.A. 2010. Application of molecular genetic and microbiological techniques in ecology and biotechnology of cyanobacteria. *Microbiology*, **79**(6), 721-734.

Kopplow, O., Barjenbruch, M., Heinz, V. 2004. Sludge pre-treatment with pulsed electric fields. *Water Science and Technology*, **49**(10), 123-129.

Kovarik, B. 1998. Henry Ford, Charles F. Kettering and the fuel of the future. *Automotive History Review*(32), 7-27.

Kubicková, I., Snåre, M., Eränen, K., Mäki-Arvela, P., Murzin, D.Y. 2005. Hydrocarbons for diesel fuel via decarboxylation of vegetable oils. *Catalysis Today*, **106**(1-4), 197-200.

Lalman, J.A., Bagley, D.M. 2004. Extracting long-chain fatty acids from a fermentation medium. *Journal of the American Oil Chemists' Society*, **81**(2), 105-110.

Lee, I.-S., Parameswaran, P., Alder, J.M., Rittmann, B.E. 2010a. Feasibility of Focused–Pulsed treated waste activated sludge as a supplemental electron donor for denitrification. *Water Environment Federation*, **82**.

Lee, J.Y., Yoo, C., Jun, S.Y., Ahn, C.Y., Oh, H.M. 2010b. Comparison of several methods for effective lipid extraction from microalgae. *Bioresource Technology*, **101**, S75-S77.

Lee, S.J., Yoon, B.D., Oh, H.M. 1998. Rapid method for the determination of lipid from the green alga *Botryococcus braunii*. *Biotechnology Techniques*, **12**(7), 553-556.

Lee, T.W., Ho, A. 2010. Scaling of the urban heat island effect based on the energy balance: nighttime minimum temperature increase vs. urban area length scale. *Climate Research*, **42**(3), 209-216.

Lepage, G., Roy, C.C. 1984. Improved recovery of fatty-acid through direct trans-esterification without prior extraction or purification. *Journal of Lipid Research*, **25**(12), 1391-1396.

Levario, T.J., Dai, M., Yuan, W., Vogt, B.D., Nielsen, D.R. 2011. Rapid adsorption of alcohol biofuels by high surface area mesoporous carbons. *Microporous and Mesoporous Materials*, DOI:10.1016/j.micromeso.2011.08.001.

Li, Q., Du, W., Liu, D.H. 2008. Perspectives of microbial oils for biodiesel production. *Applied Microbiology and Biotechnology*, **80**(5), 749-756.

Li, X.F., Xu, H., Wu, Q.Y. 2007. Large-scale biodiesel production from microalga *Chlorella protothecoides* through heterotropic cultivation in bioreactors. *Biotechnology and Bioengineering*, **98**(4), 764-771.

Liberton, M., Berg, R.H., Heuser, J., Roth, R., Pakrasi, H.B. 2006. Ultrastructure of the membrane systems in the unicellular cyanobacterium *Synechocystis* sp. strain PCC 6803. *Protoplasma*, **227**(2-4), 129-138.

Lin, J.H., Liu, D.Y., Yang, M.H., Lee, M.H. 2004. Ethyl acetate/ethyl alcohol mixtures as an alternative to Folch reagent for extracting animal lipids. *Journal of Agricultural and Food Chemistry*, **52**(16), 4984-4986.

Liu, B., Zhao, Z. 2007. Biodiesel production by direct methanolysis of oleaginous microbial biomass. *Journal of Chemical Technology and Biotechnology*, **82**(8), 775-780.

Liu, W.T., Marsh, T.L., Cheng, H., Forney, L.J. 1997. Characterization of microbial diversity by determining terminal restriction fragment length polymorphisms of genes encoding 16S rRNA. *Applied and Environmental Microbiology*, **63**(11), 4516-4522.

Liu, X.J., Jiang, Y., Chen, F. 2005. Fatty acid profile of the edible filamentous cyanobacterium *Nostoc flagelliforme* at different temperatures and developmental stages in liquid suspension culture. *Process Biochemistry*, **40**(1), 371-377.

Liu, X.Y., Fallon, S., Sheng, J., Curtiss, R. 2011a. CO_2-limitation-inducible Green Recovery of fatty acids from cyanobacterial biomass. *Proceedings of the National Academy of Sciences of the United States of America*, **108**(17), 6905-6908.

Liu, X.Y., Sheng, J., Curtiss, R. 2011b. Fatty acid production in genetically modified cyanobacteria. *Proceedings of the National Academy of Sciences of the United States of America*, **108**(17), 6899-6904.

Lopez-Archilla, A.I., Moreira, D., Lopez-Garcia, P., Guerrero, C. 2004. Phytoplankton diversity and cyanobacterial dominance in a hypereutrophic shallow lake with biologically produced alkaline pH. *Extremophiles*, **8**(2), 109-115.

Mahlmann, D.M., Jahnke, J., Loosen, P. 2008. Rapid determination of the dry weight of single, living cyanobacterial cells using the Mach-Zehnder double-beam interference microscope. *European Journal of Phycology*, **43**(4), 355-364.

Mata, T.M., Martins, A.A., Caetano, N.S. 2010. Microalgae for biodiesel production and other applications: A review. *Renewable & Sustainable Energy Reviews*, **14**(1), 217-232.

Matyash, V., Liebisch, G., Kurzchalia, T.V., Shevchenko, A., Schwudke, D. 2008. Lipid extraction by methyl-*tert*-butyl ether for high-throughput lipidomics. *Journal of Lipid Research*, **49**(5), 1137-1146.

McCarty, P.L. 2007. Thermodynamic electron equivalents model for bacterial yield prediction: Modifications and comparative evaluations. *Biotechnology and Bioengineering*, **97**(2), 377-388.

McCree, K.J. 1981. Photosynthetically active radiation. in: *Encyclopedia of plant physiology I*, (Eds.) O.L. Lange, P.S. Nobel, C.B. Osmond, H. Ziegler, Vol. 12A, Springer. Berlin Heidelberg New York, pp. 443-455.

Meher, L.C., Sagar, D.V., Naik, S.N. 2006. Technical aspects of biodiesel production by transesterification - a review. *Renewable & Sustainable Energy Reviews*, **10**(3), 248-268.

Meseck, S.L. 2007. Controlling the growth of a cyanobacterial contaminant, *Synechoccus* sp., in a culture of *Tetraselmis chui* (PLY429) by varying pH: Implications for outdoor aquaculture production. *Aquaculture*, **273**(4), 566-572.

Metcalf, J.S., Codd, G.A. 2000. Microwave oven and boiling waterbath extraction of hepatotoxins from cyanobacterial cells. *FEMS Microbiology Letters*, **184**(2), 241-246.

Miao, X.L., Wu, Q.Y. 2006. Biodiesel production from heterotrophic microalgal oil. *Bioresource Technology*, **97**(6), 841-846.

Middelberg, A.P.J. 1995. Process-scale disruption of microorganisms. *Biotechnology Advances*, **13**(3), 491-551.

Min, S., Evrendilek, G.A., Zhang, H.Q. 2007. Pulsed electric fields: Processing system, microbial and enzyme inhibition, and shelf life extension of foods. *IEEE Transactions on Plasma Science*, **35**(1), 59-73.

Molina Grima, E., Acien Fernandez, F.G., Garcia Camacho, F., Chisti, Y. 1999. Photobioreactors: light regime, mass transfer, and scaleup. *Journal of Biotechnology*, **70**(1-3), 231-247.

Molina Grima, E., Belarbi, E.H., Acien Fernandez, F.G., Robles Medina, A., Chisti, Y. 2003. Recovery of microalgal biomass and metabolites: process options and economics. *Biotechnology Advances*, **20**(7-8), 491-515.

Molina Grima, E., Robles Medina, A., Gimenez Gimenez, A., Sanchez Perez, J.A., Garcia Camacho, F., Garcia Sanchez, J.L. 1994. Comparison between extraction of lipids and fatty-acids from microalgal biomass. *Journal of the American Oil Chemists' Society*, **71**(9), 955-959.

Mullineaux, C.W. 1999. The thylakoid membranes of cyanobacteria: structure, dynamics and function. *Australian Journal of Plant Physiology*, **26**(7), 671-677.

Murata, N. 1989. Low-temperature effects on cyanobacterial membranes. *Journal of Bioenergetics and Biomembranes*, **21**(1), 61-75.

Murata, N., Wada, H. 1995. Acyl-lipid desaturases and their importance in the tolerance and acclimatization to cold of cyanobacteria. *Biochemical Journal*, **308**, 1-8.

Na, J.G., Yi, B.E., Kim, J.N., Yi, K.B., Park, S.Y., Park, J.H., Kim, J.N., Ko, C.H. 2010. Hydrocarbon production from decarboxylation of fatty acid without hydrogen. *Catalysis Today*, **156**(1-2), 44-48.

Nakamura, Y., Kaneko, T., Hirosawa, M., Miyajima, N., Tabata, S. 1998. CyanoBase, a WWW database containing the complete nucleotide sequence of the genome of *Synechocystis* sp. strain PCC6803. *Nucleic Acids Research*, **26**(1), 63-67.

Nielsen, D.R., Amarasiriwardena, G.S., Prather, K.L.J. 2010. Predicting the adsorption of second generation biofuels by polymeric resins with applications for *in situ* product recovery (ISPR). *Bioresource Technology*, **101**(8), 2762-2769.

Nielsen, D.R., Prather, K.J. 2009. In situ product recovery of *n*-butanol using polymeric resins. *Biotechnology and Bioengineering*, **102**(3), 811-821.

Novak, J.T., Kraus, D.L. 1973. Degradation of long-chain fatty-acids by activated-sludge. *Water Research*, **7**(6), 843-851.

Nyren, V., Back, E. 1958. The ionization constant, solubility product and solubility of lauric and myristic acid. *Acta Chemica Scandinavica*, **12**(6), 1305-1311.

Ogawa, T., Kaplan, A. 2003. Inorganic carbon acquisition systems in cyanobacteria. *Photosynthesis Research*, **77**(2-3), 105-115.

Ohkawa, H., Price, G.D., Badger, M.R., Ogawa, T. 2000. Mutation of *ndh* genes leads to inhibition of CO_2 uptake rather than HCO_3^- uptake in *Synechocystis* sp strain PCC 6803. *Journal of Bacteriology*, **182**(9), 2591-2596.

Owen, R.W., Weisgerber, U.M., Carr, J., Harrison, M.H. 1995. Analysis of calcium-lipid complexes in feces. *European Journal of Cancer Prevention*, **4**(3), 247-255.

Pimentel, D., Marklein, A., Toth, M.A., Karpoff, M., Paul, G.S., McCormack, R., Kyriazis, J., Krueger, T. 2008. Biofuel impacts on world food supply: Use of fossil fuel, land and water resources. *Energies*, **1**(2), 41-78.

Pinto, A.C., Guarieiro, L.L.N., Rezende, M.J.C., Ribeiro, N.M., Torres, E.A., Lopes, W.A., Pereira, P.A.D., de Andrade, J.B. 2005. Biodiesel: An overview. *Journal of the Brazilian Chemical Society*, **16**(6B), 1313-1330.

Pulz, O. 2001. Photobioreactors: production systems for phototrophic microorganisms. *Applied Microbiology and Biotechnology*, **57**(3), 287-293.

Quintana, N., Van der Kooy, F., Van de Rhee, M., Voshol, G., Verpoorte, R. 2011. Renewable energy from cyanobacteria: energy production optimization by metabolic pathway engineering. *Applied Microbiology and Biotechnology*, **91**(3), 471-490.

Ragauskas, A.J., Williams, C.K., Davison, B.H., Britovsek, G., Cairney, J., Eckert, C.A., Frederick, W.J., Hallett, J.P., Leak, D.J., Liotta, C.L., Mielenz, J.R., Murphy, R., Templer, R., Tschaplinski, T. 2006. The path forward for biofuels and biomaterials. *Science*, **311**(5760), 484-489.

Rasmussen, P., Barbez, P.H., Burgoyne, L.A., Saint, P. 2008. Rapid preparation of cyanobacterial DNA for real-time PCR analysis. *Letters in Applied Microbiology*, **46**(1), 14-19.

Rippka, R., Deruelles, J., Waterbury, J.B., Herdman, M., Stanier, R.Y. 1979. Generic assignments, strain histories and properties of pure cultures of cyanobacteria. *Journal of General Microbiology*, **111**(MAR), 1-61.

Rittmann, B.E. 2008. Opportunities for renewable bioenergy using microorganisms. *Biotechnology and Bioengineering*, **100**(2), 203-212.

Rittmann, B.E., Krajmalnik-Brown, R., Halden, R.U. 2008a. Pre-genomic, genomic and postgenomic study of microbial communities involved in bioenergy. *Nature Reviews Microbiology*, **6**(8), 604-612.

Rittmann, B.E., Lee, H.S., Zhang, H.S., Alder, J., Banaszak, J.E., Lopez, R. 2008b. Full-scale application of focused-pulsed pre-treatment for improving biosolids digestion and conversion to methane. *Water Science and Technology*, **58**(10), 1895-1901.

Rittmann, B.E., McCarty, P.L. 2001. *Environmental biotechnology: Principles and applications*. McGraw-Hill Co., New York.

Salerno, M.B., Lee, H.S., Parameswaran, P., Rittmann, B.E. 2009. Using a pulsed electric field as a pretreatment for improved biosolids digestion and methanogenesis. *Water Environment Research*, **81**(8), 831-839.

Sarcina, M., Murata, N., Tobin, M.J., Mullineaux, C.W. 2003. Lipid diffusion in the thylakoid membranes of the cyanobacterium *Synechococcus* sp.: effect of fatty acid desaturation. *FEBS Letters*, **553**(3), 295-298.

Sato, N., Murata, N. 1988. Membrane-lipids. *Methods in Enzymology*, **167**, 251-259.

Schafer, K. 1998. Accelerated solvent extraction of lipids for determining the fatty acid composition of biological material. *Analytica Chimica Acta*, **358**(1), 69-77.

Schenk, P.M., Thomas-Hall, S.R., Stephens, E., Marx, U.C., Mussgnug, J.H., Posten, C., Kruse, O., Hankamer, B. 2008. Second generation biofuels: High-efficiency microalgae for biodiesel production. *Bioenergy Research*, **1**(1), 20-43.

Schirmer, A., Rude, M.A., Li, X.Z., Popova, E., del Cardayre, S.B. 2010. Microbial biosynthesis of alkanes. *Science*, **329**(5991), 559-562.

Schoenbach, K.H., Joshi, R.P., Stark, R.H., Dobbs, F.C., Beebe, S.J. 2000. Bacterial decontamination of liquids with pulsed electric fields. *IEEE Transactions on Dielectrics and Electrical Insulation*, **7**(5), 637-645.

Shastri, A.A., Morgan, J.A. 2005. Flux balance analysis of photoautotrophic metabolism. *Biotechnology Progress*, **21**(6), 1617-1626.

Sheng, J., Kim, H.W., Badalamenti, J.P., Zhou, C., Sridharakrishnan, S., Krajmalnik-Brown, R., Rittmann, B.E., Vannela, R. 2011a. Effects of temperature shifts on growth rate and lipid characteristics of *Synechocystis* sp. PCC6803 in a bench-top photobioreactor. *Bioresource Technology*, **102**(24), 11218-11225.

Sheng, J., Vannela, R., Rittmann, B.E. 2011b. Disruption of *Synechocystis* PCC 6803 for lipid extraction. *Water Science and Technology*, DOI: 10.2166/wst.2011.879.

Sheng, J., Vannela, R., Rittmann, B.E. 2011c. Evaluation of cell-disruption effects of pulsed-electric-field treatment of *Synechocystis* PCC 6803. *Environmental Science & Technology*, **45**(8), 3795-3802.

Sheng, J., Vannela, R., Rittmann, B.E. 2011d. Evaluation of methods to extract and quantify lipids from *Synechocystis* PCC 6803. *Bioresource Technology*, **102**(2), 1697-1703.

Smedes, F., Thomasen, T.K. 1996. Evaluation of the Bligh & Dyer lipid determination method. *Marine Pollution Bulletin*, **32**(8-9), 681-688.

Snoeyink, V.L., Jenkins, D. 1980. *Water chemistry*. John Wiley & Sons, New York.

Snyder, L.R. 1974. Classification of solvent properties of common liquids. *Journal of Chromatography*, **92**(2), 223-230.

Somerville, C., Browse, J. 1991. Plant lipids - metabolism, mutants, and membranes. *Science*, **252**(5002), 80-87.

Somolinos, M., Garcia, D., Condon, S., Manas, P., Pagan, R. 2007. Relationship between sublethal injury and inactivation of yeast cells by the combination of sorbic acid and pulsed electric fields. *Applied and Environmental Microbiology*, **73**(12), 3814-3821.

Sousa, D.Z., Smidt, H., Alves, M.M., Stams, A.J.M. 2009. Ecophysiology of syntrophic communities that degrade saturated and unsaturated long-chain fatty acids. *FEMS Microbiology Ecology*, **68**(3), 257-272.

Speight, J.G. 2005. Lange's handbook of chemistry. 16th ed, McGraw-Hill. New York.

Steen, E.J., Kang, Y.S., Bokinsky, G., Hu, Z.H., Schirmer, A., McClure, A., del Cardayre, S.B., Keasling, J.D. 2010. Microbial production of fatty-acid-

derived fuels and chemicals from plant biomass. *Nature*, **463**(7280), 559-U182.

Summerfield, T.C., Sherman, L.A. 2008. Global transcriptional response of the alkali-tolerant cyanobacterium *Synechocystis* sp. strain PCC 6803 to a pH 10 environment. *Applied and Environmental Microbiology*, **74**(17), 5276-5284.

Sundararaj, S., Guo, A.C. 2008. *E. coli* statistics. http://www.ccdb.ualberta.ca/CCDB/cgi-bin/STAT_NEW.cgi.

Sung, D.Y., Kaplan, F., Lee, K.J., Guy, C.L. 2003. Acquired tolerance to temperature extremes. *Trends in Plant Science*, **8**(4), 179-187.

Terry, K.L., Raymond, L.P. 1985. System-design for the autotrophic production of microalgae. *Enzyme and Microbial Technology*, **7**(10), 474-487.

Torzillo, G., Giovannetti, L., Bocci, F., Materassi, R. 1984. Effect of oxygen concentration on the protein-content of *Spirulina* biomass. *Biotechnology and Bioengineering*, **26**(9), 1134-1135.

Tran, H.L., Hong, S.J., Lee, C.G. 2009. Evaluation of extraction methods for recovery of fatty acids from *Botryococcus braunii* LB 572 and *Synechocystis* sp. PCC 6803. *Biotechnology and Bioprocess Engineering*, **14**(2), 187-192.

Tredici, M.R., Zittelli, G.C. 1998. Efficiency of sunlight utilization: Tubular versus flat photobioreactors. *Biotechnology and Bioengineering*, **57**(2), 187-197.

U.S. Energy Information Administration. 2010a. Annual energy review. http://www.eia.gov/totalenergy/data/annual/.

U.S. Energy Information Administration. 2010b. International energy outlook 2010. http://www.eia.gov/oiaf/ieo/index.html.

U.S. EPA. 2009. IRIS toxicological review of methanol (external review draft), U.S. Environmental Protection Agency. Washington, DC.

U.S. National Research Council. 2008. *Water implications of biofuels production in the United States*. The National Academy Press, Washington, D.C.

Unal, R., Yousef, A.E., Dunne, C.P. 2002. Spectrofluorimetric asessment of bacterial cell membrane damage by pulsed electric field. *Innovative Food Science and Emerging Technologies*, **3**(3), 247-254.

van de Meene, A.M.L., Hohmann-Marriott, M.F., Vermaas, W.F.J., Roberson, R.W. 2006. The three-dimensional structure of the cyanobacterium *Synechocystis* sp. PCC 6803. *Archives of Microbiology*, **184**(5), 259-270.

van der Horst, D., Vermeylen, S. 2011. Spatial scale and social impacts of biofuel production. *Biomass & Bioenergy*, **35**(6), 2435-2443.

van der Staay, G.W.M., Staehelin, L.A. 1994. Biochemical characterization of protein composition and protein phosphorylation patterns in stacked and unstacked thylakoid membranes of the prochlorophyte *Prochlorothrix Hollandica*. *Journal of Biological Chemistry*, **269**(40), 24834-24844.

Van Gerpen, J., Shanks, B., Pruszko, R., Clements, D., Knothe, G. 2004. Biodiesel production technology. Subcontractor report to National Renewable Energy Laboratory (NREL). NREL/SR-510-36244.

Vannela, R., Verma, S.K. 2006. Cu^{2+} Removal and recovery by *Spi*SORB: batch stirred and up-flow packed bed columnar reactor systems. *Bioprocess and Biosystems Engineering*, **29**(1), 7-17.

Vermaas, W. 1996. Molecular genetics of the cyanobacterium *Synechocystis* sp. PCC 6803: Principles and possible biotechnology applications. *Journal of Applied Phycology*, **8**(4-5), 263-273.

Vermaas, W.F.J. 2001. Photosynthesis and respiration in cyanobacteria. in: *eLS*, John Wiley & Sons, Ltd.

Vorum, H., Brodersen, R. 1994. Adsorption and physical state of medium-chain and long-chain fatty-acids in neutral aqueous buffer solution. *Chemistry and Physics of Lipids*, **74**(1), 43-48.

Wada, H., Gombos, Z., Murata, N. 1994. Contribution of membrane lipids to the ability of the photosynthetic machinery to tolerate temperature stress. *Proceedings of the National Academy of Sciences of the United States of America*, **91**(10), 4273-4277.

Wada, H., Murata, N. 1989. *Synechocystis* PCC6803 mutants defective in desaturation of fatty-acids. *Plant and Cell Physiology*, **30**(7), 971-978.

Wada, H., Murata, N. 1990. Temperature-induced changes in the fatty-acid composition of the cyanobacterium, *Synechocystis* PCC6803. *Plant Physiology*, **92**(4), 1062-1069.

Wang, J.F., Shu, Q., Nawaz, Z., Gao, J.X., Liao, Y.H., Zhang, Q., Wang, D.Z. 2010. Synthesis of biodiesel from a model waste oil feedstock using a carbon-based solid acid catalyst: Reaction and separation. *Bioresource Technology*, **101**(14), 5374-5384.

Weaver, J.C., Chizmadzhev, Y.A. 1996. Theory of electroporation: A review. *Bioelectrochemistry and Bioenergetics*, **41**(2), 135-160.

Weier, D., Muller, C., Gaspers, C., Frentzen, M. 2005. Characterisation of acyltransferases from *Synechocystis* sp. PCC6803. *Biochemical and Biophysical Research Communications*, **334**(4), 1127-1134.

Westphal, S., Heins, L., Soll, J., Vothknecht, U.C. 2001. Vipp1 deletion mutant of *Synechocystis*: A connection between bacterial phage shock and thylakoid biogenesis? *Proceedings of the National Academy of Sciences of the United States of America*, **98**(7), 4243-4248.

Wouters, P.C., Bos, A.P., Ueckert, J. 2001. Membrane permeabilization in relation to inactivation kinetics of *Lactobacillus* species due to pulsed electric fields. *Applied and Environmental Microbiology*, **67**(7), 3092-3101.

Wouters, P.C., Dutreux, N., Smelt, J., Lelieveld, H.L.M. 1999. Effects of pulsed electric fields on inactivation kinetics of *Listeria innocua*. *Applied and Environmental Microbiology*, **65**(12), 5364-5371.

Xu, H., Miao, X.L., Wu, Q.Y. 2006. High quality biodiesel production from a microalga *Chlorella protothecoides* by heterotrophic growth in fermenters. *Journal of Biotechnology*, **126**(4), 499-507.

Yoke, J.T. 1958. The solubility of calcium soaps. *Journal of Physical Chemistry*, **62**(6), 753-755.

Zhang, H., Banaszak, J.E., Parameswaran, P., Alder, J., Krajmalnik-Brown, R., Rittmann, B.E. 2009a. Focused-Pulsed sludge pre-treatment increases the bacterial diversity and relative abundance of acetoclastic methanogens in a full-scale anaerobic digester. *Water Research*, **43**(18), 4517-4526.

Zhang, L.F., Yang, H.M., Cui, S.X., Hu, J., Wang, J., Kuang, T.Y., Norling, B., Huang, F. 2009b. Proteomic analysis of plasma membranes of cyanobacterium *Synechocystis* sp. strain PCC 6803 in response to high pH stress. *Journal of Proteome Research*, **8**(6), 2892-2902.

Zhang, P.Y., Zhang, G.M., Wang, W. 2007. Ultrasonic treatment of biological sludge: Floc disintegration, cell lysis and inactivation. *Bioresource Technology*, **98**(1), 207-210.

Zhang, Y., Dubé, M.A., McLean, D.D., Kates, M. 2003. Biodiesel production from waste cooking oil: 1. Process design and technological assessment. *Bioresource Technology*, **89**(1), 1-16.

Zhu, X.-G., Long, S.P., Ort, D.R. 2008. What is the maximum efficiency with which photosynthesis can convert solar energy into biomass? *Current Opinion in Biotechnology*, **19**(2), 153-159.

Zittelli, G.C., Tomasello, V., Pinzani, E., Tredici, M.R. 1996. Outdoor cultivation of *Arthrospira platensis* during autumn and winter in temperate climates. *Journal of Applied Phycology*, **8**(4-5), 293-301.

Zsiros, O., Kis, M., Mustardy, S., Farkas, T., Varkonyi, Z., Gombos, Z., Szalontai, B. 2002. Light-driven structural changes in thylakoid and cytoplasmic membranes of a cyanobacterium, *Synechocystis* PCC 6803. *Journal of Plant Physiology*, **159**(4), 403-414.